THE UNIVERSITY

of LIVERPOOL

Processing and Characterisation of the Mechanical Properties of Novel Fibre-Metal Laminates

Thesis submitted in accordance with the requirements of The University *of* Liverpool for the degree of Doctor in Philosophy by

Germán Reyes Villanueva

Department of Engineering

March 2002

ACKNOWLEDGEMENTS

I would like to give thanks to God for giving me life and the peace and love of my wonderful family – they are more than I could ever wish for.

I also would like to express my gratitude to CONACYT (National Council for Science and Technology of Mexico) for sponsoring me throughout the duration of my PhD studies, making possible this life changing experience at the University of Liverpool.

The enjoyable time I spent in Liverpool is due to a number of people. Within the department, the technical staff including Dave, Chris, Monica and Pete deserve recognition; the secretarial staff, especially Pat, many thanks for your friendship!

Above all, I would like to express my sincere gratitude to Professor Wesley J. Cantwell whose experience and advice has proved invaluable in the completion of this programme. Thanks for being the best supervisor anyone could ask for. Wesley, thanks for your sincere friendship!

Thanks to my friends and colleges in the composites team, especially Lukas and Graham for all the meaningful discussions over the past few years and lunchtime chats.

To my parents, parents in law and all my family for your love and support, although far in Mexico, I always kept every one of you all the time in my heart.

Finally, thanks to mi morcito! Gisvi Yalid for your infinite love and patience, thanks for being my strength and inspiration in this precious part of my life. I love you! and I always will. To mi enano! Sergio Germán for being my motivation all the time and to mi cachetona! Giovanna Yalid for bringing your happiness and sunshine to our lives. The three of you fulfil my existence, I love you all!

I dedicate this Thesis to Gisvi Yalid, Sergio Germán and Giovanna Yalid.

LIST OF PUBLICATIONS

Some of the proceeding work has appeared or will appear in the following publications:

1.- **Reyes, G., Cantwell, W.J.**, Interfacial fracture in composite-metal laminates, 5th International Conference in Composite Engineering, (1998), pp 757-758.

2.- **Reyes, G., Cantwell, W.J.**, Interfacial fracture in fibre-metal laminates based on glass fibre reinforced polypropylene, Advance Composite Letters, **7** (1998), pp 97-103.

3.- **Reyes, G., Cantwell, W.J.**, The effect of strain rate on the interfacial fracture properties of carbon fibre-metal laminates, Journal of Materials Science Letters, **17** (1998), pp1953-1955.

4.- **Reyes, G., Cantwell, W.J.**, The properties of high performance fibre-metal laminates, 20th International SAMPE EUROPE Conference of the Society for the Advancement of Material and Process Engineering, (1999), pp 151-160.

5.- **Reyes, G., Cantwell, W.J.**, The mechanical properties of fibre - metal laminates based on glass fibre reinforced polypropylene, Composites Science and Technology, **60** (2000), pp 1085-1094.

6.- **Reyes Villanueva, G., Cantwell, W.J.**, The fracture properties of fibre-metal laminates, 7th International Conference in Composite Engineering, (2000), pp 897-898.

7.- **Cantwell, W.J., Compston, P., Reyes, G.**, The fracture properties of novel aluminium foam sandwich structures, Journal of Materials Science Letters, **19** (2000), pp 2205-2208.

8.- **Reyes, G., Cantwell, W.J.**, Energy absorption in hybrid composite structures Institution of Mechanical Engineers, Materials and structures for energy Absorption, (2000), pp 33-54.

9.- **Reyes, G., Compson, P., Guillen, F., Cantwell, W.J., Jones, N.**, The impact resistance of thermoplastic-based fibre metal laminates, Presented at the 13th International Conference on Composite Materials, (2001).

10.- **Cantwell, W.J., Wade, G., Guillen, J.F., Reyes Villanueva, G., Jones, N.,** The high velocity impact response of novel fibre metal laminates, Proceeding of the International Mechanical Engineering Congress and Exhibition, (2001).

11.- **Cantwell, W.J., Jones, N., Wade, G.A., Reyes, G., Guillen, J.F.,** The impact response of novel fibre-metal laminates, Proceedings of the First International Conference on High Performance Structures and Composites, (2002).

ABSTRACT

This study examines the mechanical properties of novel fibre-metal laminates under quasi-static and dynamic loading conditions. Here, fibre-metal laminates based on a woven carbon fibre reinforced epoxy (CFRE) and on a tough glass fibre/polypropylene (GFPP) have been manufactured and characterised. Initial tests on the plain composites have shown that these systems exhibited excellent interlaminar fracture properties over a range of loading rates. Here, the interlaminar fracture toughness of the plain composites was directly related to the ability of the material to dissipate energy in form of plastic deformation within the matrix material. Single cantilever beam tests on model aluminium/CFRE samples have shown that a simple abrasion-wipe procedure is sufficient for achieving an excellent level of adhesion at quasi-static and dynamic rates of loading. In addition, SCB tests have shown that a high level of adhesion between aluminium and GFPP can be achieved by surface-treating the aluminium and incorporating an interlayer based on a maleic anhydride-modified polypropylene polymer at the bi-material interface. Here, it has been shown that the interfacial fracture properties of these systems remained high over a wide rage of loading rates. Subsequent testing of a number of laminates has shown that the flexural properties of these layered systems are dependent on the volume fraction of composite. In addition, it has been shown that the tensile properties of thermosetting and thermoplastic-based fibre metal laminates can be fully controlled by altering the volume fraction of composite material.

Low velocity impact testing on three different stacking sequences has shown that these materials offer an excellent resistance to dynamic loading. In addition, it has been shown that the thermoplastic-based fibre-metal laminates offer a superior resistance to low velocity impact loading than its thermosetting counterpart. Here, it was shown that the laminates were capable of absorbing significant energy through extensive plastic deformation in the aluminium and composite layers and localised fibre fracture and matrix cracking in the thermosetting and thermoplastic composite layers respectively. Subsequent tensile tests on the impact-damaged coupons from both systems have shown that fibre-metal laminates offer excellent residual properties with the (4/3) laminates suffering only a 20% reduction in strength following a 20 Joule impact. High velocity impact tests on a series of thermosetting and thermoplastic-based fibre-metal laminates have shown that the GFPP-based fibre-metal systems offer a very good perforation resistance over the CFRE-based fibre-metal laminates. Indeed, the specific perforation energy of this system was over seventy percent higher than that offered by the thermosetting-based fibre metal laminates. Here, failure mechanisms such as extensive plastic drawing in the aluminium layers and fibre fracture and matrix cracking in the composite plies have been shown to contribute to the superior perforation resistance of these systems.

TABLE OF CONTENTS

1. INTRODUCTION

1.1 COMPOSITE MATERIALS

In the continuing quest for improved performance, which may be specified by various criteria including reduced weight, enhanced strength and lower costs, materials scientists and engineers are continuously striving to improve traditional materials and to produce completely new and novel high performance engineering such as advanced composites. The word composite describes a multi-phase material where the interaction of the two or more phases yields a material that offers a wide range of outstanding mechanical and physical properties.

1.1.1 Origins

The use of fibrous structures for load-bearing purposes has its origins in nature. The structure of a tree is a good example of a composite material consisting of strong cellulose fibres bonded to the lignin oriented in the direction of the principal stresses. Wood remains one of the most widely used structural materials at the present time. In the pioneering days of flight, aircraft structures were essentially based on composites, being composed largely of wood, wire and fabric. Light aluminium alloys took over in the 1930's and these materials have dominated the aircraft industry to the present day. The emergence of a new class of composite materials for use in aircraft design has its origin in a number of technical and scientific developments. The starting point for this development was the discovery of synthetic organic materials derived originally from vegetation and coal. These developments have been used to produce plastics, rubbers, adhesives and paints. A major step forward coincided with the production of phenolic resins during the early part of this century. Since then, a whole range of thermosetting resins and such as polyesters, polyimides, silicones and epoxy adhesives have been developed. The production of glass fibres increased the development of thermosetting resins for structural purposes. Both materials were combined to produce good quality laminates with

attractive mechanical properties. In 1944, the first training aircraft built from a sandwich construction of a glass fibre-reinforced polyester laminate incorporating a honeycomb core was built and flown.

In the post-war period, the development of the epoxy resins with superior properties has resulted in the replacement of polyester resins for most structural applications. The potentially high strength and stiffness to weight ratios of the glass fibres have led to their use in aerospace applications. Similarly, both boron and carbon fibres became available in limited quantities during the 1960's. Boron fibres were developed in USA using chemical vapour deposition techniques. The development of carbon fibres had to overcome the problem of aligning the graphite crystal from which these fibres are produced. This problem was cleverly solved by W. Watt in the UK. In the 1970's the aramid fibres that became available in the USA were the first to exploit the high strength and stiffness of the highly aligned carbon polymer chains. The straightforward requirements for weight reduction in the aerospace industry clearly favoured the use of composites. In addition, the more widespread availability of carbon and aramid fibres, resulted in the manufacture of a composite horizontal tail section of the Boeing 737 based on a carbon fibre-skinned honeycomb section with integral stiffeners [1].

In recent years, composite materials have found applications in almost all transportation sectors, sport and space structures, making composites one of the key materials for the developments of the future.

1.1.2 Advantages and potential of composites

Composite materials have established themselves as high performance engineering materials and are now relatively commonplace in a wide range of structural applications. Presently, the aircraft, automotive, marine, leisure, electronic and medical industries make extensive use of fibre-reinforced plastics. Composites are currently used to provide huge benefits with an emphasis on lower production and lifetime costs featuring prominently. One of the main characteristics of composites is the possibility of optimising the fibre stacking sequence to provide

solutions for structural needs. In many future aircraft and helicopter designs, the levels of flight performance envisaged will only be possible because of composites. Among the advantages of high performance polymer matrix composites are the following:

- Weight savings are significant, frequently ranging from 25 to 50 % of the weight of conventional metallic designs.
- The high torsional stiffness requirements of various vehicles, particularly high-speed aircraft, can be satisfied.
- Corrosion resistance is outstanding.
- Fatigue and fracture attributes are numerous.
- Impact and damage tolerance characteristics are excellent.
- Improved dent resistance is normally achieved (composite panels do not damage as easily as thin sheet metals).
- Flexibility in selection and changing of styling and product aesthetic considerations is an important feature.
- Thermoplastics have rapid processing cycles, making them attractive for high-volume commercial applications which traditionally have been the domain of sheet metals. Furthermore, thermoplastics can be re-formed and re-shaped.
- Thermoplastics have indefinite shelf lives.
- Low thermal expansion can be achieved.
- Manufacturing and assembly are simplified because of part integration (joint/fastener reduction) which reduces costs.
- Orientation of fibres in the direction where the strength/stiffness is needed.
- Composites absorb microwaves (stealth capability), etc. [2,3].

1.1.3 Types of materials

1.1.3.1 Reinforcing fibres

A wide range of fibrous materials is used to make plastics, metals and ceramics stronger, stiffer or tougher. In addition to this reinforcing role, some of these fibres

also possess other useful properties, such as a low density, low electrical conductivity and a superior heat resistance. The four reinforcing fibres that are currently finding widespread use in aircraft structures are aramid, boron, carbon and glass fibres[1].

There are a number of commercially available ***aramid fibres,*** e.g., Kevlar (Du pont), Twaron (Arkzo) and Technora (Teijin); of these, Kevlar is probably the most well known. Aramid fibres can be viewed as being based on polyamide with extra benzene rings in the polymeric chain to increase stiffness. The stiff aramid molecule is shown in Figure 1.1.

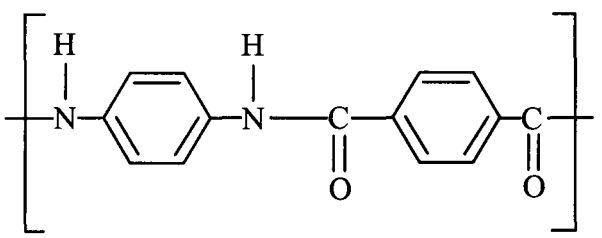

Figure 1.1 *The molecular structure of aramid*

The alignment of the molecules is enhanced during the fibre production process by spinning and extrusion, and by any subsequent mechanical treatments. Aramid fibres have good high temperature properties for a polymeric material. They have a glass transition temperature of approximately 360 °C and burn with difficulty. A loss in performance due to carbonisation occurs at around 425 °C however they can be used at elevated temperatures for sustained periods and even at 300 °C for a limited time. In addition, aramid fibres do not degrade in sunlight and their dimensional stability is good, since the coefficient of thermal expansion is low. Other properties, which are important in certain applications, are low electrical and thermal conductivity and high thermal capacity [4].

Boron fibres are unlike any of the other reinforcements. Each filament consists of a core of both tungsten wire or carbon fibre, and a sheath of boron which as been vapour-deposited upon the core from boron trichloride-hydrogen mixture. After manufacture, the fibre may be subjected to an annealing procedure to reduce residual stresses and to a chemical treatment to remove surfaces flaws and hence increase strength. Boron and carbon were selected for development as reinforcing fibres because they are the two lightest solid elements that it is practical to use [1].

Carbon fibres are produced by many companies and world production currently exceeds 12,000 tons. In spite of this large production capacity, carbon fibres are still relatively expensive. The structure and properties of these fibres vary considerably and new fibres are always being developed. As far as fibre technology is concerned, graphite is the most important structural form of carbon. Carbon fibres are produced mainly from polyacrylonitrile (PAN) and have a high degree of orientation in filament form. The first stage in the production of carbon fibres involves stretching and oxidation. Stretching of 500 – 1300% and heating to 200 – 280 °C results in an intramolecular rearrangement to give a ladder-like polymer. This is followed by oxidation whereby two-thirds of the oxygen sites are filled slowly with the release of H_2O; the product is sometimes called oxiPAN.

Heating oxiPAN in nitrogen or argon at temperatures between 900 and 1200 °C produces low modulus, high strength carbon fibres, which have fine well-oriented crystals parallel to the fibre axis. However, they have a fair degree of porosity and their density is only 1,740 kg/m^3. Heating in argon up to 2800 °C causes graphitization and produces high modulus fibres of increased density up to 2,000 kg/m^3. A three dimensional representation of the arrangement of the basal planes in PAN based carbon fibres is shown in Figure 1.2.

Carbon fibres have the highest combination of stiffness and strength properties. They are used mainly as continuous fibre reinforcement for epoxy resins, although more recently they have been incorporated in thermoplastic resins such as PEEK.

Some chopped fibres are also used in thermoplastics such as polyamide 6,6 for injection moulding.

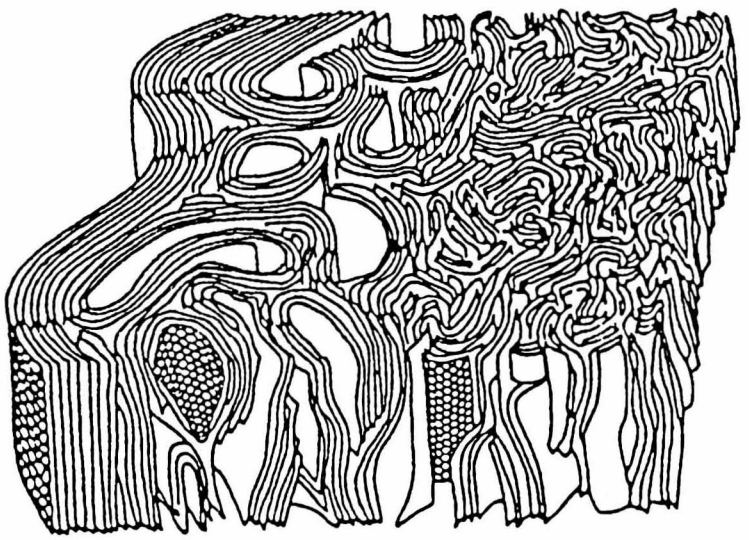

Figure 1.2 *Schematic representation of the three dimensional structure of the orientation of the basal planes of the graphite in a carbon fibre [4].*

Carbon fibre reinforced plastics (CFRP) are used primarily in applications where their high stiffness to weight ratios combined with good creep and fatigue resistance are required, and where costs are not critical. The main market for these fibres is in aerospace applications such as the space and satellite structures, military aircraft wing and fuselage panels, and internal fittings in commercial aircraft such as in seats and floors. The second largest market, which uses about 30% of carbon fibres, is in high performance structures such as power boats and racing cars, and sport goods such as tennis racquets, skis and golf clubs [4,5].

Glass fibres are the principal reinforcement for plastics, supplying about 98% of the fibre reinforcement market. They are used as continuous reinforcement primarily with polyester and epoxy resins, in chopped form as reinforcement for thermoplastic injection moulding materials such as polyamide and polypropylene, and in various types of fabric.

Glass fibres are produced from molten glass by drawing them through bushings having, normally, either 102 or 204 holes, at high speed (3000 – 4000 m/min) thus stretching the filaments and reducing their diameter. The filaments cool very rapidly by radiation and convection before being treated with a size which prevents the filaments from abrading each other as they come together to form a strand. This is wound into a package which is dried and baked.

A number of different glass compositions are used to provide particular properties: *A-glass*, the material used for windows, is now obsolete for fibres but it is cheap and has good acid resistance. The need for special electrical properties led to the development of *E-glass,* which is now the variety produced on the largest scale. *C-glass* was developed for its chemical resistance; *D-glass* has improved electrical properties and *S- or R-glass*, the American and European versions respectively, offer higher strength and modulus than conventional E-glass fibres. Glass fibres are relatively cheap; they have a high strength to weight ratio, and good thermal and electrical insulation characteristics. In addition, they are easily handled and processed into composite components using a wide range of fabrication techniques. As a result, glass fibre reinforced plastics (GRP) are widely used in all of the main industrial sectors, in particular for boat building, chemical plant pipework, food storage vessels, building panels, automotive components and sport goods [1,4,5]. In addition, glass fibres can be recycled from scrap thermoset composites using a fluidised bed combustion method. Here, the modulus of the recovered fibres is affected with the tensile strength suffering a 50% maximum reduction. Nevertheless, fibres can be successfully reused in DMC formulations and veil products [6,7]. A comparison of the properties of the four important reinforcing fibres is shown in Table 1.1.

1.1.3.2 Matrices

The resin is the polymeric material into which the fibre reinforcement is embedded. The matrix material surrounds the fibre reinforcement serving to transfer loads to and between the fibres and to protect them from damage, mechanical or

environmental. There are two principal types of polymeric matrices: thermosetting and thermoplastic.

Material	Young's modulus GPa	Tensile strength GPa	Density gcm^{-3}
Aramid	124	3.6	1.45
Boron	400	3.5	2.58
Carbon UHM	690	3.3	2.17
HM	400	3.5	1.86
IM	295	5.6	1.74
VHS	238	4.3	1.81
HS	235	3.5	1.76
Glass E	71	2.4	2.54
R	86	3.1	2.55

Table 1.1 *Comparison of the properties of aramid, boron, carbon and glass fibres.*

There are a number of ***thermosetting resins*** currently in use with high performance reinforcements, the most widely used being epoxy resins as a result of their outstanding mechanical and physical characteristics. The other common thermosetting resins include polyesters, vinyl, phenolics, polyimides and bismaleimides. *Polyester* resins are the cheapest, have good properties at normal temperatures and are widely used for large structures, such as boats, and volume production. *Vinyl* ester resins are mainly made from epoxy resins and are cured similar to unsaturated polyesters, and have cost and mechanical properties, between those of polyester and epoxy resins. *Phenolic* resins have lower mechanical properties but retain these properties to high temperatures. In addition, they do not produce toxic smoke on burning. *Polyimides* can withstand the highest temperatures of any thermoset and the latest versions can be processed as easily as epoxy resins. *Bismaleimide* resins are a recent development for use in aircraft applications and are designed to withstand the hot-wet conditions in which many epoxy resins lose strength, without incurring the extra cost of polyimides [1].

Thermosetting resins become hard, infusible solids when subjected to a cure reaction with a hardener which in some cases involves heating (hence the name), although some cold cure resin systems are used. Thermosets are resins which readily crosslink during curing. These strong bonds associated with the crosslinks have the effect of pinning the chains together. This restricts the movement of the polymer chains thereby increasing the glass transition temperature of the polymer. Epoxy resins are more expensive and more viscous than polyester resins making impregnation of woven fabrics more difficult. Although curing may require temperatures of up to 180 °C, epoxies have the major advantage that they are usually cured in two or more stages. This allows preforms to be pre-impregnated with an epoxy in a particular cured state. The pre-preg may be stored, often at sub-zero temperatures, for a reasonable length of time before being moulded into the final shape and then cured [4]. Figure 1.3 shows general epoxy structure.

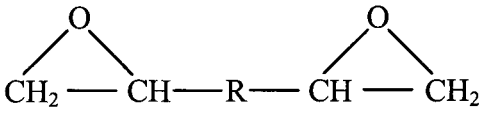

Figure 1.3 *Schematic representation of the epoxy general structure.*

Thermoplastics flow readily under stress at elevated temperature, allowing them to be fabricated into the required component and retain their shape when cooled to room temperature. Depending on the thermoplastic used, which can be of any wide range including polyamides (PA), polypropylene (PP), and many advanced engineering thermoplastics such as polyphenylene sulphide (PPS), polyetherimide (PEI), polyethersulphone (PES) and polyetheretherketone (PEEK) the mechanical, thermal and chemical properties can be selected for the application. The mechanical properties, strength and modulus will largely be controlled by the fibre used, the arrangement of it and the volume fraction incorporated. Chemical and thermal properties are controlled by the matrix selected for the particular application.

Thermoplastics are linear polymers, they do not crosslink to form a rigid network although the chains may be branched. Bonding between the chains in a thermoplastic is due to weak van der Waals forces, which are easily broken by the combined action of thermal activation and applied stress. This explains why thermoplastics flow at elevated temperature. Provided the chains of a thermoplastic are relatively simple without bulky side-groups, they are likely to fold back on themselves to form crystalline regions. Most thermoplastics are crystalline but the extent of crystallisation depends on details of the molecular structure. Polypropylene is a semi-crystalline polymer belonging to the polyolefin group. It is cheap and widely used [1,4,5]. Figure 1.4 shows the polypropylene repeating structure [8].

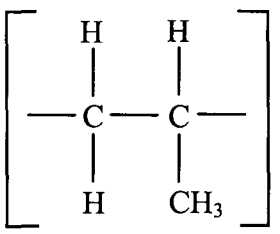

Figure 1.4 *Repeating structure of polypropylene.*

Reinforced thermoplastics are produced in two forms: continuous-fibre reinforced and short-fibre reinforced. For general engineering applications, polypropylene (PP) or polyamide (PA) plastics are generally used. Some advantages and disadvantages of thermosetting and thermoplastic resins are shown in Table 1.2 [5].

1.1.4 Applications

1.1.4.1 Road transportation

The versatility of composites as engineering materials suggests numerous parts and assemblies for highway vehicles that might use reinforced plastics to advantage. The strength to weight ratio of any material used in a moving vehicle its always

important because of its direct relation to energy requirements, performance and payload [9]. Clearly, fuel consumption is related to vehicle mass. A car with lighter body can use a lighter engine, suspension and a less elaborate structure. The use of composites as a weight reduction strategy is well established, but is clear that applications will only succeed when multiple constraints are satisfied [10]. In order to be competitive with alternate materials for high volume applications, composites must lend themselves to good reproducibility, reliable processing with semi-skilled workers, and consistent, predictable properties.

Thermosets	**Thermoplastics**
FOR • Cold cure resins simplify processing • Low pressure moulding • Good temperature and fire resistance • Contact moulding suitable for large manufacturing. AGAINST • User must control chemical reactions and cure process • Liquid resins have limited shelf life • Health hazards from resin handling • Recycling not easy • Resins can be brittle, leading to composites with low toughness	FOR • Can by processed quickly by hot pressing or injection moulding • Minimal knowledge of resin chemistry needed • Ductility gives tougher composite materials • Waste can be recycled • Good environmental resistance AGAINST • High temperature and pressure moulding • Resins soften and might burn at high temperatures • Temperature and chemical resistance varies widely • Tooling needs high-volume production to be cost effective

Table 1.2 *Advantages and disadvantages of thermoplastic and thermosetting polymer materials.*

All of the common thermoplastics have been used with reinforcing fibres in parts produced by various methods. The nature of the part, the volume of parts

required, appearance requirements and environment, as well as economics and mechanical strength have a strong bearing on the selection of the materials. Thermosetting resins are generally preferred for body parts that must accept conventional paint finishes. Thermoplastics generally are more adaptable to pigmenting and versatility in part designs where appearance in the moulded condition is important [9]. The present market is dominated by reinforced thermoplastics and glass mat thermoplastics (GMT) [10]. Some successful applications of composites in road transportation are passenger cars, highway tractors, truck bodies and trailers, recreation vehicles and racing cars.

1.1.4.2 Civil aircraft

The application of composite materials to civil aircraft structures and power plants represents one of the most significant improvements available to aeronautical engineers in recent times. Aircraft are distinguished from other vehicles by the fact that their power to weight ratios are high. The weight problem has continuously driven aircraft technology in search of improved materials, new structural concepts, comprehension of structural behaviour and the analysis of such behaviour. The selection of materials and the design of a structure for any given component or part must be made not only on the basis of the mechanical and structural functions, but must also consider the operational and cost parameters for civil aircraft [9]. Figure 1.5 shows the use of composite materials in the Airbus A320 aircraft [1].

Fortunately for the aeronautical industry and largely as a result of finding support from it, composite materials for several years, have been considered as engineering materials, they are based on low density-high strength constituents. Composite materials are presently finding use in many aircraft structures; some of them are listed below [1,3,9].

- Airbus A380 Family
- Boeing B737, 747, 757,767, 777
- Lockheed L1011
- McDonnell-Douglas MD 11, MD80, MD90, etc.

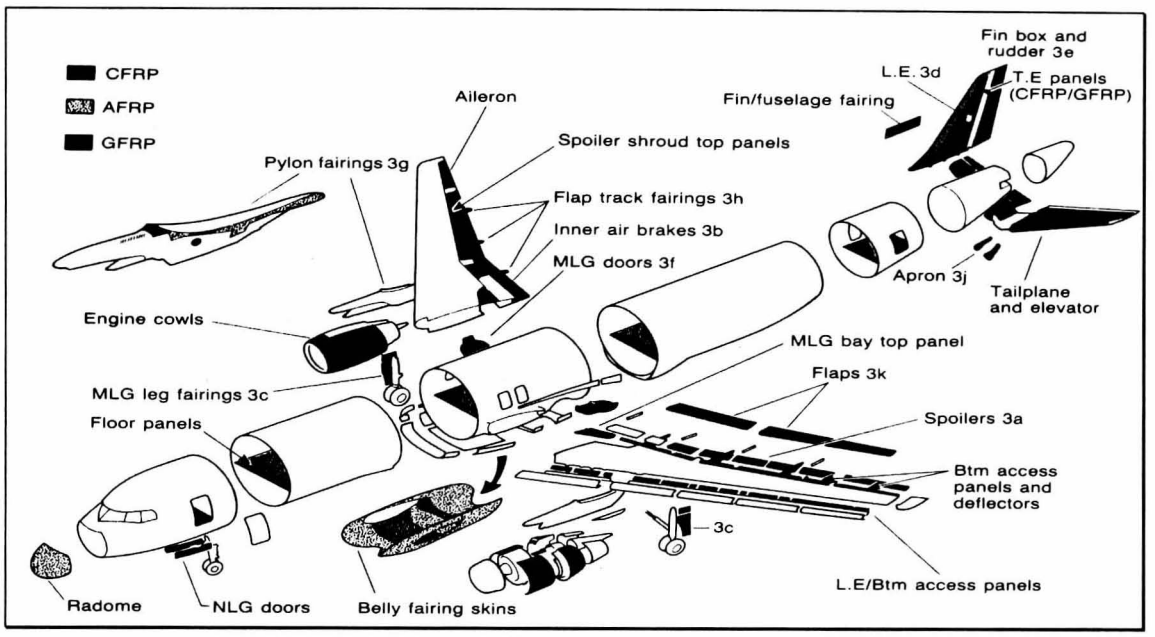

Figure 1.5 *Composite structures in the A320 aircraft [1].*

1.1.4.3 Space vehicles

The space programme demands the highest degree of structural efficiency and reliability. Since high-performance reinforced composites emerged in the 1960's, their development for spacecraft applications has been emphasised. As a rule, the service life demands for aircraft structures vary widely from those of space vehicles. In the past, a space vehicle was a one-shot structure. The major structural loads occur in the first few minutes during boost, and the major thermal loads occur either during the boost or re-entry phases. With the advent of the Space Shuttle vehicle, designers must now take into consideration fatigue and creep loads in order to extend vehicle's life.

The most efficient composite structures are those in which the load paths are uniaxial. This allows maximum advantage to be taken from the reinforcement properties. These properties depend on the type of reinforcements used, their volume fraction, their orientation and the type of matrix chosen. Composite materials have proved to be cost-effective and they play a key role in the advance and development

of space structures. Some space applications of composite material include boosters, satellites, space shuttle, space stations, etc. [3,9]

1.1.4.4 Military aircraft

Military aircraft, around 1940 were probably the first to use fibreglass composites in significant quantities. The success achieved from the introduction of advanced composites in the manufacture of aircraft structures led to the development, test and evaluation of low cost-high performance composites. Over the years, military aircraft have required increased capabilities, along with more stringent aircraft specifications. The rapid rise in the use of composites is driven by the need to reduce rapidly rising production costs. Composites are effective by reducing the weight of the aircraft, by providing higher heat resistance, better stiffness and superior fatigue resistance. The most common fibres are carbon, aramid and glass fibres, used alone or in hybrid combinations. The resin matrix is usually an epoxy-based system requiring curing temperatures between 120 and 175 °C.

The largest application by far of composite materials is in military programmes, which constitute more that 40% of the total U.S. aerospace usage. About twenty six percent of the structural weight of the U.S. Navy's AV-8B is carbon fibre reinforced composites. Components include the wing box, forward fuselage, horizontal stabiliser, elevators, rudder and other control surfaces. Trends clearly indicate that the use of composite structures will continue to grow in military aircraft [1-3,9]. A good example of this growth can be seen in the B-2 Flying wing aircraft (Figure 1.6). The B-2 is the biggest all-composite airframe structure ever built. Some other military applications include the F-14, F-15, F-16, F-18, F-22, A-6, V-22 V/STOL, Jaguar, Alpha Jet, Tornado, F-111, ATF, etc.[3].

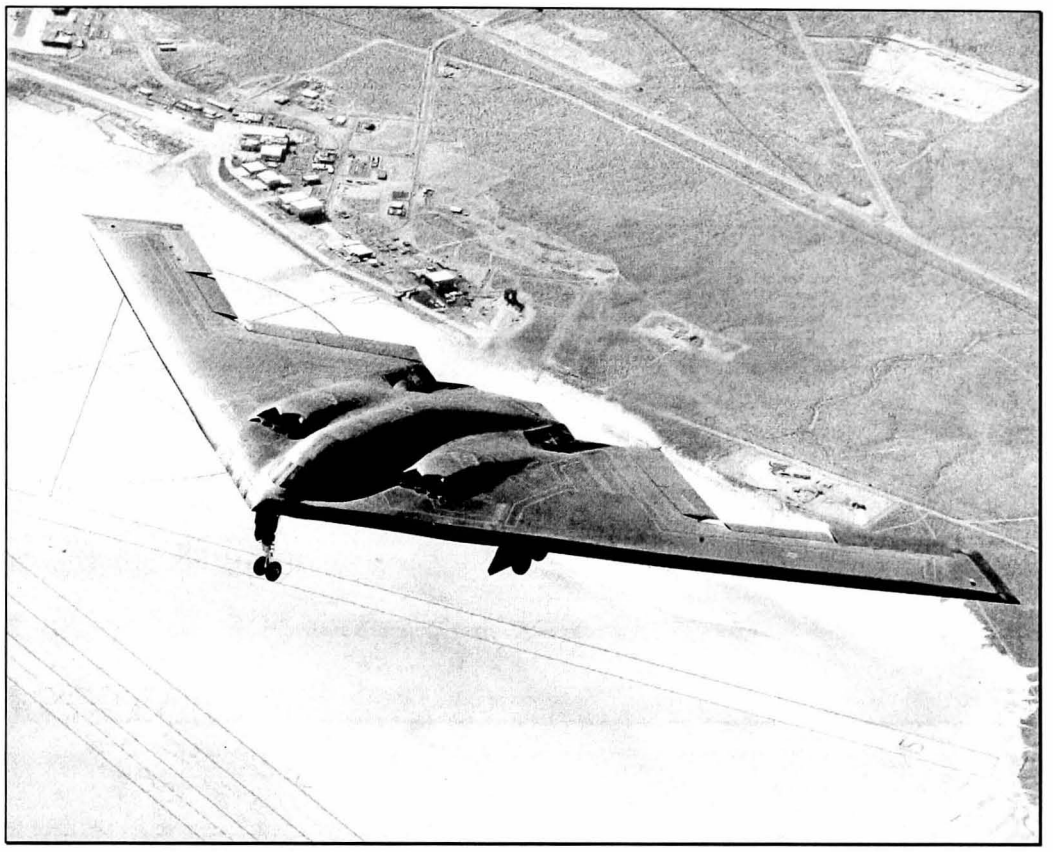

Figure 1.6 *All-composite B-2 Flying Wing Aircraft.*

1.1.4.5 Other applications

The outstanding properties of composite materials have led to their use in a wide range of structures. The marine industry is also a major employer of composite materials. The marine environment presents a challenge for engineering materials. Materials that cannot withstand this severe environment are subjected to corrosion, rot, decay and loss of strength when used in marine applications. Composite materials have proven their ability to withstand this environment, and in many cases, have essentially replaced less suitable materials. A good example is the rapid and nearly total replacement of wood with glass reinforced plastics in small pleassure boats [9]. The use of composite materials in high-speed boats also reflects the high performance of these materials in marine environments. Other applications for composite materials can be found in freight containers, the ocean engineering industry, the building industry, chemical plants, appliances, sport equipment, etc.

1.1.5 Hybrid composites

A hybrid is a composite laminate consisting of laminae of two or more composite material systems, a combination of two or more different fibres, such as carbon and glass or carbon and aramid, into a structure. Tapes, fabrics and other forms can be combined, usually only the fibres differ [2]. Hybrids offer many of the advantages exhibited by composite materials, such as excellent specific stiffness and strength, ease of fabrication and elevated corrosion resistance combined with a capability for reduced cost and optimised performance. It is possible, for example, to enhance the modulus, strength and fatigue performance of glass reinforced plastics (GRP) through the inclusion of carbon fibres, or the impact energy of carbon fibre reinforced plastics (CFRP) through the inclusion of some glass or aramid fibres. Structures subjected to tensile loads on one side and compressive loads on the other (e.g. tennis rackets, skis, yacht hulls, etc.) represent excellent applications for hybrid composite materials [11].

1.1.6 Disadvantages of composites

Despite the outstanding characteristics offered by composite materials, and although current applications of high performance composites in many products and complex engineering systems are impressive, a number of disadvantages have been identified [2,3]. These disadvantages include:

- Material cost.
- Combustion and toxic smoke generation characteristics.
- Expertise is required for the successful application of composites.
- Manufacturing processes for composites are complex, they must take place in special environments, and can be costly to control.
- Unique assembly processes are required, for example, high-temperature ovens and autoclaves, and integrally-heated tools.
- Special precautions are often necessary to prevent occurrences that would cause part rejection, such as composite dust being introduced during priming for adhesive application.

- Manufacturing defects in composites have a strong influence on the properties of the structure. Those defects include delamination, voids, porosity, inclusions, resin variations, fibre variations, etc.

1.2 ALUMINIUM ALLOYS

Aluminium alloys, which are usually called light alloys, have been developed in order to increase the strength of the base metal, aluminium, which is very ductile and corrosion resistant. During the First World War, aluminium alloys were first employed on a large scale. Since then, aluminium alloys have been widely and successfully used in the aeronautical industry.

1.2.1 Classification

Aluminium alloys are usually classified either with respect to the fabrication process (casting and wrought alloys) and to the heat treatment (heat-treated and non-heat treated alloys), or with respect to their chemical composition. This classification allows aluminium alloys to be grouped into different families exhibiting similar mechanical and technological characteristics. Aluminium alloys are currently classified using a numerical designation. This designation is derived from the American nomenclature (Aluminum Association). This type of nomenclature, which is used for wrought aluminium alloys, is represented by a four digit number. An initial digit of 1 denotes that the aluminium content is greater than 99 percent. Initial digits from 2 to 8 denote other alloys: the figure identifying the main alloying element. This is shown below.

1xxx	pure aluminium (greater than 99 percent)
2xxx	copper
3xxx	manganese
4xxx	silicon
5xxx	magnesium
6xxx	magnesium and silicon

7xxx	zinc
8xxx	other elements
9xxx	unused series

In the first group (called pure aluminium), the third and fourth figures represent the percentage of aluminium above 99 percent. The second figure represents the level of impurities. This figure is equal to zero if the impurities are uncontrolled, and can vary between 1 and 9 depending upon the impurity content. In the other groups, the second figure is equal to zero for the main alloy and varies between 1 and 9 for its modifications. The third and fourth figures identify the specific alloy within each group.

The metallurgical state of an alloy is usually identified by a symbol, which follows the chemical composition symbol. This symbol can be formed by letters and numbers. The following symbols are use by the Aluminium Association [12]:

F *rough state of fabrication*

O *annealed state*

H *work-hardened state*

W *tempered non-stabilised stage*

T *heat-treated stage*

1.2.2 Applications

1.2.2.1 Road transportation

Aluminium alloys have for many years been used in the road transportation for pistons, cylinder heads and sumps on account of their lightness and high thermal conductivity. They are presently being used increasingly for cylinder blocks. The use of aluminium alloy sheet for bodywork is increasing but price is an obstacle to its universal acceptance. The use of such materials instead of steel gives a weight saving together with a very much improved corrosion resistance. The lightweight of aluminium wheels can contribute significantly to the road-holding capabilities of

sport cars. In commercial vehicles, where weight savings can be directly related to financial return, aluminium alloy sheet and extrusions are extensively used in their bodywork. In addition, these isotropic materials are also used in many special purpose vehicles such as road tankers [13,14].

1.2.2.2 Marine industry

The use of aluminium alloys in the marine industry has a good record. These materials offer good durability and resistance to corrosion under a range of marine conditions. The hulls and superstructures of fast patrol launches are frequently made from aluminium. The reduction in weight without any loss in structural stability has resulted in its use in warship construction, where radar dishes and aerials have to be carried high above the decks [13]. Aluminium alloys have been developed and presently about fifty per cent of outboard motors are made of aluminium. Passenger liners also use aluminium; large structures may contain as much as 2,000 tonnes of aluminium, resulting in a considerable weight reduction over their steel counterparts. Fast ferries, with speeds of up to 35-50 knots, are revolutionising transport over short sea routes. These structures are weight-critical, and aluminium is the preferred material. A modern ferry can use up to 400 tonnes of aluminium [14].

1.2.2.3 Aerospace industry

Since the mid 1930's aluminium alloys have been the accepted materials for airframe construction. Introduced in 1933, the Boeing's 247 was considered the first truly modern airliner. It was an all-metal, low-wing monoplane, with retractable landing gear, an insulated cabin, and room for 10 passengers [15]. The main structural members, wing spars, fuselage and landing gear are good examples of the use of aluminium alloys in an aircraft. Aluminium alloys made possible the manufacture of the supersonic Concorde back in the 1960's [13]. In those days aluminium alloys represented the most widely used materials in the manufacture of commercial aircraft. Figure 1.7 shows a modern Boeing 747-400 aircraft, where the aluminium alloys still represent the principal structural material [14,15].

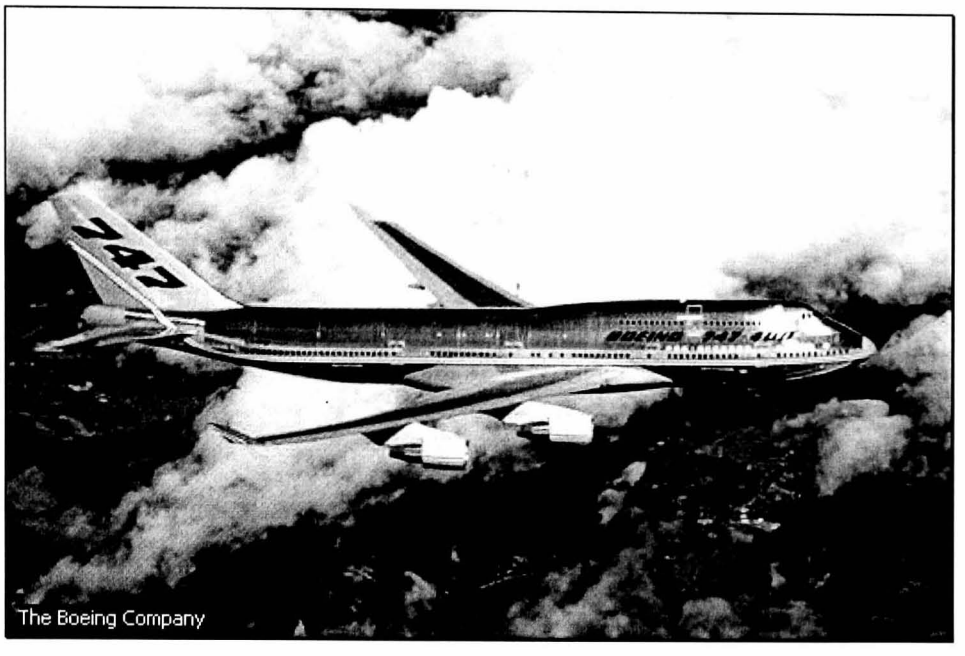

Figure 1.7 *Boeing 747-400.*

1.2.2.4 Other applications

Aluminium alloys are finding increasing use in modern day architecture, for both structural and ornamental purposes. Aluminium storm windows and foil make excellent insulators. The metal is also used as a material in low-temperature nuclear reactors because it absorbs relatively few neutrons. Aluminium becomes stronger and retains its toughness as it gets colder and is therefore used at cryogenic temperatures. Because of its lightweight, ease of forming, and compatibility with foods and beverages, aluminium is widely used for containers, flexible packages, and easy-to-open bottles and cans. A wide variety of coating alloys and wrought alloys can be prepared that give the metal greater strength, castability, or resistance to corrosion or high temperatures. Some new alloys can be used as armour plate for tanks, personnel carriers, and other military vehicles [13,15].

1.2.3 Disadvantages of aluminium alloys

Aluminium alloys remain as one of the most widely used materials for transport applications where manufactures are always in search of an improved

performance. However, there are still a number of disadvantages associated with these materials. Disadvantages associated with metals include [3]:

- Relatively high weight
- Relative sensitivity to corrosion
- Low resistance to fatigue loading
- Strength and stiffness can not be tailored to meet loads
- Propagation of damage through thickness cracks
- High coefficient of thermal expansion
- High number of assemblies and fasteners required, etc.

1.2.4 Surface treatments for aluminium alloys

Most metal surfaces, in particular aluminium alloys, react with their natural environment to form a complex interface. The longer a metal surface is exposed to its environment, the more likely it is that it will be contaminated. A surface treatment is a transformation process, changing the aluminium surface with unknown and perhaps undesirable properties to a surface with known desirable properties [16].

1.2.4.1 Solvent cleaning

Aluminium alloy surfaces are frequently contaminated with oils, greases, etc. and a common pre-treatment is degreasing either with steam, or by wiping the surface with solvent-dipped clean cloths. Following the removal of the greases and oils, the residual contaminants are usually removed with an alkaline cleaner which emulsifies the surface contaminants and keeps them in suspension. The alkaline cleaning process is often followed by a mechanical or chemical treatment since the alkaline cleaning leaves the surface unreceptive to many adhesives.

1.2.4.2 Mechanical abrasion

The methods available include wire brushes, sand and emery papers, abrasive pads and grit or shot blasting. The main purpose of this treatment is to generate a random roughened surface that could be effective in preventing small cracks, flaws,

voids or other points of stress concentration from aligning and rapidly propagating along any line of interfacial weakness in a joint [17].

1.2.4.3 Chemical treatments

Chemical treatments are required to remove soils or oxides, to smooth surfaces and to develop several types of protective or decorative coatings. Through choice of chemical treatment the surface of aluminium alloys can be left intact or altered substantially in appearance and adhesiveness. Chemical treatments usually involve two or more constituents. Alkaline or acid compounds are employed as cleaning agents to dissolve the oxide films or to etch the metal. Inhibitors are introduced to control these reaction rates; addition agents are employed to control the solubility and physical form of precipitating products. Chemical conversion coatings are considered among the chemical treatments. Conversion coating describes a surface film formed by a reaction in which a portion of the base metal is converted to one of the components of the film. As a result of this reaction and conversion, the film becomes an integral part of the metal surface, exhibiting excellent adhesion properties. Amorphous chromate coatings are currently the most widely employed conversion coatings for aluminium. They are applied as acid solutions, and provide ease and economy of operation, good adhesion properties for organic coatings and improved resistance to corrosion [18].

1.2.4.4 Anodising treatments

Anodising is an electrolytic oxidation process in which the surface of a metal, when anodic is converted to a coating having desirable protective and other properties. When aluminium is made the anode in a suitable electrolyte, with a metal or carbon cathode, and an electric current is passed through the cell, the aluminium surface is converted to an aluminium oxide coating. The oxide coating is integral with the aluminium, and has excellent adherence.

One of the most widely used anodising processes for producing thick porous-type anodic coatings on aluminium is that employing sulphuric acid as the

electrolyte, this process is called sulphuric acid anodisation. In addition to its advantage of yielding coatings having a wide range of desirable properties, sulphuric acid is inexpensive [18].

1.3 SUMMARY

The characteristics of many polymer matrix composite materials have been outlined. The development of these composite materials has resulted in their application in almost all types of transportation and leisure products. The specific properties of composite materials made them the ideal candidates for use in aircraft structures. In addition, they have been used extensively by the military industry. Until recently, composite materials have been used predominately in secondary structures in commercial aircraft, such as cargo doors, floors, etc. A number of disadvantages associated with composite materials have limited their use in primary aircraft structures. An example of this is the relatively poor performance of composite materials under low velocity impact, such as that associated with dropped tools, etc. The impact event results in a delamination within the composite, which is difficult to detect by a simple optical inspection and requires expensive and time-consuming inspection techniques. On the other hand, aluminium alloys have been widely adopted in the design of a wide range of commercial aircraft. These materials have been used in the manufacture of primary and secondary load-bearing aircraft structures. However, in order to increase aircraft efficiency and therefore capacity, a weight reduction coupled with an improvement in the performance of the candidate materials must be achieved. This drive for higher performance systems has resulted in the development of a new range of hybrid materials termed fibre-metal laminates (FML). Fibre-metal laminates combine the high specific properties of lightweight composite materials with the isotropic properties, ease of fabrication and durability of aluminium alloys.

In this research project, novel fibre-metal laminates will be manufactured and tested. Initial attention will focus on optimising the adhesion between aluminium

and composite materials. A number of surface treatments will be applied to the aluminium substrates in order to optimise the interfacial fracture energy. These model systems will be tested over a range of crosshead displacement rates, and the resulting failure modes will be elucidated and characterised. Several stacking sequences will be manufactured and tested. The influence of varying the volume fraction of the composite within the fibre-metal laminates on the tensile and flexural properties will be assessed. The static and dynamic mechanical properties of the fibre-metal laminates will be evaluated and their failure modes characterised and discussed. The post-impact residual strength of these novel fibre-metal laminates will be evaluated. Finally, the high velocity impact response of thermosetting and thermoplastic-based fibre-metal laminates will be investigated.

If this project is successful, it will lead to the development of an entirely new range of fibre-metal laminates based on thermoplastic matrices. Thermoplastic fibre-metal laminates are expected to offer a number of distinctive advantages over conventional thermosetting-based fibre-metal laminates including short processing times, high damage tolerance and ease of repair.

Before undertaking this study, a thorough evaluation of the relevant literature must be undertaken. Previous work in this area is reviewed in the next chapter, enabling the precise aims and objectives of the current research project to be identified.

1.4 REFERENCES

[1] **Middleton, D.H.**, Composite Materials in Aircraft Structures, Longman Group UK Limited, 1990.

[2] **ASTM International**, Engineered Materials Handbook, **1**, Composites, 1987.

[3] **Niu, M.C.Y.**, Composite Airframe Structures, Hong Kong Conmilit Press Ltd., 1996.

[4] **Matthews, F.L., Rawlings, R.D.**, Composite Materials: Engineering and Science, Chapman and Hall, 1996.

[5] **Mayer, R.M.**, Design with Reinforced Plastics, The Design Council, 1993.

[6] **Kennerley, J.R., Fenwick, N.J., Pickering, S.J., Rudd, C.D.**, ANTEC, (1996), pp 890-894.

[7] **Pickering, S.J., Kelly, R.M., Kennerley, J.R., Rudd, C.D., Fenwick, N.J.**, Composites Science and Technology, **60** (2000), pp 509-523.

[8] **Callister, Jr.W.D.**, Materials Science and Engineering, an Introduction, John Wiley and sons, Inc., 1997.

[9] **Broutman, L.J., Krock, R.H., Noton, B.R.**, Composite Materials, **3**, Academic Press, 1974.

[10] **Rudd, C.D.**, Materials Technology and Advanced Performance Materials, **15** (2000), pp 255-265.

[11] **Hancox, L.N.**, Fibre Composites Hybrid Materials, Applied Science Publishers Ltd., 1981.

[12] **Mazzolani, F.M.**, Alluminum Alloy Structures, Pitman Publishing Inc., 1985.

[13] **Varley, P.C.**, The Technology of Aluminium and its Alloys, Butterworth & Co. Ltd., 1970.

[14] International Primary Aluminium Institute, World Aluminium, www.world-aluminium.org, 2000.

[15] Aluminum, *Microsoft® Encarta® Encyclopedia*, 1999.

[16] **Thrall, E.W., Shannon, R.W.**, Adhesive Bonding of Aluminum Alloys, Marcel Dekker, Inc., 1985.

[17] **Kinloch, A.J.**, Adhesion and Adhesives, Chapman and Hall Ltd., 1987.

[18] **Van Horn, K.R.**, Aluminium, III, American Society for Metals, 1967.

2. LITERATURE REVIEW

2.1 INTRODUCTION

Before undertaking a full investigation of the fracture properties of the fibre-metal laminates investigated during the course of this research study, it is necessary to consider any previous work of relevance. This review will cover a number of key areas. Initially, the development and basic configurations of the various types of fibre metal laminate will be considered. Following this, the static mechanical properties of fibre-metal laminates will be discussed. Finally, in order to obtain a better understanding of the dynamic properties of these multi-layered systems, the low and high velocity impact performance of fibre-metal laminates will be discussed.

One of the main characteristics of fibre-metal laminates is their high resistance to fatigue loading conditions. The crack propagation mechanisms under such conditions will be reviewed in this section. In addition, the stability and durability of these novel materials will be examined and the associated properties highlighted.

Fibre-metal laminates have been used in a number of applications and this will be discussed. This procedure will enable a visualisation of future applications and for the development of a new type of fibre-metal laminates. A thorough examination of the previously-published work will assist in the establishment of the appropriate test procedures for the characterisation of the fracture properties of novel fibre-metal laminates. In addition, a review of the literature will enable the aims and objectives of the present research project to be clearly established.

2.2 DEVELOPMENT OF FIBRE-METAL LAMINATES (FML's)

The origin of fibre-metal laminates has it roots in the development of layered structures by Fokker Aircraft in the 1970's. Their research established that thin

sheets of aluminium adhesively-bonded together resulted a significant increase in fracture toughness and damage tolerance over a monolithic material of the same thickness as the laminate [1]. Schijve *et al.* [2] studied the fatigue properties of adhesively bonded laminated sheet material of aluminium alloys. They fatigue-tested centrally-cracked specimens of solid aluminium sheet and laminated sheet and showed that through cracks in laminated specimens with a central crack grow at a lower rate than in the solid material. For part through cracks (i.e. cracks with a depth that is less than the specimen thickness, crack growth was much lower in the laminated material than in its solid counterpart. After testing a full-scale wing panel, they concluded that he use of adhesively-bonded laminates significantly improved the damage tolerance of an aircraft structure.

It was a small step for Fokker to introduce high performance fibres to reinforce the adhesive in the bondline. This procedure resulted in a significant increase in the fatigue strength and life of the laminate. Subsequently, Fokker collaborated in a research project with the Delft University of Technology, ALCOA (suppliers of aluminium), ENKA (producer of aramid fibres), 3M (producer of adhesives), AKZO (manufactures of fibres and aerospace chemicals) and the Dutch National Aerospace Laboratory. From this co-operative project, ARALL (Aramid Aluminium Laminates) were first manufactured by ALCOA in 1983. Subsequently, a second generation of laminates, based on R and S2 glass fibres was developed and marketed by AKZO under the trade name of GLARE [1].

2.3 EXISTING FML's AND CONFIGURATIONS

ARALL and GLARE consist of thin sheets of aluminium alloy bonded together by a fibre reinforced epoxy adhesive in the form of prepreg material. A schematic representation of a fibre-metal laminate is shown in Figure 2.1. The laminate properties depend on various factors such as the fibre-resin system, the

aluminium alloy material, stacking sequences, fibre orientations, surface preparation techniques and the degree of post-cure stretching or forming.

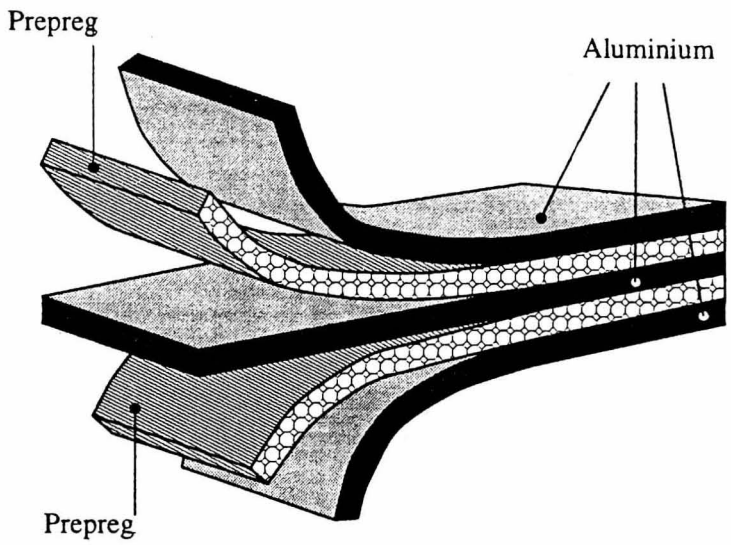

Figure 2.1 *Schematic illustration of a fibre-metal laminate.*

Of the several different combinations possible, four types of ARALL and four types of GLARE have been standardised for commercial production. These combinations are listed in Table 2.1 [1]. ARALL is over fifteen percent lighter than aluminium, whereas GLARE is only ten percent less dense than monolithic aluminium. Both ARALL and GLARE are available in several through-the-thickness configurations, such as 2/1, 3/2, 4/3 and 5/4 [1]. This nomenclature indicates the ratio of the number of aluminium layers to the number of prepreg layers. For example a 3/2 configuration is based on 3 layers of aluminium (top, middle and bottom) and two intermediate layers of the prepreg, as shown before in Figure 2.1. Clearly, the aluminium to prepreg ratios affects not just the thickness but also the properties of the resulting laminate.

Prior to lay-up and cure, the aluminium sheets are degreased, pickled in chromic-sulphuric acid, and the surfaces are anodised with phosphoric or chromic acid and primed to provide a good bond integrity and to inhibit bond-line corrosion in the event of moisture ingression [3].

ARALL laminates	**GLARE Laminates**
Unidirectional adhesive epoxy prepreg with high modulus Aramid fibres (V_f= 0.5)	Unidirectional or cross-ply adhesive epoxy prepreg with R-Glass fibres (V_f= 0.6)
ARALL-1 Aluminium alloy 7075-T61 120 °C cure prepreg 0.4 % permanent stretch	**GLARE-1** Aluminium alloy 7475-T76 Unidirectional R-glass 120 °C cure prepreg 0.5 % permanent stretch
ARALL-2 Aluminium alloy 2024-T3 120 °C cure prepreg with or without 0.4 % stretch	**GLARE-2** Aluminium alloy 2024-T3 Unidirectional R-glass 120 °C cure prepreg no permanent stretch
ARALL-3 Aluminium alloy 7475-T761 120 °C cure prepreg 0.4 % permanent stretch	**GLARE-3** Aluminium alloy 2024-T3 Cross-ply (50 % L, 50 % LT) 120 °C cure prepreg no permanent stretch
ARALL-4 Aluminium alloy 2024-T8 175 °C cure prepreg with or without 0.4 % stretch	**GLARE-4** Aluminium alloy 2024-T3 Cross-ply (67 % L, 33 % LT) 120 °C cure prepreg no permanent stretch

V_f = Volume fraction of reinforcing fibres in the prepreg.

L, LT = Long (grain) and long transverse directions, respectively of aluminium.

Table 2.1 *Commercial combinations of ARALL and GLARE laminates [1].*

2.4 STATIC MECHANICAL PROPERTIES

2.4.1 Ultimate strength

A summary of typical room temperature properties of the 3/2 configurations of the ARALL and GLARE laminates is given in Table 2.2. It is clear that the ultimate strengths of the ARALL laminates are approximately seventy percent grater than those of the constituent aluminium alloys in the longitudinal direction; but they are approximately thirty percent lower in the transverse direction. This is obviously due to the unidirectional nature of the lay-ups.

Laminate	Tensile ultimate strength **MPa**	Ultimate tensile strain %	Tensile Modulus **GPa**	Yield Strength **MPa**
ARALL-1	800 (L) 386 (LT)	1.9 7.9	68 48	545 333
ARALL-2	717 (L) 317 (LT)	2.5 12.7	64 49	360 228
ARALL-3	828 (L) 373 (LT)	2.2 ----	68 51	305 283
ARALL-4	731 (L) 338 (LT)	2.6 4.6	61 49	352 255
GLARE-1	1282 (L) 352 (LT)	4.2 7.7	65 50	641 331
GLARE-2	1214 (L) 317 (LT)	4.7 10.8	66 50	359 228
GLARE-3	717 (L) 716 (LT)	4.7 4.7	58 58	587 317
GLARE-4	1027 (L) 607 (LT)	4.7 4.7	57 50	373 317
Al 2024-T3	455 (L, LT)	19	72	359

L, LT = Directions parallel and perpendicular to the fibre reinforcement, respectively.

Table 2.2 *Typical room temperature static properties of ARALL and GLARE Laminates [1].*

The GLARE-1 and GLARE-2 laminates are approximately fifty percent stronger than the ARALL laminates in the longitudinal direction, but the transverse ultimate strengths are again thirty percent lower than that of monolithic aluminium. However, the ultimate strengths of the cross-ply GLARE laminates are far superior to the aluminium alloys in either direction.

2.4.2 Tensile properties

As previously mentioned, fibre-metal laminates offer higher tensile properties than monolithic aluminium alloys. However, in order to fully evaluate the tensile properties of these hybrid materials, a number of parameters have to be taken into account. Wu and Wu [4] studied specimen size and alignment effects in ARALL laminates under tensile loading conditions. They investigated the effect of using straight-sided and dog-bone shape specimens on the tensile properties of fibre-metal laminates. Their results showed that the ultimate tensile strength, the tensile yield strength and the tensile modulus are independent of the geometry of the specimen. They recommended the use of straight-sided fibre-metal laminates specimens for tension testing. However, they noted that if a good alignment of the testing machine could be achieved, dog-bone shape specimens could also be used. The effect of size (width) on the tensile strength of fibre-metal laminates was insignificant over the range of specimen widths investigated.

The post-cured versions of the ARALL laminates, namely, ARALL-1, ARALL-3 exhibit higher yield strengths than those in the as-cured condition. This was attributed, in part to the strain hardening of the aluminium during stretching, and in part to the residual compressive stress in the aluminium layers following post stretching. Typical tensile and compressive stress-strain curves for a 3/2 ARALL-1 laminate and its constituents are shown in Figure 2.2 [3]. This figure clearly shows that the tensile properties of the fibre-metal laminates are influenced by the properties and orientation of its constituent materials.

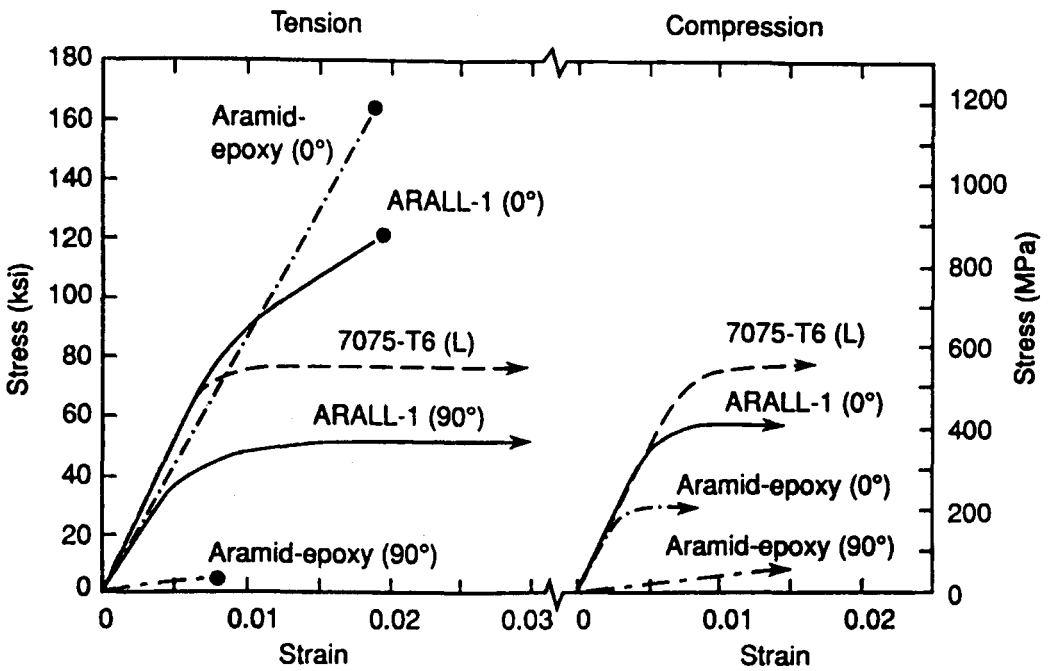

Figure 2.2 *Tensile and compressive stress-strain behaviour of an ARALL-1 laminate at room temperature [3].*

In order to evaluate the relationship between mechanical properties and the volume fraction of the constituent materials, Wu and Wu [4] conducted an analytical and experimental investigation on GLARE-4. Tensile specimens were tested to determine the influence of volume fraction of aluminium on the tensile properties of this hybrid system, and these results are plotted in Figure 2.3.

The results show that the tensile strength and tensile modulus of the laminates are linear functions of the volume fraction of aluminium alloy. The tensile modulus can be predicted using a rule of mixtures, which is the addition of the tensile moduli of the constituents whilst accounting for the thickness of the separate layers. They concluded that a simple rule of mixtures could be applied to predict some key mechanical properties of fibre-metal laminates.

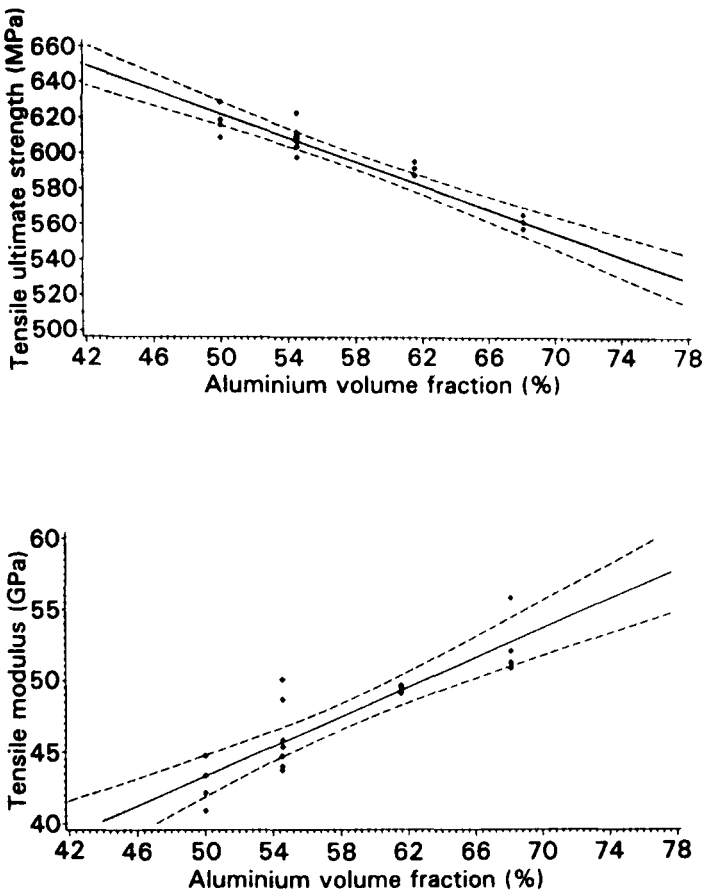

Figure 2.3 *Tensile strength and modulus of GLARE-4 variation with aluminium volume fraction [5].*

2.4.3 Fracture toughness and residual strength

The residual strength of fibre-metal laminates depends on the integrity of the fibres in the wake of the defect or crack. If the fibres are intact, hybrid laminates offer an improved performance over their monolithic counterparts. However, if the fibres are broken, the performance of fibre-metal laminates is usually inferior or comparable to that of their aluminium counterparts [1]. A number of studies have been carried out in order to evaluate the fracture toughness and residual strength of fibre-metal laminates under static loading conditions [6-9]. Macheret and Bucci [6] conducted a number of tensile tests on unstiffened centrally-slotted ARALL

laminates panels. During the test, the load and crack opening displacement were recorded and the effective crack length, needed for crack growth resistance calculations, was determined from a compliance calibration curve. Figure 2.4 shows crack growth resistance for a series of ARALL laminates. Their results showed that fibre-metal laminates, like metals, exhibit slow stable tearing prior to rapid fracture. The crack resistance behaviour of ARALL laminates was directly related to the toughness of the metal constituents and the resistance curve of each laminate was virtually independent of the initial slot length. Vermeeren [7] studied the residual strength of GLARE-2 and GLARE-3 laminates using centre-cracked tensile specimens. Figure 2.5 shows a schematic of a typical failure mode in a fibre-metal laminate. His model assumed that both the fibre layer and the aluminium layer are cut over a certain length due to the notching process. At the tip of the saw cut, there are sectioned fibres neighbouring undamaged fibres. Under tensile loading conditions, the load that should be carried by the sectioned fibres at the tip of the saw cut is transmitted to the neighbouring intact fibres and to the aluminium layers.

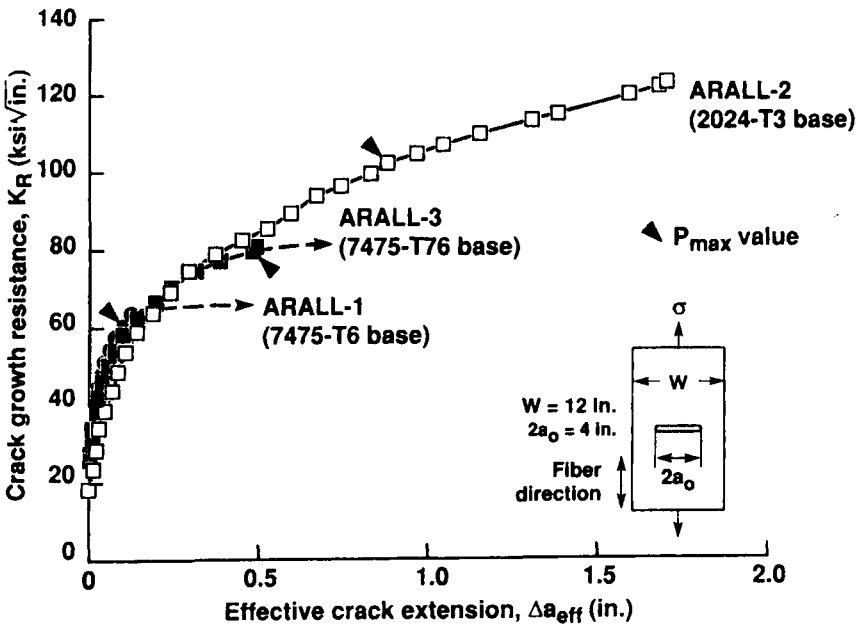

Figure 2.4 *Effect of aluminium alloy on crack growth resistance curves for 3/2 ARALL laminates [6].*

When the shear load becomes too high for the material to withstand, the transfer of load can lead to splitting in the composite plies and delamination at the bi-material interface.

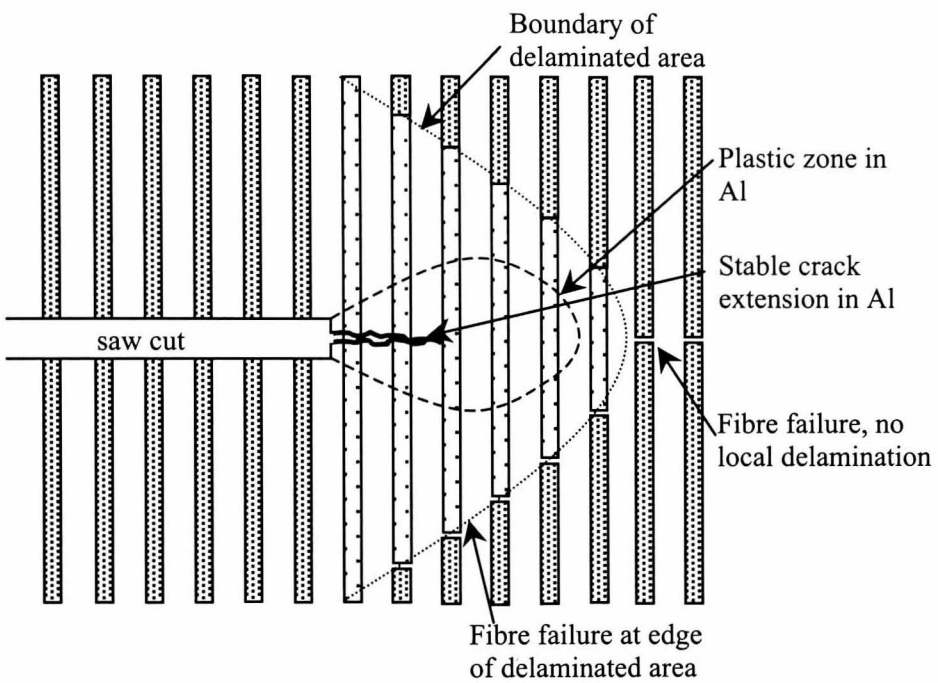

Figure 2.5 *Basic failure modes in notched fibre-metal laminates [7].*

De Vries and Vlot [8] investigated the influence of the properties of the metal layer on the fracture toughness of fibre-metal laminates. Tests on centre-cracked tension (CCT) GLARE-3 specimens were performed using a number of aluminium alloy variants and Table 2.3 shows the residual strength results. The authors concluded that the residual strength of the fibre-metal laminates was sensitive to the plastic reserve (amount of plasticity available in the material after yielding) of GLARE. The results highlighted a higher residual strength in materials with a higher plastic reserve, see Figure 2.6. In addition, they revealed that the high resistance to fracture of GLARE could be attributed to the redistribution of the load from the aluminium to the fibres. Thus, in developing fibre-metal laminates with a high

fracture toughness is necessary to ensure that the fibres carry the load in place of the aluminium.

Material	Crack initiation stress **MPa**	Ultimate strength **MPa**
GLARE 2024-T3	121	240
GLARE 2024-T81	98	228
GLARE 7075-T6	94	221
GLARE 7475-T761	146	230
GLARE 6013-T6	139	229

Table 2.3 *The influence of the properties of the aluminium alloy on the strength of GLARE 3/2 laminates [8].*

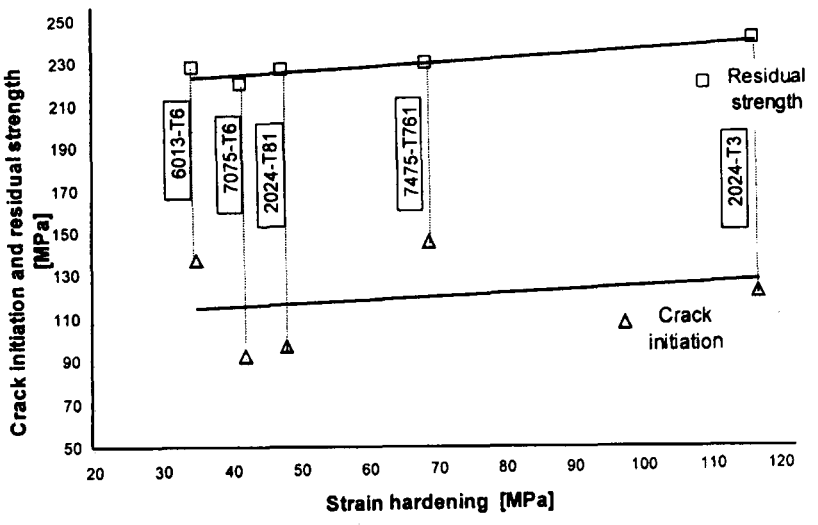

Figure 2.6 *Residual strength of GLARE laminates as a function of the plastic reserve of the Al alloy [8].*

2.5 IMPACT PERFORMANCE AND DAMAGE RESISTANCE

2.5.1 Low velocity impact

One of the major advantages of aluminium alloys over composites is their high resistance to impact loading. Indeed aluminium structures hardly suffer any

damage from low energy impacts and any minor damage is immediately visible as a dent on the surface of the metal [10]. On the other hand, fibre reinforced plastics are highly susceptible to damage, even from relatively low energy impacts. Damage from low velocity impact loading is generally internal, taking the form of delaminations, that may not be readily detectable, but never the less reduce the stiffness of the laminate considerably [10]. In this respect, the presence of aluminium on the surface of fibre metal laminates is highly advantageous, in that they provide a ready mechanism (in the form of indentations), by means of which impact damage in the laminate can easily be detected.

A number of studies had been carried out in order to evaluate the low velocity impact performance of both types of fibre-metal laminates (ARALL and GLARE) [11-16]. Vlot and Fredell [11] conducted a number of low velocity impact tests on ARALL and GLARE laminates. The tests were performed using an instrumented drop-weight impact tester, with an impactor mass of 575 grams capable of achieving a maximum velocity of 10 m/s. Their results showed that fibre-metal laminates based on glass fibre reinforced epoxy (GLARE) offer a superior resistance to low velocity impact loading than a monolithic aluminium alloy and a carbon fibre/thermoplastic composite. The fibre-metal laminates exhibited either a fibre-critical or an aluminium-critical behaviour. In the case of fibre-critical failure, a crack occurred perpendicular to the outer fibre direction. No fibre failure was observed without the generation of a simultaneous crack in the outer aluminium layer. During an aluminium-critical failure, the crack extended in the rolling direction of the aluminium layers which was generally the same as fibre direction in the laminates. Figure 2.7 illustrates an aluminium-critical failure in a 2/1 GLARE laminate [12].

Under low velocity impact loading conditions, GLARE laminates exhibited a minimum cracking energy that was fifteen percent greater than that of monolithic aluminium [13]. The minimum cracking energy defines the minimum energy required to cause visible cracking. The impact damage resistance of these fibre-metal laminates increases with increasing glass/epoxy content. This is partly due to

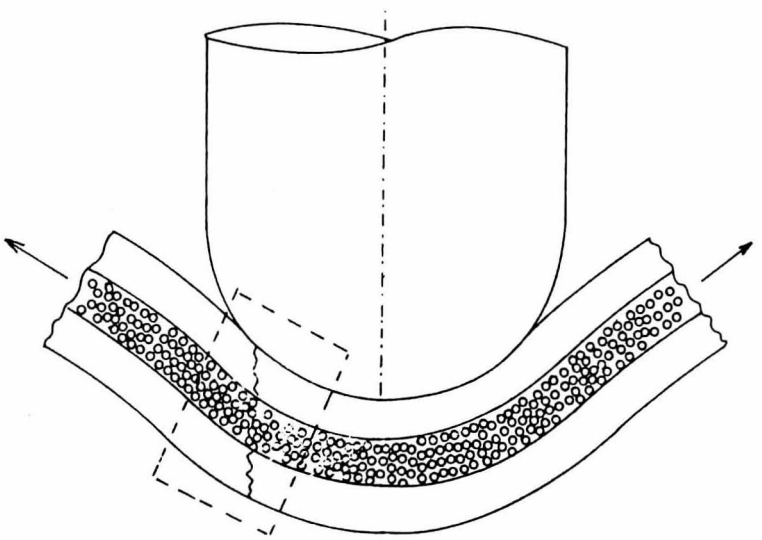

***Figure 2.7** Aluminium critical failure in 2/1 GLARE-2 (low velocity impact at 12 J) [12].*

the strain-rate sensitivity of the glass fibres. During the impact event, delamination occurs in fibre-metal laminates, and consequently the individual plies in the laminate will be loaded in a membrane deformation instead of the dominant bending response of the monolithic material. Figure 2.8 shows the damage width of carbon/PEI and GLARE laminates [13]. Compared to fibre-metal laminates, Carbon/PEI thermoplastic composites exhibit a poor impact damage resistance.

Following low velocity impact on GLARE, the dent depth was similar to that in an aluminium 2024-T3. The permanent dent in the FML had a depth of approximately two thirds of the maximum displacement of the target. The dent depth in the carbon/PEI thermoplastic was very small up to the penetration threshold [15]. No failure of the glass fibres was observed without associated cracking of the aluminium layers. First failure at low impact energies took the form of a crack in the outer aluminium layer in the fibre direction on the non-impacted side of the fibre-metal laminates. At energies above the threshold for first cracking, failure in

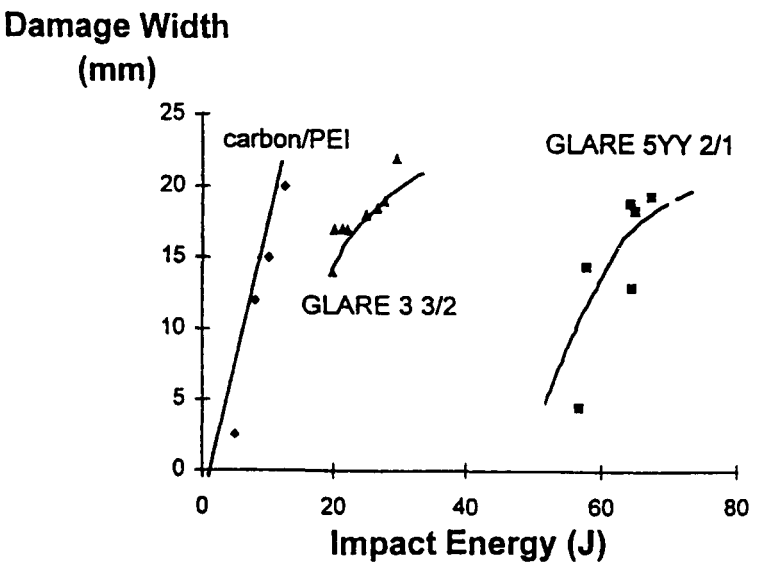

Figure 2.8 *Damage width for carbon/PEI and GLARE laminates [13].*

the aluminium layer initiated on the impacted surface and a through crack was created. Fibre failure occurred at very low energies in the thermoplastic composites on the non-impacted surface of the specimen [15].

2.5.2 High velocity impact

During their operational life, many aerospace structures are subjected to localised impact loading. High velocity impact damage can be caused by a number of sources such as runaway debris, hail, bird strikes, ice from propellers striking the fuselage, engine debris and tire shrapnel from tread separation and tire rupture [16]. The high velocity impact performance of fibre-metal laminates has been investigated in a number of studies [11-16]. A gas gun was used in order to undertake high velocity tests at velocities in the order of 100 m/s. In order to evaluate the impact damage zone in fibre-metal laminates, the aluminium outer layers need to be removed. Unfortunately, FML specimens cannot be C-scanned because the plastically deformed dent resulting from the impact event reflects the ultrasonic waves [12].

Vlot *et al* [13,15] studied the impact resistance of different types of fibre-metal laminates and compared their response with monolithic aluminium and carbon/PEI composites. Their results showed that GLARE laminates exhibited a higher specific cracking energy defined as the energy divided by the areal density (mass per m^2). In addition, increasing the number of layers of glass/epoxy in the fibre-metal laminates increased its specific cracking energy as shown in Table 2.4 [13].

Material	Lay-up	Thickness (mm)	Areal density (kg/m^2)	Specific cracking energy (Jm^2/kg)
Al 2024-T3	-	1.6	4.45	9.7
GLARE-3	3/2	1.4	3.49	19.9
GLARE-5YY	2/1	1.6	3.65	34.7
Carbon/PEI	0/90	2	3.46	0.86

Table 2.4 *Specific cracking energies at high velocity impact loading [13].*

In this case, GLARE-5YY represents a 2/1 laminate with eight layers of glass fibre/epoxy in a cross-ply stacking sequence. The influence of impact energy on the damage width under high velocity impact loading is shown in Figure 2.10 [15]. These results show that under high velocity impact conditions, fibre-metal laminates exhibit a superior minimum cracking energy (by approximately 2 to 3.5 times) to that of monolithic aluminium. The damage zone in these laminates tends to be smaller as the number of layers of glass fibre/epoxy is increased. Thin aluminium sheets are able to absorb greater amounts of incident energy because they exhibit membrane deformation compared to the dominant bending behaviour in thicker sheets. This is another explanation for the fact that GLARE laminates perform better under low and high velocity impact conditions.

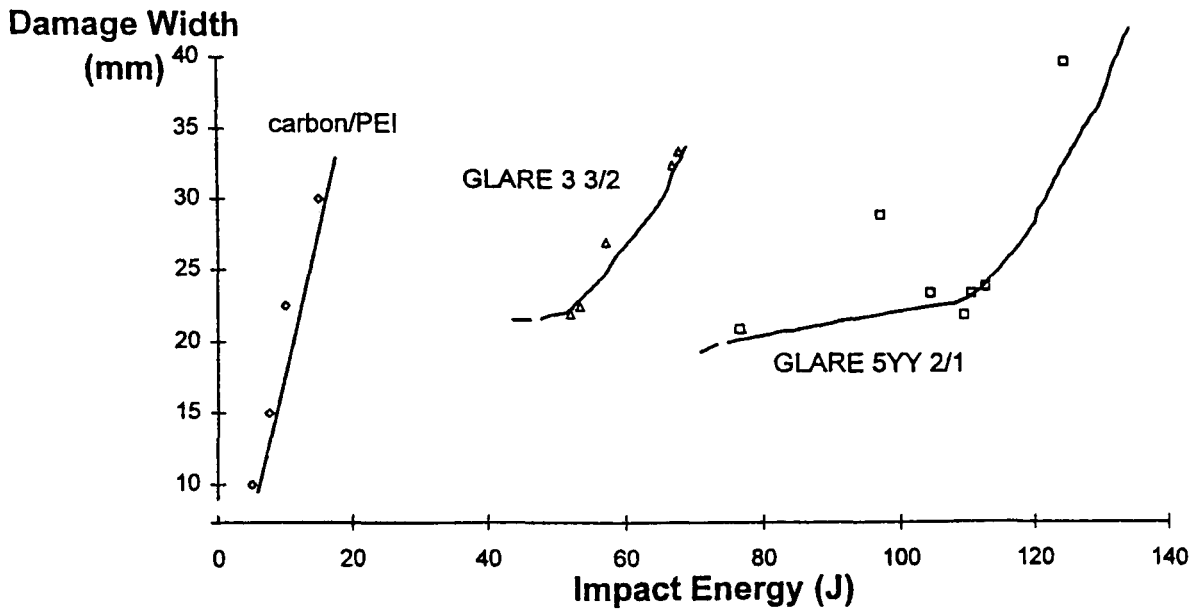

Figure 2.10 *Damage width of GLARE laminates and carbon/PEI composites at high velocity impact [15].*

Lawcock *et al* [14] studied the effect of varying the level of fibre surface treatment on the impact resistance of a carbon fibre/epoxy based fibre-metal laminate. The fibre-metal laminates with high levels of surface treatment exhibited a smaller reduction in damage area after high velocity impact tests than those with lower treatment levels. Tests on ARALL laminates indicated that their impact resistance is relatively low compared to monolithic aluminium, but considerably higher than typical quasi-isotropic carbon and aramid fibre reinforced thermoset systems [10]. The low strain to failure of aramid fibres and the relatively low flexural stiffness of ARALL in the direction perpendicular to the fibres have been identified as the two factors that contribute to their low impact resistance [10]. The latter causes large deformations precipitating premature failure of the composite layers and/or the aluminium layers. It appears that in ARALL laminates, failure initiates in the composite layer farthest form the impacted surface, wherein the fibres break, leading to the failure of the aluminium layers and the development of a through-the-thickness crack [1].

2.6 FATIGUE PERFORMANCE

The catastrophic failure of the Aloha Airlines Boeing 737 in April 1988 drew engineers' attention to the importance of structural damage tolerance. The aircraft lost a major portion of the upper fuselage near the front of the plane in full flight at 24,000 feet. Miraculously, the pilot managed to land the plane on the island of Maui, Hawaii. Surprisingly, only one life was lost in the accident. Multiple site fatigue damage was found in the aircraft, which led to structural failure during flight [17,18]. ARALL and GLARE laminates were primarily developed with the objective of increasing the life of structural aluminium; enhanced fatigue life is therefore the primary advantage offered by fibre-metal laminates over conventional aluminium alloys [1]. During the development of ARALL laminates, the design and manufacture of a realistic aircraft component was tested under fatigue loading and compared with an equivalent aluminium structure. The tests clearly demonstrated the advantages offered by lightweight fibre-metal laminates [19].

2.6.1 Fracture toughness and residual strength

Numerous research studies have been undertaken to characterise and quantify the fatigue performance of fibre-metal laminates [1,16,20-24]. In general, the results indicate that under conditions where loading is tension dominated and directed parallel to the direction of the fibre reinforcement, hybrid laminates exhibit a significant superior fatigue life compared to monolithic aluminium. Since much of the increased fatigue life of fibre-metal laminates is due to the restraint on crack growth provided by the reinforcing fibres, the fatigue performance is greatly reduced when the fibres are cut, as in the case of saw-cut cracks. Young *et al* [20] studied the crack growth and residual strength of GLARE-3 and GLARE-4 using the specimen geometry shown in Figure 2.11 and compared it with its monolithic aluminium counterparts. Their results indicated that GLARE specimens tested under constant amplitude load exhibited superior fatigue crack growth behaviour. For GLARE-3,

the improvement in fatigue life over monolithic 2024-T3 aluminium was of the order of one hundred times, whilst that for GLARE-4 the improvement was of the order of fifty times. Residual strength tests showed that GLARE-4 and GLARE-3 exhibited an improvement of 20 to 40 per cent and 25 per cent respectively over monolithic aluminium.

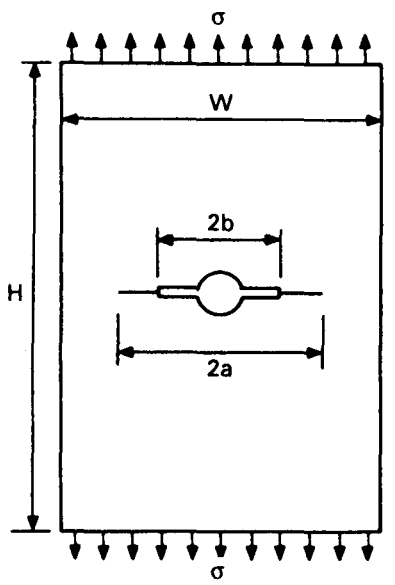

Figure 2.11 *Centrally-notched fatigue specimen geometry [20]*

When tested under fatigue loading, ARALL laminates has been shown to exhibit an improved performance over monolithic aluminium [1,19]. Teply [21] studied the fracture toughness and fatigue crack growth of ARALL laminates. Here, it was shown that the fracture and fatigue performance of these laminates is closely related to their ability to delaminate. In these systems, delamination was followed by fibre crack bridging which in turn was accompanied by an increase in fracture toughness and fatigue crack growth resistance. He suggested that the residual strength of these laminates strongly depended on the fibre bridging length. The effect of biaxial loading plays an important role in determining the fatigue response of aircraft structures [1]. Tests using lateral restraints (which provide a stress in the direction perpendicular to the axis of loading due to the Poisson effect) have shown

that a biaxial stress field results in a longer fatigue life than in uniaxial tension fatigue. In this case, fibre failure is delayed by the presence of delamination around the crack tip. Figure 2.12 shows the effect of biaxial loading on crack growth in ARALL laminates [1].

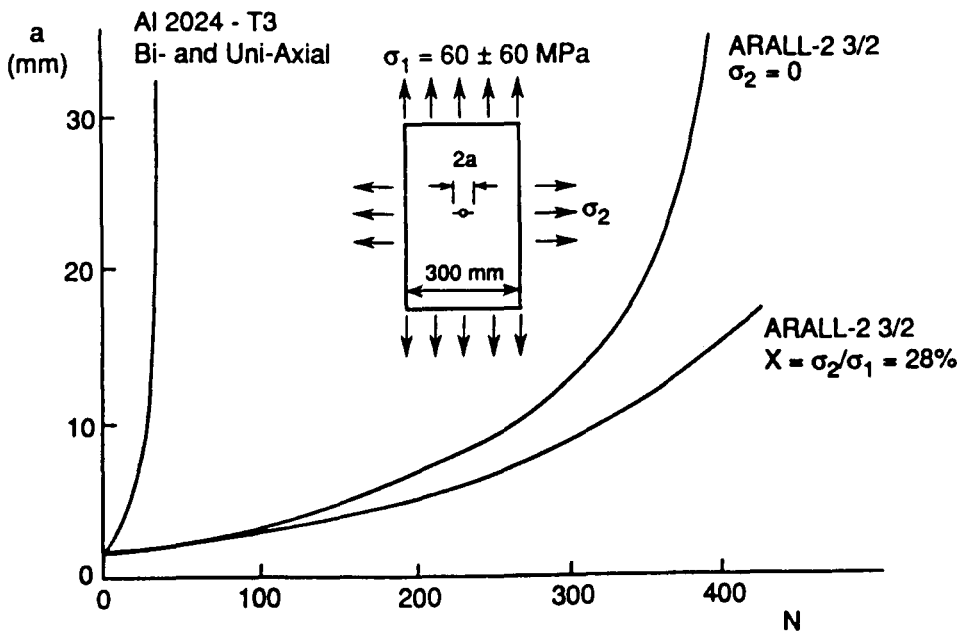

Figure 2.12 *Effect of biaxial loading on crack growth in ARALL laminates [1].*

Papakyriacou *et al* [22] studied the fatigue crack growth behaviour of GLARE-1 with blunt notches and compared it with aluminium 7475 laminates. Their results showed that for the aluminium specimens with cracks of 3 to 3.5 mm, the crack growth rates were higher as the notch root radius was reduced, but the difference decreased at larger crack lengths. Figure 2.13 shows the influence of notch radius on the fatigue crack growth rate for both aluminium and GLARE-1 laminates under tension-tension fatigue loading conditions (R= -1). These results show that GLARE-1 exhibits a superior fatigue crack growth performance to that offered by aluminium 7475. The aluminium 7475 alloy exhibited the typical response associated with a metal involving the initiation and propagation of a single crack and an increasing crack growth velocity as the crack developed. In contrast,

multiple crack initiation and propagation occurred in GLARE-1 where a decreasing crack growth rate was observed with increasing crack propagation. In addition, cracks in this multilayered material propagated independently from each other (i.e. without mutual interference) as single cracks and with similar crack growth rates.

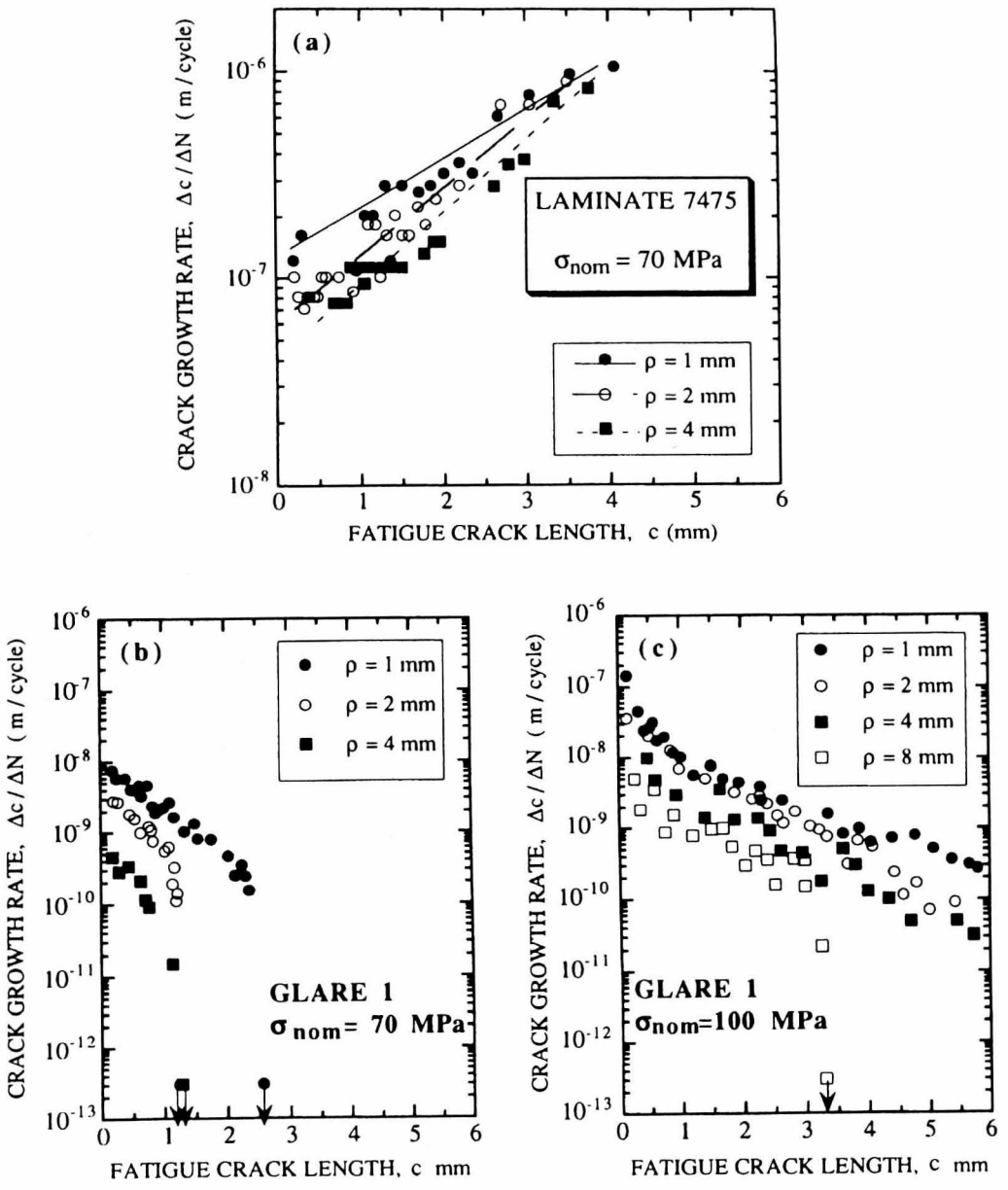

Figure 2.13 *Influence of the notch radius on fatigue crack growth rates in the width direction of the sample. (a) aluminium 7475 at 70 MPa. (b) GLARE-1 at 70 MPa. (c) GLARE-1 at 100 MPa [22].*

These results were attributed to crack bridging due to the unbroken fibres. Here, cracking in the fibre layer was very limited and the fibre layer acted as a barrier between cracks in the two adjacent metal layers. It also enabled independent cracks to develop in the same metallic layer. From this study, it was also established that the notch radius influences the crack initiation phase and the early stage of crack propagation in GLARE-1, as well as its behaviour at long crack lengths. The fatigue crack growth rates were greater for small notch root radii for crack growth in both the thickness and width directions. The superiority of GLARE samples with a large notch radii was attributed to lower effective stress intensity factors at the same nominal stress intensity value due to lower local stresses in the crack tip area. The lower stress level leads to less fibre failure at the crack tip of notches with larger radii and therefore greater fibre bridging along the whole crack path.

Vlot et al [16] evaluated the fatigue performance of a number of fibre-metal laminates under simulated fuselage loading conditions in samples containing a central saw cut and compared their response with their monolithic counterparts. Their results showed that while the crack growth rate of the aluminium 2024-T3 alloy increased rapidly with increasing crack length, the fibre-metal laminates exhibited an almost constant slow crack growth behaviour. Figure 2.14 compares the fatigue performance of cross-plied GLARE-3, unidirectional reinforced GLARE-2, ARALL-2 and monolithic aluminium 2024-T3. They suggested that under realistic loading conditions, fibre-metal laminates exhibited crack growth rates 10 to 100 times lower than their monolithic aluminium counterparts. In addition, they proposed that GLARE excels under all types of fatigue loading situations and that inspection of the structure for fatigue damage was, in many cases, not necessary during the whole operational life of an aircraft.

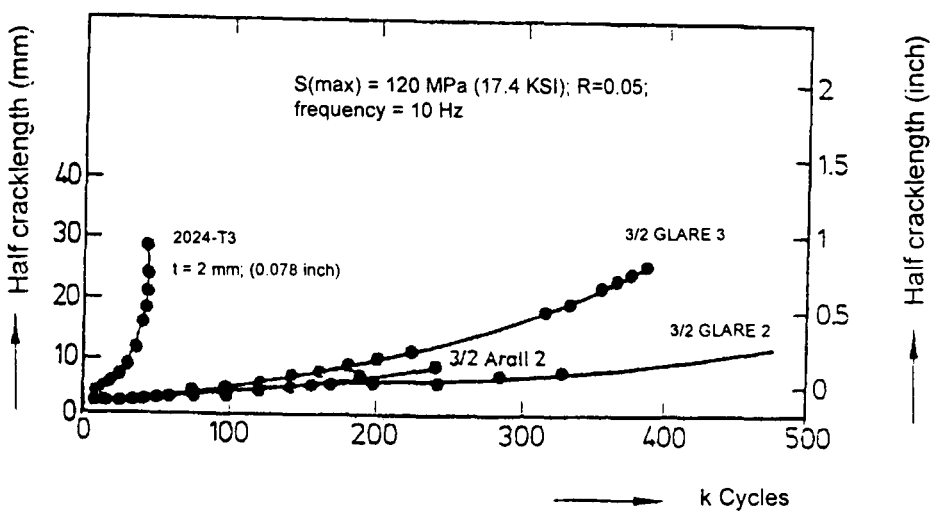

Figure 2.14 *The crack growth behaviour of GLARE-3, GLARE-2, ARALL-2 and aluminium 2024-T3 for fuselage loading conditions[16].*

Studies of the fatigue properties of similar types of fibre-metal laminates have been undertaken in order to assess their fatigue damage resistance [23,24]. Senatorova and co-workers [23] studied the fatigue fracture resistance of GLARE-type fibre-metal laminate and compared their response with monolithic aluminium. The behaviour of the composite layer in the fibre-metal laminate was examined using metallographic and fractographic techniques. The laminate consisted of unidirectional glass fibre and duralumin alloy sheets. Fatigue crack growth rates and fracture toughness properties were determined on the centre-notched (hole + saw cut + cracks) specimens. Their results showed that fibre-metal laminates exhibited a very high resistance to fatigue crack propagation; the fibres remained intact and restricted the crack tip opening in the aluminium sheets. The fracture toughness values were higher in samples where the fatigue crack was restricted to the thin aluminium sheets rather than through the thickness of the laminate. Microscopic observations of fatigue failure revealed that a crack (or a few cracks) always started from the hole in outer aluminium layers and propagated perpendicular to free

surface. No fibre failure was observed after removing the outer aluminium layer. They concluded that GLARE-type fibre-metal laminates exhibit a superior fatigue fracture resistance than monolithic aluminium and that the fatigue life of fibre-metal laminates with an open hole increases as the number of metallic and polymer layers increases and their thickness decreases.

Austin *et al* [24] studied the progress of fatigue damage in a carbon fibre reinforced aluminium alloy laminate (CARALL). The strain within a defined area in the vicinity of the crack was measured directly by means of fibre optic sensors. A two-dimensional array of optical fibre sensors was embedded within the composite to map the strain field. The growth of the delamination zone was successfully related to the strain field in the vicinity of the crack and the development of a typical zone within a 4-ply CARALL fatigue-loaded laminate is shown in Figure 2.15.

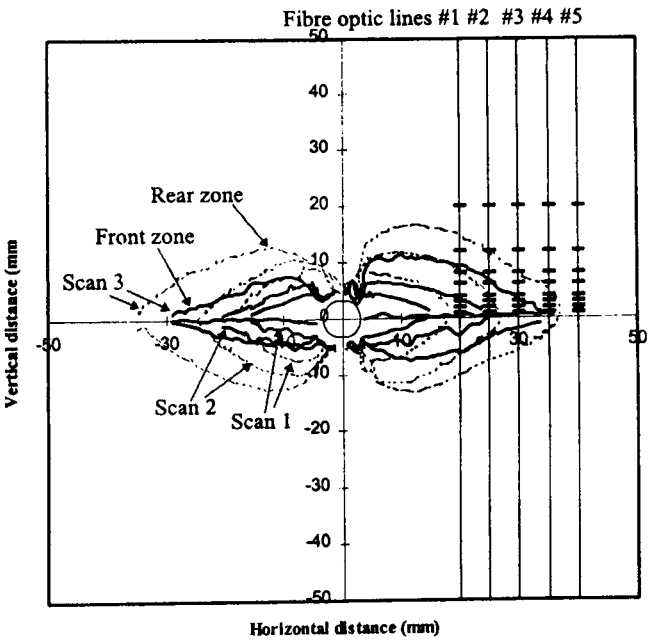

Figure 2.15 *Development of delaminated regions in CARALL laminates subjected to fatigue [24].*

This figure shows three ultrasonic scans, the unbroken lines indicate the boundaries of delamination zones between the front alloy skin and the composite, while the dashed lines depict the rear zones. Their results showed that CARALL laminates typically presented a triangular shaped delamination zone, which tended to become more elliptical as the delamination progressed. They suggested that the growth of the delaminated area could be related to the strain amplitude. Changes in the strain field were related to both fatigue crack growth and the presence of delaminations between the composite and aluminium skins.

2.6.2 Crack propagation mechanisms

The improved fatigue performance of fibre-metal laminates can partly be attributed to their layered structure, since it is well established that laminates based on thin sheets bonded together exhibit superior crack growth resistance and damage tolerance compared to those of the constituent material [2]. However, the primary factor that contributes to their vastly superior fatigue life comes from the crack bridging effect of the reinforcing fibres embedded in the polymeric matrix. In contrast to the behaviour of the conventional metallic materials, crack growth rates in fibre-metal laminates are found to decrease with continued load cycling. This effect is attributed to a reduction in the effective stress intensity factor at the crack tip, caused by the crack bridging effect of the fibres in the wake of the crack [1,16,20-24].

Ritchie *et al* [25] studied the fatigue crack propagation behaviour of ARALL-2 laminates in order to elucidate the mechanisms associated with crack-tip shielding. Their results suggested that the interface between the aluminium sheet and the epoxy, and between the resin-rich and fibre-rich layers within the epoxy, only suffered minor delamination. However, extensive separation was apparent among various bundles of fibres, implying that the failure of individual fibre/epoxy interfaces was the primary source of delamination.

The influence of the location and size of the bridging zone of unbroken fibres behind the crack tip in fatigue-loaded ARALL-2 laminates (Figure 2.16) was also evaluated [25]. They concluded that the superior crack growth resistance of fibre-metal laminates was associated with crack-tip shielding primarily as a result of crack bridging by unbroken fibres in the wake of the crack-tip. The effect of crack bridging was promoted by controlled delamination, principally along the fibre/epoxy interfaces. The length of the crack over which the fibres remained unbroken in the wake of the crack-tip, i.e. the bridging zone was found to be between 3 and 5 mm.

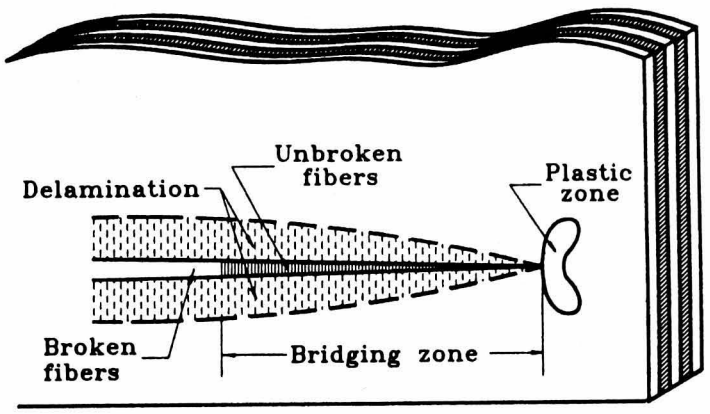

Figure 2.16 *Schematic illustration of a fatigue crack in an ARALL-2 laminate [25].*

The excellent fatigue resistance of GLARE laminates resulted from the crack closure mechanism exerted by the fibres on the fatigue crack in the aluminium. Fibres bridging the fatigue crack, as shown in Figure 2.17, lowered the stress concentration at the crack tip, thus retarding or arresting crack growth [1,12,20,26]. In addition, as the crack grows, a zone of delamination is created at the prepreg/aluminium interface [26]. The effect of this delamination was to increase the free length over which the fibres were strained in order to cover the opening of the

crack faces. This had the negative effect of reducing the efficiency of crack bridging; but its more important and positive effect was that it reduced the tensile stress in the fibres, thereby delaying their ultimate fracture [26].

Another fracture mechanism, shear deformation in the adhesive between the aluminium and the fibres, also played a similar dual role. This mechanism reduced the crack bridging efficiency and delayed fibre fracture by allowing only a fraction of the crack opening displacement to be transferred to the fibres [1].

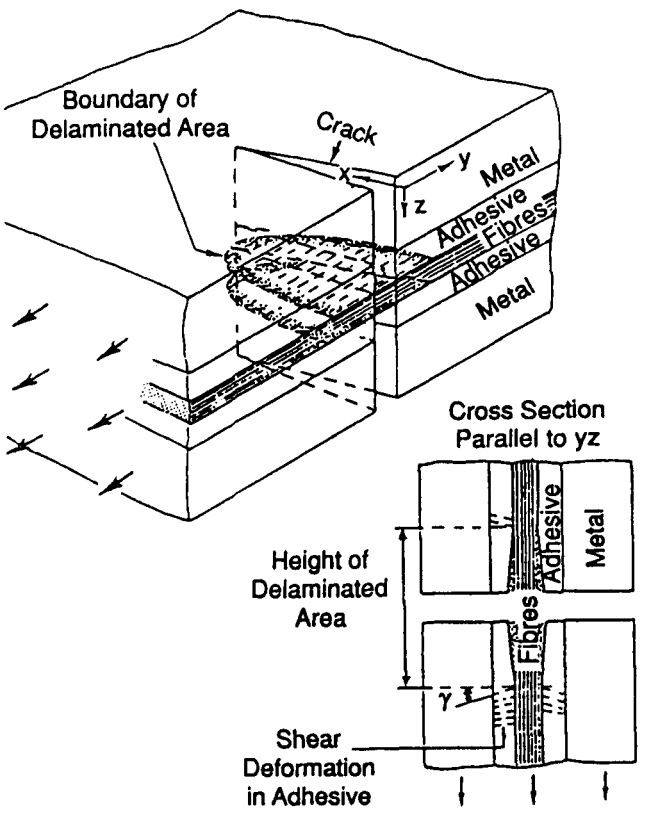

Figure 2.17 *Schematic illustration of crack bridging by fibres in a fibre-metal laminate [26].*

2.7 STABILITY AND DURABILITY

The durability of aluminium is primarily governed by its fatigue and crack initiation behaviour. Once the crack initiates, its subsequent propagation leading to

catastrophic failure (if unchecked) is only a matter of time, since the crack growth rate increases with increasing crack length in metals. The initiation of cracks is greatly influenced by environmental effects [27]. Micro-cracks initiate in areas of high stress concentration associated with holes, changes in cross-sectional area or where the surface has suffered extensive pitting due to corrosion. The presence of stress concentrations coupled with corrosion yields to a much earlier initiation of cracks. In ARALL and GLARE laminates, cracks initiate in the aluminium layers after approximately the same number of cycles as in their monolithic aluminium counterparts. However, the subsequent growth of these micro-cracks into macro-cracks is substantially delayed or even prevented by the crack-restraining influence of the embedded fibres in the hybrid laminates. Thus, the stability and durability of fibre-metal laminates is highly dependent on the environmental resistance of the fibres and adhesive matrix in the composite material. Fortunately, the composite layers are largely protected from hostile environments by the aluminium outer sheets, making fibre-metal laminates inherently more durable than both plain metallic panels and bulk composite materials [28].

2.7.1 Moisture absorption

Compared to plain composite materials, moisture absorption in fibre-metal laminates is negligible, particularly for thin systems. This superior moisture resistance is due in part to the protective barriers offered by the aluminium face sheets, which restrict moisture ingress through the surface of the laminate [29]. Adhesion between aramid fibres and the matrix is decreased in the presence of moisture, which in turn affects the peel strength and the shear fracture properties [28]. The fibre/epoxy layers are only exposed at the edges of the laminates.

Moisture penetration is therefore limited. Under realistic cyclic temperature and humidity conditions as encountered during aircraft service, the influence of moisture is small, as is also the case for conventional glass/epoxy composites and

bonded aluminium structures [16]. While aramid fibres (organic) absorb water, glass fibres (inorganic) do not absorb moisture [30]. Therefore, the moisture absorption rate of GLARE is small compared to ARALL. Further, the diffusion of moisture into GLARE is limited to the exposed edges of the laminate, whereas in ARALL moisture can diffuse along the length of the fibres [27]. In addition, the moisture weakens the bi-material interfaces, leading to a greater amount of delamination and reductions in the load-carrying capacity under flexural fatigue loading conditions [31]. In contrast, the development of a larger delamination zone in the presence of a high humidity environment in ARALL laminates, contributes to a lower crack growth rate (compared to a normal laboratory environment), and hence a longer fatigue life [32].

2.7.2 Bondline corrosion

Bondline corrosion is a typical service type of fracture, characterised by debonding of the aluminium/adhesive interface, followed by severe corrosion of the aluminium. ARALL laminates when subjected to salt spray, salt-water exposure and moisture absorption up to 50 %, experience virtually no degradation in interlaminar shear strength even after exposure for periods up to eight weeks [33]. As mentioned earlier, ARALL offers a relatively poor peel strength, due to the poor adhesion between the aramid fibres and the epoxy system. Therefore, the peel strength of ARALL laminates decreases with increasing exposure to salt spray environment. In contrast, no bondline corrosion was observed after fifteen months. In the case of exposure to the hydraulic oil used in aircraft systems, virtually no deterioration of the peel strength was observed [34].

All aluminium sheets used in the production of fibre-metal laminates are anodised and coated with a corrosion-inhibiting primer prior to the bonding process. Furthermore, outer aluminium surfaces can be supplied with a thin clad layer to improve surface corrosion resistance. Through the thickness corrosion is prevented

by the barrier role played by the fibre/epoxy layers. This barrier effect limits the extent of corrosion damage in severe environments. Under acid bath corrosion, fibre-metal laminates are only pitted to the first fibre/epoxy interface while their monolithic counterparts are fully penetrated [16,35].

2.7.3 Seacoast environment

The environmental resistance of ARALL laminates when tested under accelerated conditions (continuous exposure to hot and humid air, salt fog and thermal cycling) and exposed to a seacoast atmosphere exhibit no appreciable loss in peel strength. However, a reduction of twenty per cent in peel strength in the transverse direction is observed. In addition, the exposure of ARALL laminates to a salt fog environment produces a marginal reduction in tensile strength, mainly due to the severe corrosion of the outer aluminium layers. Interestingly, the residual stresses introduced whilst processing ARALL-2 were completely relaxed after exposure to this severe environment [36].

Exposure to hostile environments can result in corrosion through the thickness of the material in monolithic aluminium [1]. However, in bonded laminates, corrosion is prevented from spreading from the outer layers to the inner metallic layers by the adhesive layers in the laminate. Reinforcing the adhesive with polymer fibres enhances this preventive mechanism, so that corrosion, however severe, is restricted to the outermost aluminium laminae in ARALL and GLARE laminates [36].

2.8 RESIDUAL STRESSES

One of the drawbacks of fibre-metal laminates in the as-cured condition is the state of the residual stresses introduced by the differential thermal expansion of the aluminium and prepreg layers during the curing process. Since aluminium has a

higher coefficient of thermal expansion than the composite material, the process of curing introduces residual compressive stresses in the prepreg and tensile stresses in the aluminium [1,10-11,12-13,15,20]. As it is, the aramid prepreg has a poor resistance to compression due to their propensity to suffer micro buckling. The effect of a residual compressive stress in the prepreg is to lower the value of its compressive resistance. Therefore, even when subjected to fatigue cycles with stress ratio greater that zero, the aramid fibres go through a compressive phase, resulting in substantial fibre failure and a consequent reduction in fatigue life. This behaviour intensifies as the frequency of loading decreases [10].

Krishnakumar [1] cited a range of techniques and procedures for introducing a more favourable residual stress-state in a fibre-metal laminate, these include (a) pre-tensioning of the fibres, (b) post-stretching and (c) rolling. The introduction of tensile residual stresses in the prepreg layers greatly improved the fatigue performance of ARALL laminates. In addition, the procedure also improved the performance of laminates subjected to tension-dominated loading, making them practically insensitive to fatigue crack growth as shown in Figure 2.18. This is because the reversed residual stress state in ARALL laminates has two beneficial effects: Firstly, the tensile residual stresses in the prepreg reduce the extent of micro-buckling failure of the aramid fibres, providing improved crack bridging. Secondly, the compressive residual stresses in the aluminium have a crack closing effect, and hence retard the propagation of the crack in the metallic layers [1].

In contrast to ARALL, GLARE performs very well in fatigue loading with low or negative stress ratios, even in its as-cured condition. This is because, glass does not share the tendency of the aramid fibres to suffer micro-buckling under compressive stresses.

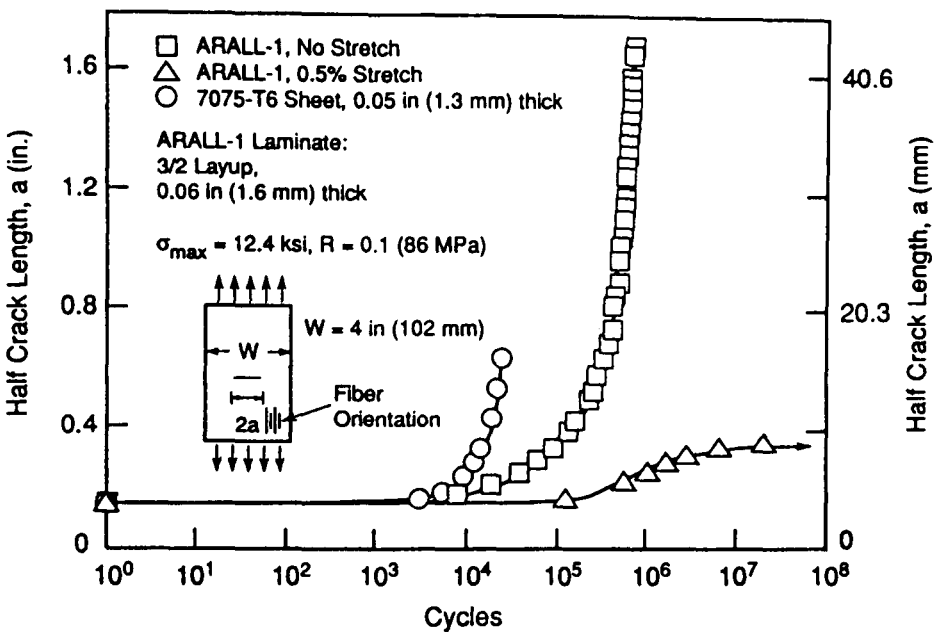

Figure 2.18 *Fatigue crack growth in ARALL-1 under constant cyclic loading [1].*

Hence, in many situations GLARE can be used in the as-cured condition [1]. This is particularly important, since the post-stretching of long panels with fibres in the width direction is practically impossible on a commercial basis. Such panels are highly desirable in order to avoid a large number of transverse joints in fuselage skins. The prestraining of the laminate, however, considerably enhances the performance of GLARE laminates, mostly as a result of the crack closing effect of the compressive stresses in the aluminium [1,11,20].

Post-stretching of fibre-metal laminates after curing is accompanied by plastic deformation. This causes a reversal of the internal stresses due to curing, which is favourable for the fatigue properties of these hybrid systems. Vlot and Van Ingen [37] studied the delamination resistance of post-stretched fibre-metal laminates. They highlighted the possible effects of the internal stress system on the stress-state around the crack in the outer aluminium layers, see Figure 2.19.

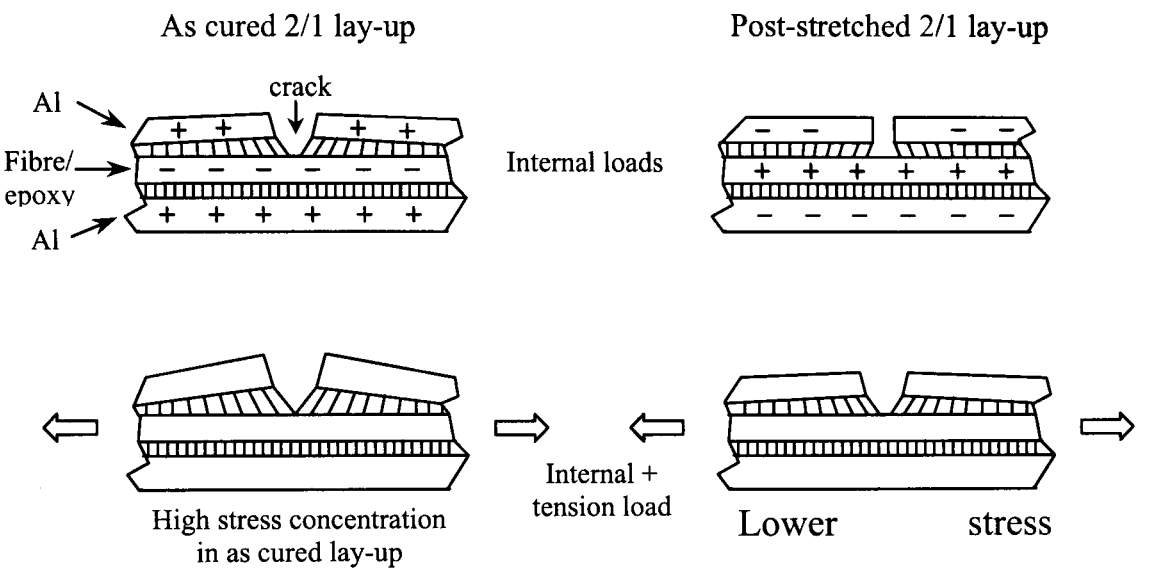

Figure 2.19 *The influence of internal stresses in fibre-metal laminates on the shear stress at the crack [37].*

The authors suggested that in the as-cured condition, a shear stress is present in the resin-rich layer at the interface between the aluminium and fibre/epoxy layer, since the aluminium edge in the gap is stress free. This shear stress tends to open the gap and acts in the same direction as the stress induced by a tensile load on the laminate. In the post-stretched condition, the sign of the shear stress due to the internal stresses is reversed, which has a favourable effect on the delamination resistance of these lightweight materials [37]. The effect of a second cure cycle on the residual stresses and the mode I delamination resistance of fibre-metal laminates was also investigated [37]. Vlot and Van Ingen showed that post-stretching ARALL laminates decreased their mode I delamination resistance by fifteen per cent whilst no significant influence on the mode II delamination resistance was found. In addition, post-stretching GLARE laminates did not influence the mode I delamination resistance of the system and had only a small positive influence on the mode II delamination resistance.

Furthermore, GLARE laminates exhibited superior mode I and mode II delamination resistances to ARALL laminates. Post-curing of fibre-metal laminates has been shown to increase the mode I delamination resistance of ARALL laminates, whereas no effect was observed in GLARE laminates [37]. In addition, it was shown that post-curing caused a relaxation of the internal stresses in post-stretched ARALL laminates of up to twenty per cent.

2.9 ADDITIONAL PROPERTIES

2.9.1 Formability and machinability

Fibre-metal laminates combine the excellent fatigue and fracture resistance of lightweight composite materials and the isotropic properties, traditional durability and ease of fabrication associated with metals [38]. The formability and machinability of fibre-metal laminates has been studied by Sinke and de Jong [38]. They suggested that, due to its constituents and lay-up structure, the formability of fibre-metal laminates was limited. The major limitations stemmed from the fibres and the interfaces between the layers: fibre-metal laminates fail by metal fracture, fibre failure or by delamination. Furthermore, the folding of ARALL laminates requires special attention due to the limited strain to failure of the aramid fibres and the possibility of delaminations forming. Their results suggested that when manufacturing structural components, fibre-metal laminates could be treated as hybrid materials where workshop practices for metals such as bending, roll forming, machining and drilling could be applied along with composite production processes such as the lay-up of single and double-curved parts. Waterjet cutting of fibre-metal laminates has also been investigated [27]. It was suggested that abrasive waterjet cutting, using an abrasive to increase the cutting power of the water showed excellent results. In particular, when the cutting line started at the edge of the workpiece, no problems were encountered and the laminates were cut at an acceptable speed.

In addition, Sinke and de Jong concluded that existing forming and machining processes could be applied to fibre-metal laminates, but due to their layered structure, special attention should be paid to some production aspects to prevent delamination, premature failure or excessive tool wear. In contrast, Graaf and Meijer [39] studied laser cutting techniques for aluminium-synthetic laminates. They suggested that these fibre-metal laminates materials could be cut at the same speed as homogeneous aluminium alloys, although some damage to the synthetic layers was apparent. A damage zone of 0.6 mm depth was observed at the maximum cutting speed.

2.9.2 Production and splicing

The fibre layers used to produce a fibre-metal laminate are supplied in pre-impregnated layers, so-called prepregs. After lay-up, the whole laminate is cured in an autoclave under controlled temperature and pressure conditions. This process yields the ready-to-use fibre-metal laminate [16]. The thin aluminium sheets used to produce fibre-metal laminates limit the size of the panel to be manufactured. From an aircraft manufactures' point of view, the most efficient way of building aircraft is to use large skin panels. This approach reduces the number of riveted joints, thereby not only reducing production time, but also reducing possible structural critical areas [16,40]. In order to be able to produce these large fibre-metal laminate panels, the splicing concept has to be applied. With this approach, the size of the panels can be increased by having the aluminium sheets overlap each other. Since there is no size limitation for the prepreg layers, this results in a continuous laminate [16]. Figure 2.20 shows a schematic representation of the splicing concept.

It was stated that the fracture toughness of the splice area should not be lower than that of a non-spliced laminate [16]. This was achieved through the application

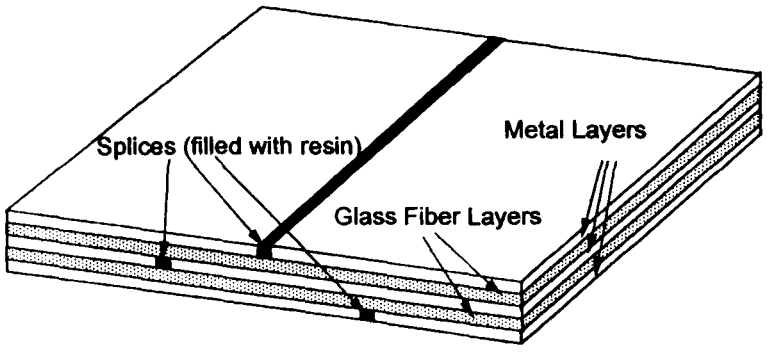

Figure 2.20 *Schematic representation of the splicing concept [40].*

of a doubler over the splice area. This original configuration performed very well under fatigue and residual strength tests. However, static delamination of the bonded-on doubler and subsequent delamination in the laminate from splice to splice, occurred well before the static strength of the unspliced laminate was reached. In order to resolve this, a change in the splice geometry was made. Here, the location of the critical splice was moved. Additional testing on a full-scale fuselage barrel (focusing on the tensile strength, bunt-notch strength, off-axis tensile loading, crack initiation, crack growth, delamination and riveting) showed that the splice area performed satisfactorily [16,40].

2.9.3 Flame resistance

The flame resistance of GLARE laminates was evaluated by Vogelesang and co-workers [16,35]. Their results showed that the flame resistance of GLARE laminates is superior to that of monolithic aluminium alloys. They suggested that current aircraft fuselages with their aluminium alloy skins will melt away in twenty to thirty seconds in case of an outside kerosene fire. Consequently, passengers will be exposed to these flames because at least ninety seconds of escape time is required

to rescue the passengers. GLARE laminates showed a capability to resist fire conditions for much longer periods. The glass fibres with their high melting point protected the second aluminium layer from melting for a significantly increased time period and will therefore protect the passengers from this threat. Standard aluminium alloy fuselage structures have a firewall liner on the interior side of the structure. However, when the unprotected outside skin structure melts away, the interior of the aircraft which is attached to this fuselage structure will easily collapse and injure the passengers. Vogelesang and co-workers [16,35] concluded that the use of GLARE laminates in fuselage skins will protect the structure against outside fires for longer fire periods and will keep the interior side intact as well.

2.9.4 Inspectability and repair

One of the advantages of fibre-metal laminates over composite materials is their easy inspectability. Damage due to impact is detectable as readily as in metals due to the indentation produced in the outer layers. In addition, other forms of damage, such as corrosion and fatigue cracking, usually initiate in the surface ply. Therefore, the same inspection techniques (eddy current, dye penetrant, etc.) that are used for aluminium alloys can also be employed for inspecting fibre-metal laminates [1]. The inspectability and repair characteristics of fibre-metal laminates have been reported in a number of studies [16,35,41-43]. Vlot and co-workers [16,35] suggested that when cracks occur in fibre-metal laminates, they might initiate below the outer surface. Internal cracking was characterised using eddy current techniques. This method was capable of finding small cracks (3 mm in length) in the third aluminium layer of a 3/2 laminate with ninety per cent accuracy. In addition, larger cracks were easier to locate. However, as with any non-destructive inspection technique, good training and the availability of reference standards are the key to successful detection. A quality control method for the ultrasonic inspection of fibre-metal laminates was developed and established by Coenen and co-workers [41-42].

This advanced inspection system was developed in order to verify the correct processing route and clarify the internal structure of these hybrid laminates. This was accomplished by comparing the actual C-scanning recordings with a semi-synthetic C-scan image generated by combining data from a lay-up simulation system with information from the curing process and historical records. They reported that by applying this method, many production errors could be traced. These include delaminations, inclusions, lay-up errors and erroneous processing parameters. In contrast, Fahr et al [43] stated that the C-scanning technique could in fact be used to map delaminations caused by fatigue and impact loading. However, if impact loading causes a severe dent on the surface, the scattering of the ultrasonic beam at the dent will influence the C-scan response thereby reducing its accuracy. The authors indicated that the use of the eddy current technique to detect cracks in the first or second layers yielded good accuracy.

Fibre-metal laminates are also attractive as a result of their easy repair procedures. It has been shown that the repair techniques that have been established for conventional aluminium structures can be employed for fibre-metal laminates [1]. Conventional riveted or bonded patch techniques perform well and fibre-metal patches can be used to repair conventional aluminium structures [16,35,44]. In addition, strips of ARALL and GLARE bonded on to monolithic aluminium have been found to be very effective as crack stoppers [45]. A very promising application of GLARE-3 and GLARE-4 is in the damage-tolerant repair of cracked aluminium skins. The high blunt notch strength, moderate stiffness and excellent fatigue resistance of cross-ply GLARE laminates make them an ideal choice for the repair of incidental damage in monolithic fuselage [16,35]. An interesting repairing technique using unidirectional GLARE laminates is the adhesively bonded patching of cracks. The moderate thermal expansion properties of GLARE make it an ideal patch material for the life extension of ageing transport fuselage skins suffering from multiple site fatigue damage [16,35,44].

2.9.5 Cost considerations

Fibre-metal laminates are relatively costly compared to the conventional aluminium alloys used in aircraft construction. This is partly due to the high cost of the composite prepreg, as well as the manufacturing costs associated with the processes of bonding, curing and post-stretching [1]. The use of fibre-metal laminates in aircraft structures may provide substantial savings in production costs as well as operating costs compared to monolithic aluminium [16,20]. The higher fatigue and static strength properties of these hybrid laminates can be exploited to design structures with less number of doublers and other local reinforcements which are widely used in aluminium structures, leading to a reduction in parts count and thereby production cost savings [1]. The excellent fatigue and corrosion resistance properties of fibre-metal laminates ensure a prolonged repair-free life and potentially extended inspection periods. These should translate to reduced operation and maintenance costs [16]. In addition, the potential weight savings of between twenty and thirty percent offered by fibre-metal laminates also contribute to significant reductions in the aircraft operating costs [16,20]. Thus when all the cost components are taken into account, fibre-metal laminates prove to be a cost effective alternative to conventional aluminium structures.

2.10 STRUCTURAL APPLICATIONS

The impressive fatigue, mechanical and anti-corrosion properties of fibre-metal laminates make them candidates for a wide range of applications including marine and offshore structures, containers, cars, bridges, tubes and space structures. However, the majority of applications that have been proposed and studied so far have been in the aircraft industry, wherein these hybrid laminates offer the greatest potential for improvement due to their combination of high strength, light weight and excellent damage tolerance characteristics [1]. Fibre-metal laminates are ideally suited for fatigue-intensive, preferably tension-loaded applications, the most likely

components for construction in ARALL have been identified as the lower wing, speed brakes and ailerons [1]. GLARE is being promoted specially for fuselage applications where high damage tolerance and exceptional fatigue properties are essentials. With GLARE, a good compromise exists between the outstanding properties of aluminium and glass fibres. This is giving the aircraft industry a higher confidence level for the use of non-monolithic metal for primary aircraft structures [20]. ARALL laminates have already been used in a number of aircraft structures; these include the Fokker F-27 lower wing structure, the F-50 underwing inspection access door and wing panel, and the McDonnell Douglas C-17 aft cargo door principally [46].

GLARE laminates are finding significant use with Airbus Industrie. This hybrid material is a strong contender for use in the fuselages of the ultra-large 480 to 650-seater Airbus A380 'super jumbo' that will enter in service in the year 2006 [16,35,47-49]. Figure 2.21 shows the Airbus A380, that is destined to become be the world's largest passenger aircraft [50].

Figure 2.21 *The Airbus A380 [50].*

2.11 SUMMARY

This section has reviewed much of the published data and information on fibre-metal laminates and multilayered materials. It is evident that these new hybrid laminates offer a number of distinct advantages when compared to conventional aluminium alloys and fibre reinforced plastics. Compared to conventional aluminium alloys, these layered laminates offer superior specific strengths and stiffnesses as well as exhibiting an excellent crack growth resistance and fatigue performance. In comparison to composites, they offer superior machinability, formability and inspectability, higher impact resistance and reduced susceptibility to environmental degradation. Due to their unique arrangement of alternating layers of aluminium and composite material, fibre-metal laminates are more environmentally durable and damage tolerant than either monolithic aluminium or plain composites. The aluminium face sheets minimise moisture absorption into the composite layers, while the adhesive prepreg prevents corrosion in the outer aluminium sheets from spreading through the thickness. Similarly, the aluminium face sheets protect the brittle composite from accidental damage and matrix cracking, while the reinforcing fibres arrest the propagation of the cracks in the aluminium layers.

The research and development activities to date have covered a variety of important aspects pertaining to the development of these new materials. However, there are still many areas where insufficient information is available in the published literature. Much of the work published in the literature has been conducted on fibre-metal laminates based on unidirectional composites with relatively brittle thermosetting matrices. One of the aims of the present research programme is to investigate the mechanical properties of a fibre-metal laminate based on a rubber-toughened epoxy resin in a carbon fibre plain woven composite.

Previous work [51] has shown that increasing the toughness of the matrix in a carbon fibre reinforced plastic can yield to a significant reduction in the size of the resulting impact damage zone and an improvement in the post-impact compression properties. Furthermore, woven composites offer a number of advantages over unidirectional tapes. Significant cost savings are often realised during the manufacturing operation since lay-up labour requirements are reduced and complex shapes produced in a single operation [52]. In the present work, the fracture properties of a multilayered fibre-metal laminate based on a rubber-toughened carbon fibre reinforced composite will be investigated. Initial attention will focus on optimising the adhesion between the aluminium and composite materials. A number of surface treatments will be applied to the aluminium substrates. Once this has been achieved, the in-plane fracture properties, the low velocity impact resistance and post-impact residual strength of these lightweight systems will be investigated. In addition, the work of fracture and high velocity impact response of these thermosetting-based fibre-metal laminates will be evaluated.

One of the disadvantages associated with almost all fibre-metal systems is the relatively long processing cycle required to ensure complete curing of the thermosetting matrix and optimised bonding across the composite-metal interface. In principle, this problem can be overcome through the use of a thermoplastic-based composite that can be moulded, bonded to a metal substrate and shaped in a simple one-shot manufacturing operation. This procedure clearly offers and attractive option for reducing both the cycle time and the associated manufacturing costs. Other benefits are likely to include: (i) the possibility to reform and reshape components following manufacture procedures, (ii) ease of repair, (iii) excellent energy-absorbing characteristics and (iv) high resistance to localised impact loading. At present, very little work has been undertaken in an attempt to investigate the mechanical properties of thermoplastic-based fibre-metal laminates. Chinsikirul *et al* [53] showed that polypropylene can be successfully bonded to aluminium through

the introduction of a polypropylene cohexenol copolymer at the critical interface. Laminates based on this system exhibited a seven to ten fold increase in peel strength over acid-etched samples. However, no attempt was made to characterise the properties of laminates based on these materials. In this research programme, the fracture properties of fibre-metal laminates based on a tough glass fibre reinforced polypropylene composite will be investigated. Initial attention will focus on characterising the fracture properties of the interface between the two constituent materials. Following this, the quasi-static, low velocity impact and post-impact properties of these novel lightweight systems will be investigated. Subsequent testing will focus on evaluating the work of fracture and characterising the high velocity impact response of these thermoplastic-based fibre-metal laminates.

2.12 REFERENCES

[1] **Krishnakumar, S.**, Materials and Manufacturing Processes, **9** (1994), pp 295-877

[2] **Schijve, J., Van Lipzing, H.T.M., Van Gestel, G.F.J.A., Hoeymakers, A.H.W.**, Engineering Fracture Mechanics, **12** (1979), pp 561-579.

[3] **Bucci, R.J.**, Treatise on Materials Science and Technology, **31**, Academic Press Inc., 1989.

[4] **Wu, H.F., Wu, L.L.**, Journal of Materials Science, **29** (1994), pp 5847-5851.

[5] **Wu, H.F., Wu, L.L.**, Journal of Materials Science, **29** (1994), pp 4583-4591.

[6] **Macheret, J., Bucci, R.J.**, Engineering Fracture Mechanics, **45** (1993), pp 729-739.

[7] **Vermeeren, C.A.J.R.**, 30th International SAMPE Technical Conference, (1998), pp 471-483.

[8] **De Vries, T., Vlot, A.**, 30th International SAMPE Technical Conference, (1998), pp 484-493.

[9] **Lawcock, G.D., Ye, L., Mai, Y.W., Sun, C.T.**, Composites Science and Technology, **57** (1997), pp 1609-1619.

[10] **Vogelesang, L.B.**, 16th International Council of Aeronautical Sciences, (1988), pp 1615.

[11] **Vlot, A., Fredell, R.S.**, 9th International Conference on Composite Materials, **6**, (1993), pp 51-58.

[12] **Vlot, A.**, International Journal of Impact Engineering, **18** (1996), pp 291-307.

[13] **Vlot, A., Krull, M.**, Journal de Physique, IV **7**(1997), pp 1045-1050.

[14] **Lawcock, G.D., Ye, L., Mai, Y.W., Sun, C.T.**, Composites Science and Technology, **57** (1997), pp 1621-1628.

[15] **Vlot, A., Kroon, E., La Rocca, G.**, Key Engineering Materials, **141-143** (1998), pp 235-276.

[16] **Vlot, A., Vogelesang, L.B., De Vries, T.J.**, 30th International SAMPE Technical Conference, (1998), pp 456-470.

[17] AvStop Magazine on Line, Lessons from Aloha, http://avsopt.com, 2000.

[18] Corrosion Doctors, The Aloha Incident, www.corrosion-doctors.org, 2000.

[19] **Gunnik, J.W.**, Composite Structures, **4**, Elsevier Applied Science, 1987, pp 1.162-1.177.

[20] **Young, J.B., Landry, J.G.N., Cavoulacos, V.N.**, Composite Structures, **27** (1994), pp 457-469.

[21] **Teply, J.L.**, Materials Research Society Symposium Proceedings, **434** (1996), pp 15-25.

[22] **Papakyriacou, M., Schijve, J., Stanzl-Tschegg, S.E.**, Fatigue and Fracture of Engineering Materials and Structures, **20** (1997), pp 1573-1584.

[23] **Senatorova, O.G., Anihovskaya, L.I., Sidelkinov, V.V., Sandler, V.S., Zhegina, I.P., Fridlyander, J.N., Filimonov, A.A.**, Materials Science Forum, **217-222** (1996), pp 1745-1750.

[24] **Austin, T.S.P., Gregson, P.J., Dakin, J.P., Powell, P.M., Singh, M.M.**, 5th International Conference on Deformation and Fracture of Composites, (1999), pp 191-200.

[25] **Ritchie, R.O., Yu, W., Bucci, R.J.**, Engineering Fracture Mechanics, **32** (1989), pp 361-377.

[26] **Marissen, R.**, Fatigue Crack Growth in Arall, DFVLR-FB-88-56, Germany, 1988.

[27] **Verbruggen, M.L.C.E.**, Influence of Prestrain Level on the Crack Propagation under a Mode I Condition, VTH-M-480, Netherlands, 1983.

[28] **Verbruggen, M.L.C.E.**, Thesis, Delft University of Technology (1980).

[29] **Verbruggen, M.L.C.E.**, Moiture Absorption on Arall compared to Carbon and Aramid Reinforced Composites, VTH-M-506, Netherlands, 1984.

[30] **Barbero, E.J.**, Introduction of Composite Materials Design, Taylor & Francis Inc., 1998.

[31] **Cook, J., Donnellan, M.E.**, Flexural Fatigue Behaviour of Arall Laminates, NADC-90073-60, Naval Air Development Center, 1990.

[32] **Ruschau, J.J.**, Fatigue Crack Growth Characteristics of Arall-1, AFWAL-TR-88-4075, US Air Force, 1988.

[33] **Donnellan, M.E., Cook, J., Skowronek, C.**, Evaluation of Arall-4, NADC-89100-60, Naval Air Development Center, 1989.

[34] **Verbruggen, M.L.C.E.**, Bondline Corrosion Properties of Arall in Salt Spry Environment, VTH-M-495, Netherlands, 1983.

[35] **Vogelesang, L.B., Vlot, A.**, Journal of Processing Technology, **103** (2000), pp 1-5.

[36] **Lee, S., Kipp, T.R.**, 20th International SAMPE Technical Conference, (1988), pp 617

[37] **Vlot, A., Van Ingen, J.W.**, Journal of Composite Materials, **32** (1998), pp 1784-1805.

[38] **Sinke, J., de Jong, T.W.**, 30th International SAMPE Technical Conference, (1998), pp 494-500.

[39] **Graaf, R.F., Meijer, J.**, Journal of Materials Processing Technology, **103** (2000), pp 23-28.

[40] **De Vries, T.J., Vlot, A., Hashagen, F.**, Composite Structures, 46 (1999), pp 131-145.

[41] **Coenen, R.A.M., Vogelesang, L.B.**, 29th International SAMPE Technical Conference, (1997), pp 168-178.

[42] **Coenen, R.A.M.**, 30th Internatinal SAMPE Technical Conference, (1998), pp 501-514.

[43] **Fahr, A., Chapman, C.E., Laliberte, J.F., Poon, C.**, Seventh Annual International Conference on Composite Engineering, (2000), pp 219-220.

[44] **Vlot, A., Soerjanto, T., Yeri, I., Schelling, J.A.**, 41st International SAMPE Symposium, (1996), pp 888-902.

[45] **Schijve, J.**, Engineering Fracture Mechanics, **37** (1990), pp 405-421.

[46] Aircraft Engineering, April 1988, pp 10-12.

[47] Flight International, July 1998, pp 28.

[48] Reinforced Plastics, January 1999, pp 28-32.

[49] Fokker Aerostructures B.V. Glare leaflet, (2000).

[50] Airbus Industrie, www.airbus.com, 2000.

[51] **Abrate, S.**, Impact on Composite Structures, Cambridge University Press, 1998.

[52] **Niu, M.C.Y.**, Composite Airframe Structures, Hong Kong Conmilit Press Ltd., 1996.

[53] **Chinsirikul, W., Chung, T.C., Harrison, I.R.**, Proceedings of the American Society for Composites, (1992), pp.42-56.

3. EXPERIMENTAL PROCEDURE

A number of earlier studies on fibre-metal laminates have been discussed in the preceding chapter. Even though much of this work represents a useful source of information for establishing the current experimental procedure, the originality of the present work necessitates the definition of carefully chosen testing procedures.

Initially, the manufacturing procedures for the plain composites will be established. Following this, the test procedures for the characterisation of the interlaminar properties of the plain composites will be outlined. Once this has been achieved, a test procedure for evaluating the level of adhesion at the bi-material interface will be described. In addition, the test procedures for the characterisation of the flexural, tensile, low velocity impact, post impact, work of fracture and high velocity impact properties will be outlined.

3.1 FRACTURE PROPERTIES OF COMPOSITE MATERIALS

The characteristics of composite materials in a fibre-metal laminate play a very important role in determining the fracture properties of these novel materials. Therefore, prior to manufacturing these multi-layer systems, the mode I, mode II and mixed-mode interlaminar fracture properties of the composite materials need to be fully characterised. During the course of this study, two different types of composite were used, further details of which will be given below.

3.1.1 Manufacturing procedures

3.1.1.1 Woven carbon fibre reinforced epoxy

The carbon fibre reinforced composite material employed in this study was Stesapreg EP121-C15-53 from Stesalit Ltd. (Switzerland). The composite consisted of a plain weave carbon fabric impregnated with epoxy resin. This particular prepeg material has been developed for the manufacture of lightweight structures that offer

very high specific mechanical properties. The nominal fibre volume fraction (V_f) of the prepreg was approximately 40 per cent.

In order to obtain panels for testing, sixteen 0.28 mm thick composite plies were placed in a picture frame mould with dimensions 200 x 240 mm (Fig. 3.1). For the interlaminar fracture testing of composite materials, a starter defect or pre-crack is required. Ideally, this film should be as thin as possible in order to minimise the disturbance of the fibres in the interlaminar region [1]. Here, a 25 μm thick folded aluminium foil with dimensions 50 x 240 mm was employed as a pre-crack as shown in Figure 3.1. In addition, a thermocouple wire was placed within the composite plies in order to monitor the curing temperature.

Once the correct number of plies and the starter defect had been placed in the lower mould, the upper mould was positioned on the top of the stack.

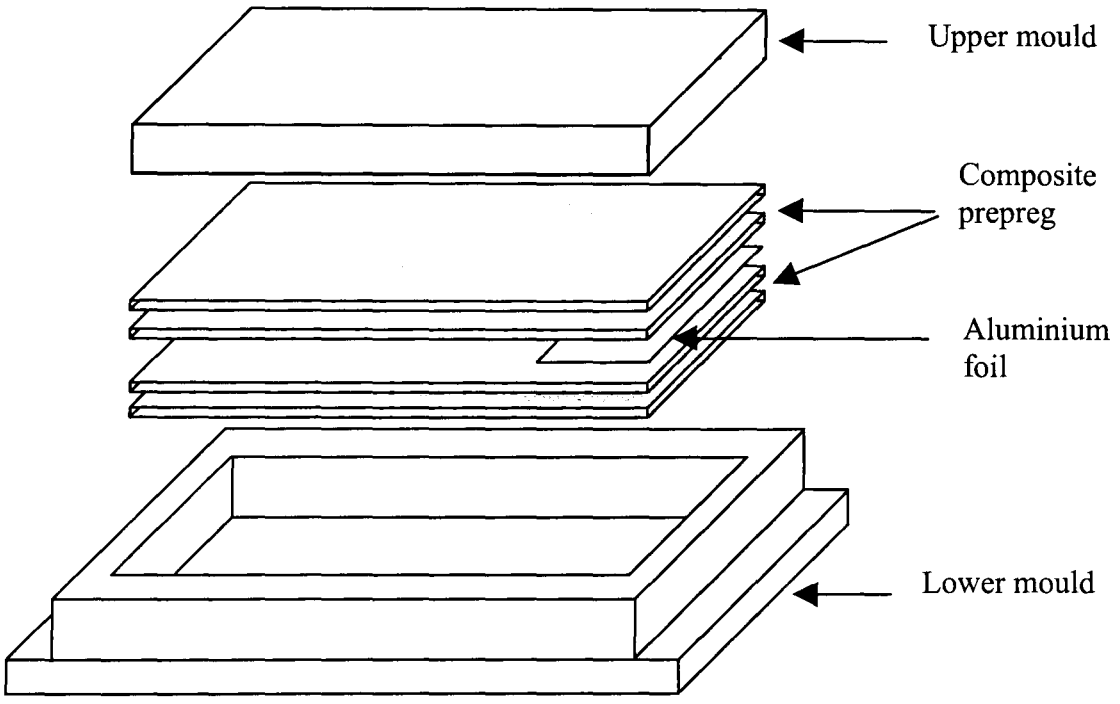

Figure 3.1 *The stacking arrangement of the composite and the starter defect in the picture frame mould .*

The mould was then placed in the hydraulic press shown in Figure 3.2. A pressure of approximately 6 bars was applied and the following curing cycle recommended by the manufacturers was employed.

- Heating from room temperature to 120 °C at a heating rate of 3 °C/min.
- A minimum curing time of 90 min at 120 °C.
- Cooling at about 4 °C/min to 60 °C.

Once the mould had cooled to approximately 30 °C, the pressure was released, and the mould was removed from the press. The panel was then carefully removed from the mould and inspected optically.

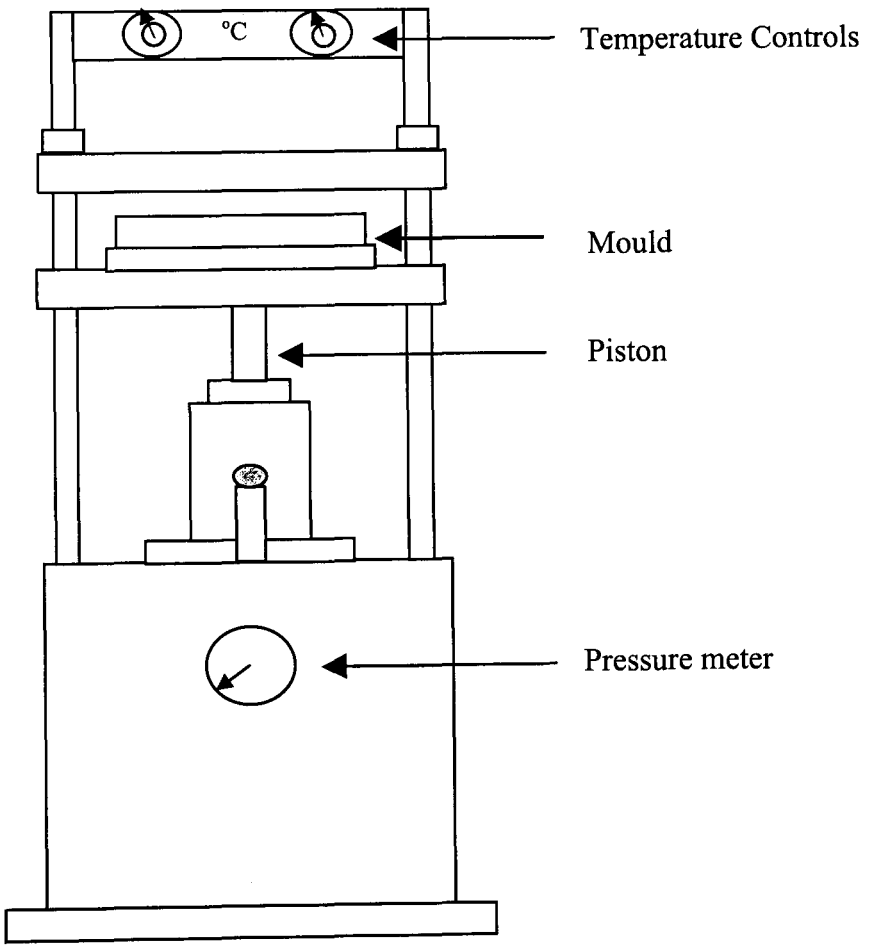

Figure 3.2 *Hydraulic press used for the manufacture of plain composites and the fibre-metal laminates.*

3.1.1.2 Unidirectional glass fibre reinforced polypropylene

This composite material, referred to as Plytron, is manufactured by Borealis Ltd. (Norway) and supplied by BI Composites Ltd. (United Kingdom). The composite consists of unidirectional E-glass fibres embedded in a semicrystalline polypropylene matrix. The nominal fibre volume fraction (V_f) of the prepreg is approximately 35 %.

In order to achieve the required specimen thickness for the interlaminar fracture testing, ten 0.54 mm thick layers of prepreg were placed in the picture frame mould as shown in Figure 3.1. As before, an aluminium foil starter defect was placed between the centremost composite plies. In addition, a thermocouple wire was placed within the composite layers in order to monitor the processing temperature. The mould was then placed in an air-circulating oven and the following processing cycle was employed:

- Heating from room temperature to 185 °C at a heating rate of 3 °C/min.
- Holding time of approximately 4 min. at 185 °C.

The hot mould was then placed in a cold press under a pressure of approximately 4 bar (Fig. 3.2) to ensure a fast cooling rate and a low degree of crystallinity [2]. This procedure resulted in a cooling rate of approximately 19 °C/min between 185 and 60 °C.

Once the mould had cooled to approximately 30 °C, the pressure was released and the mould was removed from the press. The panel was then removed from the mould and inspected optically.

3.1.2 Specimen preparation and mechanical testing

3.1.2.1 Mode I interlaminar fracture testing

The mode I interlaminar fracture properties of the fibre reinforced composites were studied using the double cantilever beam (DCB) geometry shown in Figure 3.3. The basic dimensions of the specimens were chosen in accordance with the ESIS (European Structural Integrity Society) protocol [3].

The DCB specimens were cut from the laminates and the hinges were fixed to one end for loading (opening). A ratio of opening displacement divided by crack length (δ/a) of less than 0.4 was employed to avoid large displacement effects. For the glass fibre/polypropylene samples, the specimen with (B) was nominally 20 mm, the thickness (2h) was approximately 4.8 mm and the specimen length was 200 mm. The length of the starter defect (a) was initially 50mm, but the bonding of the hinges, reduced the true initial crack length to 35 mm. Due to material limitations, the specimen width (B) of the woven carbon fibre/epoxy materials was nominally 15 mm. The thickness of the samples (2h) was approximately 4.8 mm and the specimen length was 135 mm. The initial length of the starter defect (a) was 35 mm and the initial crack length following bonding of the hinges was 25 mm.

Crack advance was monitored by applying a thin layer of correction fluid to one of the edges of the specimen. A scale was then marked over the region of anticipated crack growth.

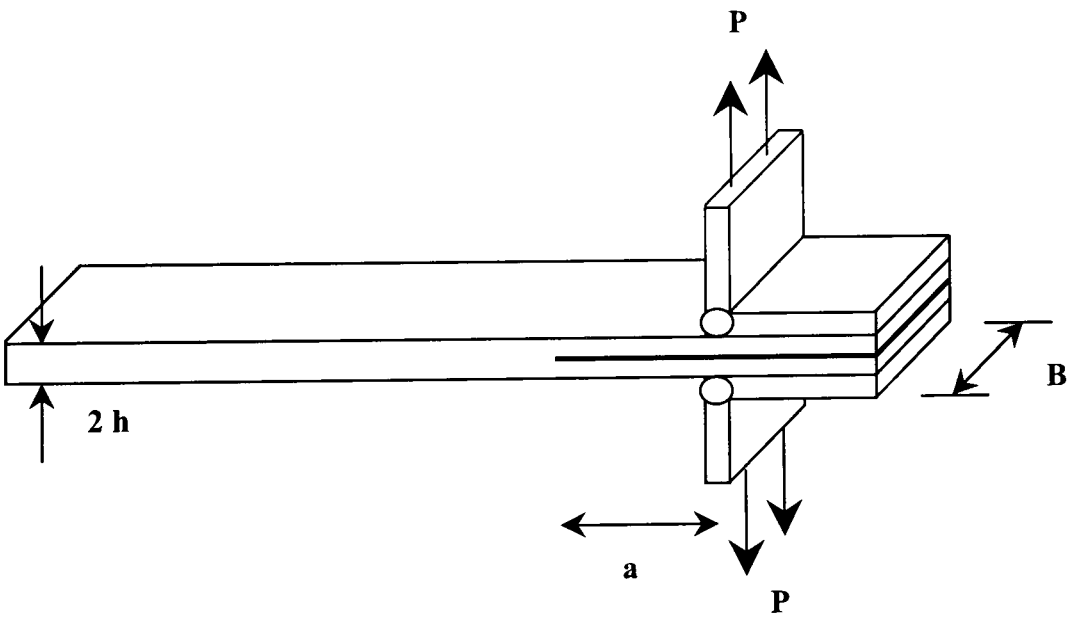

Figure 3.3 *Double cantilever beam (DCB) specimen.*

The DCB specimen was mounted in an Instron 4505 screw-driven universal test machine and the load was introduced via two piano stock hinges as shown in Figure 3.3. The use of piano hinges allowed free rotation and minimal stiffening of the specimen. The crosshead displacement rate was 1 mm/min. This rate was chosen in order to allow crack propagation to be followed and recorded easily. The specimen was loaded continuously in a displacement-control mode and the point on the load-displacement plot at which the crack initiated from the insert was recorded along with the corresponding load and displacement values. Subsequently, crack lengths were noted every five millimetres until the crack had propagated approximately 50 mm from the starter defect. The specimen was then unloaded. At least four specimens were tested for each loading condition.

The mode I interlaminar fracture energy was determined using Berry's experimental compliance calibration method. This technique assumes a compliance relationship of the form:

$$C = Ka^n \tag{3.1}$$

where **K** and **n** are experimentally-determined constants. The mode I interlaminar fracture energy was then determined using (see appendix A.1):

$$G_{Ic} = \frac{nP\delta}{2Ba} \tag{3.2}$$

where P= load, δ= displacement, B= specimen width and a= crack length.

This approach was used to determine the mode I interlaminar fracture energy of the two composite systems examined in this investigation.

3.1.2.2 Mode II interlaminar fracture testing

The mode II interlaminar fracture properties of fibre reinforced composites was studied using the end notched flexure (ENF) geometry shown in Figure 3.4. The specimen dimensions were selected following the ESIS protocol [3]. This test method yields the critical strain energy release rate, G_{IIc}, for the initiation of delamination under mode II (in-plane shear) loading conditions. The specimen configuration (i.e. the width, thickness and distance between supports) was chosen to avoid large displacements and to minimise transverse shear effects.

P

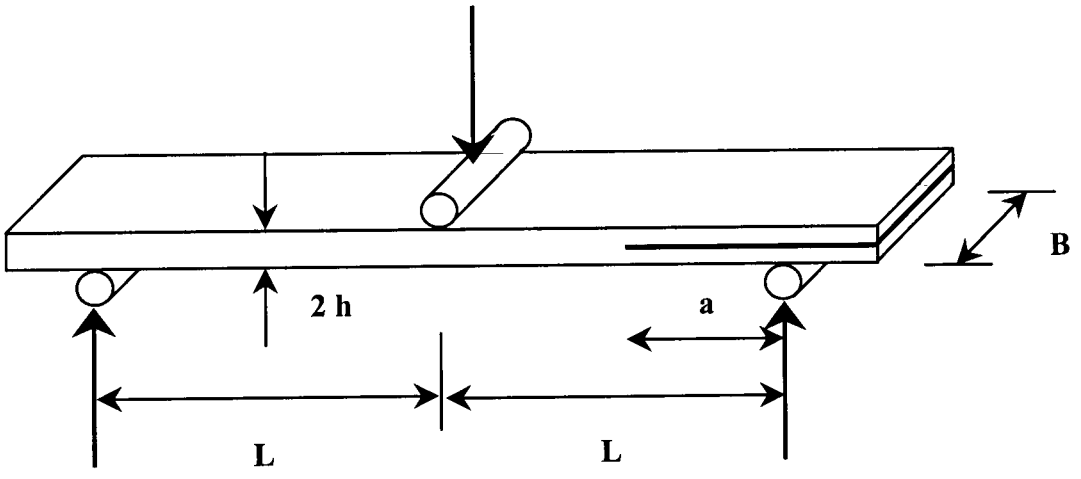

Figure 3.4 *End notched flexure (ENF) specimen.*

The nominal specimen thickness (2h) of all specimens was 4.8 mm and the width was approximately15 mm. In the case of the woven carbon fibre/epoxy composite, the total specimen length was nominally 135 mm and the distance

between the supports (2L) was 100 mm. The length of the pre-crack (a) was 25 mm, yielding a crack length to half span ratio (a/L) of 0.5.

For the glass fibre/polypropylene composite, the specimen length was approximately 200 mm and the distance between the supports was 60 mm. This reduced distance was selected to avoid top surface buckling failure of the samples [2]. For the tests, the aluminium pre-crack (a) was 15 mm long, thereby maintaining a ratio of a/L of 0.5. The width of the sample was approximately 20 mm.

The specimens were supported using the three-point bend fixture shown schematically in Figure 3.4. The specimen edges were coated with a thin layer of water-soluble typewriter correction fluid from the end of the pre-crack. The support locations were marked to enable the initial crack length to be measured accurately from the load point. The specimen was loaded in a displacement-control mode at a crosshead displacement rate of 1 mm/min. The application of the load caused a crack to propagate from the tip of the insert. As soon as the load started to drop, the specimen was unloaded and removed from the test machine. The load-displacement data were recorded and plotted.

The mode II interlaminar fracture energies, G_{IIc}, of both composite systems were determined using the direct beam theory technique where (see appendix A.2):

$$G_{IIc} = \frac{9a^2 P\delta}{2B\left(2L^3 + 3a^3\right)} \tag{3.3}$$

where a= initial crack length, P= load, δ= displacement, B= specimen width and L= half of the distance between supports.

3.1.2.3 Mixed-mode interlaminar fracture testing

The mixed-mode interlaminar fracture energy was studied using the mixed-mode flexural (MMF) geometry shown in Figure 3.5. This geometry is similar to the ENF specimen, except that the load is applied to one arm only as shown in the figure. This test geometry yields a G_I/G_{II} ratio of 1.33 [4].

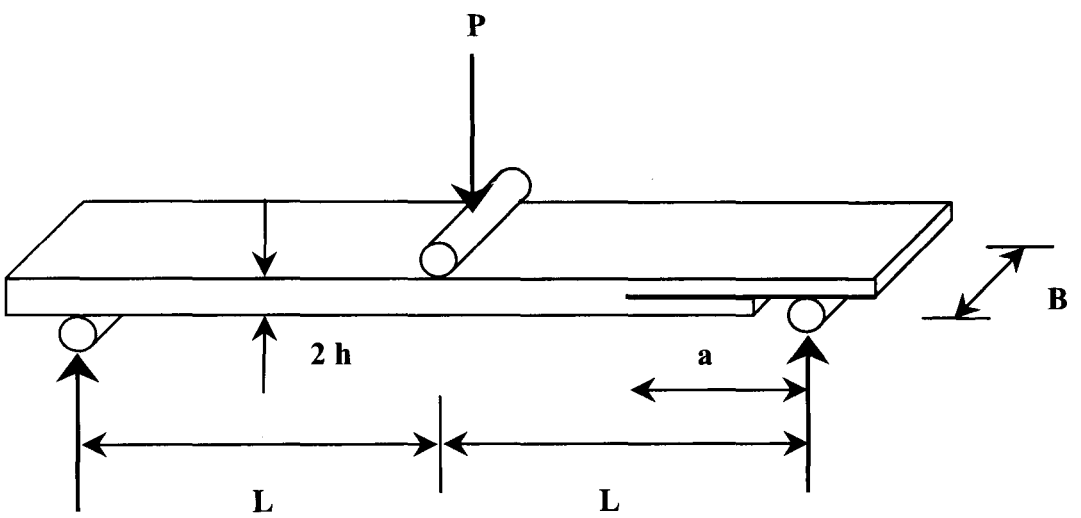

Figure 3.5 *Mixed-mode flexure (MMF) specimen.*

The specimen dimensions were the same for both the carbon fibre reinforced epoxy and glass fibre reinforced polypropylene systems. Here, the specimen thickness (2h) was 4.7 mm, the total specimen length was 200 mm and the distance between supports (2L) was 140 mm. In addition, the length of the starter defect (a) was 35 mm yielding a ratio of crack length to half span, (a/L) of 0.5. The specimen width (B) was 20 mm approximately.

The specimen was supported using the three-point bend fixture shown schematically in Figure 3.5. The specimen edges were coated with a thin layer of water-soluble typewriter correction fluid from the end of the pre-crack. The support

locations were marked to enable the initial crack length to be measured accurately from the load point.

The specimen was loaded in a displacement-control mode at a crosshead displacement of 1 mm/min forcing a crack to propagate from the insert tip. As soon as the load started to drop, the specimen was unloaded and removed. The load-displacement data was recorded and plotted. At least four specimens were tested for each material system.

The mixed-mode interlaminar fracture energy, $G_{I/IIc}$, was calculated using [5] (see appendix A.3):

$$G_{I/IIc} = \frac{21P^2a^2C}{2B\left(7a^3 + 2L^3\right)} \tag{3.4}$$

where a= crack length, P= load, C= the specimen compliance (δ/P), B= specimen width and L= half of the distance between supports.

The mixed-mode interlaminar fracture tests were performed at crosshead displacement rates between 0.1 mm/min and 2 m/s. For rates above 100 mm/min, optical monitoring was no longer possible and an inverse compliance calibration was applied using the initial and final crack lengths and the corresponding compliances. Here, intermediate crack lengths were determined by calculating the slope of the graph of 'log C' vs. 'log a'. This equation gives a relationship of the form:

$$a = 10^{\left(\frac{\log C - b}{n}\right)} \tag{3.5}$$

where a= crack length, C= the specimen compliance (δ/P) and b and n= experimentally-determined constants.

3.2 INTERFACIAL FRACTURE PROPERTIES OF THE FIBRE-METAL LAMINATES

Fibre-metal laminates (FML) are bonded arrangements of high strength aluminium sheets and fibre reinforced plastics. The most critical region in these materials is the interface between the aluminium layers and the composite plies. Therefore, the characterisation of the interfacial fracture properties of these be-material systems is highly important. The level of adhesion between the two materials was assessed using the two different composite systems.

3.2.1 Manufacturing procedures

3.2.1.1 Carbon fibre/epoxy based-FML

These fibre-metal laminates were based on type 2024-0 aluminium alloy sheets and the woven carbon fibre/epoxy (Stesapreg EP121-C15-53) described previously. Initial attention focused on optimising the interface between the composite and the aluminium substrate. Here, bi-material panels were obtained by stacking eight layers of the woven fibre composite prepreg on a 2 mm thick aluminium sheet. A folded aluminium foil with dimensions 50 x 240 mm was incorporated as a starter defect

and placed in a picture frame mould with dimensions 200 x 240 mm, as shown in Figure 3.6.

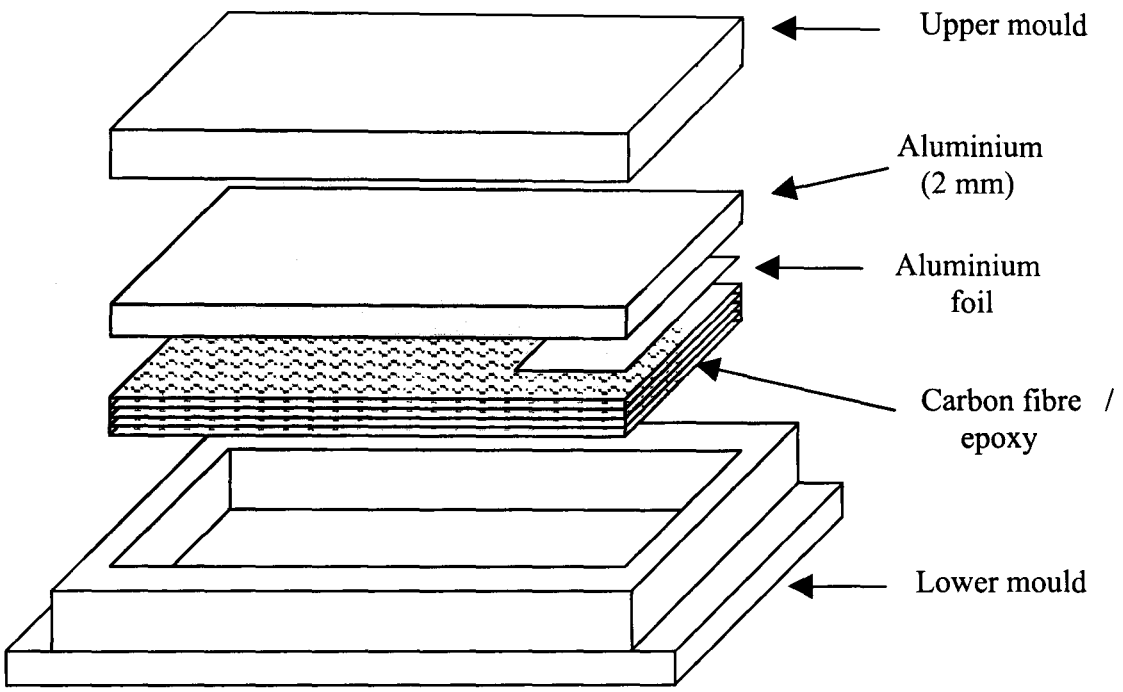

Figure 3.6 *The stacking arrangement of the carbon fibre/epoxy prepreg and the 2 mm thick aluminium sheet in the picture frame mould.*

Prior to laminating, several pre-treatments were applied to the aluminium substrate in a bid to ensure optimum adhesion to the composite plies. The pre-treatments are shown in Figure 3.7 and were:

i)- Sulphuric acid anodisation

ii)- Z6040 Silane coupling agent

iii)- Amorphous chromate coating, using hexavalent chromium, a fluoride and an accelerator.

iv)- Simple abrasion-wipe, using 1200 grit sanding paper and acetone cleaning

Treatments (i) and (iii) were undertaken by Runcorn Anodisers.

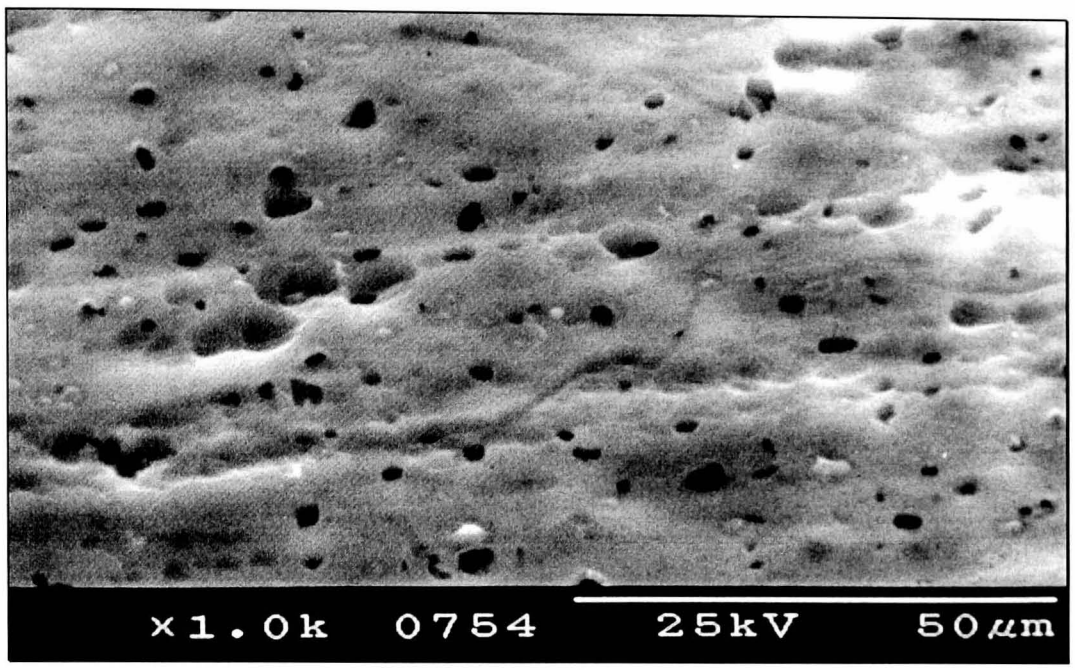

(i) *Sulphuric acid anodisation treatment*

(ii) *Silane coupling agent treatment*

Figure 3.7 *Micrographs showing the pre-treatments applied to the aluminium substrates.*

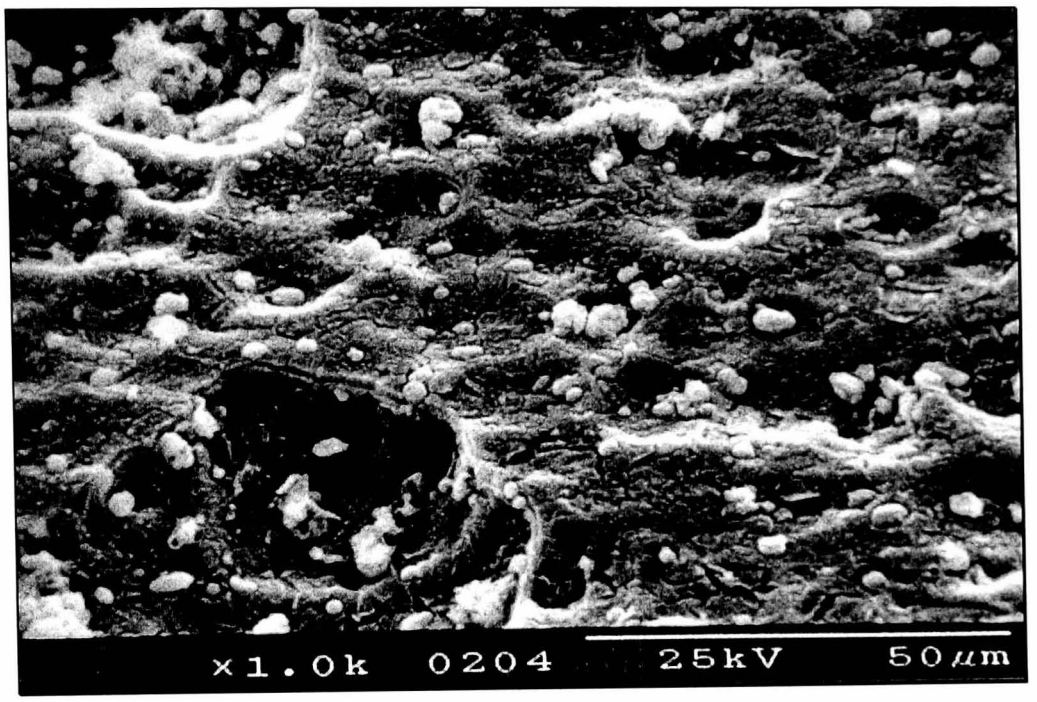

(iii) *Amorphous chromate coating treatment*

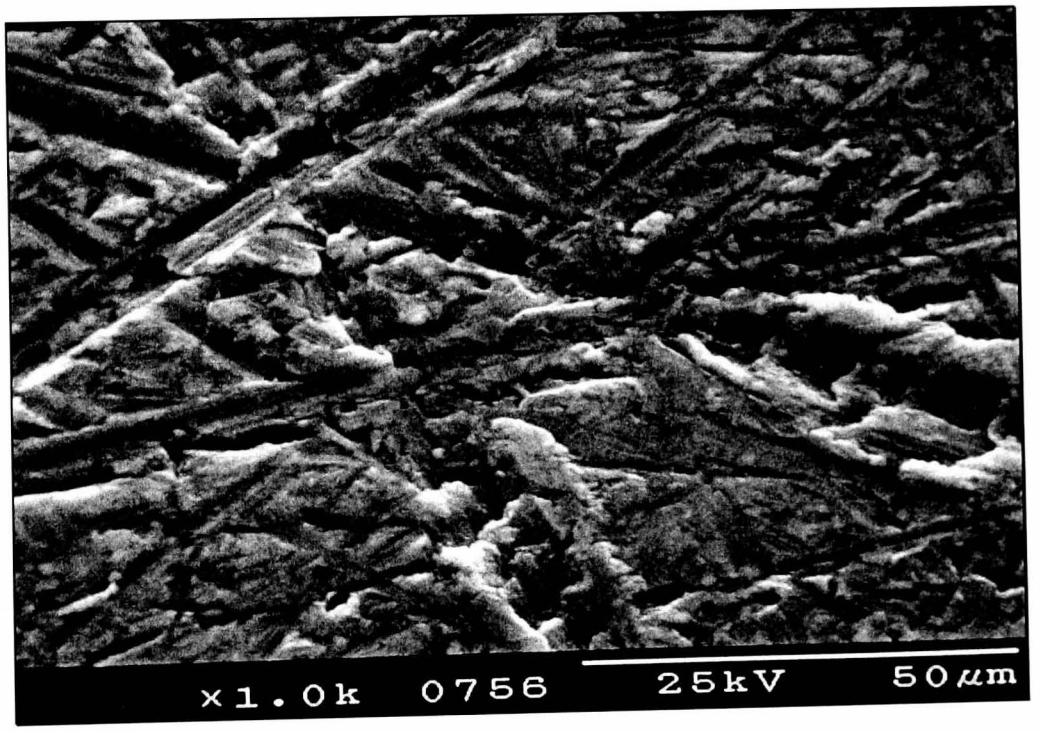

(iv) *Simple abrasion-wipe treatment*

Figure 3.7 (Cont.) *Micrographs showing the pre-treatments applied to the aluminium substrates.*

The aluminium was aligned so that the rolling direction was parallel to the fibre direction. The mould was then placed in the press under a pressure of 6 bar and the processing cycle was the same as that employed in the manufacture of the plain composite materials. Once the mould had cooled sufficiently, the pressure was released and the mould was removed from the press. The panel was then removed from the mould and visually inspected for quality.

3.2.1.2 Glass fibre/polypropylene-based FML

These fibre-metal laminates were based on type 2024-0 aluminium alloy sheets and the unidirectional glass fibre/polypropylene (Plytron) described previously. Here, bi-material panels were obtained by stacking five layers of the unidirectional fibre composite prepreg on a 2 mm thick aluminium sheet. A folded aluminium foil with dimensions 50 x 240 mm was incorporated as a starter defect and placed in a picture frame mould of dimensions 200 x 240 mm as shown in Figure 3.6.

In order to ensure optimum adhesion between the composite and the aluminium constituents, a surface treatment based on an amorphous chromate coating was applied to the aluminium alloy prior to laminating. A 0.20 mm thick pre-manufactured layer of maleic anhydride modified polypropylene (Fusabond M613-05 from DuPont de Nemours) was incorporated at the composite-metal interface to improve the adhesion.

As before, the aluminium was aligned so that the rolling direction was parallel to the fibre direction. The mould was then placed in the press under a pressure of 4 bar and the processing cycle was the same as that employed in the manufacture of the plain composite.

Once the mould had cooled sufficiently, the pressure was released and the mould was removed from the press. The panel was then removed from the mould and visually inspected for quality.

3.2.2 Specimen preparation and mechanical testing

3.2.2.1 Mixed-mode interfacial fracture tests using the single cantilever beam geometry

The single cantilever beam (SCB) specimen was used in order to investigate the interfacial fracture properties and failure mechanisms occurring within the fibre-metal laminates. The nature of this geometry yields mixed-mode loading conditions at the crack tip. The test involved bi-material specimens obtained from the panels described above, the typical specimen thickness (2h) was 4.5 mm and the total specimen length was 200 mm. The distance between the supports (L) was 100 mm, the length of the starter defect (a) was 40 mm and the width (B) was 20 mm approximately.

The specimen was supported and clamped in a steel fixture as shown in Figure 3.8. In order to facilitate the observation of the primary crack, the specimen edges were coated with a thin layer of water-soluble typewriter correction fluid starting at the end of the pre-crack. The support location was marked to enable the initial crack length to be accurately measured from the load point.

The specimen was loaded in a displacement control mode at one end forcing a crack to propagate from the tip of the insert. The point on the load displacement plot at which the crack was first observed to grow from the insert was recorded along with the corresponding load and displacement.

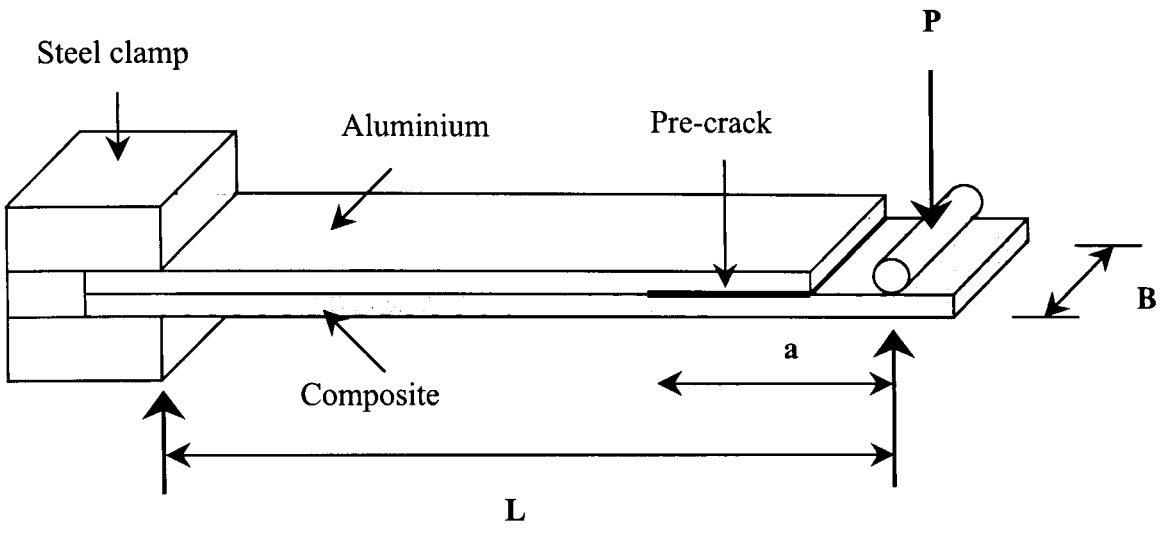

Figure 3.8 *Schematic of the mixed-mode single cantilever beam (SCB) specimen.*

As the test progressed, crack lengths were noted every 5 mm along the bi-material interface, until the crack had propagated approximately 40 mm from the starter defect. The specimen was then unloaded and removed from the test machine. The test was performed on at least four specimens. The mixed-mode interlaminar fracture energy was determined using the experimental compliance calibration method. This technique assumes a compliance vs. crack length relationship of the form:

$$C = C_o + ma^3 \tag{3.6}$$

where $\mathbf{C_o}$ and **m** are experimentally-determined constants. In this study 'm' was determined by measuring the slope of the graph of the compliance 'C' versus the cube of the crack length 'a^3'. The mixed-mode interlaminar fracture energy was then determined using (see appendix A.4):

$$G_{I/IIc} = \frac{3P^2ma^2}{2B} \tag{3.7}$$

where P= load and B= specimen width.

The mixed-mode interfacial fracture tests were performed at crosshead displacement rates between 0.1 mm/min and 2 m/s. For rates above 100 mm/min, optical monitoring was no longer possible and the inverse compliance calibration was applied. Here, the initial and final specimen compliances were determined from the initial and final slopes of the load-displacement plot. In addition, the initial and final crack lengths were measured before and after completion of the test. These two pairs of crack length and compliance data were used to establish a plot of compliance vs. the cube of the crack length (C vs. a^3). A straight line was then plotted through these two points yielding values for the slope, m, and the intercept, C_o. The crack length at any point on the load-displacement curve was then determined by inserting the compliance of the specimen, C, at that point into the following equation:

$$a = \sqrt[3]{\frac{C - C_o}{m}} \tag{3.8}$$

The tests at 2 m/s were performed using an instrumented falling-weight impact tower. Again, an inverse compliance calibration procedure was used under impact conditions. Here, however, the initial and final compliances were determined at 1 mm/min using the Instron universal test machine.

3.2.2.2 Double mixed-mode interfacial fracture tests (DMMF)

In order to gain a greater understanding of the interfacial failure mechanisms occurring in the fibre-metal laminates, the double mixed-mode flexure (DMMF) specimen shown in Figure 3.9 was used. The specimen thickness was 4.5 mm, the width was approximately 15 mm and the total specimen length was 130 mm. The distance between the supports (L) was 100 mm and the length of the starter defect (a)

was 25 mm. The starter defect was based on the same aluminium foil used in the single cantilever beam tests.

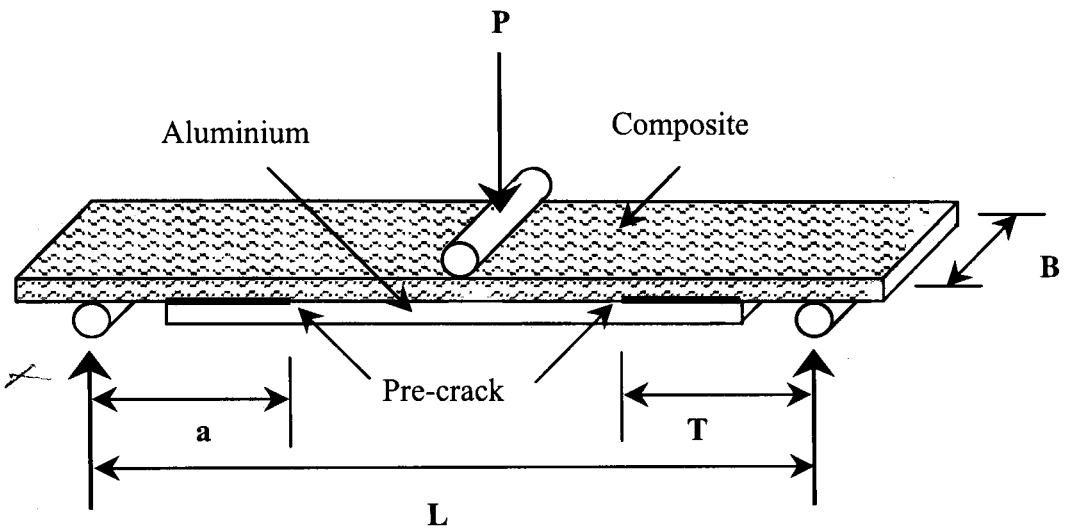

Figure 3.9 *Schematic of the double mixed-mode flexure (DMMF) specimen.*

DMMF specimens were prepared by polishing one edge of a sample containing pre-cracks at each end to a one micron finish. Prior to testing, the polished edge was coated with a thin layer of silver in a S150 sputter coater to facilitate a subsequent SEM analysis.

The specimen was supported in a three point bend fixture as shown in Figure 3.9 and loaded in a displacement-control mode. Once one of the cracks started to propagate from the aluminium pre-crack, the test was stopped and the sample was unloaded. The specimen was then removed from the fixture and both the propagated and unpropagated cracks were examined in the scanning electron microscope. In order to investigate the interfacial failure mechanisms at the same crosshead displacement rates that were applied in the SCB specimens, the double mixed-mode interfacial fracture tests were performed at crosshead displacement rates between 0.1 mm/min and 2 m/s.

The DMMF geometry clearly differs from that of the SCB configuration and does not necessarily offer the same loading conditions (G_I/G_{II}) at the crack tip. In spite of this, it was felt that this geometry offered useful information regarding the interfacial failure processes in fibre-metal laminates

3.3 MECHANICAL PROPERTIES OF THE FIBRE-METAL LAMINATES

Once the aluminium/composite interface had been optimised and the interfacial failure mechanisms highlighted, the mechanical properties of a range of fibre-metal laminates were investigated. These fibre-metal laminates were based on both the carbon fibre reinforced epoxy and the glass fibre reinforced polypropylene composite systems. A number of different stacking sequences were evaluated in this part of the research project in order to investigate the influence of varying the volume fraction (V_f) of the constituent materials on the final properties of the fibre-metal laminates.

3.3.1 Manufacturing procedures

3.3.1.1 Carbon fibre/epoxy-based FML

The carbon fibre-metal laminates were based on type 2024-0 aluminium alloy sheets and the woven carbon fibre reinforced epoxy (Stesapreg EP121-C15-53) described in Section 3.1.1.1. Here, the stacking sequences shown in Table 3.1 were manufactured using the manufacturing process outlined in section 3.2.1.1. Here, a 2/1 configuration refers to a laminate in which two 0.8 mm thick aluminium alloy sheets are situated either side of a single composite prepreg layer as shown in Figure 3.10. The aluminium and composite layers were placed in a picture frame mould of dimensions 200 x 240 mm. In all laminates the rolling direction of the aluminium layers was oriented in the direction of the fibres.

Laminate	Configuration	Laminate thickness (mm)
2/1	2 aluminium layers + 1 composite ply	1.88
3/2	3 aluminium layers + 2 composite plies	2.96
4/3	4 aluminium layers + 3 composite plies	4.02
2/5	2 aluminium layers + 5 composite plies	3.00
2/17	2 aluminium layers + 17 composite plies	6.20

Table 3.1 *Summary of the carbon fibre-based FML's investigated in this programme.*

A simple abrasion-wipe surface treatment was applied to the aluminium sheets prior to manufacturing. As a result, the degree of adhesion should be comparable to that measured on the bi-material configuration. The panel was then removed from the mould and the specimens were cut from it.

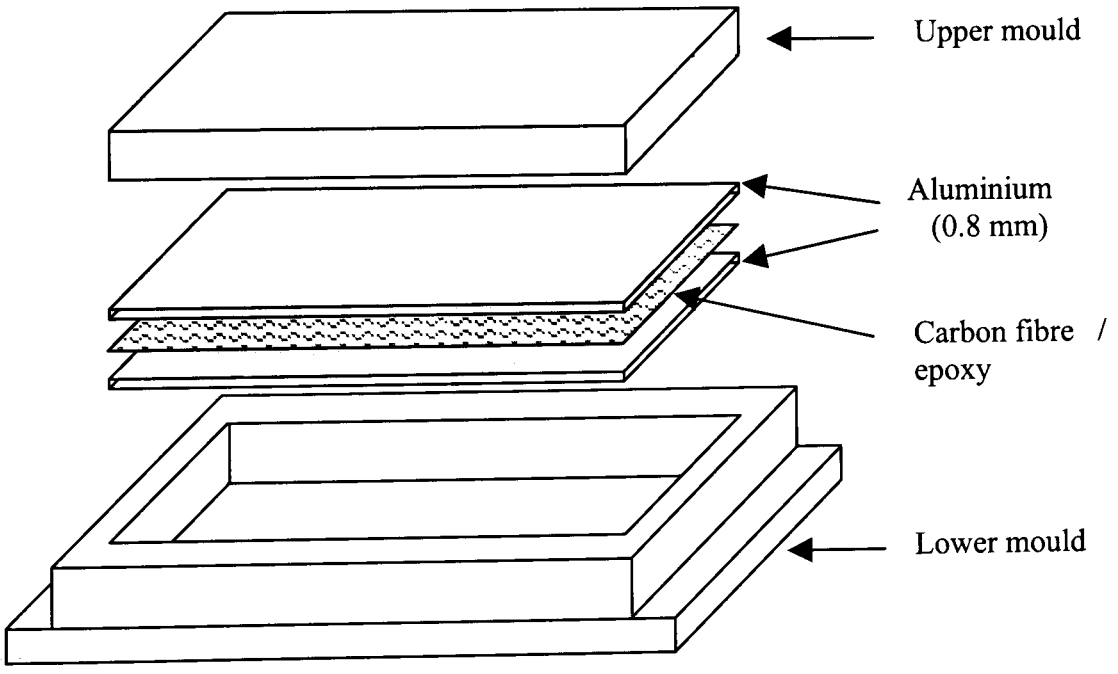

Figure 3.10 *The stacking sequence of the (2/1) carbon fibre-based fibre-metal laminate.*

3.3.1.2 Glass fibre/polypropylene-based FML

These glass fibre-metal laminates were based on layers of type 2024-0 aluminium alloy and plies of unidirectional glass fibre/polypropylene (Plytron). Tests were undertaken on the stacking sequences shown in Table 3.2 that were manufactured according to the bi-material manufacturing process.

Laminate	Configuration	Laminate thickness (mm)
2/1	2 aluminium layers + 1 composite ply	2.50
3/2	3 aluminium layers + 2 composite plies	4.30
4/3	4 aluminium layers + 3 composite plies	5.70
2/8	2 aluminium layers + 8 composite plies	6.00

Table 3.2 *Summary of the glass fibre-based FML's investigated in this programme.*

As before, a 2/1 configuration refers to a laminate based on two 0.8 mm thick aluminium alloy sheets either side of a composite prepreg layer. Both the aluminium sheets and the composite layers were placed in a picture frame mould of dimensions 200 x 240 mm. An amorphous chromate coating was applied to the surface of the aluminium sheets prior to manufacturing.

3.3.2 Specimen preparation and mechanical testing

3.3.2.1 Flexural testing

The flexural properties of the aluminium, the carbon fibre reinforced plastic and the glass fibre reinforced polypropylene materials were investigated under three point loading conditions. Following this, the flexural properties of fibre-metal

laminates based on both composite systems were evaluated in order to highlight the effect of varying the composite volume fraction (V_f) on the flexural modulus and strength. The specimens were cut from the panels parallel to rolling and fibre directions. Flexural tests were conducted according to the ASTM D 790 standard [6]. The loading regime for a (2/1) flexural specimen is shown in Figure 3.11.

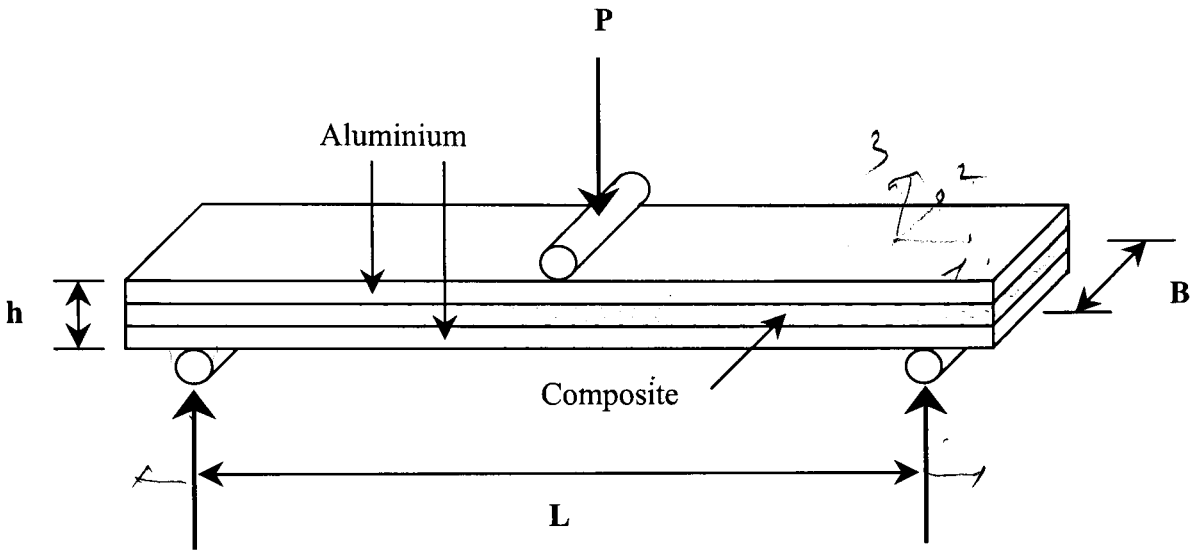

Figure 3.11 *Schematic illustration of the three point bend test geometry.*

The specimens were mounted on a three point bend fixture and loaded centrally as shown above. The specimen width (B) was 15 mm and a span/thickness (L/h) ratio of 32 to 1 was employed throughout. The specimens were loaded at crosshead displacement rates between 3.2 and 8.4 mm/min depending on the thickness (h) and span (L) of the sample. The flexural strength was calculated at the maximum stress using the following equation:

$$\sigma_f = \frac{3PL}{2Bh^2} \cdot \left[1 + 6\left(\delta/L\right)^2 - 4\left(h/L\right)\left(\delta/L\right)\right] \tag{3.9}$$

where σ_f= stress in the outer layer at midspan, P= load at a given point on the load displacement curve, L= support span, B= width of the specimen tested, h= thickness of the specimen tested and δ= the deflection of the centreline of the specimen at the middle of the support span.

The first part of the equation applies to a specimen of homogeneous, elastic material tested in flexure as a simple beam under three point bend regime. When span/thickness ratios greater than 32 to 1 are used, significant end forces are developed at the supports which affect the moment in a simply supported beam. An approximate correction factor is applied in the second part of the Equation 3.9 to correct for these end forces where relatively large deflections exist. It is worth noting that this is only a simplified approach because it assumes that the sample is isotropic.

The modulus of elasticity was calculated by drawing a tangent to the steepest initial straight line portion of the load-displacement curve and using the following equation:

$$E = \frac{L^3 m}{4Bh^3} \tag{3.10}$$

where E= modulus of elasticity in bending, L= support span, B= width of the specimen, h= thickness of the specimen and m= slope of the tangent to the initial straight line portion of the load-displacement curve.

During each test, the load-displacement data were recorded and plotted. After failure, the specimens were removed from the test fixture for optical examination of the failure mode.

A greater insight into the flexural failure mechanisms occurring during the fracture process was achieved by examining the edges of a number of samples during testing. Here, the edges of the samples were polished to a one micron finish and coated with a thin layer of silver in a S150 sputter coater in preparation for examination in the SEM. The specimens were then loaded to a pre-determined stress and unloaded. The specimens were then examined in a Hitachi S-2460N scanning electron microscope. Once this had been completed, the specimens were loaded to a higher stress and the procedure was repeated. This continued until the specimen had fractured.

3.3.2.2 Tensile testing

The tensile properties of the plain aluminium, the carbon reinforced plastic and the glass fibre reinforced polypropylene were investigated at quasi-static rates of loading. Following this, the tensile properties of fibre-metal laminates based on both composite systems were evaluated in order to highlight the effect of varying the composite volume fraction (V_f) on the tensile modulus and strength. The specimens were cut from the panels parallel to rolling and fibre directions.

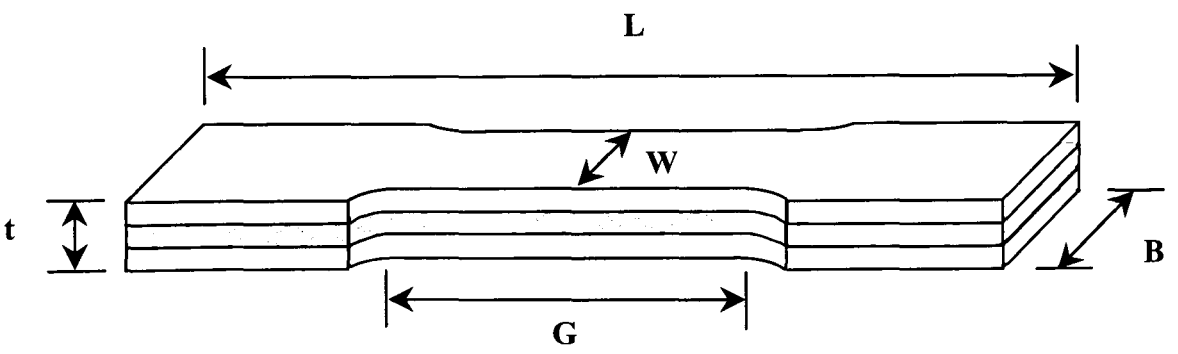

***Figure 3.12** Schematic illustration of the tensile geometry*

where, G= gauge length, W= working section width, t= thickness, B= grip section width and L= total specimen length.

Tensile tests were conducted according to the ASTM D 3039, B557M, and D638 [7,8,9] standards. A number of authors have employed straight-sided tensile specimens [10] to characterise the tensile properties of fibre-metal laminates, however more consistent and reliable data have been obtained using dog-bone shape tensile specimens. A typical (2/1) dog-bone tensile specimen is shown in Figure 3.12.

The working section of each sample was 10 x 60 mm and the length, L, was 200 mm. The specimens were placed in a screw-driven Instron 4505 universal test machine and a clip-on extensometer was attached to the gauge section to measure the elastic modulus. Testing was conducted at crosshead displacement of 1 mm/min and the load-displacement data were recorded.

The tensile strength was calculated using the following equation:

$$\sigma_t = \frac{P}{Wt} \tag{3.11}$$

where σ_t= ultimate tensile strength, P= maximum load, W= working section width and t= thickness. Again, this Equation assumes that the specimen is isotropic.

The modulus of elasticity was measured using a 12.5 mm gauge length clip-on extensometer and calculated using:

$$E = \left(\Delta P / \Delta l\right) \cdot \left(l / Wt\right) \tag{3.12}$$

where E= modulus of elasticity, $\Delta P/\Delta l$= slope of the plot of load as a function of deformation within the linear portion, l= gauge length of the extensometer, W= working section width and t= thickness. Once the specimen failed, it was removed from the grips for subsequent optical examination.

The tensile failure mechanisms occurring during the fracture process were highlighted by polishing a number of specimens to a one micron finish and coating the edge of the specimens with a thin layer of silver. The specimens were then loaded to a pre-determined stress and unloaded. The specimens were then examined in a Hitachi S-2460N scanning electron microscope. Once this had been completed, the specimens were loaded to a higher stress and the procedure was repeated. This continued until the specimen fractured

3.3.2.3 Low velocity impact testing

The dynamic properties of the fibre-metal laminates based on thermosetting and thermoplastic matrices were investigated by conducting low velocity impact tests on the instrumented falling weight impact tower shown in Figure 3.13. Here, a 2 kg carriage was released from heights of up to 0.8 metres onto plates supported on a 75 mm internal diameter circular ring. A piezoelectric load cell located just above the 12.7 mm diameter impact head was used to measure the impact force and this signal was recorded by a Packard Bell computer using the Dataflow plus software package. After impact, the carriage was caught in order to avoid secondary impacts. The impact tests were performed on 2/1, 3/2 and 4/3 thermosetting and thermoplastic based fibre-metal laminates with dimensions 100 x 100 mm approximately. Impact energies up to 20 Joules were considered.

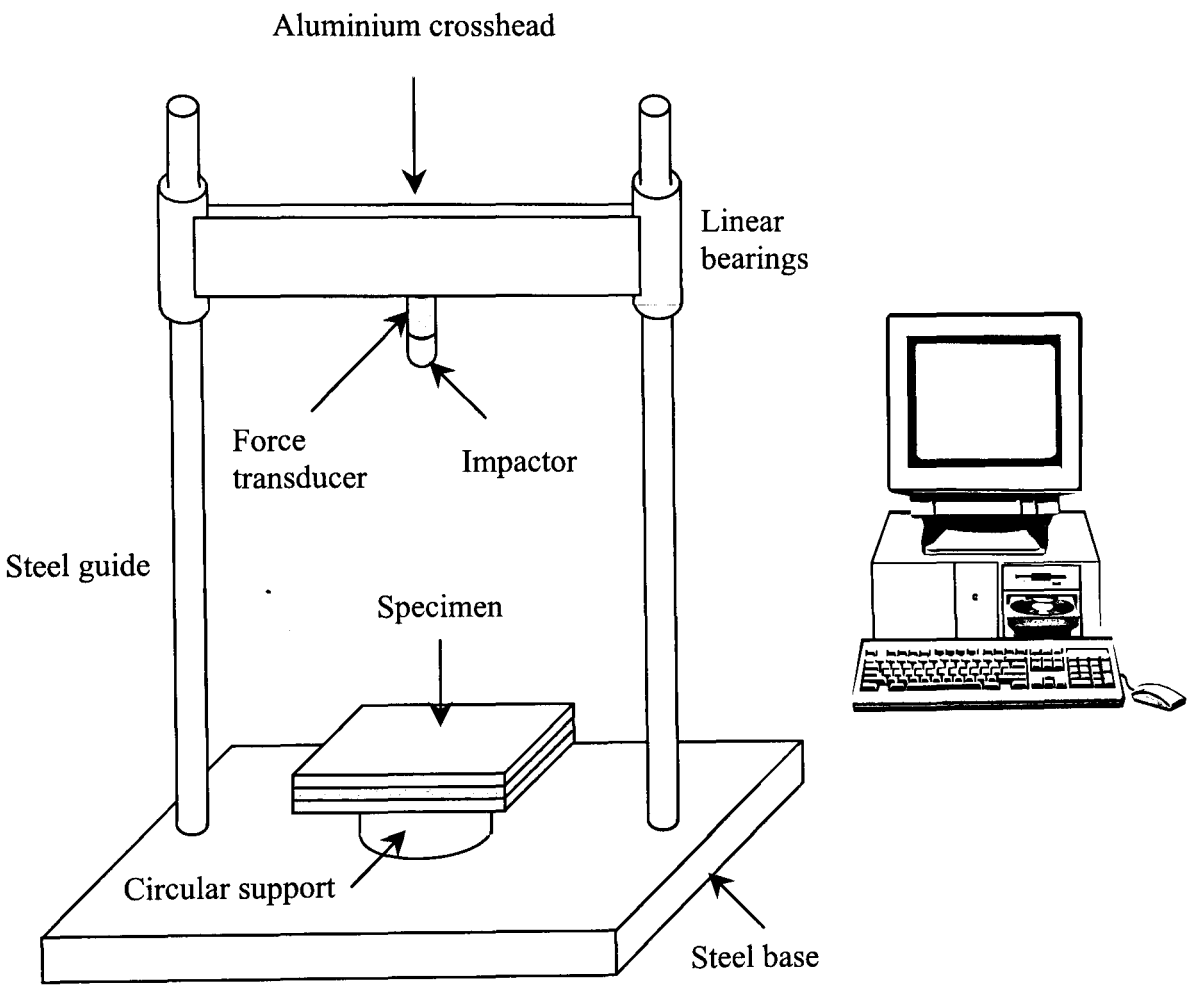

Figure 3.13 *Instrumented falling-weight impact tower.*

In order to elucidate the impact failure mechanisms occurring in both types of fibre-metal laminate, a number of impacted specimens were sectioned close to the impact site and polished for optical examination under a Wild-Heerbrugg and a Leitz Wetzlar Metalloplan optical microscope.

3.3.2.4 Post-impact tensile testing

The post-impact residual strength of the fibre-metal laminates were investigated by conducting low velocity impact tests on the instrumented falling weight impact tower shown in Figure 3.13. Here plates with dimensions 200 x 240 mm were tested and subjected to impact energies up to 20 Joules.

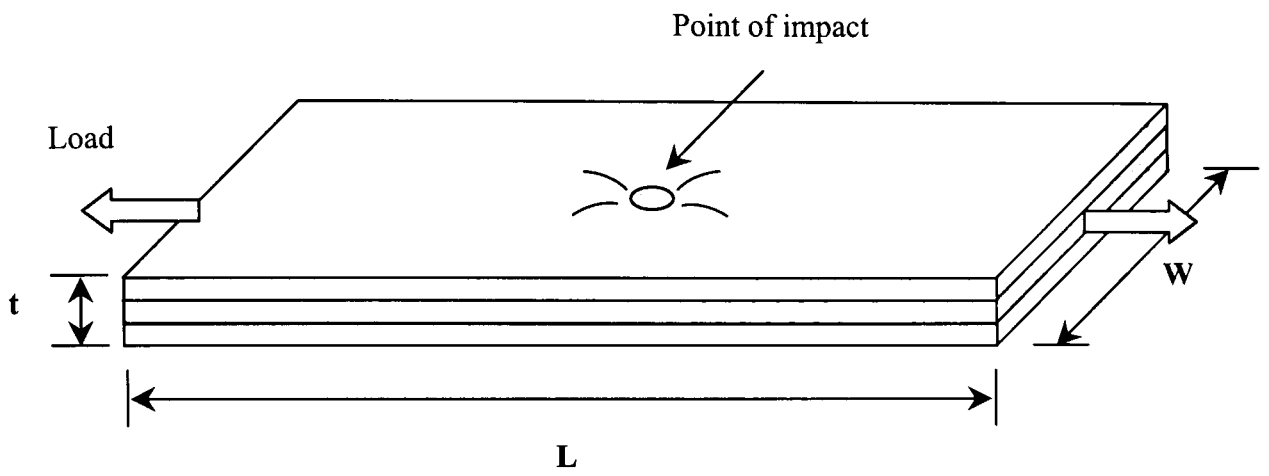

Figure 3.14 *Schematic of the test geometry for measuring the residual tensile strength of the impact-damaged laminates*

After impact, specimens with dimensions 200 x 50 mm were removed from the impacted plates using a band saw. The edges of the samples were then ground to a 600 grit finish to remove any scratches or defects. Tensile tests were conducted on the damaged specimens at 1 mm/min as shown in Figure 3.14. The tensile strength was then calculated at maximum load using Equation 3.11. After failure, the specimens were removed for examination.

3.3.2.5 Single edge notch bend tests

The work of fracture $\mathbf{W_f}$ of the plain aluminium alloy, the plain composites and the fibre-metal laminates was evaluated using the single edge notch bend (SENB) geometry shown in Figure 3.15. The dimensions of SENB specimens were 75 x 15 mm x thickness. Notches with a length to depth ratio, a/W of 0.5 were introduced at the mid-span using a saw and sharpened with a fresh razor blade. The specimens

were supported on two 6 mm diameter rollers positioned 60 mm apart and loaded at a crosshead displacement rate of 2 mm/min in the Instron 4505 universal test machine.

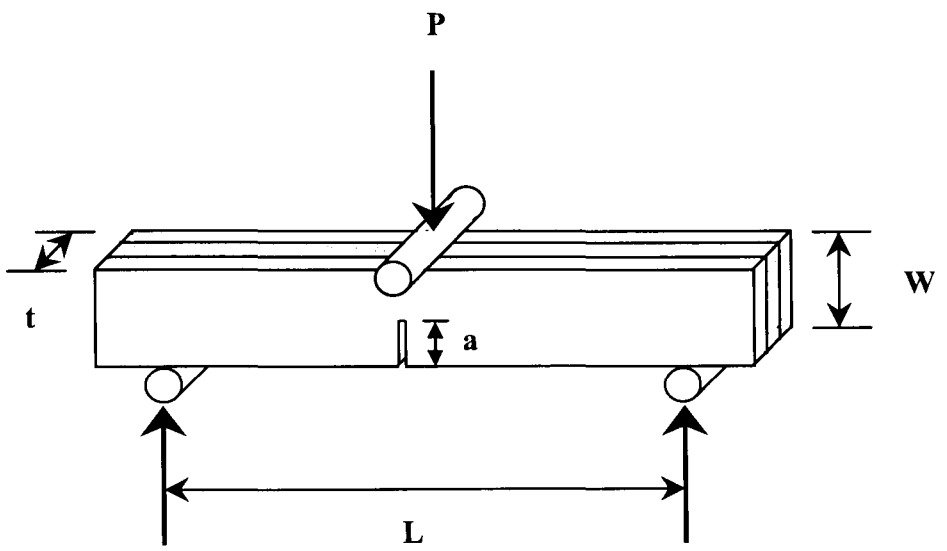

Figure 3.15 *Single edge notch bend (SENB) specimen.*

During the test, the crack propagated through the specimen thickness and the load-displacement data were recorded in order to estimate the energy absorbed by the specimen. The work of fracture was calculated using:

$$W_f = {U}/{t(W-a)} \qquad (3.13)$$

where, W_f= work of fracture, U= energy absorbed by the specimen, t= specimen thickness, W= specimen width and a= notch length. After failure, the specimen was removed from the fixture for low magnification optical examination.

At impact rates of strain, tests were undertaken using the instrumented falling weight impact tower. Here, the impact velocity was 3 m/s and the carriage weight was 9.976 kg. During the test, the force-time data were recorded.

The impact energy under the load-time trace was calculated using [11]:

$$E_{tot} = v_o . A_{tot} \left(1 - \frac{v_o . A_{tot}}{4 E_o} \right) \tag{3.14}$$

where, v_o= impact velocity just before impact, A_{tot}= total area under the curve, E_o= energy of the striker before impact. The work of fracture was then calculated by dividing the absorbed energy by the ligament of the SENB specimen.

3.3.2.6 High velocity impact testing

In order to evaluate the high velocity impact response of the thermosetting and thermoplastic-based fibre-metal laminates, a nitrogen gas gun was used. Figure 3.16 shows a schematic illustration of the test set-up used in order to assess the high velocity impact properties of these hybrid systems.

Here, square plates with dimensions 100 x 100 mm were clamped in a steel support with a 75 x 75 mm square aperture. The rig was then bolted to a steel backing plate. Once the target was in position, a velocimeter was placed between the exit of the barrel and the target in order to measure the velocity of the projectile, from which the incident impact energy was calculated. Here, the velocimeter determined the time required for the projectile to pass between two photoelectric sensors. This procedure ensured 99.6% minimum accuracy. Impact testing was conducted using a 46.8 grams steel projectile with a 12.7 diameter hemi-spherical head. The velocity of the projectile was controlled by adjusting the pressure in the main chamber of the gas gun shown in Figure 3.16.

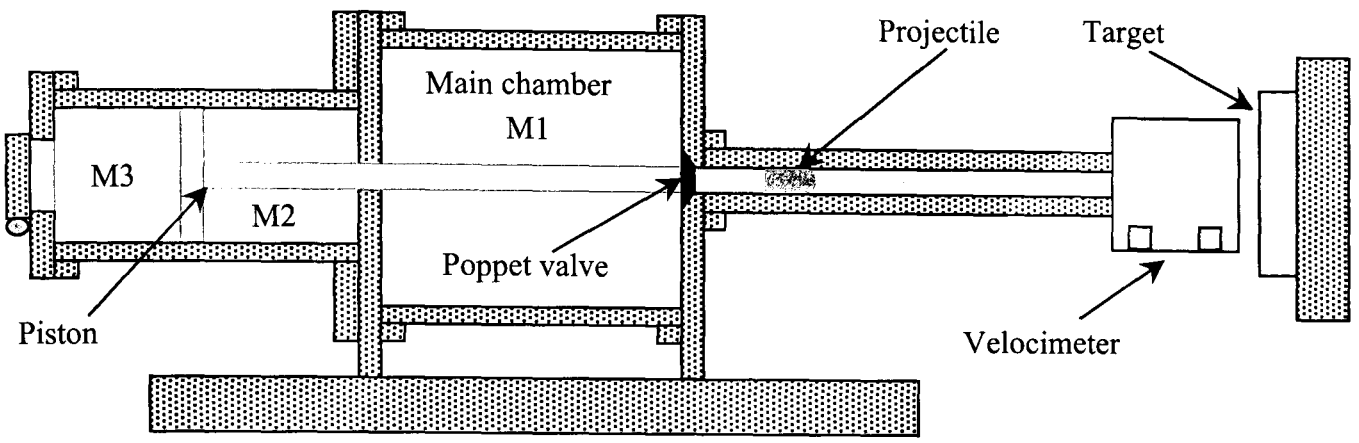

Figure 3.16 *Schematic illustration of the set-up for the high velocity impact test set-up.*

Impact testing was performed over a range of impact energies until complete perforation of the target was achieved. After testing, the specimens were removed from the rig and sectioned and polished in order to elucidate the failure mechanisms in these thermosetting and thermoplastic-based fibre-metal laminates at dynamic rates of loading. The perforation energy was then used to calculate the specific perforation energy. Here, the perforation energy was normalised by the areal density of the target.

3.4 FAILURE MECHANISMS AND DAMAGE CHARACTERISATION

During fracture testing of the plain composite materials and the fibre-metal laminates, several fractured and damaged surfaces were exposed. In this programme, the following techniques were employed to investigate the failure processes and mechanisms in the composites and fibre-metal laminates.

3.4.1 Optical microscopy

In order to identify and highlight some of the failure mechaisms a Wild-Heerbrugg M8 low power magnification microscope was used. This microscope was used to estimate the damage area in the impacted speciens as well. A Leitz Wetzlar Metalloplan optical microscope was used at higher magnifications to highlight the failure mechanisms in more detail. Both microscopes produced high quality images.

3.4.2 Scanning electron microscope

A Hitachi S-2460N scanning electron microscope (SEM) was used in a number of key areas in this study. The fracture surfaces of the tested samples and the failure mechanisms ocurring during tests on the fibre-metal laminates were examined in detail. Prior to placing the specimens in the scanning electron microscope, the fracture surface to be examined was coated with a thin layer of silver using a S150 sputter coater.

3.5 REFERENCES

[1] **Davies, P., Cantwell, W., Kausch, H.H.**, Composites Science and Technology, **35** (1989), pp.301-313.

[2] **Davies, P., Cantwell, W.J.**, Composites, **25** No.9 (1994), pp 869-877.

[3] **European Structural Integrity Society (ESIS)**, Protocols for Interlaminar Fracture Testing, Davies, P.,IFREMER (1993).

[4] **Blyton, M.**, PhD thesis, The University of Liverpool (1999).

[5] **Russell, A.J., Street, K.N.**, Delamination and Debonding of Materials, ASTM STP 876, W.S. Johnson, Ed. (1985), pp 349-370.

[6] **ASTM standard** D790-80, Annual book of ASTM standards (1981) **35**, Philadelphia, U.S.A.

[7] **ASTM standard** D3039-76, Annual book of ASTM standards (1981) **36**, Philadelphia, U.S.A.

[8] **ASTM standard** B557M-81, Annual book of ASTM standards (1982) **7**, Philadelphia, U.S.A.

[9] **ASTM standard** D638-80, Annual book of ASTM standards (1981) **35**, Philadelphia, U.S.A.

[10] **Wu, H.F., Wu, L.L.**, Journal of Materials Science **29** (1994), pp.5847-5851.

[11] **Takahashi, K., Yee, A.F.**, Impact Fracture of Polymers, Kyushu University Press, 1991, pp 425-473.

4. RESULTS AND DISCUSSION

In order to fully characterise and elucidate the mechanical and fracture properties of novel fibre-metal laminates based on thermoset and thermoplastic matrices, a number of well-defined mechanical tests have been carried out. Initially, the interlaminar fracture properties of the plain composite materials have been evaluated. Once this was achieved, attention focused on the optimisation of the level of adhesion at the bi-material interface over a range of loading rates. Subsequently, testing of the in-plane fracture properties, low velocity impact and post-impact residual strength was also performed. In addition, the work of fracture and high velocity impact response of these novel fibre-metal laminates were evaluated.

4.1 INTERLAMINAR FRACTURE PROPERTIES OF THE COMPOSITE MATERIALS

It is well known that composite structures based on plies or laminates are extremely susceptible to crack initiation and propagation along the laminar interfaces in various failure modes [1]. In fact, delamination is one of the most deleterious crack growth modes in composites, since it can cause a severe reduction in the in-plane strength and stiffness, potentially leading to catastrophic failure of the whole structure [1]. Consequently, the evaluation of these properties is an important and necessary requirement.

4.1.1 Fracture toughness and post-failure fractography

The interlaminar fracture toughness of both types of composites used in this programme were evaluated by conducting mode I, mode II and mixed-mode I/II tests at a crosshead displacement rate of 1 mm/min. In general, the initial load-displacement response of both materials exhibited a steady linear increase in load with increasing crosshead displacement. Figure 4.1 shows typical load-displacement

traces resulting from these three testing modes on the woven carbon fibre/epoxy (CFRE). The mode I load-displacement trace for this material displays a saw-tooth crack growth appearance (Figure 4.1a). Here, the delamination crack has multiple crack fronts, one in each warp yarn. Therefore, the crack advances more rapidly where the exposed yarns are aligned parallel to the crack direction. Thus, the overall crack front is discontinuous in appearance [1]. In addition, due to the woven nature of the composite material, no fibre bridging is present to stabilise crack growth [2]. After unloading, a small residual displacement is apparent on the trace, this is likely to be a result of plastic deformation within the composite substrate. The mode I interlaminar fracture energy was determined at each of the peaks on the trace. Under mode II loading, crack growth was stable with a crack propagating in a controlled manner to the centre of the sample (Figure 4.1b). As in mode I loading, a residual displacement is apparent after unloading the sample. Stable crack growth in other fibre reinforced epoxies under mode I and mode II loading conditions has been observed [3]. Surprisingly, failure in all of the mixed-mode samples occurred in a highly unstable manner with the crack propagating some distance from the starter defect (Figure 4.1c). Here, the condition for stable crack growth (dG/da) is believed to be > 0. Consequently, crack propagation was unstable under mixed-mode loading conditions.

Figure 4.2 shows a typical plot of log C vs. log a for a CFRE double cantilever beam sample tested at 1 mm/min. The data clearly fall on a straight line, which yields a value of n of 2.28. Figure 4.3 shows a typical resistance curve for mode I test on a CFRE sample. The data points indicate that the values of G_{Ic} tend to decrease with increasing crack length. The reason for this is not clear although it is possible that the stiffening effects of the piano hinges influence the load displacement response at short crack lengths. There was no evidence of crack bridging in these samples, which is to be expected since the composite is based on a woven fabric which renders bridging difficult [2]. The interlaminar fracture energies under mode I, mode II and mixed-mode I/II testing were calculated from the load-displacement data using Equations 3.2, 3.3 and 3.4 respectively.

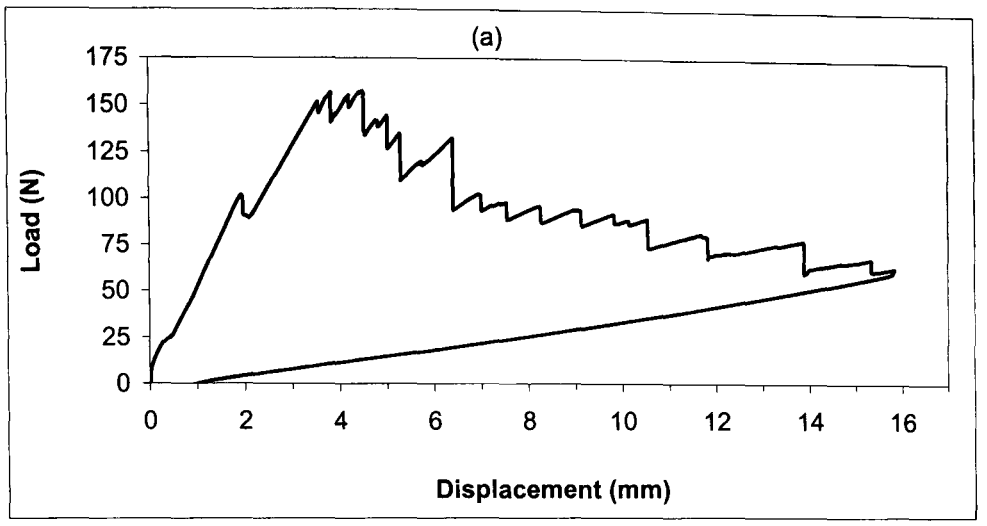

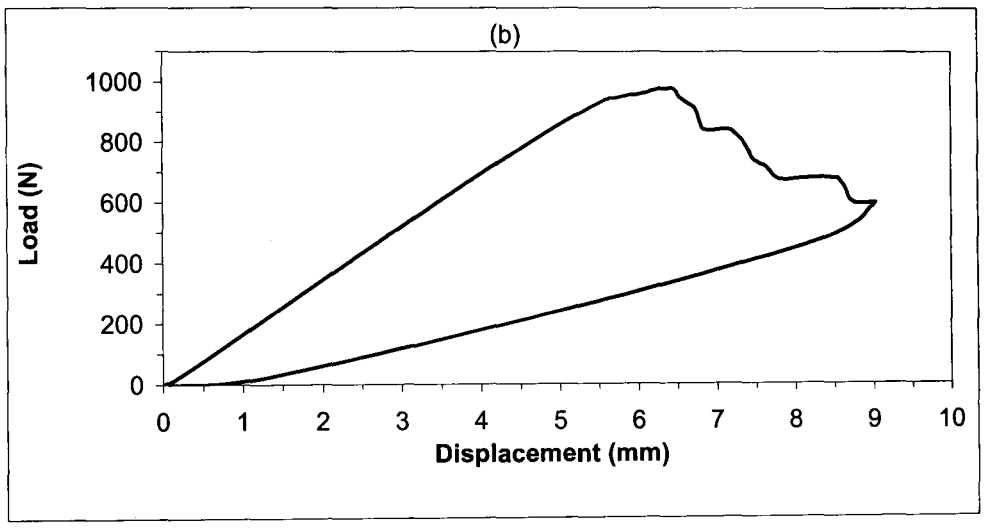

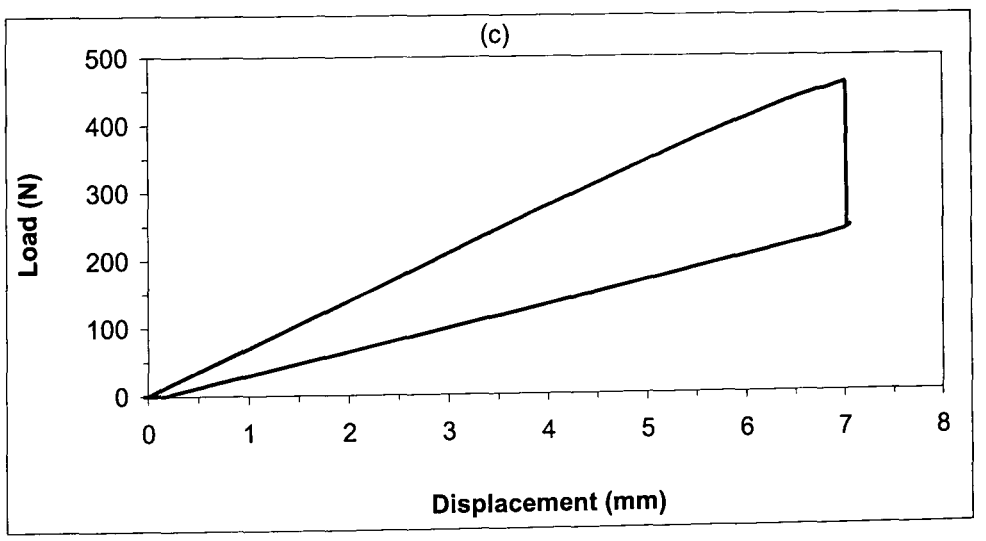

Figure 4.1 *Typical load-displacement curves following (a) mode I, (b) mode II and (c) mixed-mode I/II interlaminar loading of the CFRE composite.*

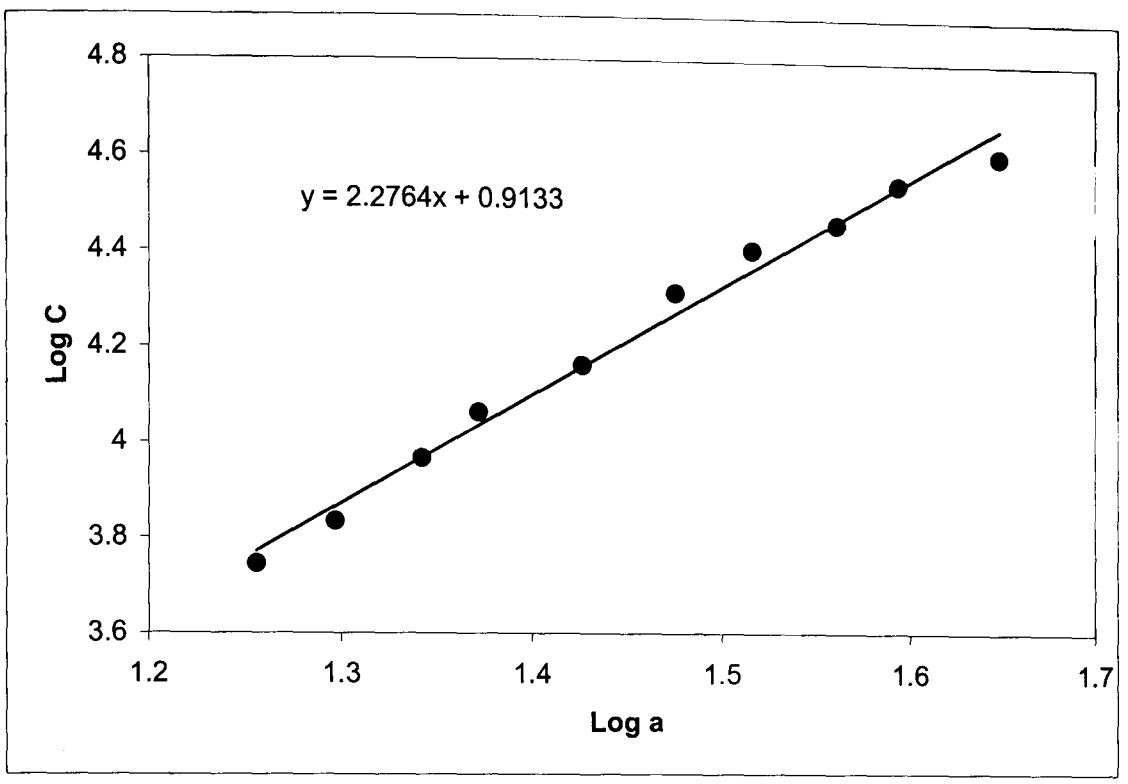

Figure 4.2 *Typical plot of log C vs. log a following a mode I test on a CFRE sample at 1 mm/min.*

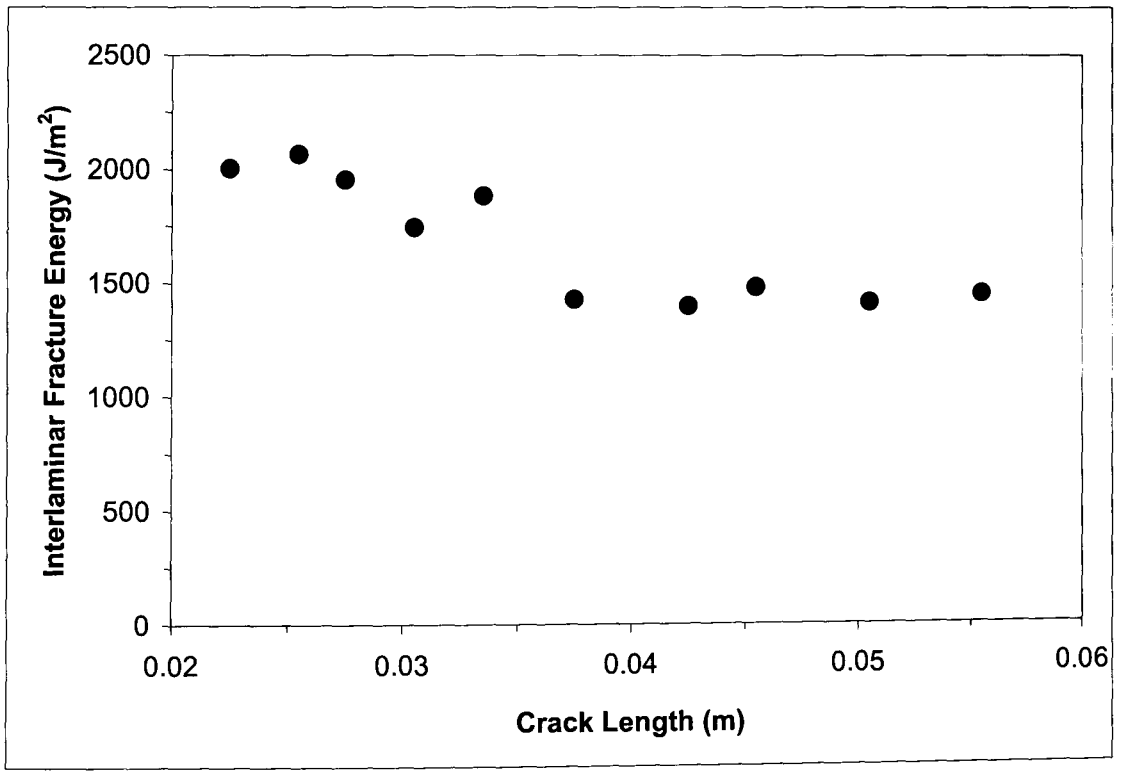

Figure 4.3 *Typical resistance curve following a mode I test on a CFRE sample at 1mm/min.*

Figure 4.4 summarises the results of the interlaminar fracture tests on the woven carbon fibre/epoxy (CFRE). The mode I interlaminar fracture tests yielded average values of G_{Ic} of 1900 J/m^2 and the mode II tests resulted in a very high average value of 4150 J/m^2. Here, the interlaminar fracture energy was calculated at the maximum load of the load-displacement trace as that shown in Figure 4.1b. Similarly, the mixed-mode I/II interlaminar fracture energy was evaluated at the maximum load point yielding an average value of 2150 J/m^2. It is worth noting that these values of G_{Ic} and G_{IIc} comfortably exceed those reported following tests on similar carbon fibre/epoxy systems [1,4], where values of G_{Ic} and G_{IIc} were of the order of 900 and 1500 J/m^2 respectively. It is interesting to note that the value of $G_{I/IIc}$ is close to that of the G_{Ic} of the composite despite the high value of G_{IIc} exhibited by this material. In this specimen the ratio of G_{Ic}/G_{IIc} is 4/3. This suggests that is the mode I effect that is heavily dominant under mixed-mode loading conditions. Similar trends have been observed for other carbon fibre reinforced epoxies [5].

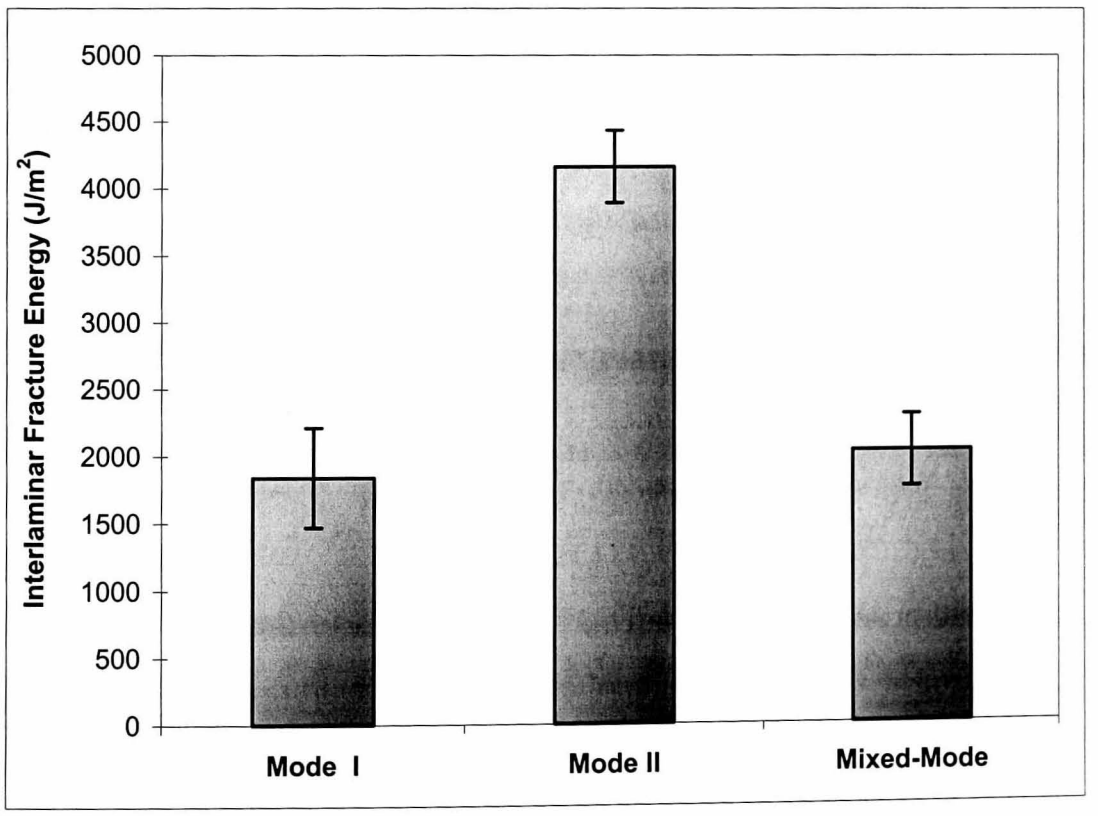

Figure 4.4 *Summary of the interlaminar fracture properties of the carbon fibre reinforced epoxy composite.*

Typical scanning electron micrographs of the fracture surfaces of the rubber toughened CFRE samples tested under the three modes of loading are shown in Figure 4.5. Here, crack propagation is from right to left. In the case of mode I fracture, the maximum principal stress lies perpendicular to the plane of failure. Consequently, brittle cleavage accompanied with traces of plastic flow of the matrix material occurs and fibre fracture rarely happens in this tough composite system. The mode I fracture surface exhibited a relatively flat appearance with a large number of chevron markings and scallops (Figure 4.5a) similar to those seen in other carbon fibre/epoxy systems [6]. Under mode II loading, the matrix is responsible for transferring the axial loads in each fibre to adjacent fibres and neighbouring plies that are not orientated in the direction of primary loading. Consequently, shear fracture tends to occur within, or adjacent to, plies that are orientated in the direction of the maximum loading [7]. In contrast to mode I failure, the mode II fracture surface shown in Figure 4.5b exhibited extensive plastic deformation and yielding.

A closer examination of the micrograph highlights the presence of what appears to be a large number of distorted hackles that have been severely deformed during the passage of the primary crack. As described by Mohr's circle, during in-plane shear loading, the principle tensile stresses are orientated at forty-five degrees to the plane of applied shear, as shown in Figure 4.6. Since matrix fracture occurs in a microscopic plane normal to resolved tensile stresses, a series of distinctive inclined microcracks are formed ahead of the main crack front. Increased loading causes these small parallel microcracks to grow and coalesce, resulting in the formation of a series of upright curved platelets [7]. Similar observations have been made following mode II test on other fibre reinforced composites [8,9]. The evidence of such extensive localised plastic flow clearly explains the impressive mode II fracture energies recorded for this material. Finally, the mixed-mode fracture surface shows a similar appearance to that observed following mode I testing on this composite, Figure 4.5c, and to other epoxy based systems where similar values of fracture energy have been recorded [10].

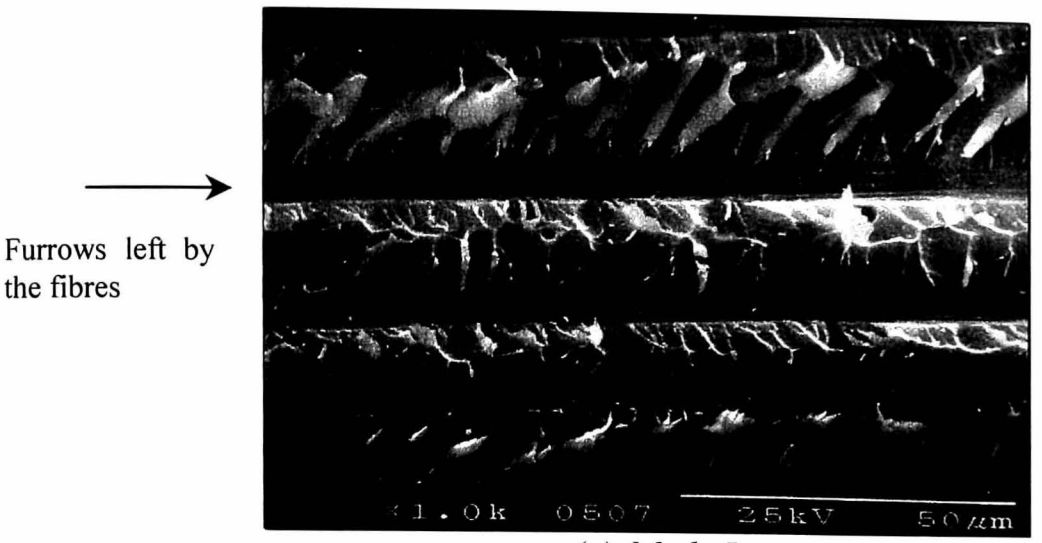

(a) Mode I

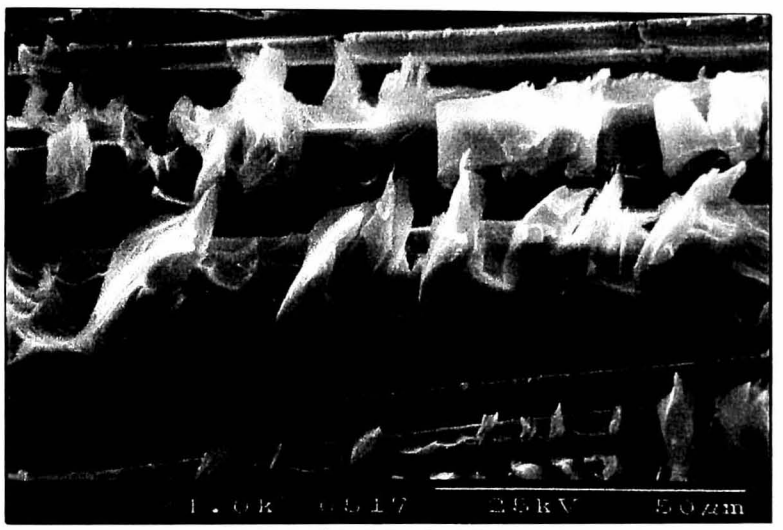

(b) Mode II

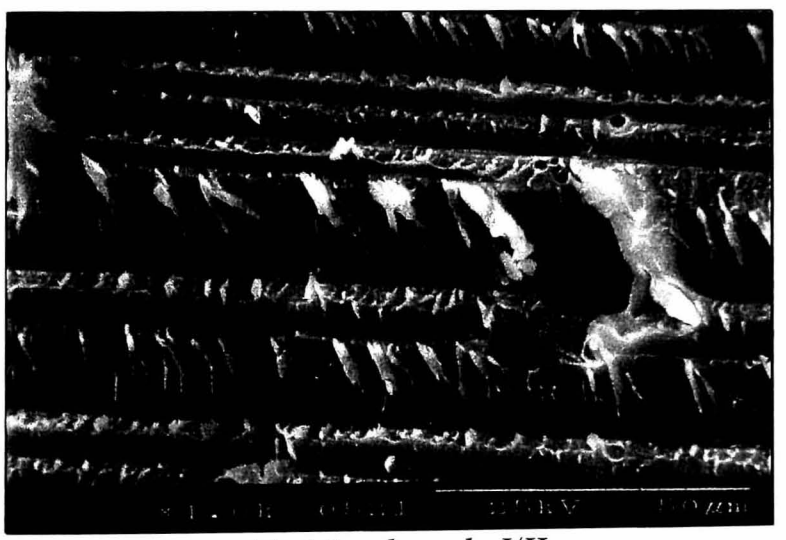

(c) Mixed-mode I/II

Figure 4.5 *Scanning electron micrographs showing the fracture surfaces following interlaminar fracture tests on the carbon fibre reinforced epoxy composite.*

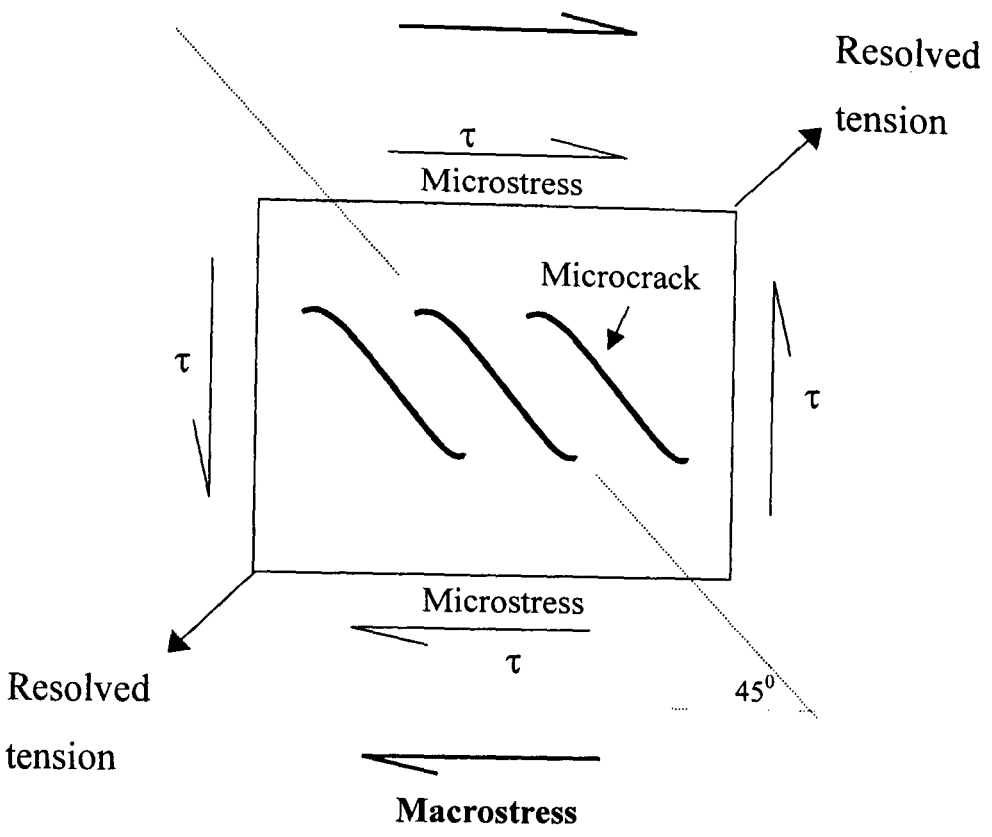

Figure 4.6 *Schematic illustration of hackle formation under mode II loading.*

This suggests that the interlaminar fracture toughness of this system is directly related to the ability of the material to dissipate energy in form of plastic deformation within the matrix material.

The mode I, mode II and mixed-mode load-displacement traces for the glass fibre/polypropylene (GFPP) are shown in Figure 4.7. The mode I curve, Fig. 4.7a, shows stable crack propagation with the crack propagating in a controlled manner from the starter defect. Fibre bridging was present during crack propagation, and is clearly a fracture mechanism that has contributed to the fracture toughness of the material. After unloading, a small residual displacement is apparent on the trace as a result of small amounts of fibre bridging being trapped between the two halves of the specimen. Stable crack propagation is also apparent in the mode II and mixed-mode

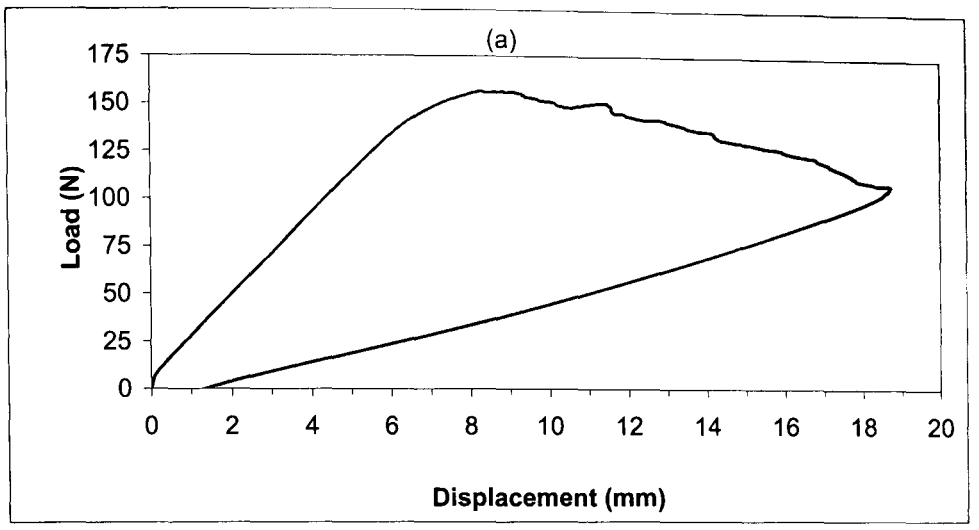

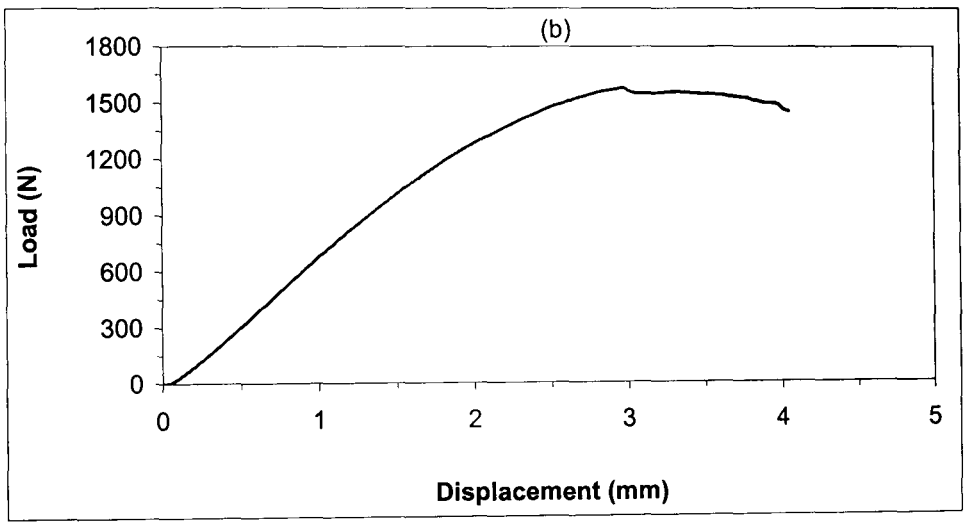

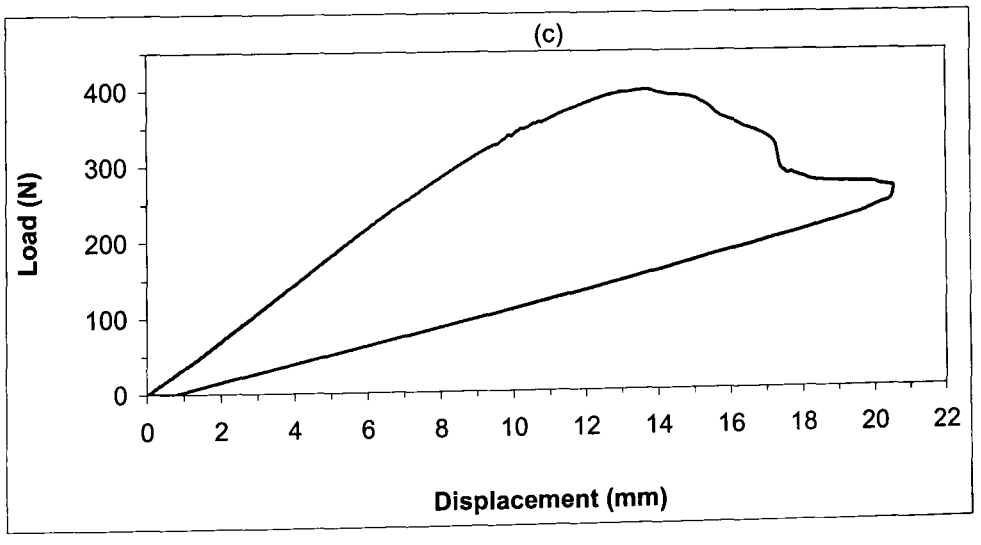

Figure 4.7 *Typical load-displacement curves following (a) mode I, (b) mode II and (c) mixed-mode I/II loading of the glass fibre polypropylene composite.*

traces shown in Figures 4.7b and 4.7c. Here, it is apparent that under mixed-mode loading conditions a small residual displacement is present after unloading of the specimen. Using the information obtained from these tests, the interlaminar fracture energies for mode I, mode II and mixed-mode loading were evaluated using Equations 3.2, 3.3 and 3.4 respectively.

Figure 4.8 shows a typical resistance curve following mixed-mode loading of GFPP at 1 mm/min. This figure clearly shows that crack initiation occurs at a value of approximately 2800 J/m^2. The value of $G_{I/IIc}$ then rises very rapidly before stabilising at approximately 4600 J/m^2. This increase in $G_{I/IIc}$ with crack length is associated with the formation of fibre bridges at the crack tip of the advancing crack. Clearly, no bridges are present at the onset of crack propagation. However, as the crack advances, these bridges develop and the fracture energy increases.

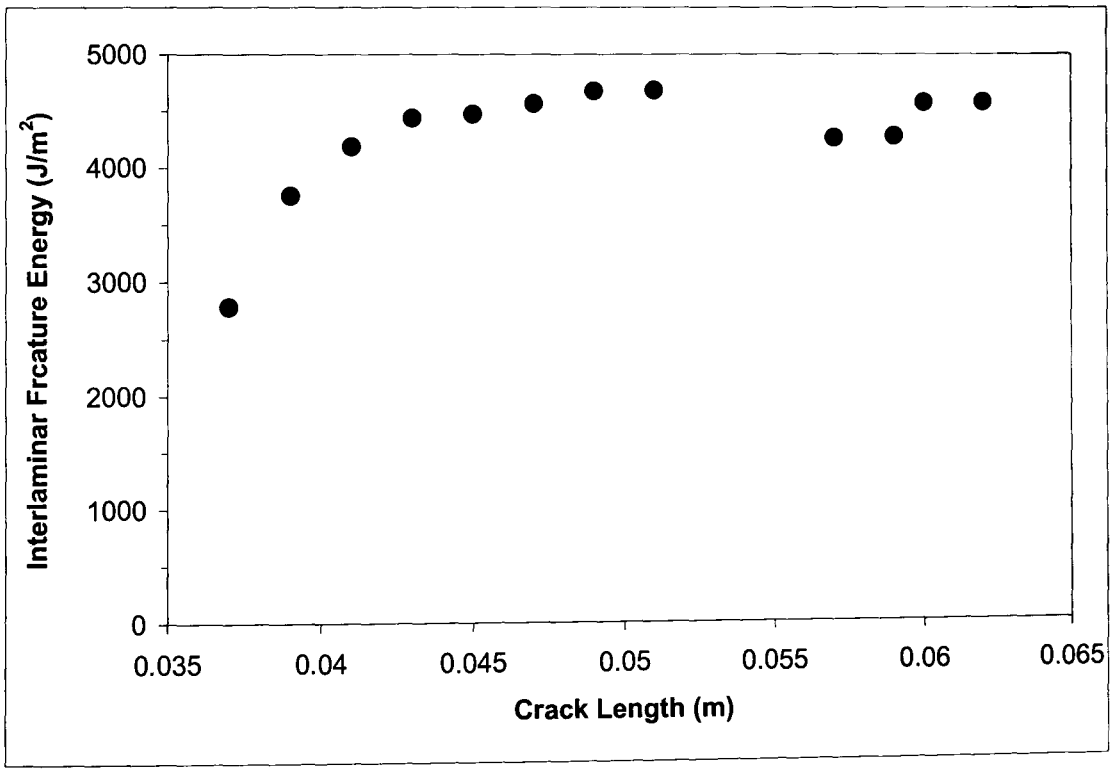

Figure 4.8 *Typical resistance curve following mixed-mode loading of GFPP at 1 mm/min.*

Figure 4.9 summarises the results of the interlaminar fracture tests on the glass fibre/polypropylene (GFPP). The G_{Ic} and $G_{I/IIc}$ values correspond to the average fracture energies during crack propagation. However, during mode II testing, it was not possible to accurately monitor crack advance, therefore, values of G_{IIc} at maximum load were used. The mode I and mode II interlaminar fracture tests yielded average values of 2500 J/m^2 and 3800 J/m^2 respectively, these being similar to those found in previous studies [11]. The mixed-mode interlaminar fracture energies are particularly impressive with average values of $G_{I/IIc}$ approaching 5000 J/m^2. In order to investigate the fracture mechanisms responsible for these impressive properties, the fracture surfaces of the failed specimens were prepared for analysis in the scanning electron microscope.

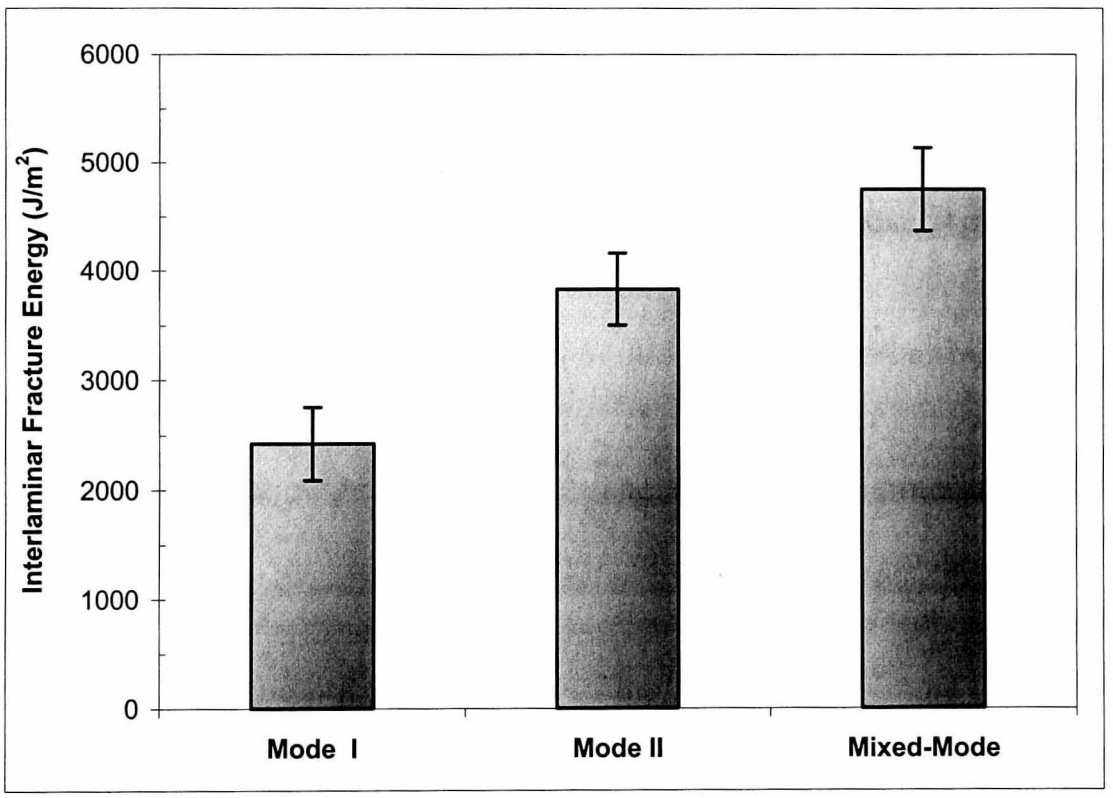

Figure 4.9 *Summary of the interlaminar fracture properties of the glass fibre polypropylene composite.*

Typical scanning electron micrographs of the fracture surfaces of samples tested under the three modes of loading are shown in Figure 4.10. In contrast to the woven CFRE, the fracture surface corresponding to the mode I test exhibits large amounts of plastic deformation within the matrix material (Fig.4.10a). Here, the strain to failure of pure polypropylene is very high and this is clearly contributing to the toughness of the composite. During the test, fibre bridging was also observed. Such fracture mechanisms were suppressed in the CFRE system as a result of the weave pattern restraining the fibres [12]. Fibre bridging was not observed in the case of mode II loading. However, the shear stresses acting during failure of the material caused the matrix to undergo considerable plastic deformation as shown in Figure 4.10b. Here, the formation of hackles as those exhibited by the CFRE was not observed. This is believed to be suppressed as a result of the high strain to failure of the polypropylene. The fracture surface corresponding to mixed-mode loading, Fig. 4.10c, shows a combination of mode I and mode II fracture. Fibre bridging was also observed during the mixed-mode interlaminar tests. Therefore, it is believed that the combination of the fibre bridging and the mixed appearance of the plastic deformation in the matrix were responsible for the high values of mixed-mode fracture energy, $G_{I/IIc}$, measured on this material.

The results obtained from the interlaminar fracture tests on the plain composites indicate that both the thermoset and thermoplastic-based systems exhibit excellent interlaminar fracture properties. This suggests, therefore, that these materials should be ideal candidates for incorporation into fibre-metal laminates.

4.2 THE INFLUENCE OF CROSSHEAD DISPLACEMENT RATE ON THE $G_{I/IIc}$ OF THE COMPOSITE MATERIALS

Interfacial fracture in the single cantilever beam (SCB) test geometry is likely to be of a mixed mode nature, therefore potential rate effects in the SCB geometry can best be understood by considering rate effects in the MMF test geometry.

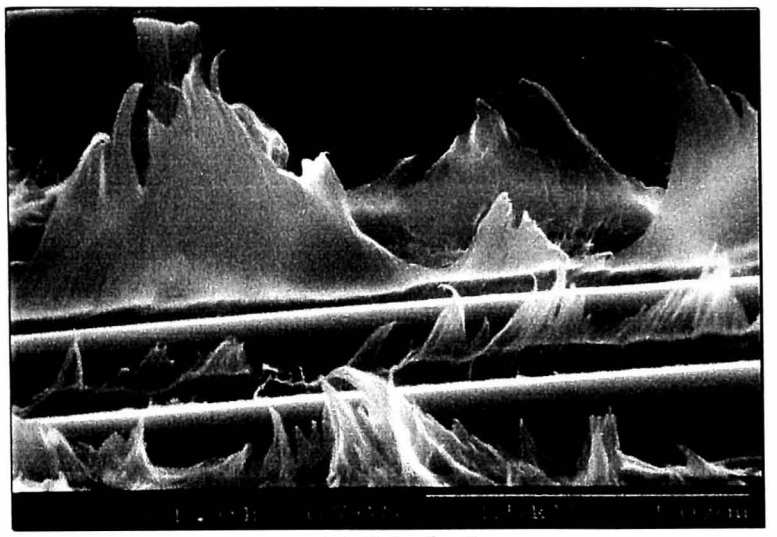

(a) Mode I

(b) Mode II

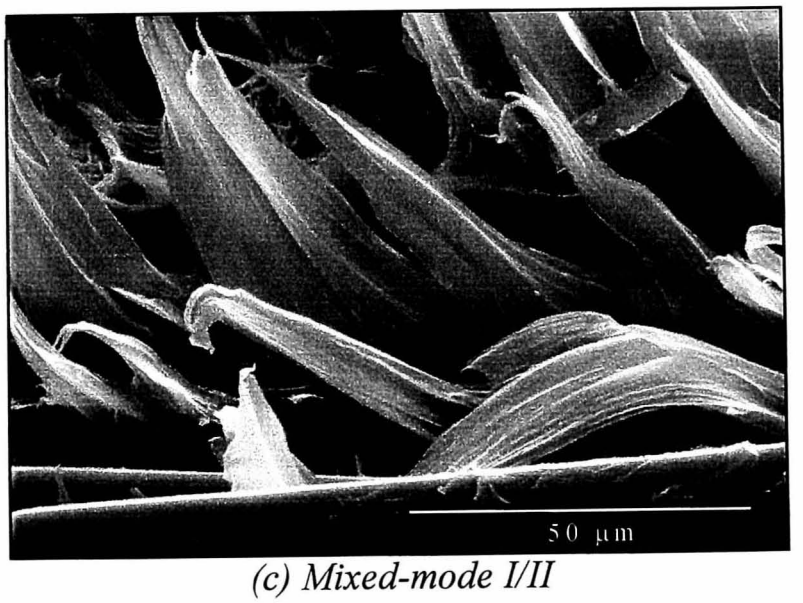

(c) Mixed-mode I/II

Figure 4.10 *Scanning electron micrographs showing the fracture surfaces following interlaminar fracture tests on the GFPP composite.*

Therefore, in order to evaluate the effect of loading rate on the mixed-mode fracture properties of the fibre-metal laminates, initial attention will focus on characterising the strain rate sensitivity of the composite materials.

4.2.1 Fracture toughness and post-failure fractography

A series of mixed-mode interlaminar fracture tests were performed in order to evaluate the influence of the crosshead displacement rate on the interlaminar fracture properties of the plain composites used in the fibre-metal laminates. The tests were conducted at crosshead displacement rates between 0.1 mm/min and 2 m/s. During each test, the load and displacement data were recorded. At low and intermediate rates, crack propagation was monitored by eye. For rates above 100 mm/min, optical monitoring was no longer possible and an inverse compliance calibration was applied. In the CFRE system, crack propagation occurred in an unstable manner at all rates of loading with the crack propagating some distance from the starter defect.

Figure 4.11 shows typical load-displacement curves following mixed-mode loading of the CFRE composite at 10 and 100 mm/min. From this figure, it is clear that crack propagation occurred in an unstable mode at both rates of loading. At 10 mm/min, the sample exhibited a linear response up to maximum load yielding a value of approximately 495 N at 7.7 mm of displacement, Figure 4.11a. At 100 mm/min, the curve exhibited a similar appearance to that tested at 10 mm/min, Figure 4.11b. These results suggest that no rate sensitivity in the CFRE is apparent over this range of loading rates. The mixed-mode interlaminar fracture energy $G_{I/IIc}$ was then calculated using Equation 3.4. It is worth noting that a number of attempts have been made to relate the measured fracture toughness to local strain rate conditions at the crack tip [13,14]. However, it was noted that the estimation of the strain rate at the crack tip was rendered difficult by the complexity of the strain field at the tip of the crack. Therefore, the use of crosshead displacement rate is believed to be an appropriate parameter to characterise strain rates effects in these materials.

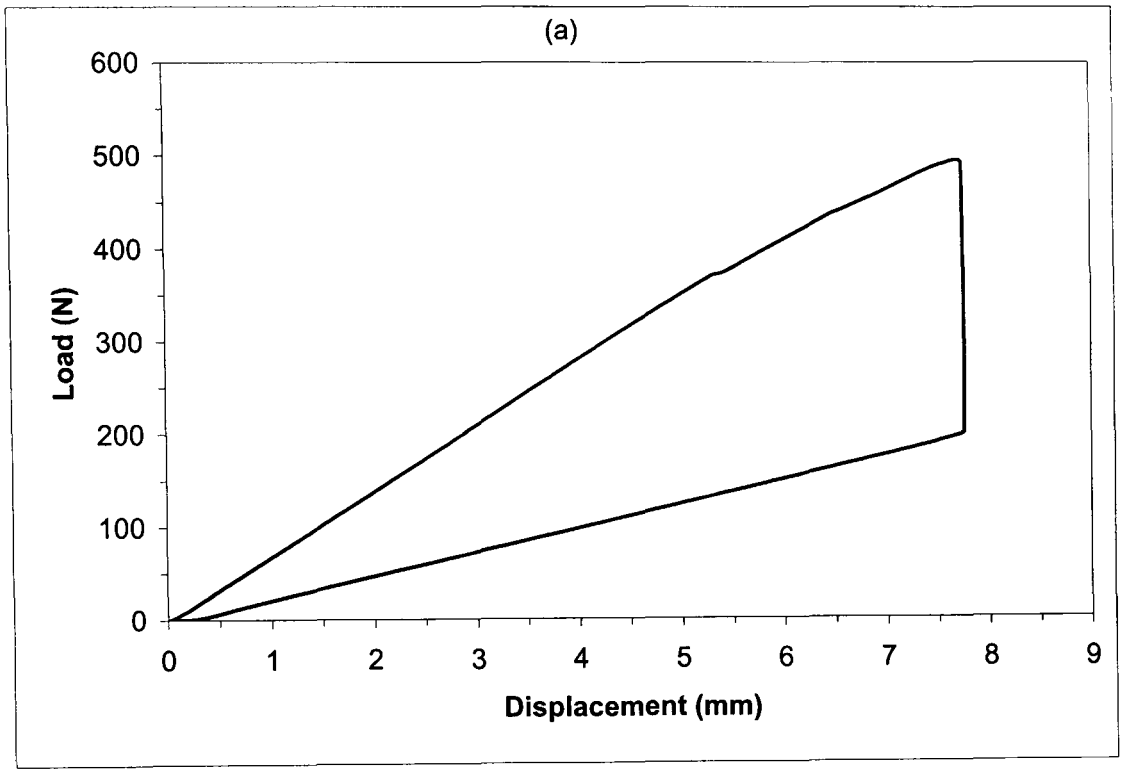

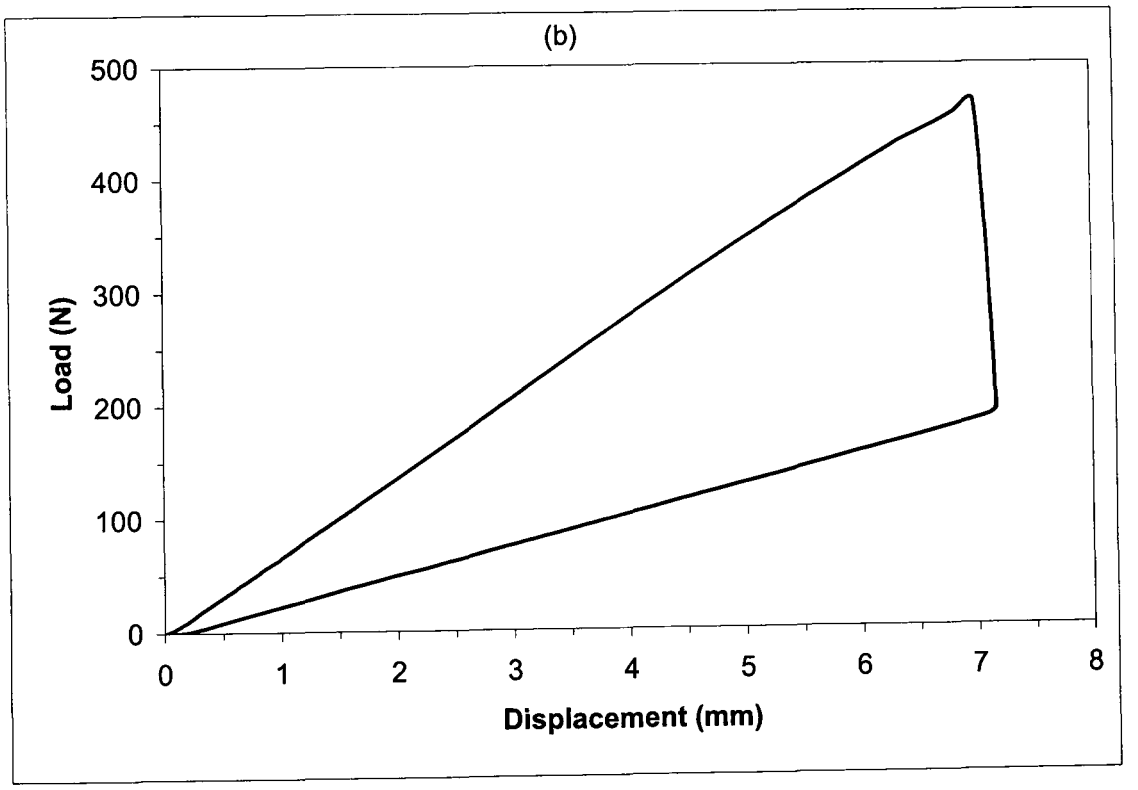

Figure 4.11 *Typical load-displacement curves following mixed-mode loading of the CFRE composite at (a) 10 mm/min and (b) 100 mm/min.*

Figure 4.12 shows the influence of the crosshead displacement rate on the interlaminar fracture properties of the woven carbon fibre/epoxy (CFRE). This figure clearly shows that at low and intermediate displacement rates, the values of interlaminar fracture energy remains roughly constant averaging approximately over 2000 J/m^2 in all cases. At higher crosshead displacement rates, the values of interlaminar fracture energy drop slightly, although under impact conditions, the value remains close to 1900 J/m^2. These values are up to three time greater that those measured on other carbon fibre/ epoxy systems [15] and are comparable with those of tough thermoplastic matrix composites such as carbon fibre reinforce PEEK [16]. These results clearly indicate that the material retains its interlaminar fracture properties at very high rates of loading suggesting an outstanding response under impact loading conditions.

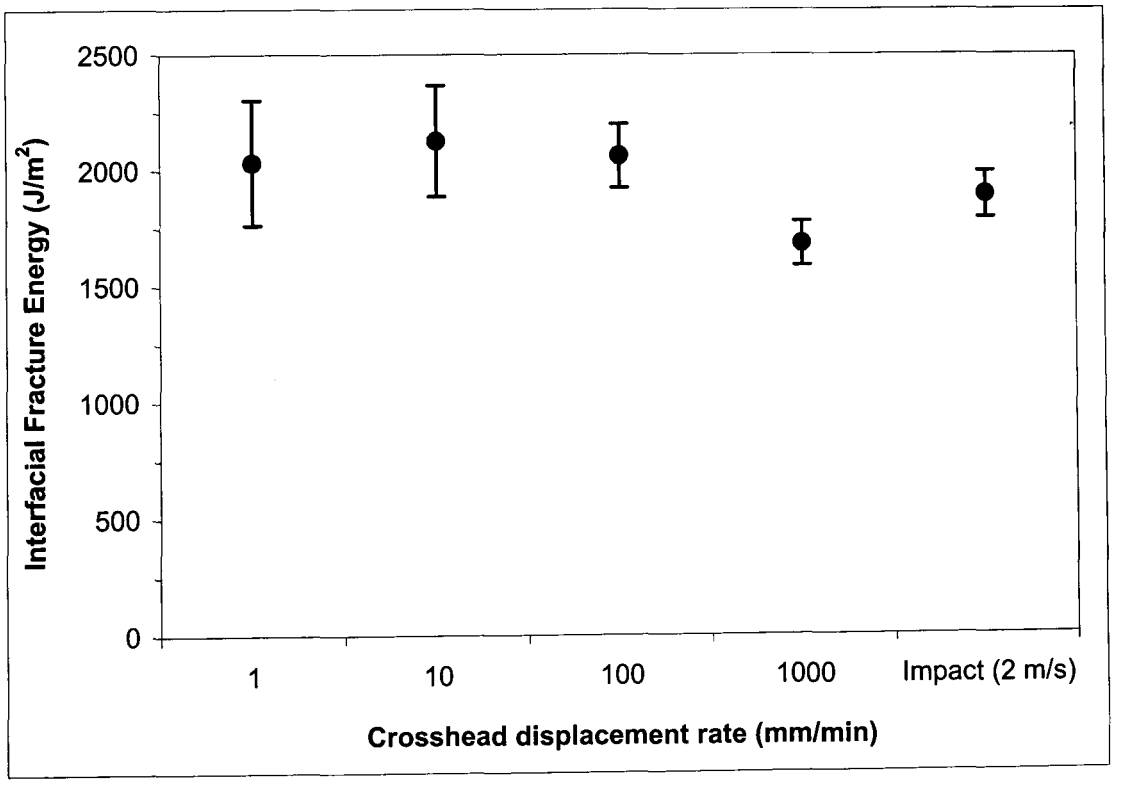

Figure 4.12 *Influence of crosshead displacement rate on the mixed-mode I/II interlaminar fracture properties of carbon fibre/epoxy (CFRE).*

A post-fracture optical examination of the failed samples highlighted the presence of significant plastic deformation in the matrix material at lower rates of loading. At higher rates, the amount of plastic deformation was reduced suggesting the presence of a ductile to brittle transition in the matrix [17]. This reduction in plastic deformation within the matrix is believed to be associated with the reduction in fracture toughness at higher rates of loading.

The influence of the crosshead displacement rate on the mixed-mode interlaminar fracture properties of the glass fibre/polypropylene (GFPP) system was evaluated using the same test arrangement used for testing the CFRE. The load-displacement traces recorded under mixed-mode loading conditions showed small regions of non-linearity and stable crack growth at all rates of loading.

Figure 4.13 shows typical load-displacement curves following mixed-mode loading of the GFPP composite at 0.1 and 1 mm/min. From the curves, it is clear that both samples failed in a stable manner along the centreline of the sample. It is also apparent that the loads and displacements are greater in the sample tested at the higher rate suggesting a positive strain rate effect Figure 4.13b.

This information was used to calculate the interlaminar fracture energy at different rates of loading. The variation of the mixed-mode interlaminar fracture energy, $G_{I/IIc}$, with crosshead displacement rate is shown in Figure 4.14. Here, at 0.1 m/min., average values of approximately 3400 J/m^2 were recorded. As the crosshead displacement rate was increased, the value of the interlaminar fracture energy also increased and at intermediate rates of loading, the average values of $G_{I/IIc}$ remained almost constant at values close to 4700 J/m^2. At higher crosshead displacement rates, a slight drop in the values of $G_{I/IIc}$ was recorded with values dropping to 3600 J/m^2 at 2 m/s. Similar reductions in $G_{I/IIc}$ have been observed in other thermoplastic matrix composites at high rates of loading [18].

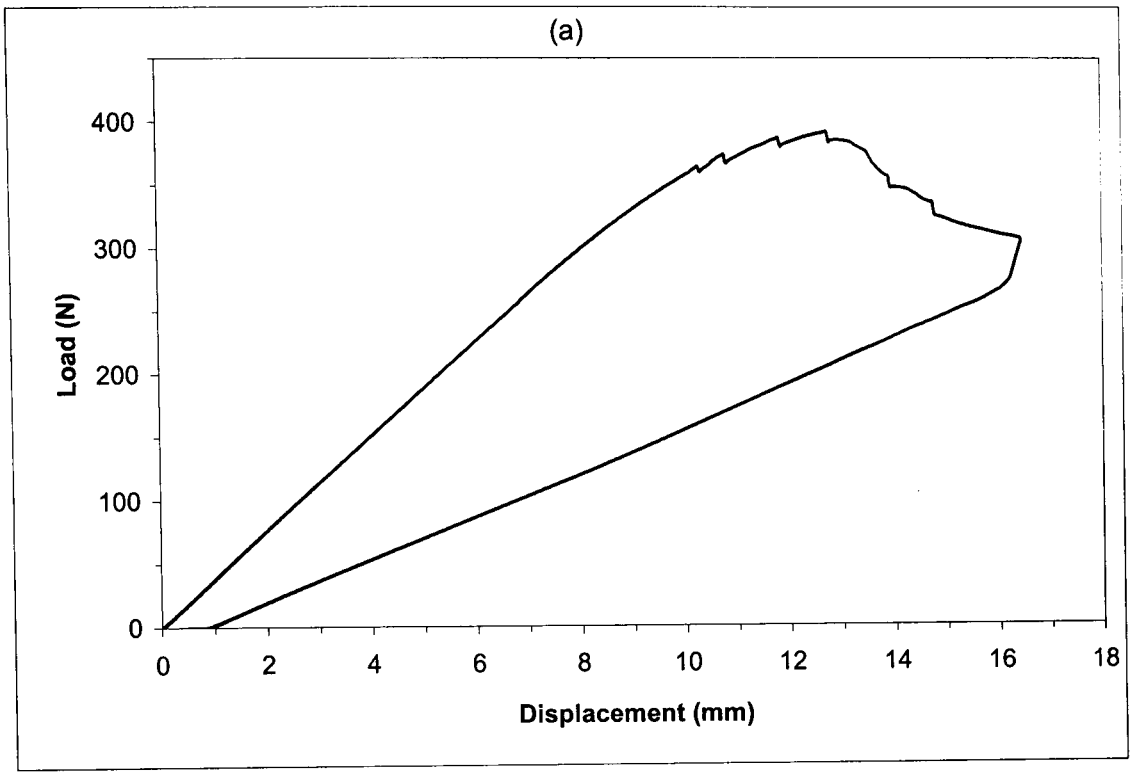

Figure 4.13 *Typical load-displacement curves following mixed-mode loading of GFPP at (a) 0.1 mm/min and (b) 1 mm/min.*

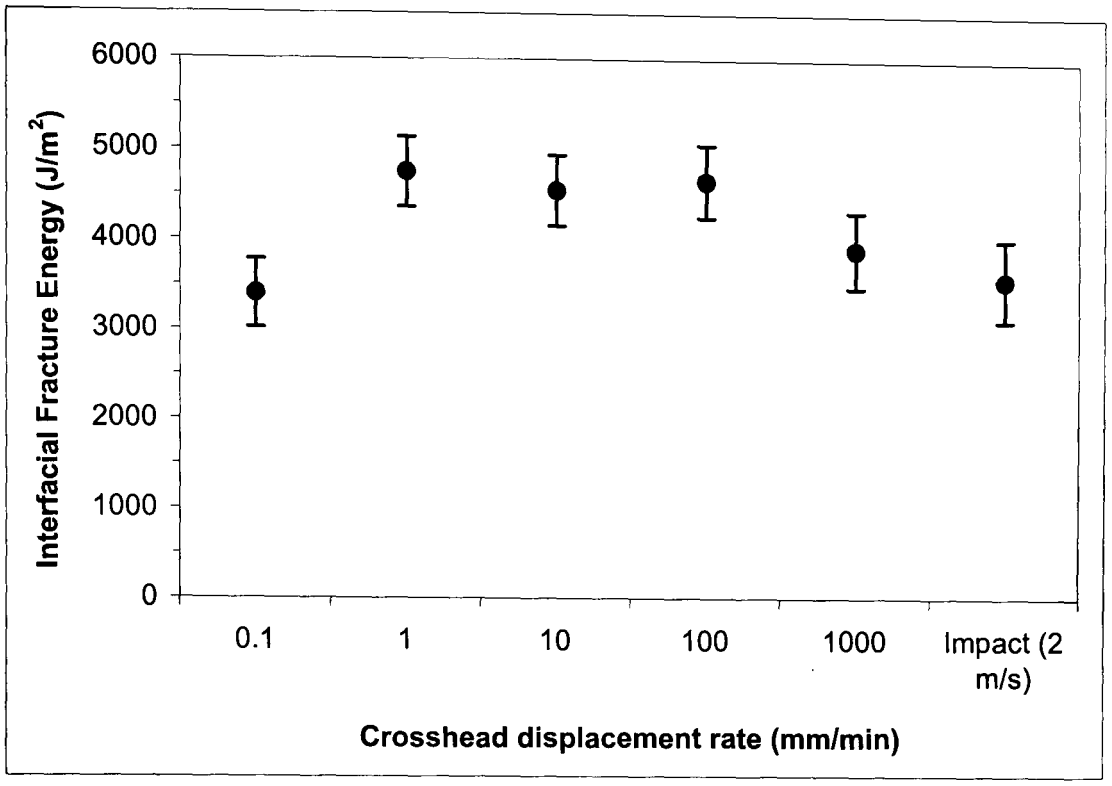

Figure 4.14 *Influence of crosshead displacement rate on the mixed-mode I/II interlaminar fracture properties of glass fibre/polypropylene (GFPP).*

An examination of the mixed-mode interlaminar fracture data suggests that the value of $G_{I/IIc}$ increases at low and intermediate crosshead displacement rates before decreasing at high rates. Clearly, the influence of crosshead displacement rate on the mixed-mode interlaminar fracture properties of a composite is likely to be complex. In the MMF samples, the ratio of mode I to mode II components at the crack tip is 4/3. To understand the influence of loading rate on these properties, one must understand how the mode I and mode II properties of the composite vary with crosshead displacement rate. For example, Mall has shown that the mode I interlaminar fracture toughness of woven carbon fibre/PEEK decreases with increasing crosshead displacement rate [19]. In contrast, other workers have shown that the mode II interlaminar fracture toughness of carbon fibre/PEEK increases before possible reaching a plateau at higher strain rates [20]. Since the mixed-mode fracture energy is likely to reflect the rate sensitivity of both the mode I and mode II

fracture properties of the composite, one could imagine the type of response outlined in Figure 4.15, where the value of $G_{I/IIc}$ increases and then decreases.

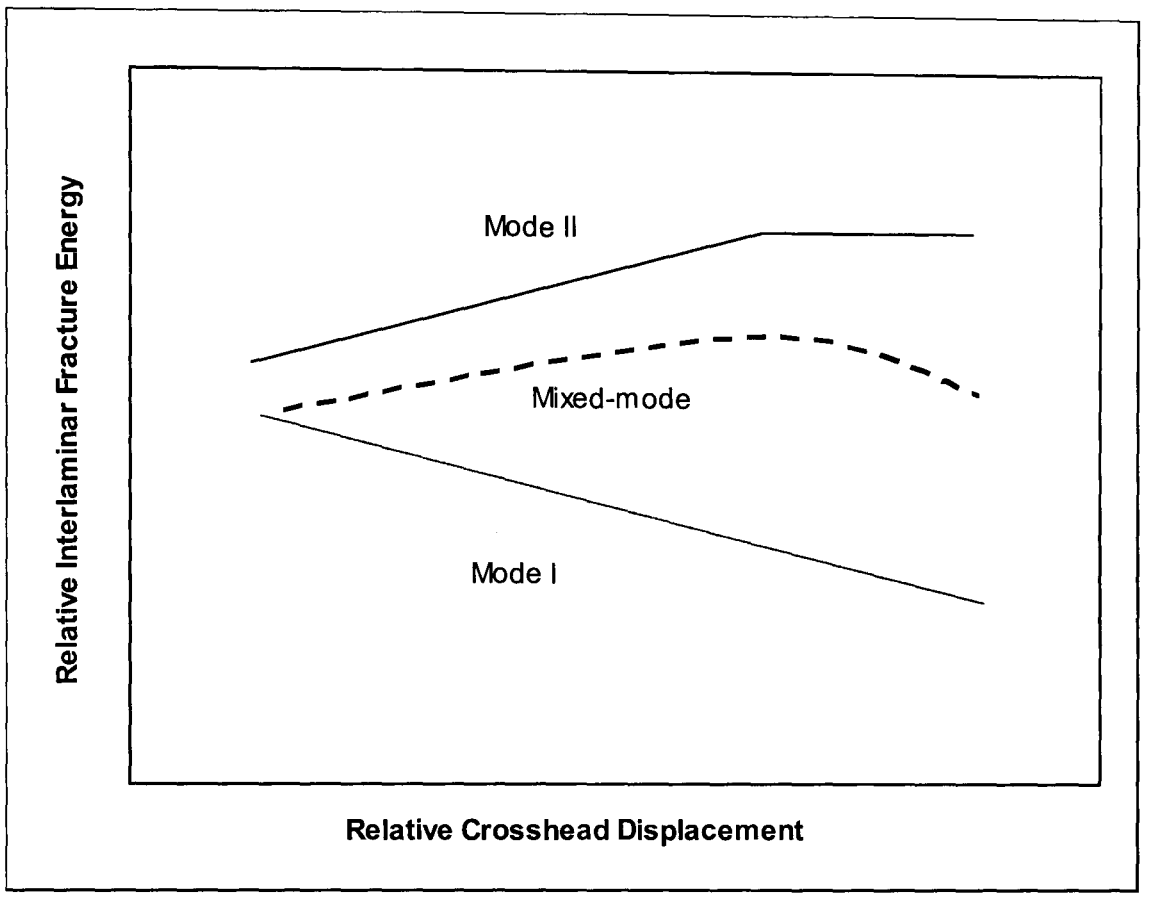

Figure 4.15 *Schematic illustration of possible effect of the crosshead displacement rate on mixed-mode interlaminar fracture.*

The mixed-mode data suggest that the crosshead displacement rate has a slight effect on the interlaminar response of the plain composite, although it has also been shown that this material retains its interlaminar fracture properties at high crosshead displacement rates.

An examination of the fracture surfaces highlighted the presence of large amounts of plastic deformation in the matrix material at low crosshead displacement rates. At intermediate rates, the amount of plastic deformation in the matrix was reduced suggesting the presence of a matrix yielding toughening mechanism [17]. Here, between 0.1 and 1 mm/min the matrix gets tougher as the loading rate is

increased. At the same time, small amounts of fibre bridging were also apparent on the fracture surface of this material. The combination of these fracture mechanisms is believed to contribute to the high interlaminar fracture energy at intermediate loading rates. At high crosshead displacement rates, the matrix material showed a reduced amount of plastic deformation. This has been associated with the presence of a ductile to brittle transition in the matrix [17,21]. Therefore, a small rate dependency is apparent in the matrix. Similar results have been observed elsewhere [22]. Nevertheless, these results show that this material retains its high interlaminar properties at high rates of loading. This suggests that both composites materials after being tested over a range of crosshead displacement rates represent ideal candidates for use in the manufacture of fibre-metal laminates.

4.3 OPTIMISATION OF THE COMPOSITE – METAL INTERFACE

Fibre-metal laminates are arrangements that combine the high specific properties of the composites with the ease of fabrication and machinability of metals. In order for these materials to be effective and interact as a whole, a strong interface has to be achieved. This interface plays an important role in transferring the applied loads from one material to the other. In order to manufacture fibre-metal laminates with a strong bi-material interface, initial attention focused on optimising the degree of adhesion between the aluminium and composite materials based on the thermosetting and thermoplastic matrices.

4.3.1 Carbon fibre/epoxy-based FML

4.3.1.1 Influence of aluminium surface treatments and post-failure fractography

The fibre-metal laminates investigated in this part of the study were based on type 2024-0 aluminium alloy sheets and the woven carbon fibre/epoxy (Stesapreg EP121-C15-53). Here, bi-material panels were manufactured by stacking eight layers of the woven fibre composite prepreg on a 2 mm thick aluminium sheet.

Prior to laminating, several pre-treatments were applied to the aluminium substrate to ensure optimum adhesion to the composite plies. These were (i) sulphuric acid anodisation, (ii) silane coupling agent, (iii) amorphous chromate coating and (iv) an abrasion-wipe. The purpose of anodising the aluminium substrate with an acid is to create a large and active surface area for the polymer to flow into and interlock with the metal. This process produces a thick porous-type anodic coating [23,24]. Silane coupling agents were created to bond inorganic materials to organic matrices by forming covalent bonds with the matrix and inorganic bonds with the metallic substrate [23]. Amorphous chromate coatings are applied in acid solutions; the coating usually consists of hexavalent chromium, a fluoride and an accelerator. They provide ease and economy of operation, good adhesion properties for organic coatings, and improved resistance to corrosion [24]. The abrasion-wipe procedure is a mechanical treatment that increases the roughness of the surface of the metallic substrate in order to promote mechanical interlocking with organic materials [25]. These surface treatments are widely used to promote good adhesion between organic and inorganic substrates.

The single cantilever beam (SCB) specimen was used in order to investigate the interfacial fracture properties and failure mechanisms occurring within the fibre-metal laminates. The specimen was supported and clamped in a steel fixture and loaded at one end in a displacement-control mode at a crosshead displacement of 1 mm/min forcing a crack to propagate from the tip of the insert. The point on the load displacement plot at which the crack was first observed to grow from the insert was recorded along with the corresponding load and displacement. As the test progressed, crack lengths were noted every 5 mm along the bi-material interface, until the crack had propagated approximately 40 mm from the starter defect.

Figure 4.16 shows typical load-displacement traces following SCB tests on aluminium/CFRE samples in which the aluminium alloy was subjected to various treatments prior to bonding. Figure 4.16a shows a typical trace for a sample, which was subjected to a sulphuric acid anodisation treatment. Here, the load-displacement

trace suggests that crack propagation occurred in a stable manner. A small residual displacement is apparent at the end of the test associated with the relief of the residual stresses during testing. Figure 4.16b shows a load-displacement trace for the silane-treated aluminium sample. The initial portion of the curve is clearly non-linear, this being associated with significant plastic deformation in the aluminium adherend. The crack then propagates in a highly unstable manner along the sample resulting in the saw-tooth appearance in the figure. From the graph, it is clear that the applied load was significantly lower than that observed in Figure 4.16a. In all subsequent testing, the aluminium alloy was reinforced to reduce the amount of non-linear plastic deformation apparent in this sample. Figure 4.16c shows a typical load-displacement trace for a sample in which the aluminium was subjected to an amorphous chromate coating treatment. This curve is similar in appearance to that exhibited by the S.A.A. sample, Figure 4.16a. Here, crack propagation occurs in a stable manner at relatively high forces. A small instability is apparent in the initial loading curve, however this is likely to be as a result of the aluminium foil sticking to itself during manufacture. Finally, the load-displacement curve for the simple abrasion-wipe procedure shown in Figure 4.16d suggests that this procedure yields very successful results. Here, the applied forces and resulting displacements are large suggesting an impressive fracture energy. In addition, crack propagation was generally stable.

The mixed-mode interfacial fracture energy for each surface treatment used was then determined using Equation 3.7. Figure 4.17 summarises the effect of the surface treatments applied to the aluminium alloy on the fracture properties of the bi-material specimens. The data indicate that three of the pre-treatment techniques yielded fracture energies in the range of 1550 to 2000 J/m^2. These values are clearly impressive for an aluminium-epoxy interface, being slightly above the mode I interlaminar fracture toughness of tough thermoplastic matrix composites such as carbon fibre reinforced PEEK [15].

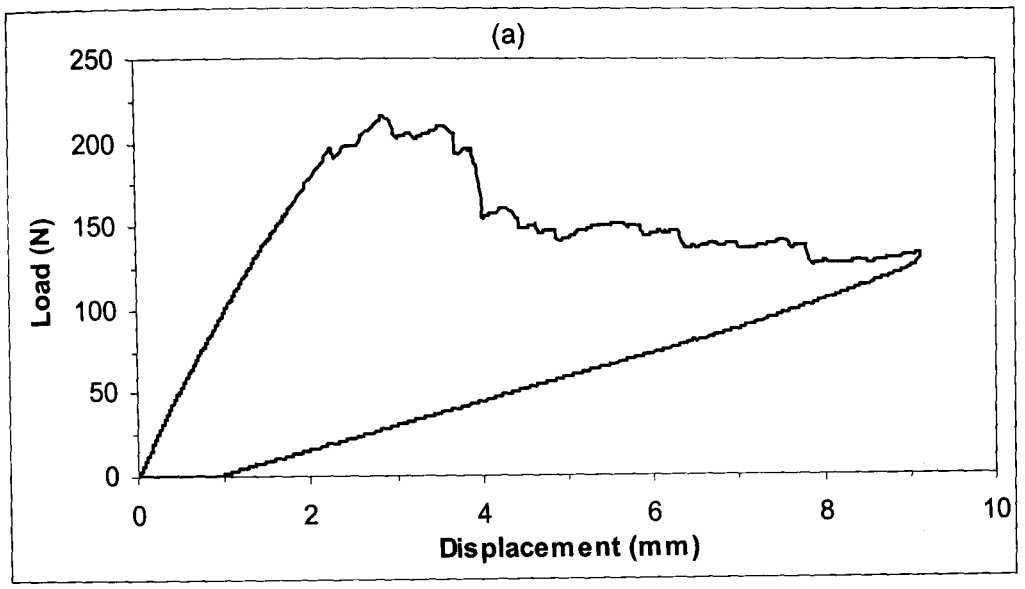
(a)
Load (N)
250
200
150
100
50
0
0
2
4
6
8
10
Displacement (mm)

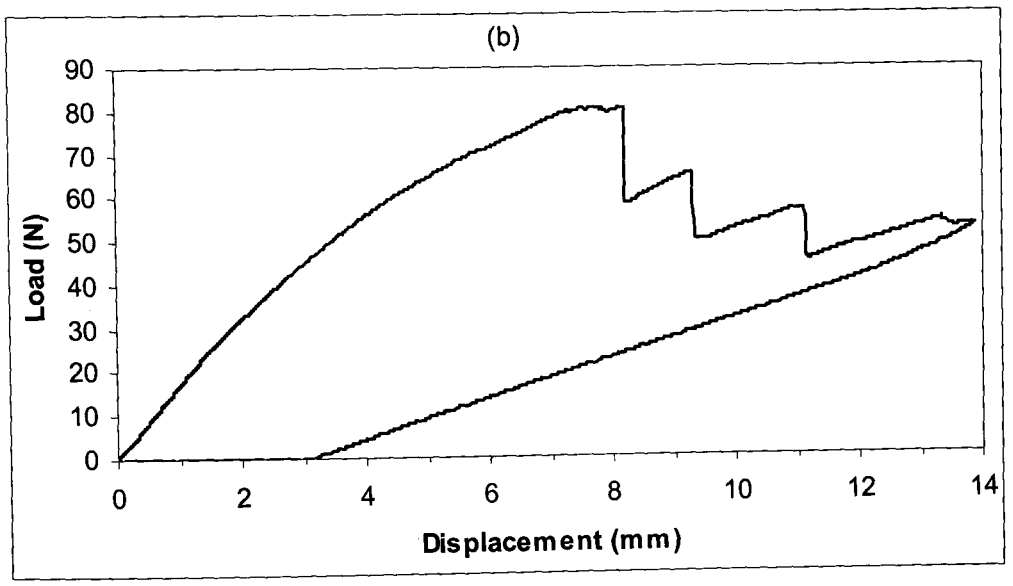
(b)
Load (N)
90
80
70
60
50
40
30
20
10
0
0
2
4
6
8
10
12
14
Displacement (mm)

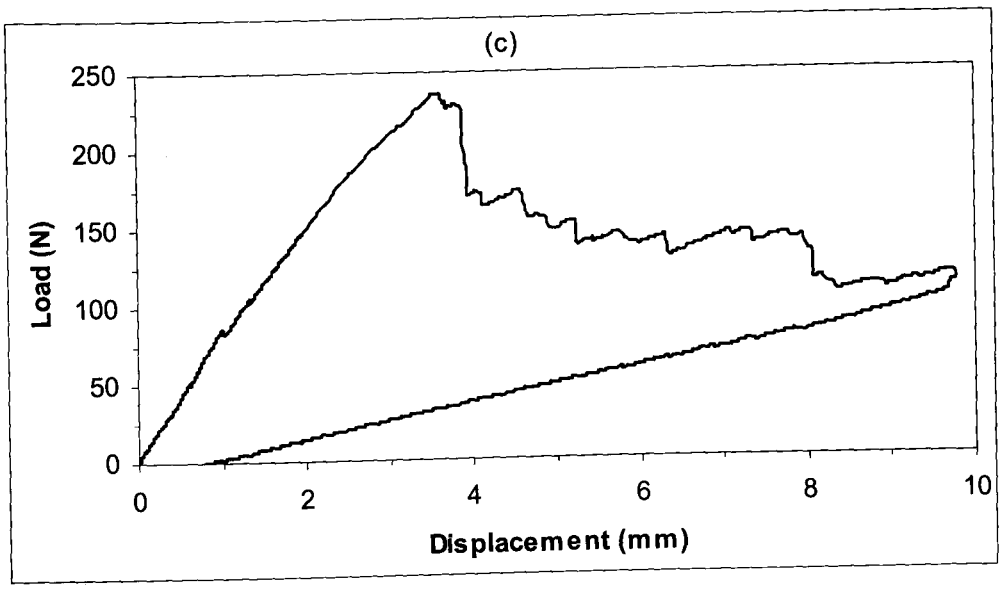
(c)
Load (N)
250
200
150
100
50
0
0
2
4
6
8
10
Displacement (mm)

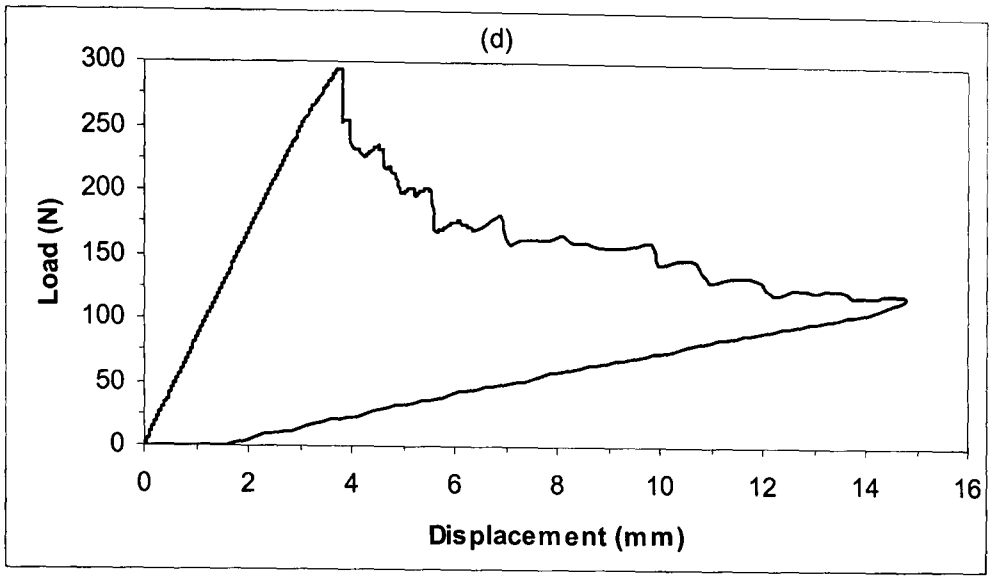

Figure 4.16 *Typical load-displacement curves following SCB tests on aluminium/CFRE samples. Prior to testing, the aluminium was treated via a (a) sulphuric acid anodisation, (b) silane coupling agent, (c) amorphous chromate coating and (d) a simple abrasion-wipe procedure.*

It is interesting to note that samples prepared using a simple abrasion-wipe procedure offered values of G_c comparable and even superior to those achieved following more complex and time-consuming surface treatments. It is also worth noting that the application of a silane pre-treatment lead to a reduction in interfacial adhesion.

A series of post-failure low magnification optical micrographs of the surface-treated aluminium substrates is shown in Figure 4.18. Crack propagation is from right to left in all cases. Here, small amounts of residual composite are apparent on the sulphuric acid anodised aluminium substrate along with regions of clean aluminium. This suggests that this treatment does not promote a strong bond between the dissimilar materials, and that the crack had propagated mainly along the aluminium-composite interface, Figure 418a. This is believed to be as a result of the

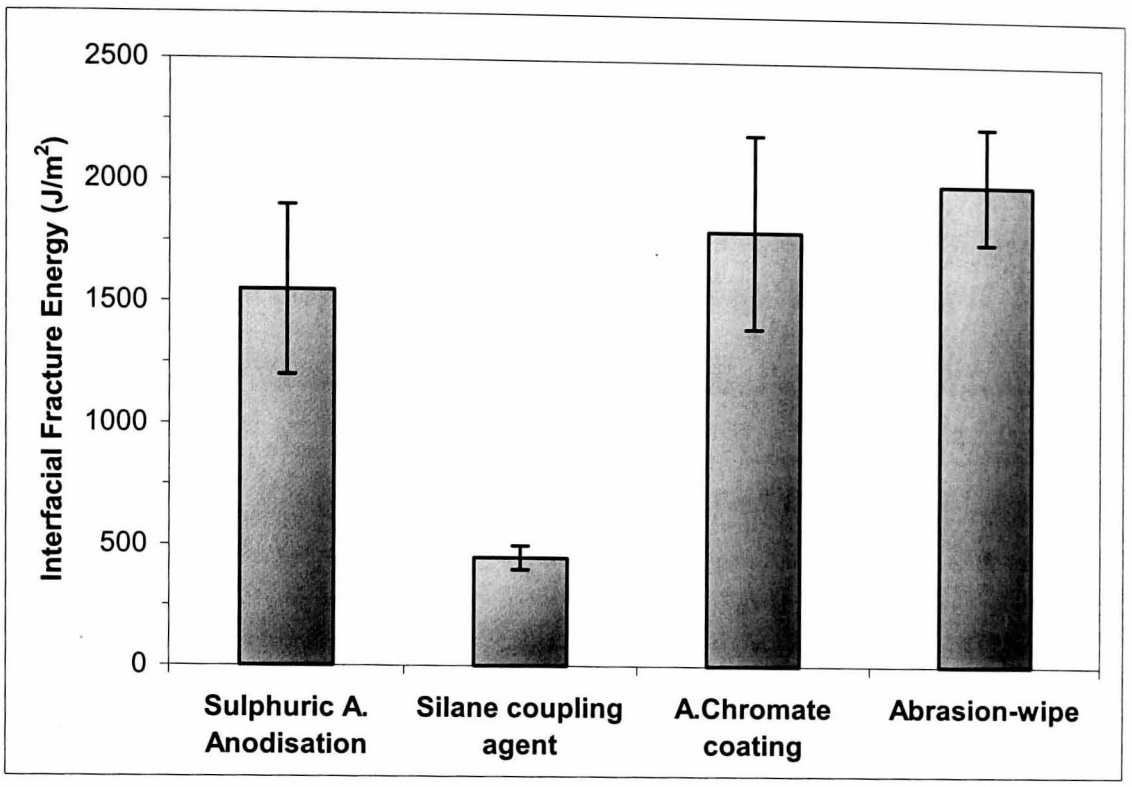

Figure 4.17 *The effect of various surface treatments on the fracture properties of the SCB bi-material specimens based on carbon fibre reinforced epoxy.*

relatively small pore size on the treated aluminium. As a result, the resin could not infiltrate the porous structure to promote a strong mechanical interlocking at the bi-material interface. The fracture surface of the aluminium substrate on which the silane coupling agent was applied shows that almost no residual composite is left after failure. Furthermore, it appears that, although the coupling agent was applied to the aluminium, it did not bond to the composite, and the crack therefore propagated between the coupling agent and composite material, Figure 4.18b. Silane coupling agents should provide a mechanism for covalent bonding between aluminium and epoxy. The reduction in adhesion could be related to the curing temperature of the epoxy system. Therefore, it is believed that the activation energy of the organofunctional silane is such that temperatures in excess of 120 °C (composite

curing temperature) are required in order to form a silane coupler/epoxide/amine network. Similar observations have been reported for other bi-materials systems [23].

Following an amorphous chromate coating treatment, the crack propagated along the bi-material interface as well as within the composite, thereby, increasing the amount of residual composite on the aluminium surface, Figure 4.18c. Here, the relatively large porous surface of the aluminium promoted good adhesion by allowing the epoxy to penetrate into it forming a high level of mechanical keying. This had a beneficial impact on the interfacial fracture energy of this system. This suggests that, as a result of its large cavities, an amorphous chrome coating offers higher adhesion properties than that offered by the sulphuric acid anodisation treatment.

Following the simple abrasion-wipe surface treatment, the crack propagated mainly within the composite and only small amounts of aluminium are left visible, suggesting that adhesion between composite and aluminium is very good, Figure 4.18d. The improvement in adhesion between the aluminium and the epoxy is believed to be as a result of high mechanical interlocking achieved at the bi-material interface. Here, the abraded aluminium surface provides a random anchor-shaped topography, which increases the wetting and surface area of the aluminium substrate. It has been suggested that this random topography has an effect on the local stress distribution [25]. Essentially, it can be effective in preventing any small cracks, flaws, voids or other points of stress concentration from aligning and rapidly propagating along any line of weakness at the interface [25]. In addition, this increase in roughness may increase the localised energy dissipation in the epoxy near the interface [25]. These results suggests that in order to promote a strong bi-material interface, large cavities are needed for the epoxy to flow into and achieve a higher level of mechanical keying. These results suggest that the values of interfacial fracture energy presented in Figure 4.17 are directly related to the degree of adhesion between the aluminium and composite materials provided by the different surface treatments.

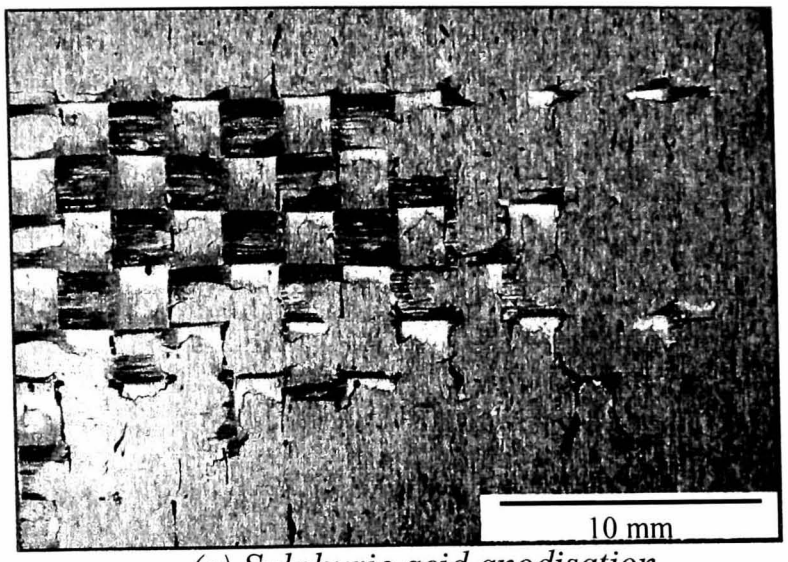

(a) Sulphuric acid anodisation

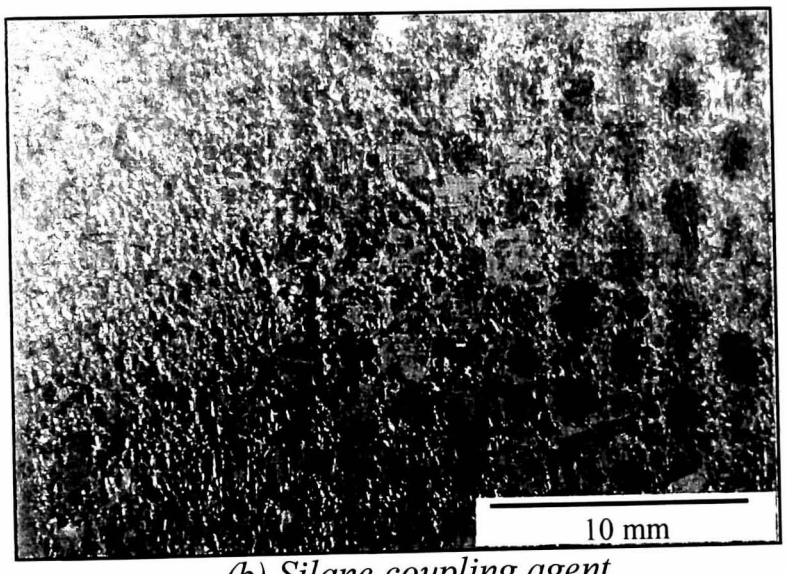

(b) Silane coupling agent

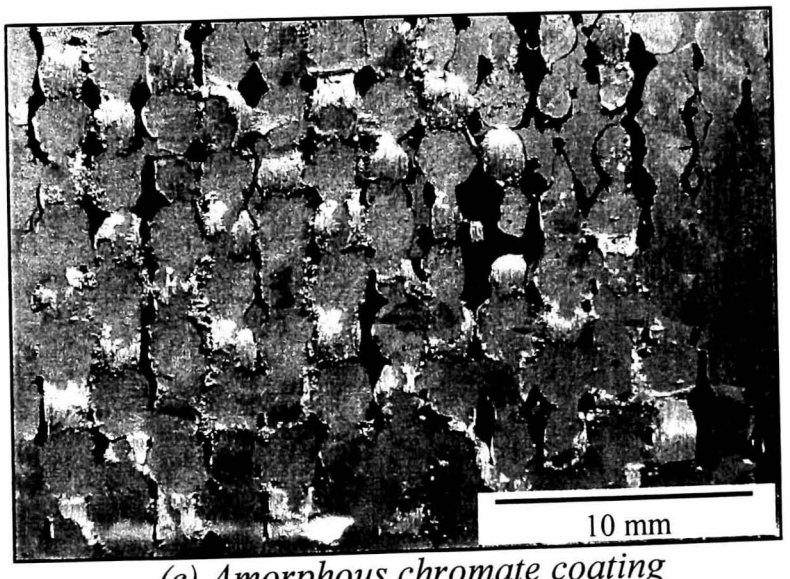

(c) Amorphous chromate coating

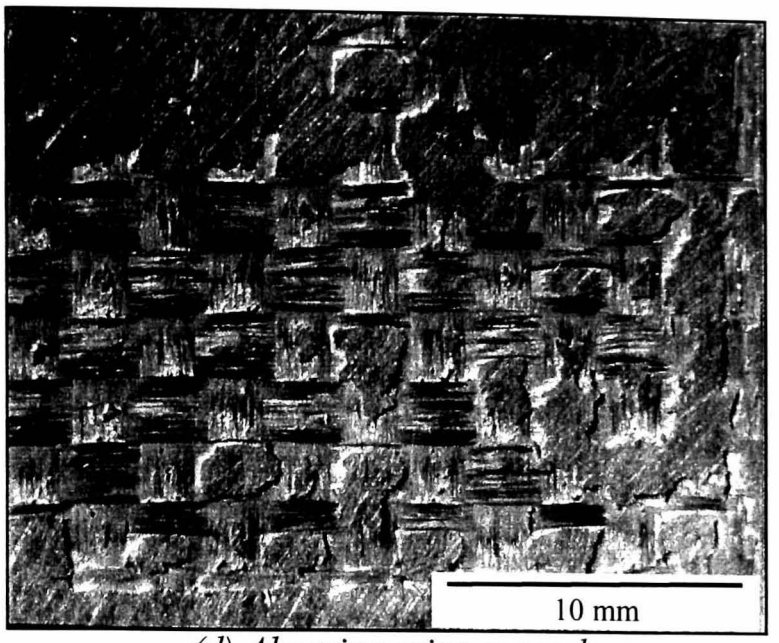

(d) Abrasion-wipe procedure

Figure 4.18 *Low magnification optical micrographs of the surface-treated aluminium substrates following SCB tests.*

It has also been shown that a simple abrasion-wipe treatment is sufficient to ensure excellent adhesion between the two constituents. This treatment was therefore used in the manufacture of the CFRE based fibre-metal laminates investigated in the remainder of this study.

4.3.2 Glass fibre/polypropylene based FML

4.3.2.1 Influence of aluminium surface treatment and copolymer interlayer material

These fibre-metal laminates were based on type 2024-0 aluminium alloy sheets and the unidirectional glass fibre/polypropylene (Plytron) described previously. Here, bi-material panels were obtained by stacking five layers of the unidirectional fibre composite prepreg on a 2 mm thick aluminium sheet. A folded aluminium foil with dimensions 50 x 240 mm was incorporated to act as starter defect.

In order to ensure optimum adhesion between the composite and the aluminium constituents, a surface treatment based on an amorphous chromate coating described previously was applied to the aluminium alloy prior to laminating. A 0.20 mm thick pre-manufactured layer of maleic anhydride modified polypropylene (Fusabond M613-05 from DuPont de Nemours) was incorporated at the composite-metal interface to improve adhesion at the bi-material interface. The modification of isostatic polypropylene by the grafting of maleic anhydride has been reported to improve the adhesion properties of polypropylene to a metallic substrate [26]. Here, the polar functional groups of the modified polypropylene form chemical bonds with the metal oxide surfaces.

As with the carbon fibre-based FML, the single cantilever beam (SCB) specimen and associated test procedure were used in order to investigate the interfacial fracture properties and failure mechanisms occurring at the bi-material interface. During the test, the load-displacement data were recorded. Figure 4.19 shows a typical load-displacement curve following an SCB test on an aluminium/GFPP sample at 1 mm/min. The initial loading curve exhibits some non-linearity which may be associated with some plasticity in the composite adherends. An examination of the curve highlights the presence of a fine saw-tooth appearance which is associated with the primary crack propagating in small jumps.

The mixed-mode interfacial fracture energy was then determined using Equation 3.7. Here, the value of the constant m is calculated from the slope of the plot of C vs. a^3. Figure 4.20 shows a typical plot of the compliance vs. the cube of crack length for an aluminium/GFPP SCB sample loaded at 1 mm/min. From the figure, it is apparent that the data lie on a reasonable straight line. A linear fit to the data yields a value for the constant m of 0.7.

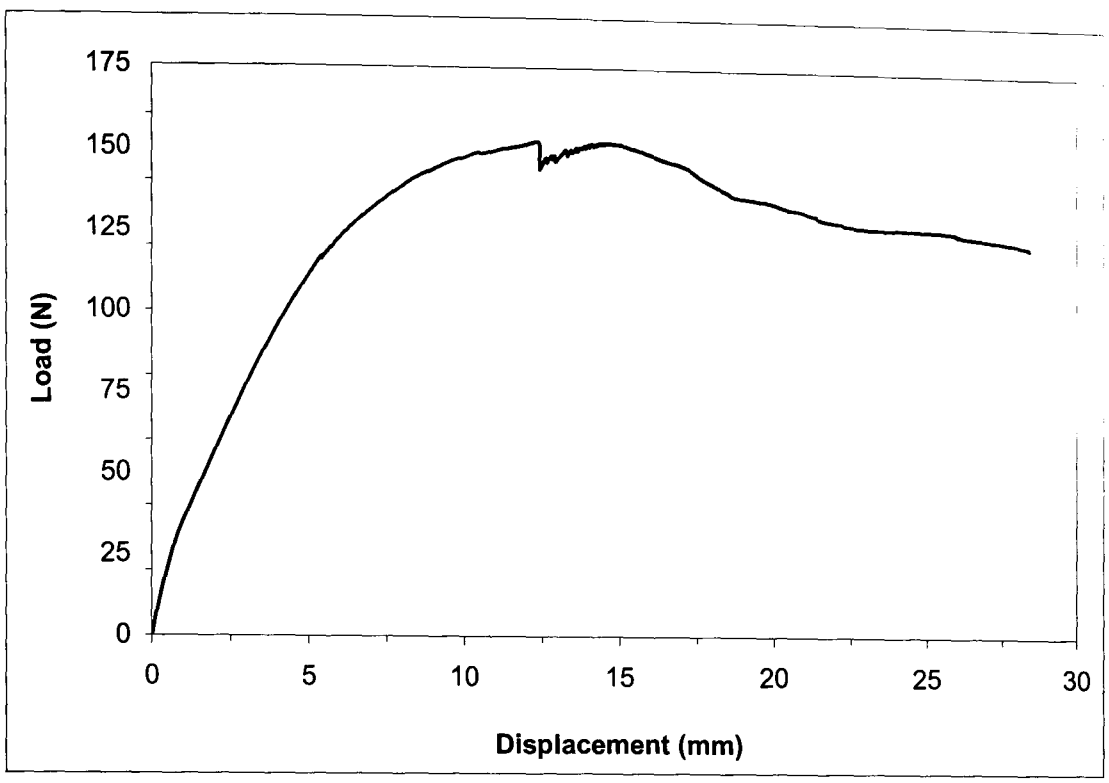

Figure 4.19 *Typical load-displacement curve following an SCB test on an aluminium/GFPP sample at 1 mm/min.*

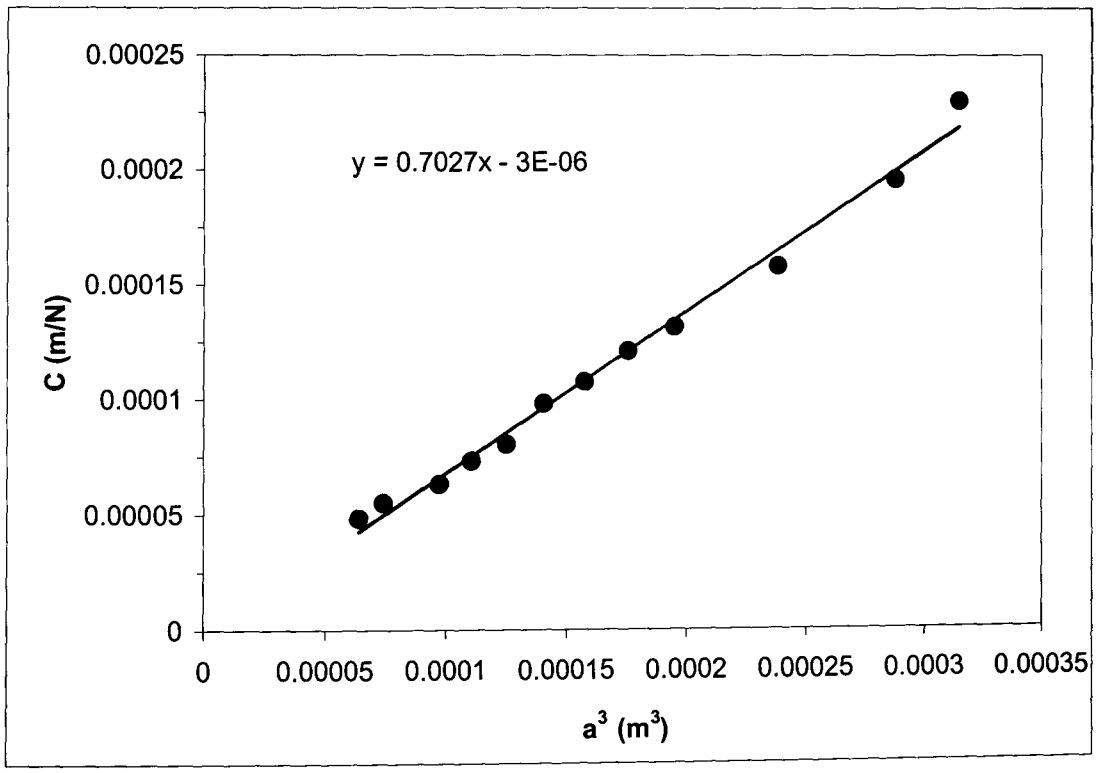

Figure 4.20 *Typical plot of C vs. a3 following an SCB test on an aluminium/GFPP sample at 1 mm/min.*

A typical resistance curve for a specimen tested at 1 mm/min is shown in Figure 4.21. From the figure, it is clear that the interfacial fracture energy rises rapidly with increasing crack length before plateauing at a value close to 3500 J/m^2. An examination of many of the specimens during testing indicated that the rising R-curve was generally associated with the development of extensive fibre bridging in the wake of the crack.

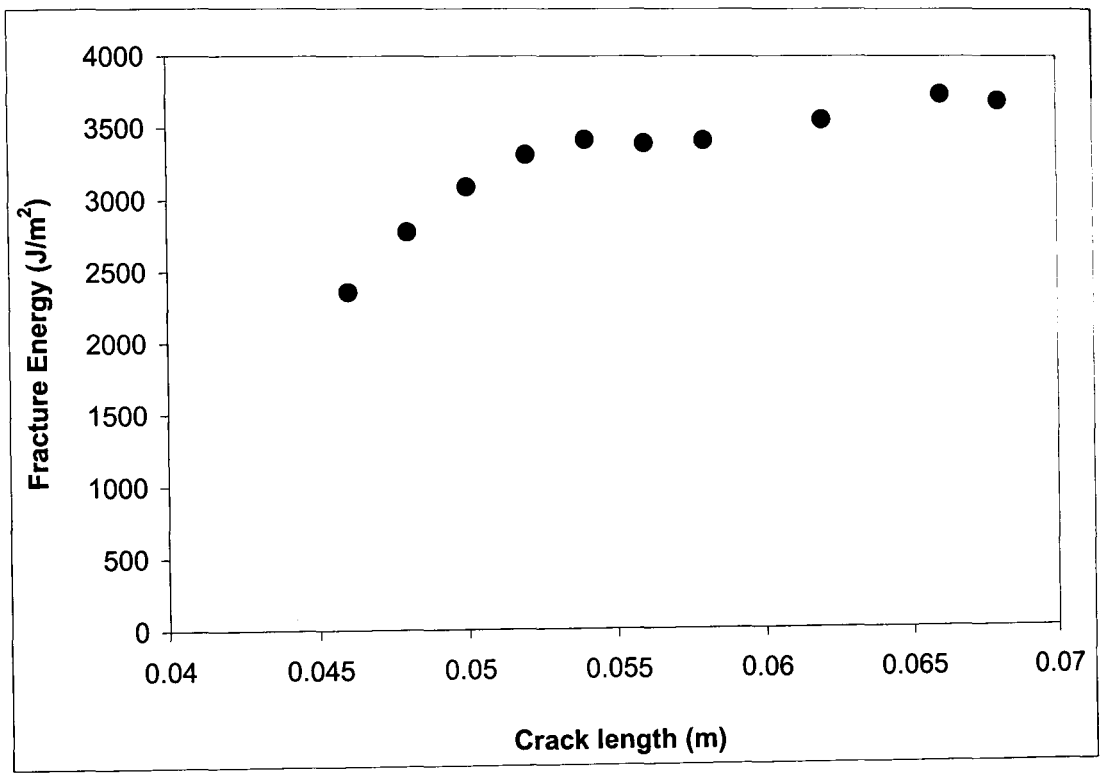

Figure 4.21 *Typical resistance curve following SCB testing at 1 mm/min on GFPP based FML.*

It is interesting to note that this value is very close to the $G_{I/IIc}$ of the plain composite. This suggests that the adhesion between the two dissimilar materials is excellent. Furthermore, the combination of an amorphous chromate coating surface treatment applied to the aluminium substrate and the incorporation of an interlayer of maleic anhydride-modified polypropylene has been proven to yield a strong bond at the bi-material interface. Therefore, this procedure should ensure excellent load

transfer between the two materials when subjected to loading conditions. It is worth noting that the thickness of the maleic anhydride-modified polypropylene interlayer should have a pronounced effect on the interfacial adhesion properties of this system. Indeed, a number of workers have observed that the thickness of the bonding interlayer has a significant effect on the interfacial fracture energy [25,27-28]. Here, increasing the thickness of the bonding interlayer resulted in a pronounced increase in fracture toughness before reaching a plateau. Continued increasing of the interlayer thickness resulted in a reduction in the fracture toughness. Therefore, in order to ensure an excellent interfacial fracture toughness between the aluminium and composite adherands an optimised interlayer thickness of 0.2 mm was used [29].

A low magnification micrograph of the aluminium fracture surface is shown in Figure 4.22. Here, crack propagation is from right to left. From this figure, it is apparent that large amounts of composite are left on the aluminium surface showing that the high degree of adhesion between the two materials has forced the crack to propagate mainly within the composite. Here, chemical interactions between the oxide/hydroxide layer on the treated aluminium and the reactive sites in the copolymer, together with mechanical interlocking due to the polymer flow into the pits on the aluminium surface, are prominent factors in achieving maximum adhesion. Similar results have been observed in other systems [30]. In addition, it can be observed that a high level of adhesion between the glass fibres and polypropylene has been developed as a result of the incorporation of the maleic anhydride interlayer. Here, modification of the polypropylene by the addition of the maleic anhydride copolymer has been reported to improve fibre/matrix adhesion and the corresponding fracture toughness of similar glass fibre/polypropylene systems [31,32]. A few broken fibres are also apparent in this micrograph. This is believed to be as a result of the fibre bridging mechanism observed during testing. The propagation of the crack mainly within the composite explains the why the mixed-mode interfacial fracture energies and interlaminar fracture energies mentioned previously are similar.

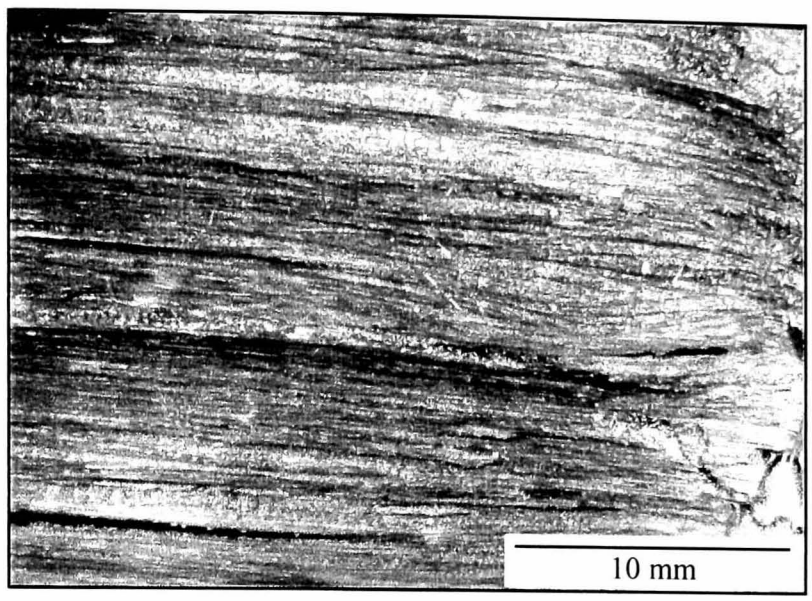

Figure 4.22 *Low magnification optical micrograph of the fracture surface of an alumium/GFPP FML following SCB testing at 1 mm/min.*

It is worth noting that for the MMF geometry, the ratio of G_I/G_{IIc} is 4/3 but for the SCB sample this ratio is likely to be different and may vary with crack length. In spite of this, agreement is still very good. In addition, it has been shown that excellent adhesion is achieved at the bi-material interface following a combination of an amorphous chromate coating to the aluminium substrate and the incorporation of an interlayer of maleic anhydride modified polypropylene. This procedure was subsequently followed throughout in the manufacture of GFPP based fibre-metal laminates.

4.4 INFLUENCE OF CROSSHEAD DISPLACEMENT RATE ON THE INTERFACIAL FRACTURE PROPERTIES OF FIBRE-METAL LAMINATES

It has been stated previously that the rate at which a structure is loaded affects the materials behaviour as well as the structural response of the target. Additionally, a strong interface must be achieved for adequate load transfer across the bondline.

Therefore, it is necessary to evaluate the effect of loading rate on the mixed-mode interfacial fracture properties of fibre-metal laminates.

4.4.1 Fracture toughness and post-failure fractography

A series of SCB mixed-mode interlaminar fracture tests was performed in order to evaluate the influence of the crosshead displacement rate on the interfacial fracture properties of fibre-metal laminates. The tests were performed at crosshead displacement rates between 1 mm/min and 2 m/s. During each test, the load and displacement data were recorded. At low and intermediate rates, crack propagation was monitored by eye. For rates above 100 mm/min, optical monitoring was no longer possible and an inverse compliance calibration was applied.

Figure 4.23 shows a typical load-displacement curves following SCB tests on the aluminium/CFRE based samples at 1 and 10 mm/min. From this figure, it is evident that crack propagation in the sample tested at the lowest rate occurred in a stable manner although some instabilities in which the crack jumped several millimetres are apparent and were observed in most specimens, Figure 4.23a. This behaviour has been associated with the presence of parallel (warp) and perpendicular (weft) yarns within the woven composite at the tip of the crack. Here, the delamination crack has multiple crack fronts one in each warp yarn. The crack advances most rapidly where the exposed yarns are aligned parallel to the crack direction, whereas the crack lags where the yarns are perpendicular to it. Therefore, the overall crack front is discontinuous in appearance [1]. Interestingly, crack propagation in the sample tested at 10 m/min was somewhat unstable with the crack propagating in a series of jumps, Figure 4.23b. Tests at higher rates of loading also resulted in an unstable mode of crack propagation suggesting that a transition from stable to unstable crack propagation exists between 1 an 10 mm/min. During the unloading phase, the curve did not return to the origin but exhibited a small residual displacement as a result of plastic deformation that had occurred during fracture of the specimen.

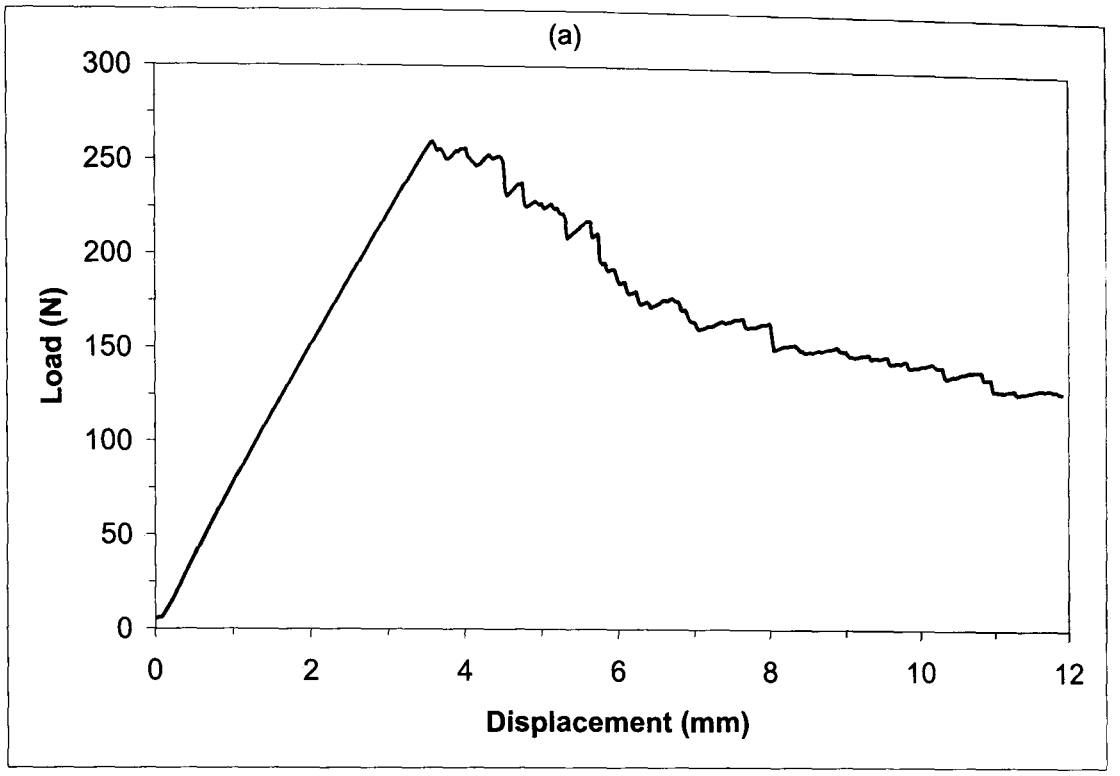

Figure 4.23 *Typical load-displacement curves following SCB tests on alumium/CFRE samples at (a)1 mm/min and (b) 10 mm/min.*

The mixed-mode interfacial fracture energy $G_{I/IIc}$ was then calculated using Equation 3.7. Figure 4.24 shows typical resistance curves resulting from the load-displacement curves in Figure 4.23. From the figure, it is clear that this system did not exhibit any pronounced R-curves with increasing crack length due to the absence of fibre bridging in this woven system. In addition, the values of interfacial fracture energy remained roughly constant plateauing at a value of approximately 2000 J/m^2 over the range of crack lengths considered. It is interesting to note that the values of $G_{I/IIc}$ are similar at both 1 and 10 m/min even though there was a change in the mode of crack propagation.

Figure 4.25 summarises the influence of the crosshead displacement rate on the interfacial fracture toughness of the CFRE based FML. This figure clearly shows that at low and intermediate displacement rates, the values of interfacial fracture energy remain roughly constant averaging approximately 2000 J/m^2 in all cases. At higher crosshead displacement rates, the values of interfacial fracture energy drop slightly although under impact conditions, the value remains close to 1700 J/m^2. These observations appear to agree with the findings of other researchers, who noted modest reductions in the mixed-mode interlaminar fracture toughness of similar carbon fibre/epoxy systems [15]. In addition, these results suggest that the interfacial properties of the CFRE-based fibre-metal laminates are still very impressive at dynamic rates of strain. It is interesting to note that these values are very close to the mixed-mode values of $G_{I/IIc}$ measured on the plain composite (Fig. 4.12), suggesting that failure in these bi-material samples is closely linked to this parameter although there was a change in the mode of crack propagation.

A post-failure examination of the failed specimens was performed in order to elucidate the fracture mechanisms occurring at the bi-material interface. Figure 4.26 shows low magnification optical micrographs of the aluminium substrates of SCB

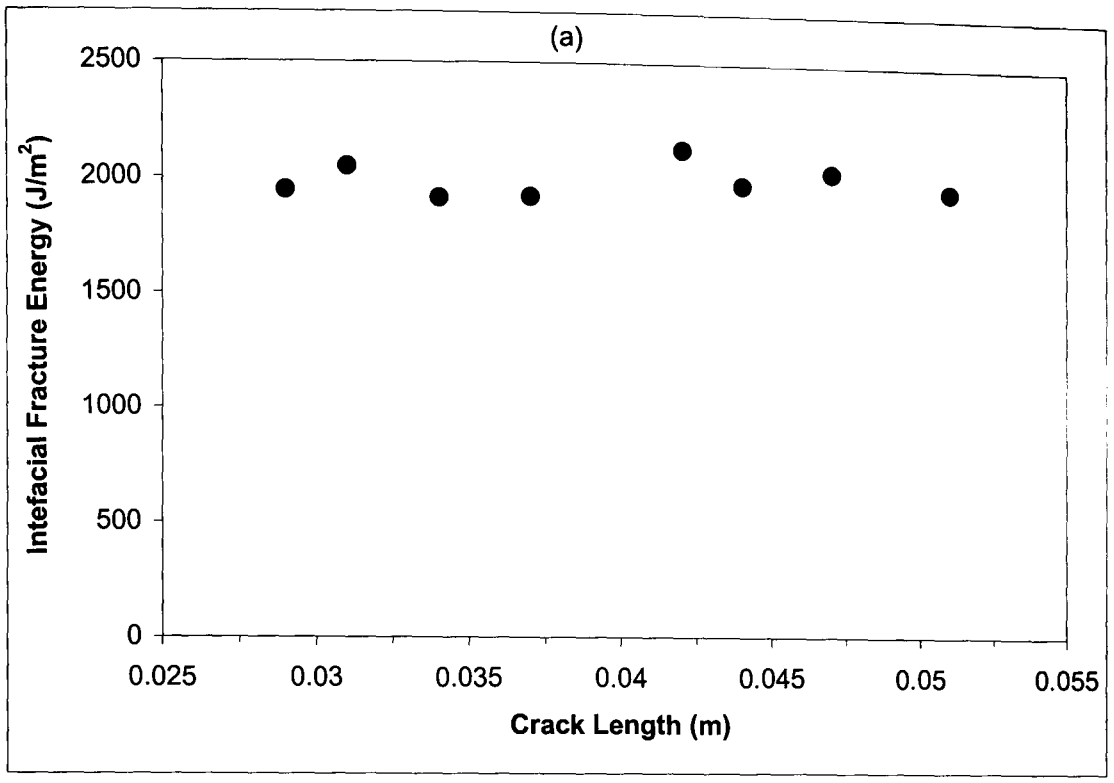

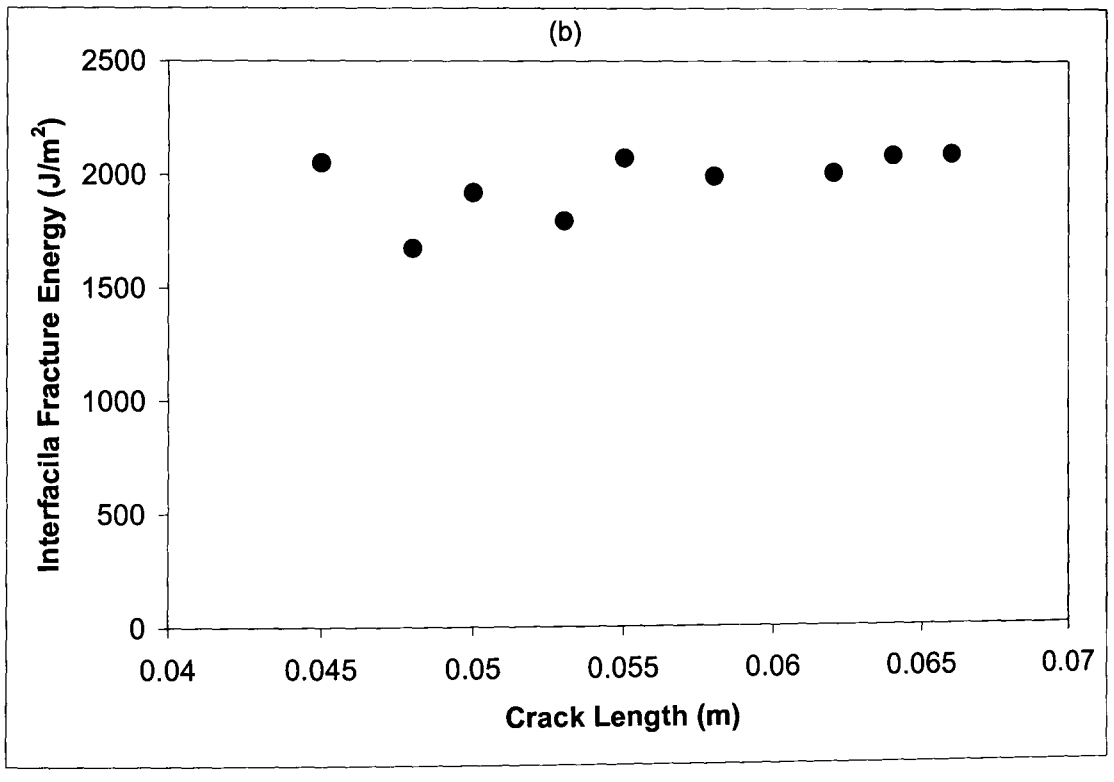

Figure 4.24 *Typical resistance curves following SCB tests on aluminium/CFRE samples at (a) 1 mm/min and (b) 10 mm/min.*

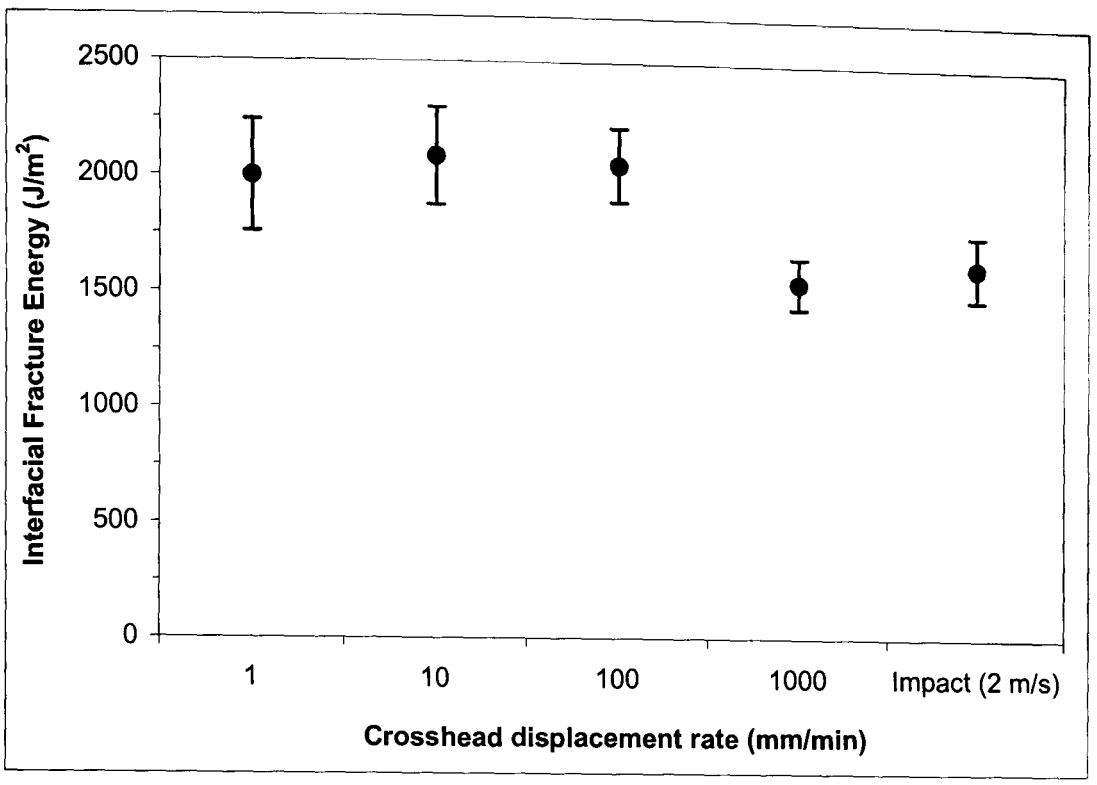

Figure 4.25 *Influence of crosshead displacement rate on the SCB mixed-mode interfacial fracture properties of CFRE based FML.*

specimens tested at 100 mm/min and 2 m/s. Crack propagation is from right to left in both cases. A closer examination of the fracture surface of the specimen tested at 100 mm/min highlights the presence of large amounts of residual composite on the aluminium substrate. This suggests that the level of adhesion between composite and aluminium is excellent at intermediate rates of loading although small areas of aluminium are still visible. In this case, the crack had propagated mainly within the composite (Figure 4.26a). Under impact loading conditions, the aluminium substrate is almost completely covered by residual composite (Figure 4.26b). Here, the crack propagates in an interlaminar mode mainly within the composite suggesting that this system exhibits an outstanding level of adhesion at higher rates of loading. This examination suggests that failure in this system changed from a mixture of

interfacial/interlaminar fracture at the lowest rate of loading to fully interlaminar fracture under impact loading conditions.

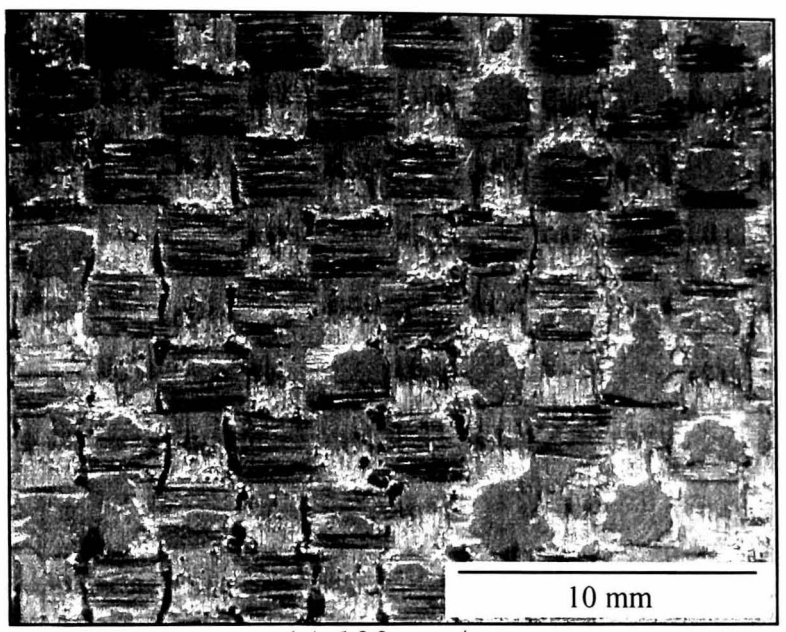

(a) 100 mm/min

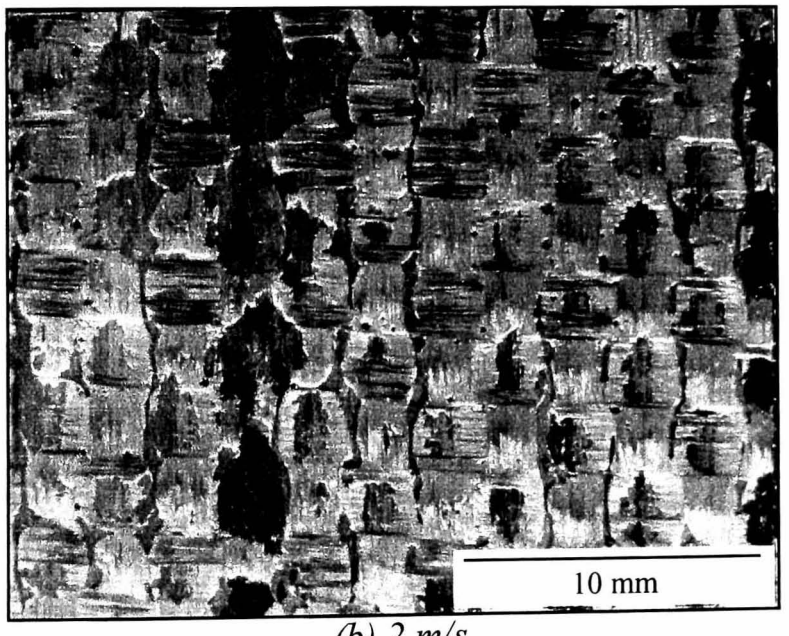

(b) 2 m/s

Figure 4.26 *Low magnification optical micrographs showing residual CFRE on aluminium substrates following SCB tests.*

In order to gain a greater insight into the fracture process, many of the samples were coated with a thin conducting layer and examined in the scanning electron microscope. Figure 4.27 shows typical SEM micrographs of residual composite on the aluminium adherands of specimens tested at 1, 100 mm/min and 2 m/s. An examination of the fracture surfaces highlights the presence of matrix ductility at a crosshead displacement rate of 1 mm/min, Figure 4.27a. A similar level of plastic deformation is apparent at 100 mm/min, Figure 4.27b. It is interesting to note that at a crosshead displacement rate of 2 m/s, the level of ductility is very similar to that observed at the lower rates of loading, Figure 4.27c. In addition, It is apparent that a number of hackles associated with mode II failure are apparent even though the values of interfacial fracture energy are very close to the mode I values of the plain composite.

The influence of the crosshead displacement rate on the mixed-mode interfacial fracture properties of the glass fibre/polypropylene-based fibre-metal laminates was evaluated using the same test arrangement as that used for testing the CFRE-based FML. The tests were performed at crosshead displacement rates between 0.1 mm/min and 2 m/s. During each test, the load and displacement data were recorded. At low and intermediate rates, crack propagation was monitored by eye. For rates above 100 mm/min optical monitoring was no longer possible and an inverse compliance calibration was applied.

Figure 4.28 shows typical load-displacement curves following SCB tests on aluminium/GFPP samples at 0.1 and 10 mm/min. At 0.1 mm/min the initial loading curve exhibits some non-linearity which may be associated with some plasticity in the composite adherends, Figure 4.28a. From this figure, it is evident that crack propagation occurred in a semi-stable manner although some instabilities giving rise to a saw-tooth appearance in the load-displacement curve are apparent. The load-displacement curve at the higher rate of loading exhibited a much smoother appearance with the crack propagating in a stable manner and only small occasioned steps are apparent.

(a) 1 mm/min

(b) 100 mm/min

(d) 2 m/s

Figure 4.27 *Scanning electron micrographs showing residual composite on the aluminium adherands following SCB tests.*

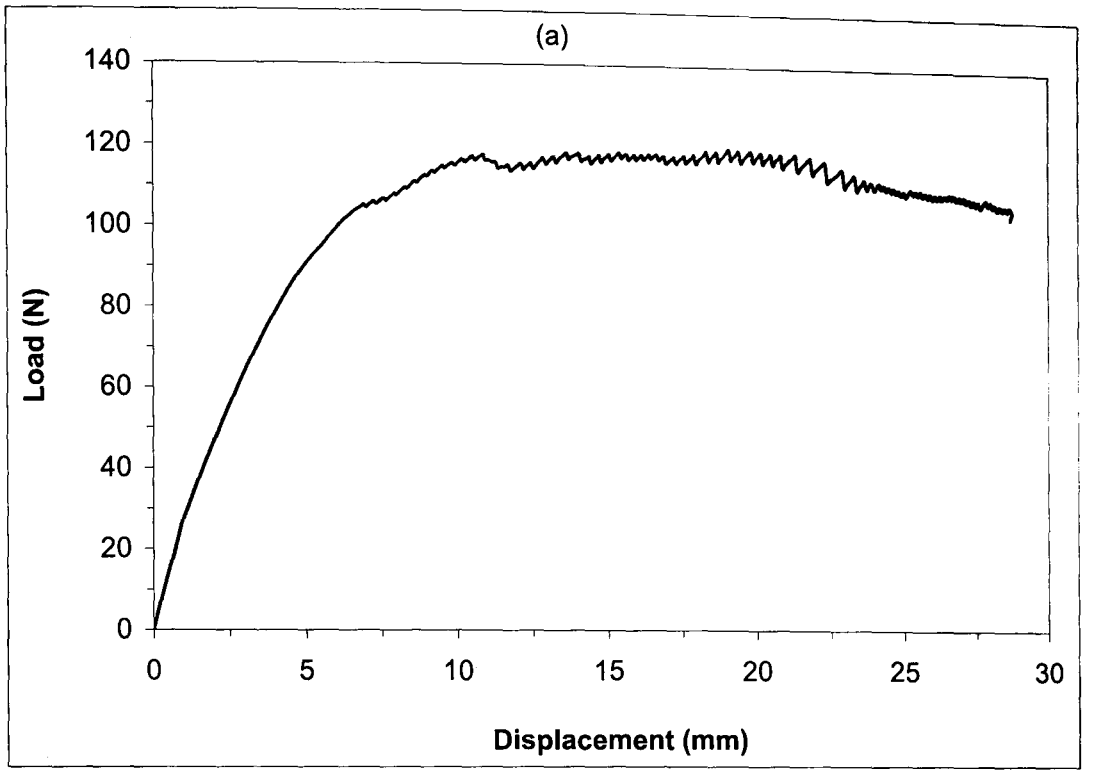

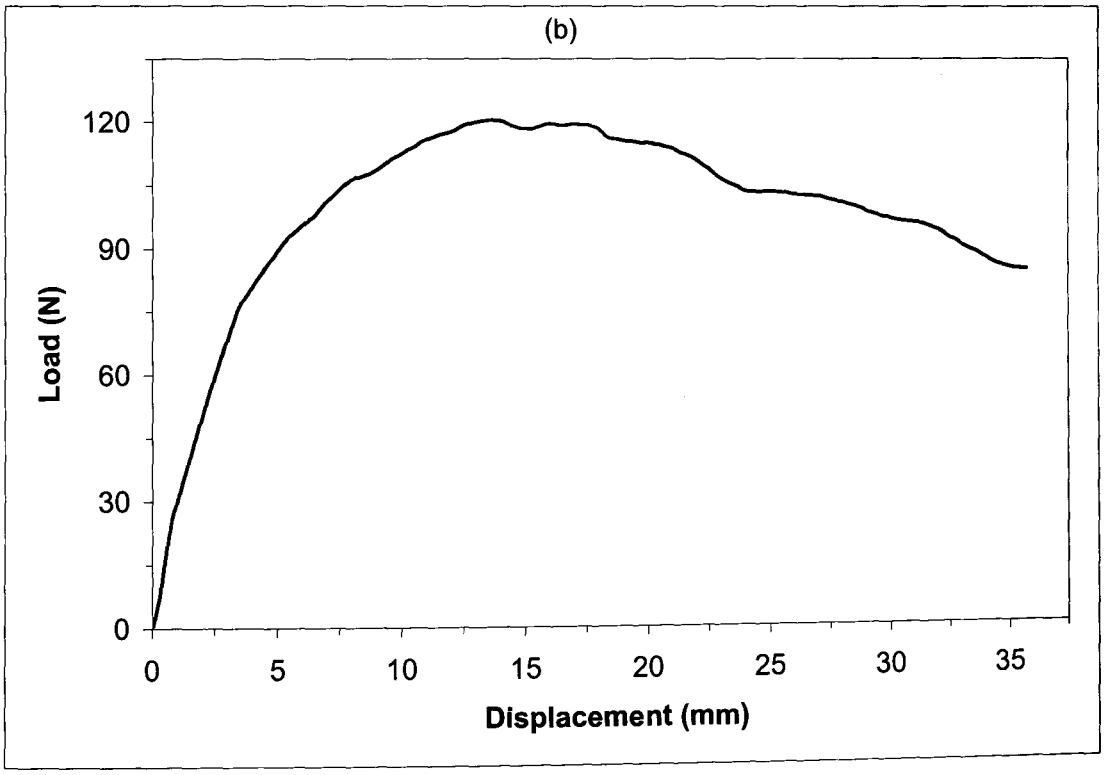

Figure 4.28 *Typical load-displacement curves following SCB tests on aluminium/GFPP samples at (a)1 mm/min and (b) 10 mm/min.*

This information was used to determine the mixed-mode interfacial fracture energy $G_{I/IIc}$, at different rates of loading.

Figure 4.29 shows typical resistance curves following SCB tests on the aluminium/GFPP samples at 0.1 and 10 mm/min. From this figure, it is clear that at the lowest rate the fracture energy increases almost continuously as crack length is increased before plateauing at a values close to 2500 J/m^2, Figure 4.29a. This is particularly pronounced over the first 15 mm of crack propagation. An examination of many of the specimens during testing indicated that the rising on the *R*-curve was generally associated with the development of extensive fibre bridging in the wake of the crack. The R-curve for the sample tested at 10 mm/min also shows an initial increase before reaching a steady-state value of around 3500 J/m^2. It is interesting to note that resistance curves effects became less pronounced as the crosshead displacement was increased. This may be due to viscoelastic effects in the polypropylene matrix.

Figure 4.30 shows a plot of compliance vs. the cube of crack length following an SCB test on an aluminium/GFPP specimen at 1 mm/min. The curve contains the initial and final compliance and crack length values. An inverse compliance calibration was then applied to the load displacement results for this test. This procedure was the used to determine the crack length at intermediate compliances and these values were compared with the experimentally-measured values of crack length to evaluate the accuracy of the inverse compliance calibration technique. Table 4.1 compares the calculated values of crack length with the values measured by aye. By comparing the data, it is apparent that the inverse compliance calibration technique successfully predicts the crack length over the range of crack lengths considered. Indeed, the error was approximately five percent. This suggests that the inverse compliance calibration technique can be used with confidence to determine intermediate crack lengths in samples tested at higher rates of loading.

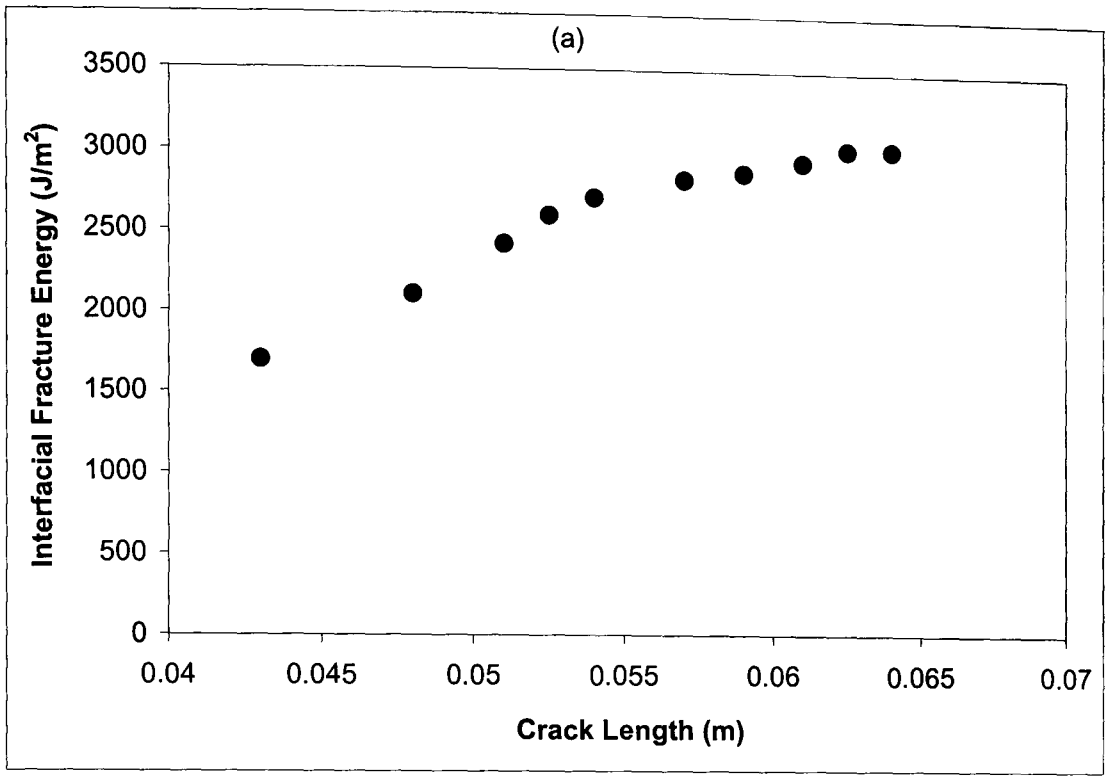

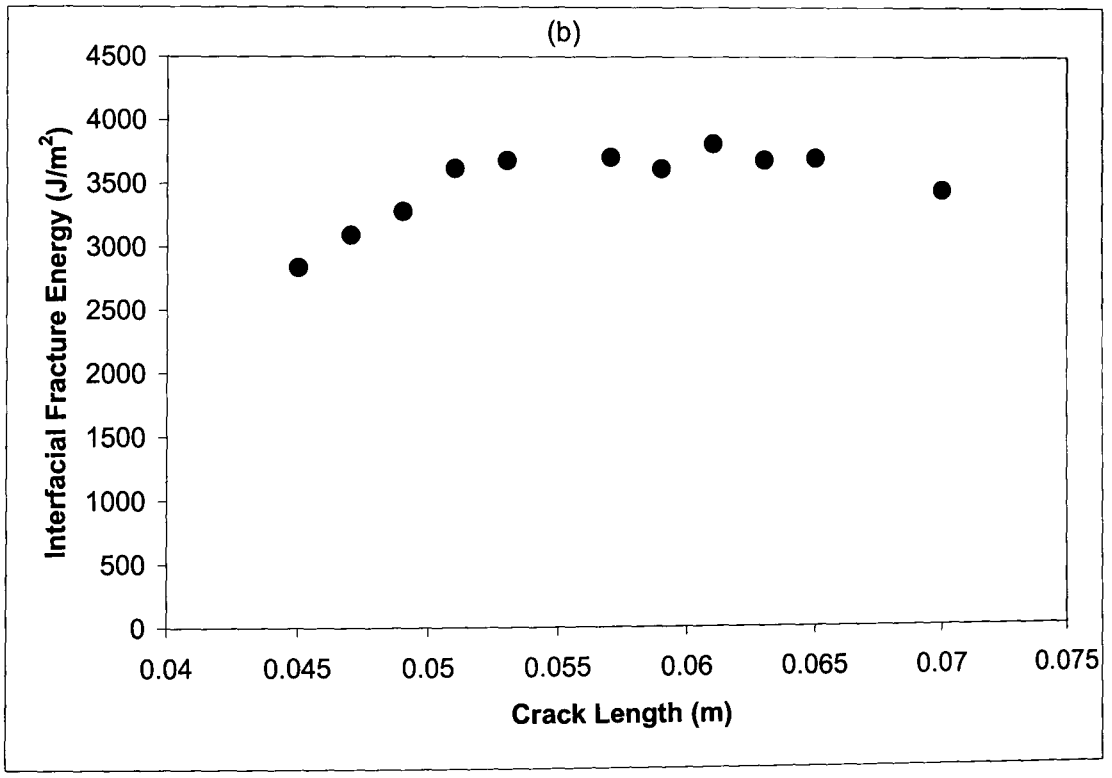

Figure 4.29 *Typical resistance curves following SCB tests on aluminium/GFPP samples at (a) 1 mm/min and (b) 10 mm/min.*

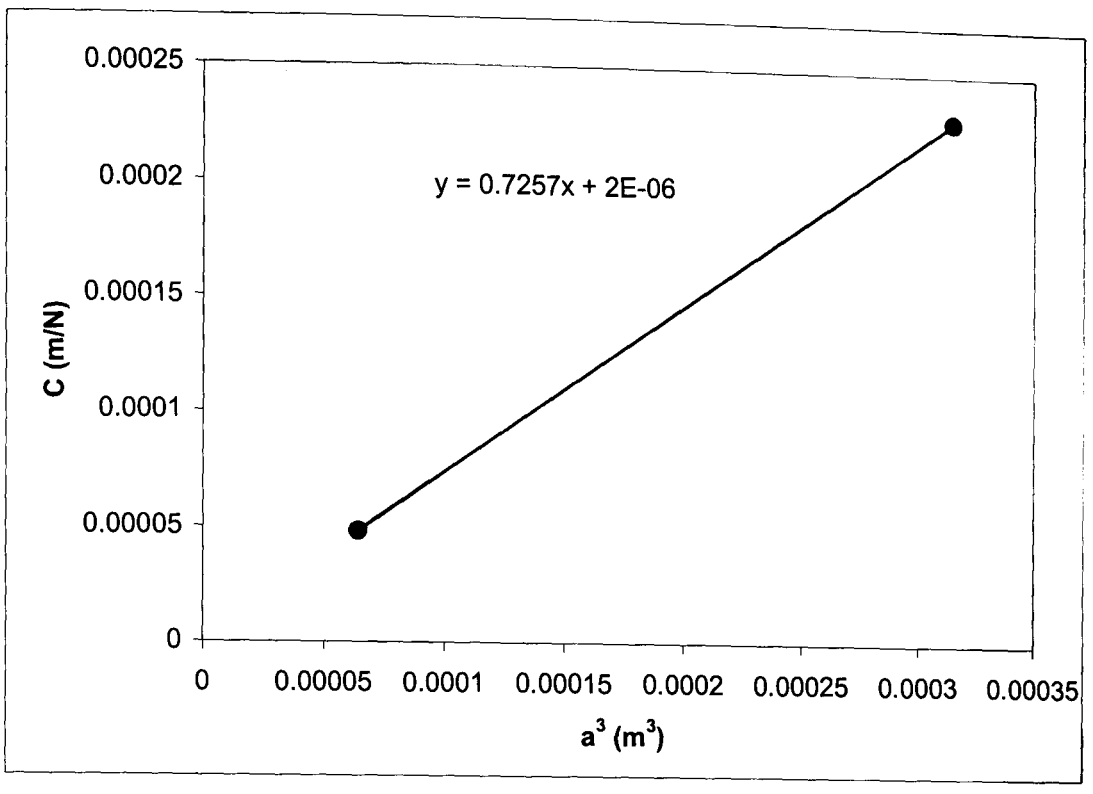

Figure 4.30 *Typical plot of initial and final compliance and a^3 data following an SCB tests on an aluminium/GFPP sample at 1 mm/min.*

Figure 4.31 shows the variation of the average of the plateau values of interfacial fracture energy with crosshead displacement rate. From this figure, it is evident that the interfacial fracture toughness is approximately 2800 J/m^2 at the lowest rate of loading. With increasing loading rate, the interfacial fracture energy increases quite rapidly reaching an average value of approximately 4700 J/m^2 at 100 mm/min. At high rates of loading, the interfacial fracture toughness begins to fall once again dropping to a value of approximately 3000 J/m^2 at impact rates of loading. It is interesting to note that the values of interfacial fracture energy of the GFPP-based fibre-metal laminates are still very impressive at dynamic rates of strain. In addition, these values are very close to the mixed-mode values of $G_{I/IIc}$ measured on the plain composite (Fig. 4.14) although most values at low and high loading rates are lower for the bi-material systems.

Compliance **C** (m/N)	**a** measured (m)	**a** calculated (m)
4.81E-05	0.040	0.040
5.49E-05	0.042	0.042
6.29E-05	0.046	0.044
7.31E-05	0.048	0.046
8.02E-05	0.050	0.048
9.80E-05	0.052	0.051
1.07E-04	0.054	0.053
1.21E-04	0.056	0.055
1.31E-04	0.058	0.056
1.58E-04	0.062	0.060
1.95E-04	0.066	0.064
2.30E-04	0.068	0.068

Table 4.1 *Measured and calculated crack lengths following an SCB test on an aluminium/GFPP sample at 1 mm/min using an inverse compliance calibration technique.*

This suggests that failure in these bi-material samples is closely linked to the $G_{I/IIc}$ of the composite. However, it is worth reiterating that the mixed-mode conditions is slightly different for both the SCB and MMF samples. In addition, the true strain rate at the crack tip in the SCB and MMF samples will be different at the same crosshead displacement rate. Furthermore, these trends suggest that there may be other competing failure mechanisms present within the crack tip region, which will be discussed below.

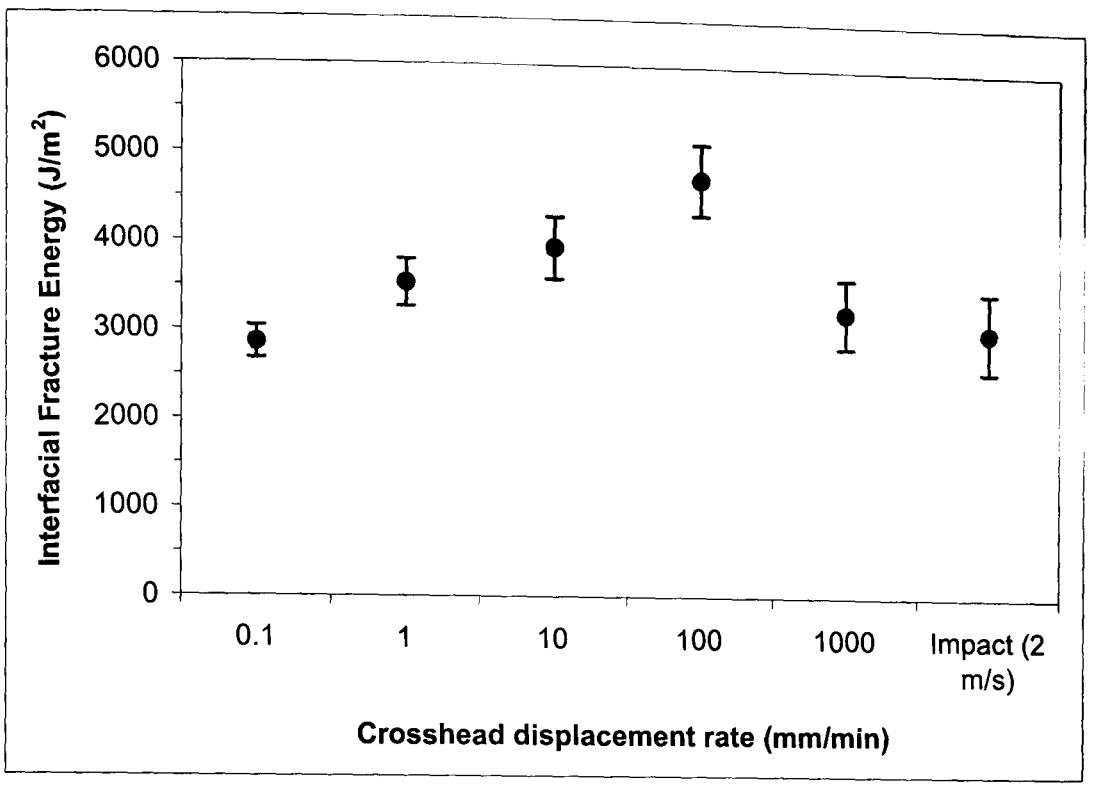

Figure 4.31 *Influence of crosshead displacement rate on the SCB mixed-mode interfacial fracture properties of the GFPP-based FML.*

A post-failure examination of the failed specimens was performed in order to elucidate the fracture mechanisms occurring at the bi-material interface. Figure 4.32 shows low magnification optical micrographs of the aluminium substrates of SCB specimens tested at 0.1,100 mm/min and 2 m/s. Crack propagation is from right to left in all cases. At the lowest rate of loading, it is clear that in certain regions the crack has propagated along the bi-material interface whereas in other areas it has extended within the fibre reinforced composite, Figure 4.32a. A closer examination of the fracture surface highlights the presence of a number of striations on the aluminium adhered. These ridges consist of pure polypropylene and are associated with the small instabilities observed in the load-displacement curve in Figure 4.28a. From the top portion of the micrograph, it is clear that a number of fibres are slightly distorted, probably as a result of localised flow during the moulding process.

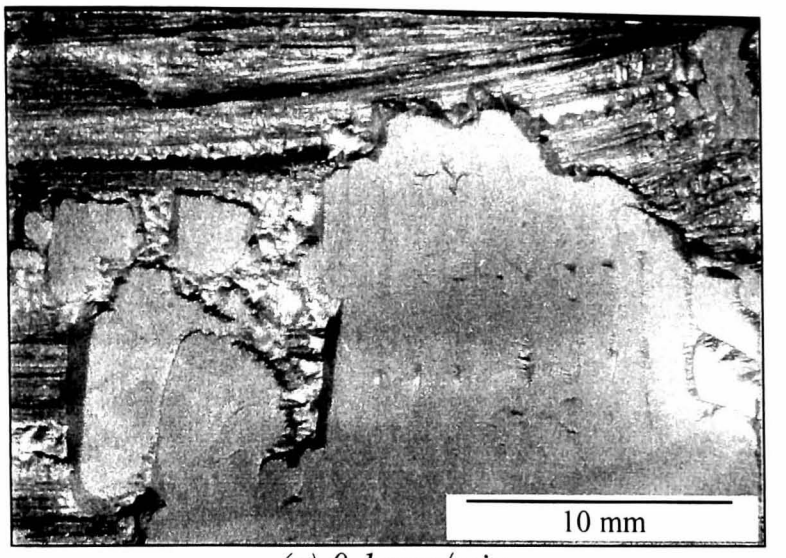

(a) 0.1 mm/min

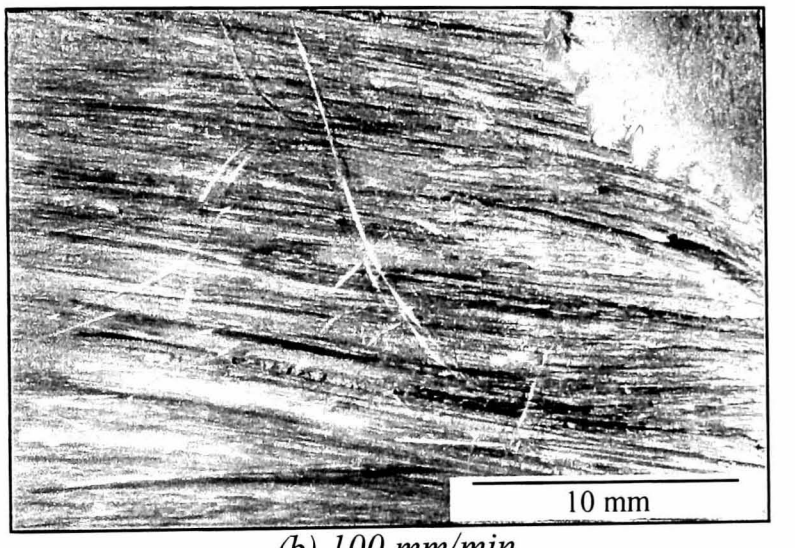

(b) 100 mm/min

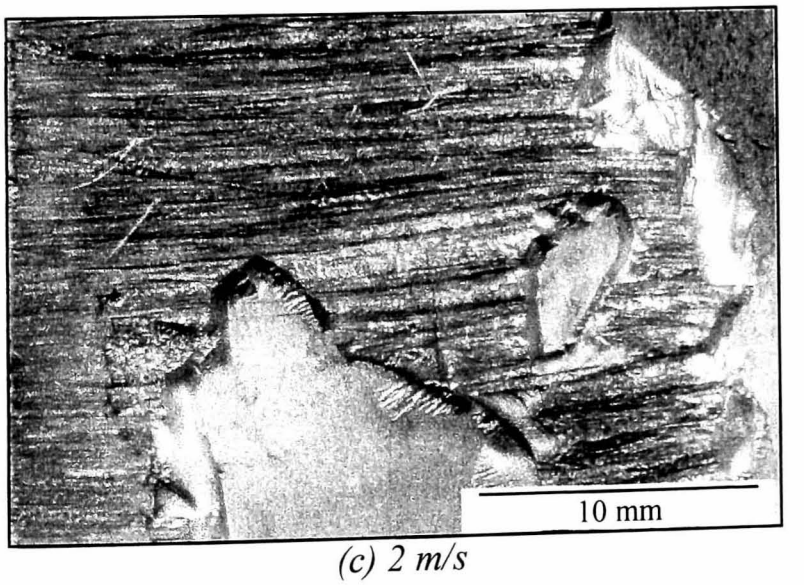

(c) 2 m/s

Figure 4.32 *Low magnification optical micrographs showing residual GFPP on aluminium substrates following SCB tests.*

At 100 mm/min, the crack remains largely within the composite although a small region of exposed aluminium was in evidence, Figure 4.32b. Here again, there is evidence of appreciable amounts of fibre movement during the manufacturing operation. In addition, a number of broken fibres are also apparent as a result of the fibre bridging during the test. This fracture mechanism is associated with the rising in the *R*-curves as mentioned previously. It is interesting to note that the values of fracture energy following SCB tests are very similar to those obtained following MMF tests. Under impact loading conditions, the fracture surface again exhibits a mixed appearance with the crack oscillating between the interface and the composite, Figure 4.32c. This change in the locus of the crack suggests that the toughness of the maleic anhydride-modified polypropylene/aluminium bond is rate sensitive. This evidence suggests that the initial increase in the interfacial fracture energy with crosshead displacement rate in Figure 4.31 may be associated with a greater tendency for the crack to propagate within the tough composite material. Furthermore, it is apparent that the reduction in the interfacial fracture toughness at impact rates of loading is associated with a tendency for the crack to propagate in a combined interfacial/interlaminar manner.

In order to gain a greater insight into the fracture process, many of the samples were coated with a thin conducting layer and examined in the scanning electron microscope. Figure 4.33 shows typical SEM micrographs of residual composite on the aluminium adherands of specimens tested at 0.1, 100 mm/min and 2 m/s. An examination of the fracture surfaces highlights the presence of significant plastic deformation in the matrix material at a crosshead displacement rate of 0.1 mm/min (Figure 4.33a). As the crosshead displacement rate is increased, the amount of plastic deformation in the matrix is slightly reduced suggesting the presence of matrix yielding, a toughening mechanism observed previously (Figure 4.33b). The fracture surfaces of samples tested under impact conditions exhibited smaller amounts of matrix ductility suggesting the presence of a ductile to brittle transition in the matrix (Figure 4.33c).

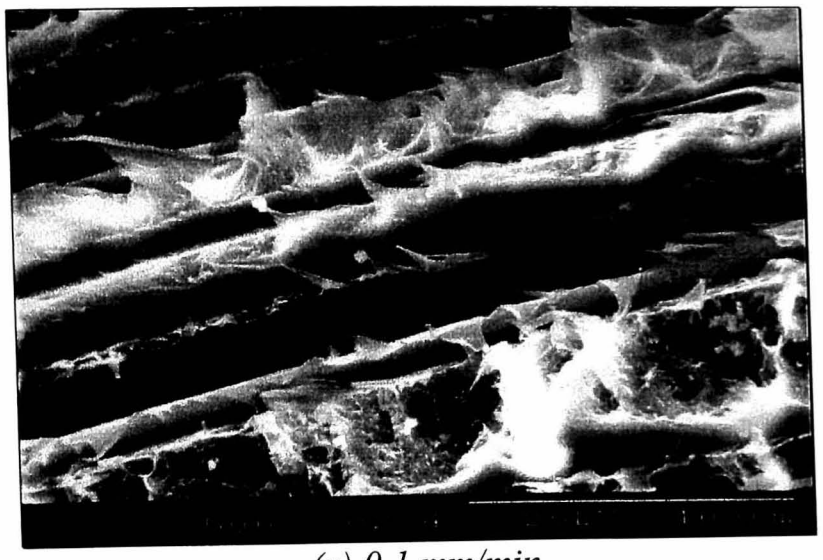

Crack propagation

(a) 0.1 mm/min

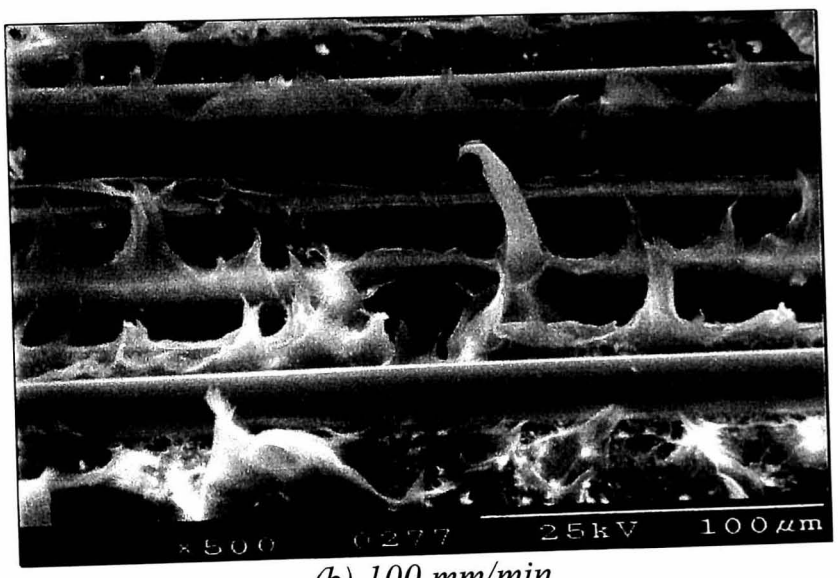

(b) 100 mm/min

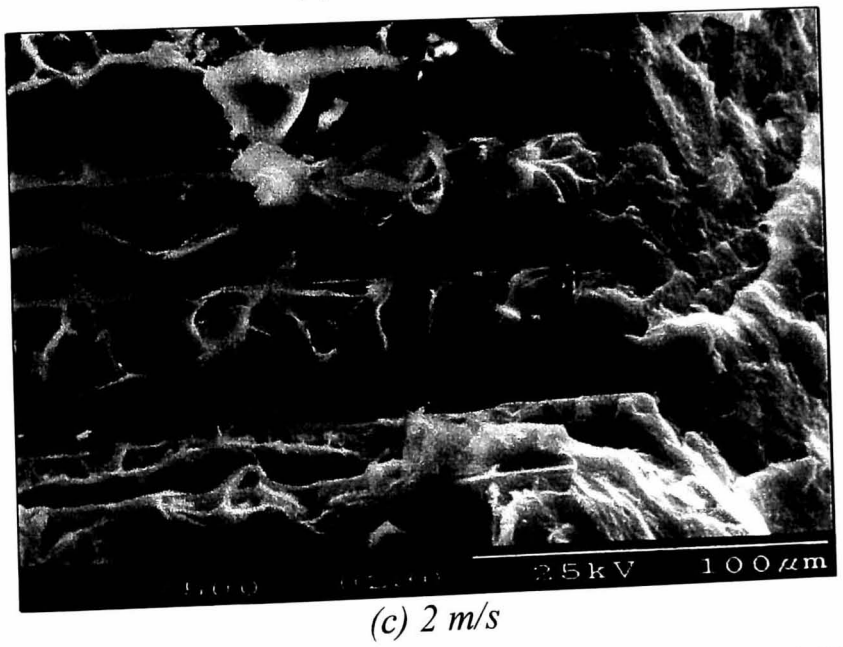

(c) 2 m/s

Figure 4.33 *Scanning electron micrographs showing residual GFPP on the aluminium adherands following SCB tests.*

Therefore, it is believed that the presence of the matrix yielding toughening mechanism, coupled with the change in failure locus, may explain the variation of the interfacial fracture toughness with crosshead displacement rate. In addition, it is interesting to note that the level of plastic deformation is less significant than that exhibited by the MMF samples suggesting that the maleic anhydride-modified polypropylene interlayer is less ductile than the plain polypropylene.

4.5 INTERFACIAL FRACTURE MECHANISMS IN THE FIBRE-METAL LAMINATES

The SCB tests on bi-material specimens based on thermoset and thermoplastic matrices highlighted the presence of a number of failure mechanisms during fracture. These tests were performed at crosshead displacement rates between 0.1 mm/min and 2 m/s. Here, matrix yielding was observed along with a ductile to brittle transition in the matrix material and a change in the locus of the primary crack between the aluminium and composite plies. This suggests that two or more competitive failure mechanisms are present during fracture.

4.5.1 Crack initiation and propagation

In order to gain a greater understanding of the fracture mechanisms occurring during failure in these bi-material specimens, the modified double end notch flexure (DENF) test geometry shown in Figure 3.9 was used. Here, prior to lamination, folded aluminium starter inserts were incorporated at each end of the bi-material samples. Prior to testing, the specimen edges were ground and polished to a one micron finish and a thin layer of silver was the sputtered onto one of the specimen edges. Three point bend tests were then undertaken at crosshead displacement rates between 0.1 mm/min and 2 m/s. The tests were stopped once a visible crack had propagated from one of the starter defects. The crack tip region around the "un-propagated" defect was then examined in the scanning electron microscope. It is worth noting that the DENF geometry is clearly different from that of the SCB

configuration and does not necessarily offer the same loading conditions at the crack tip. In spite of this, it is felt that this geometry offers useful information for understanding the failure processes in thermosetting and thermoplastic based fibre-metal laminates.

Figure 4.34 shows scanning electron micrographs taken from the crack tip region of carbon fibre / epoxy based DENF specimens tested at 1, 100 mm/min and 2 m/s. At 1 mm/min, a small crack extending from the folded aluminium pre-crack into the composite is visible, Figure 4.34ai. This information is in agreement with the observations in Figure 4.18d where a mixed interfacial/interlaminar failure was observed in which some areas of aluminium were still visible. A closer examination of the crack-tip region highlighted the presence of a number of microcracks in the matrix, Figure 4.34aii. Although it is possible that these cracks are associated with the failure of the conducting metallic layer, it is believed that their presence is indicative of significant plastic flow within the polymeric matrix as observed in Figure 4.27a. At 100 mm/min, Figure 4.34bi, the primary crack remains within the composite, propagating predominantly along fibre/matrix interfaces as a result of the excellent adhesion achieved between the aluminium and composite materials. A closer examination of the crack tip region again highlights the presence of an array of microcracks, Figure 4.34bii, generated as a result of plastic deformation within the matrix prior to crack initiation. Crack initiation and propagation in the specimens tested under impact loading conditions occurred within the composite as shown in Figure 4.34ci. At this rate of loading, there is very little evidence of plastic deformation or other energy-absorbing mechanisms in the crack tip region suggesting that the ductility of the polymer is greatly reduced at higher loading rate, Figure 4.34cii.

These results show that crack propagation in the SCB samples changes from interfacial/interlaminar to fully interlaminar with increasing crosshead displacement rate. This change in the locus of the crack is associated with an increase in interfacial fracture energy at intermediate loading rates. However, under impact

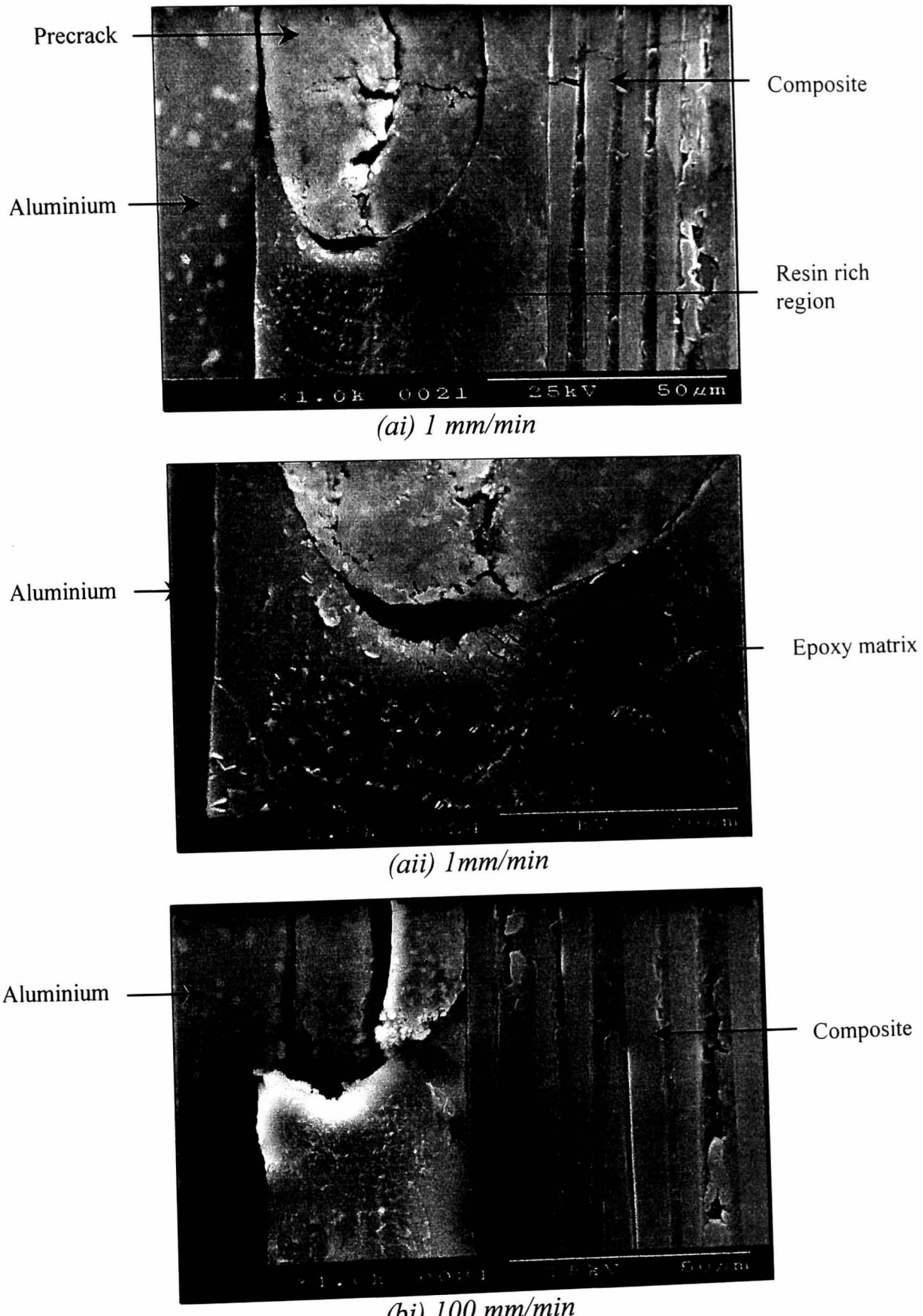

Figure 4.34 *Scanning electron micrographs of the edges of a CFRE-based FML following DENF tests.*

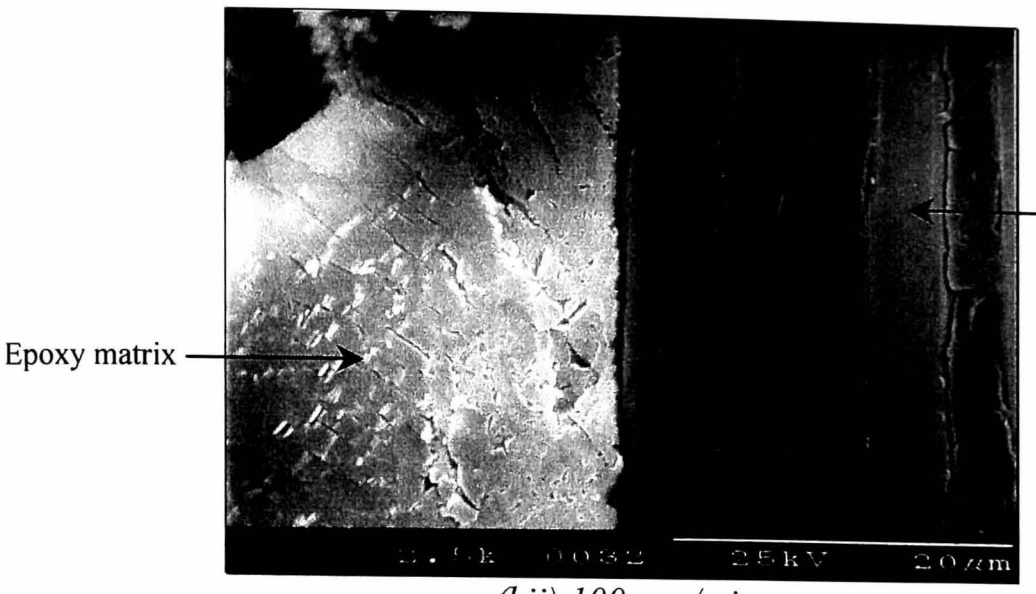

(bii) 100 mm/min

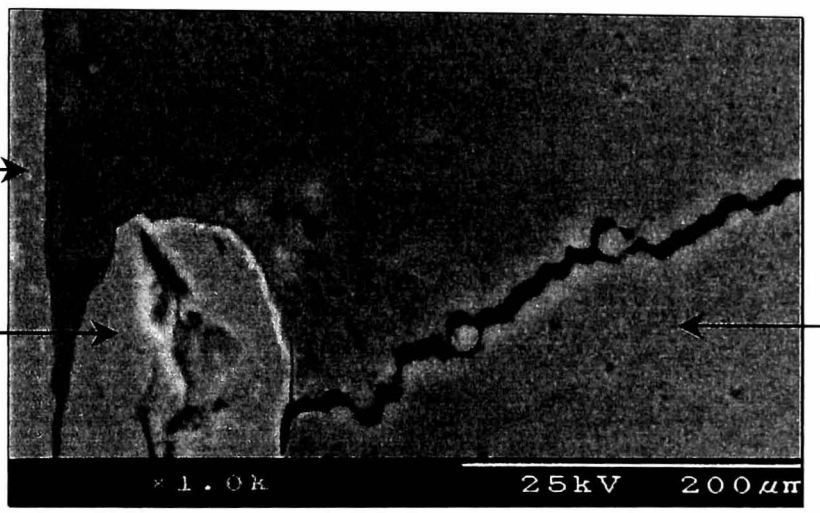

(ci) 2 m/s

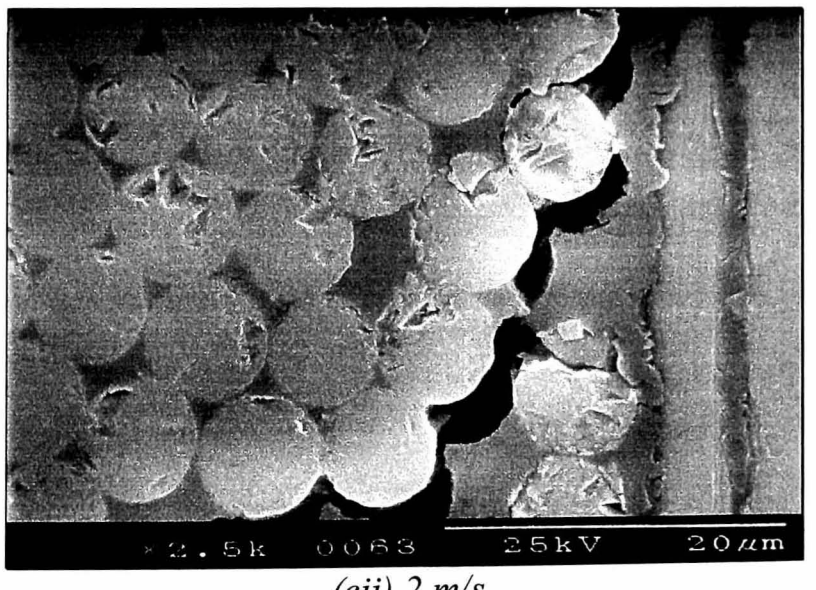

(cii) 2 m/s

Figure 4.34(Cont.) *Scanning electron micrographs of the edges of a CFRE-based FML following DENF tests.*

loading conditions, a reduction in the interfacial fracture energy was observed. This was associated with a reduction in the level of plastic deformation in the matrix material as a result of a ductile to brittle transition at higher rates of loading.

As with the CFRE-based FML, the modified double end notch flexure (DENF) test geometry shown in Figure 3.9 was used to gain a greater understanding of the fracture mechanisms occurring during failure. Figure 4.35 shows scanning electron micrographs taken from the crack tip region of glass fibre/polypropylene based DENF specimens tested at 0.1, 100 mm/min and 2 m/s. At 0.1 mm/min, a small crack extending from the folded aluminium precrack into the composite is visible along with a region of delamination between the polypropylene matrix and the aluminium substrate, Figure 4.35ai. This information is in agreement with the observations in Figure 4.32 where a mixed interfacial/interlaminar failure was observed. A closer examination of the crack tip region highlighted the presence of a number of microcracks in the thermoplastic matrix, an indication of significant plastic flow within the polymeric matrix, Figure 4.35aii. At 100 mm/min, Figure 4.35bi, the primary crack remains within the composite propagating predominantly along the fibre/matrix interface. Here, a number of broken fibres are also apparent. A closer examination of the propagation of the crack highlights the presence of extensive plastic deformation in the matrix, Figure 4.35bii. Here, it is clear that crack propagation occurred in an interlaminar mode. Under impact loading conditions, crack propagation occurred within the thermoplastic composite and the interlayer material although small regions of delamination were observed at the interface with the aluminium alloy as shown in Figure 4.35ci. At this rate of loading, there is very little evidence of plastic deformation in the matrix suggesting that the polymer's ability to flow is greatly reduced, Figure 4.35cii. A similar reduction in plastic deformation in the matrix was observed on the fracture surfaces shown previously in Figure 4.33c. These findings suggest that the locus of the crack exhibited a mixed appearance between interfacial and interlaminar propagation as a result of variations in the crosshead displacement rate.

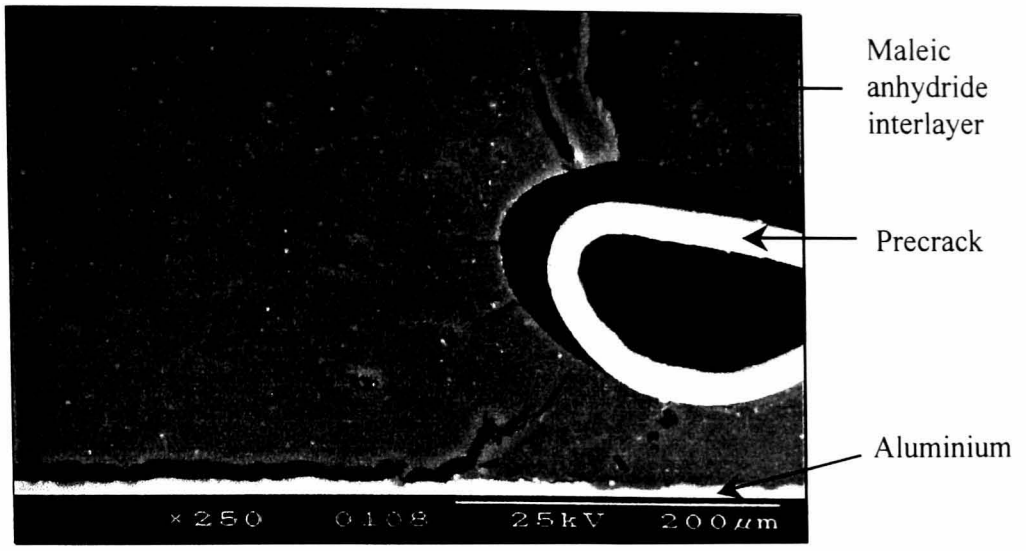

(ai) 0.1 mm/min

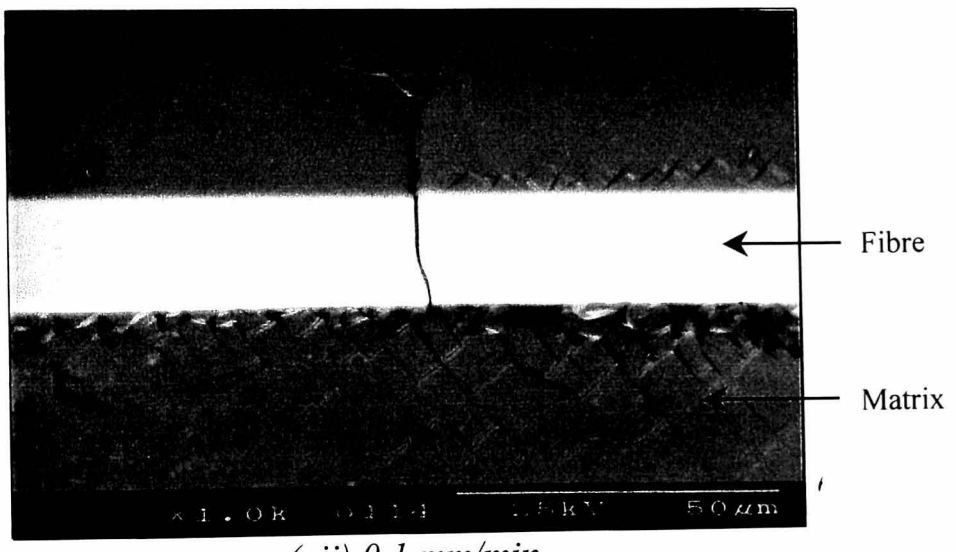

(aii) 0.1 mm/min

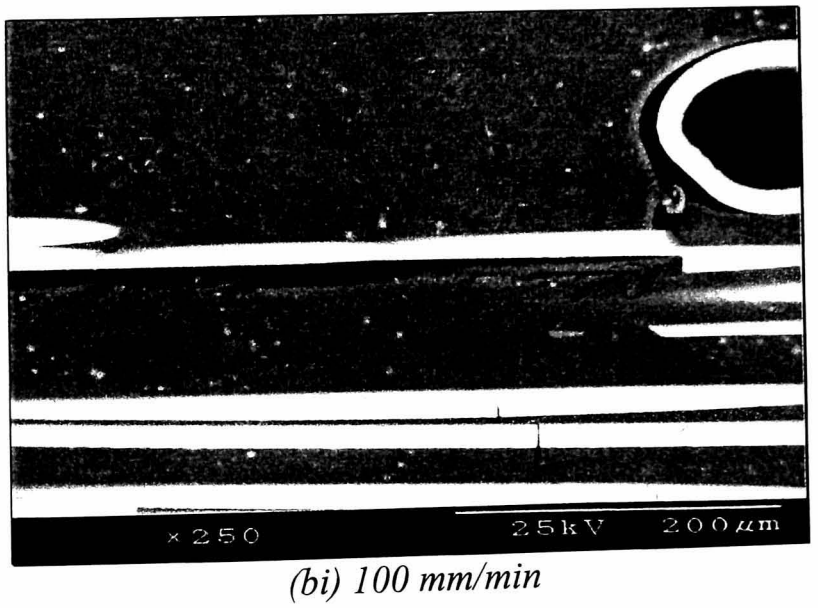

(bi) 100 mm/min

Figure 4.35 *Scanning electron micrographs of the edges of GFPP-based FMLs following DENF tests.*

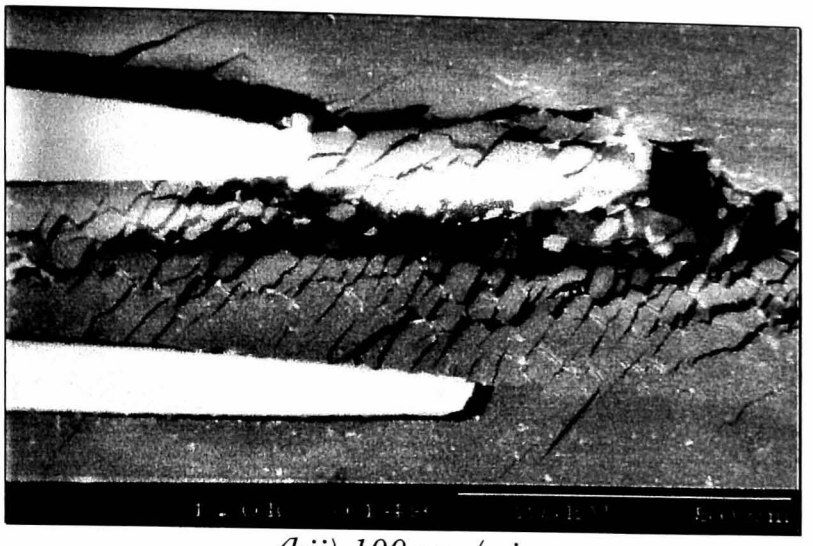

(bii) 100 mm/min

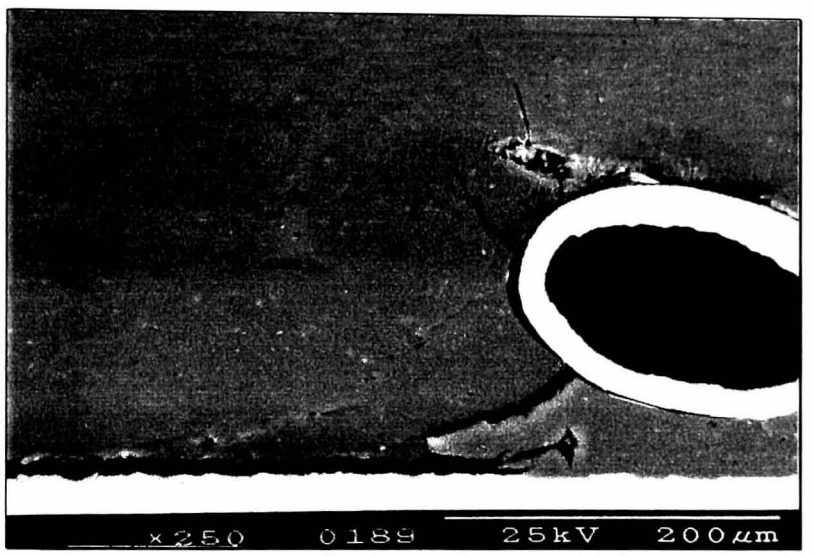

(ci) 2 m/s

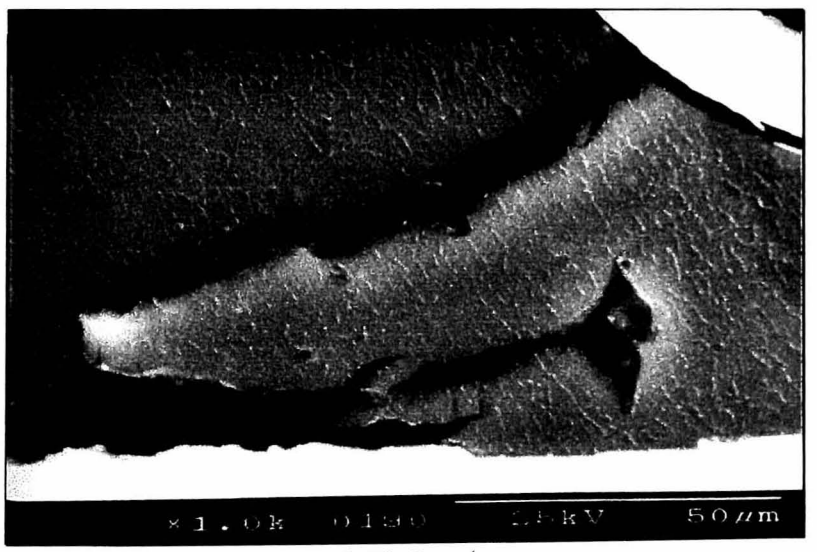

(cii) 2 m/s

Figure 4.35 (Cont.) *Scanning electron micrographs of the edges of GFPP-based FMLs following DENF tests.*

4.6 RESIDUAL STRESSES

Fibre-metal laminates are layered arrangements of aluminium alloy and composites plies. One of the drawbacks of theses hybrid systems in the as-cured condition is the state of the residual stresses introduced by the differential thermal expansion of the aluminium and composite layers during the curing and subsequent cooling processes. In order to evaluate the magnitude of the residual stresses in the thermosetting and thermoplastic-based fibre-metal laminates considered in this programme, the Utah Laminates 3.0 software was used. Here, the elastic and thermal properties of the aluminium alloy and composite materials were used along with the stress free temperatures for each system (see appendix A.5).

Table 4.2 summarises the residual stresses in the range of symmetrical CFRE-based fibre-metal laminates considered in this study. From the data, it is clear that the aluminium plies were under a tensile stress and the composite plies under a compressive stress following manufacture. This effect results from the fact that the aluminium offers a higher coefficient of thermal expansion than the carbon-reinforced epoxy. When cooled from the processing temperature the aluminium tries to contract more than the composite. Therefore, compressive stresses are introduced to the composite while the aluminium remains under tensile stresses. It is interesting to note that the tensile stresses in the aluminium layers increase as the volume fraction of the composite increases. Indeed, the calculations suggest that the residual stresses in the aluminium plies in the (2/17) laminate are as high as 120 MPa, a significant fraction of the failure strength of the aluminium alloy.

Table 4.3 shows the calculated residual stresses in the GFPP-based fibre-metal laminates. Here, the residual stresses in the in the aluminium are higher for a given configuration. In contrast, the compressive residual stresses in the glass fibre/polypropylene are lower than those exhibited by the thermosetting composite. This is believed to be as a result of the higher coefficient of thermal expansion and thickness of the composite layers in the GFPP-based fibre-metal laminates.

Laminate lay-up	Thickness (mm)	**Aluminium** Residual tensile stress (MPa)	**CFRE** Residual compressive stress (MPa)
2/1	1.88	16	95
3/2	2.96	23	92
4/3	4.02	24	90
2/5	3.00	60	72
2/17	6.20	120	42

Table 4.2 *Residual stresses present in the CFRE-based fibre-metal laminates after manufacture.*

Laminate lay-up	Thickness (mm)	**Aluminium** Residual tensile stress (MPa)	**GFPP** Residual compressive stress (MPa)
2/1	2.50	22	41
3/2	4.30	31	39
4/3	5.70	33	39
2/8	6.00	72	26

Table 4.3 *Residual stresses present in the GFPP-based fibre-metal laminates after manufacture.*

4.7 FLEXURAL PROPERTIES OF THE FIBRE – METAL LAMINATES

The flexural properties of the aluminium, the carbon fibre reinforced plastic and the glass fibre reinforced polypropylene materials were investigated under three point loading conditions. Following this, the flexural properties of fibre-metal laminates based on both composite systems were evaluated.

4.7.1 Carbon fibre/epoxy-based FML

The flexural properties of the CFRE-based fibre-metal laminates shown in Table 3.1 were evaluated according to the ASTM D790 standard. Here, specimens were cut from the panels parallel to rolling direction in the aluminium. The specimens were mounted on a three point bend fixture and loaded centrally. The specimens were loaded at crosshead displacement rates between 3.2 and 8.4 mm/min depending on the thickness (h) and span (L) of the sample. During each test, the load-displacement data were recorded and plotted.

4.7.1.1 Flexural modulus and strength

Typical load-displacement curves for the (2/1), (3/2) and (4/3) CFRE-based fibre-metal laminates are shown in Figure 4.36. From this figure, it is apparent that all systems show a region of linearity over the initial portion of the trace. As the load is increased, all systems exhibit a non-linear response associated with global plastic deformation in the laminate. The (2/1) undergoes significant non-linear plastic deformation before reaching the maximum force. In contrast, the (3/2) and (4/3) systems exhibit a pronounced drop in the load after the maximum due to failure occurring within the lowermost composite layers in an unstable manner. Continued loading of the samples resulted in the entire flexural load being carried by the aluminium plies. This stepwise failure process helped to avoid catastrophic failure of the fibre-metal laminate. A similar response was exhibited by the (2/5) and (2/17) laminates.

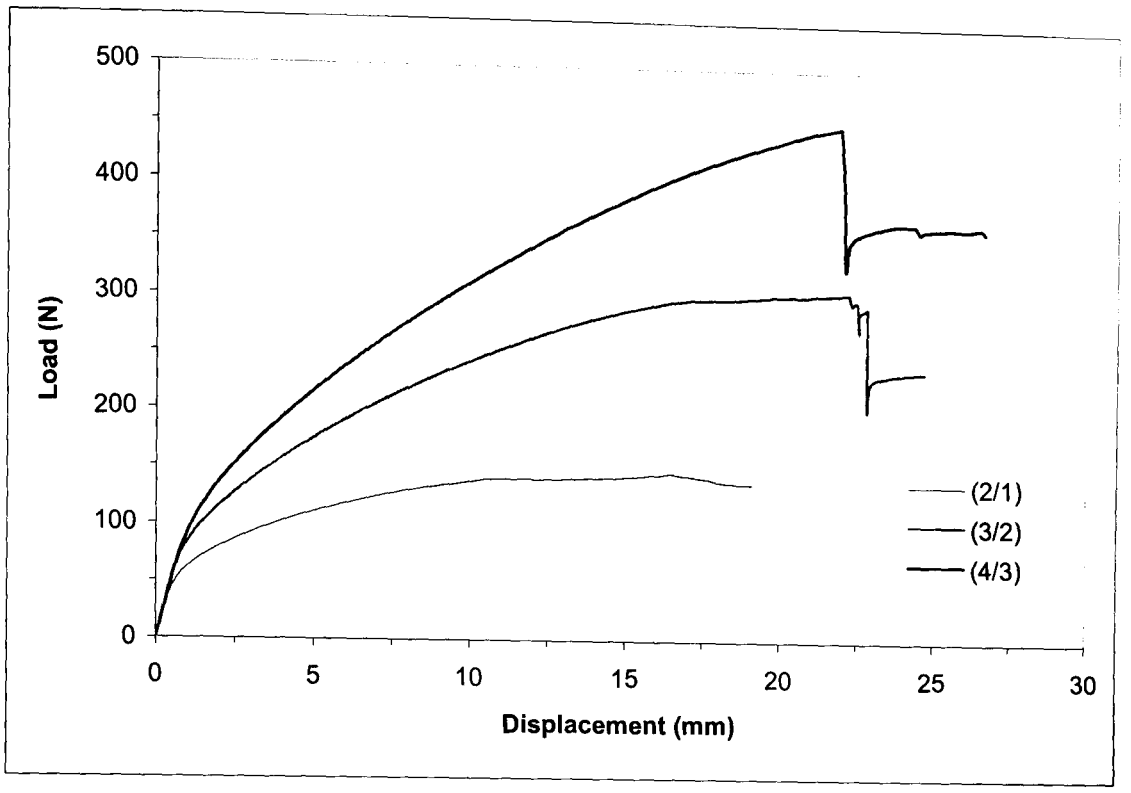

Figure 4.36 *Typical load-displacement curves of CFRE-based fibre-metal laminates following flexural tests.*

The load-displacement information was then used to calculate the flexural modulus according to Equation 3.10. Figure 4.37 presents the flexural moduli of the CFRE-based fibre-metal laminates. Included in the figure are predictions offered by Classical Laminate Theory. From the figure it is clear that the flexural modulus of the fibre-metal laminates decreases slightly with increasing composite content. This reduction results from the fact that the flexural modulus of the CFRE composite is lower than that of the aluminium. It is interesting to note that the data exhibit very little scatter and follow a linear trend. It is also worth noting that the (2/1), (3/2) and (4/3) laminates offer a flexural modulus that is just 5 to 10% lower than that of the monolithic aluminium alloy. It is also apparent that the predictions offered by Classical Laminate Theory agree very well with the experimental data for all of the systems. Clearly, the samples undergo significant non-linear deformation before

reaching the maximum load rendering the applicability of elastic beam theory questionable.

The flexural strength of the laminates was calculated at the maximum load using Equation 3.9 and the variation of the flexural strength of the CFRE-based fibre-metal laminates is shown in Figure 4.38.

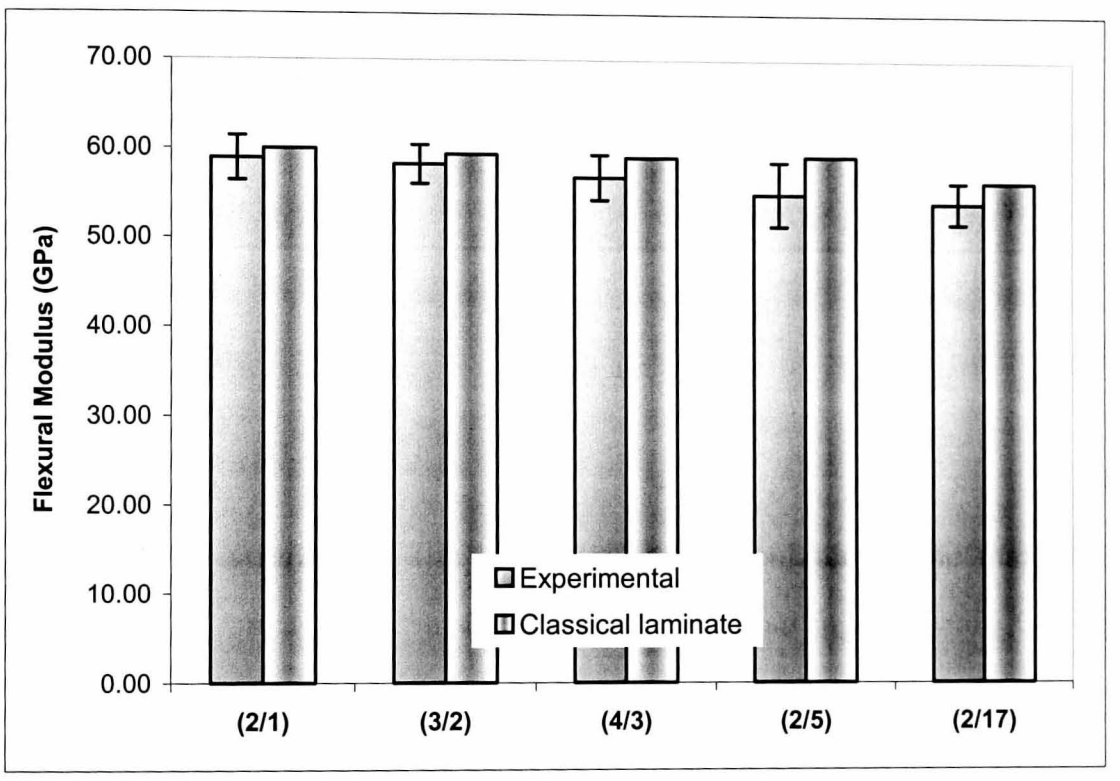

Figure 4.37 *Flexural modulus of the CFRE-based fibre-metal laminates following TPB flexural tests. The data are compared with predictions offered by classical laminate theory.*

Here, increasing the amount of carbon fibre reinforced epoxy in the laminates has a beneficial effect with the flexural strength increasing rapidly with increasing V_f. In this case, the (2/1), (3/2) and (4/3) laminates offer flexural strengths that are between

45 and 80 % higher than that of the aluminium alloy. Here again, the data exhibits very little scatter. It is worth noting that Equation 3.9 may not give the true strength since the curves are highly non-linear. However, it is believed that these results offer very useful information about the flexural behaviour of fibre-metal laminates.

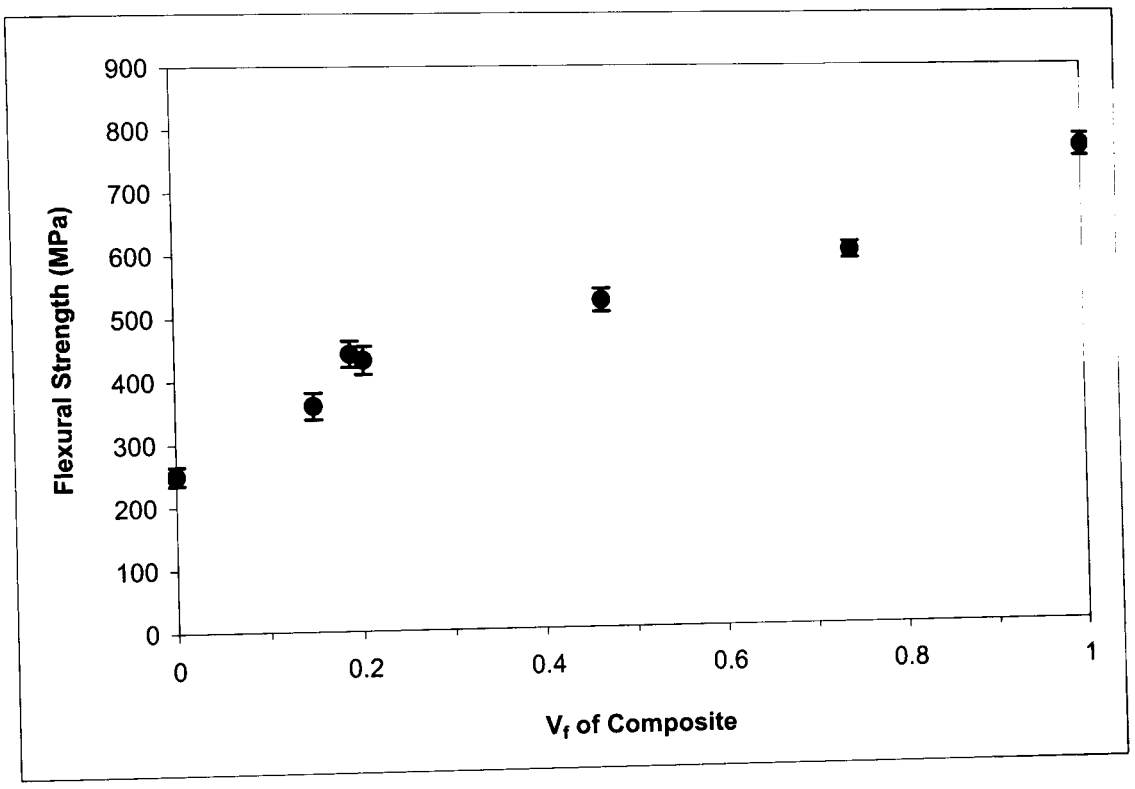

Figure 4.38 *The variation of flexural strength of the CFRE-based fibre-metal laminates with volume fraction of composite material.*

4.7.1.2 Flexural failure mechanisms

A greater insight into the flexural failure mechanisms occurring during the fracture process was achieved by examining the edges of a number of samples during testing. Here, the edges of the samples were polished to a one micron finish and coated with a thin layer of silver in a S150 sputter coater in preparation for examination in the SEM. The specimens were then loaded to a pre-determined stress

and unloaded. The specimens were then examined in a Hitachi S-2460N scanning electron microscope. Once this had been completed, the specimens were loaded to a higher stress and the procedure was repeated. This continued until the specimen had fractured.

Figure 4.39 shows scanning electron micrographs of the flexural failure of a (3/2) CFRE-based fibre-metal laminate. At 70% of the maximum load, failure is dominated by fibre/matrix debonding within the lowermost composite layer, Figure 4.39a. A number of microcracks are also apparent in this silver coating suggesting the presence of plastic deformation in the matrix. This plastic deformation may explain the aforementioned ductile behaviour exhibited by these systems, Figure 4.39b. Continued loading of the sample resulted in an increase of fibre/matrix debonding and coalesce of the microcracks. Finally, the fibre-metal laminates reached its maximum load and failed in an unstable manner within the lowermost composite layer. As this layer was loaded in tension, failure occurred between the fibres orientated perpendicular to the specimen length. From this figure, it is apparent that the material has undergone large amounts of plastic deformation in the matrix along with extensive fibre/matrix debonding before failure.

A closer examination of the bi-material interface is shown in Figure 7.39c. Here, it is evident that the main crack remains within the composite material and no damage to the interface is apparent. In addition, it is clear that the excellent high level of adhesion between aluminium and composite layers exhibited in SCB tests is retained under flexural loading conditions. Furthermore, these results suggest that flexural failure in woven CFRE-based fibre-metal laminates occurs within the lowermost composite layer. This is interesting, since the compressive properties of the composite material are poorer that the tensile properties [34]. However, it is believed that the aluminium layers located either side of the uppermost composite supported the composite by inhibiting localised composite buckling.

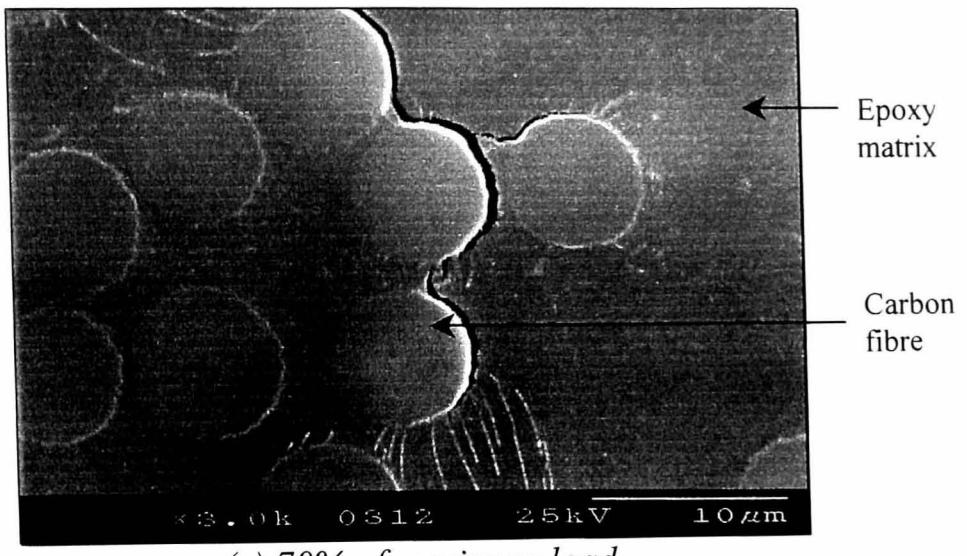

(a) 70% of maximum load

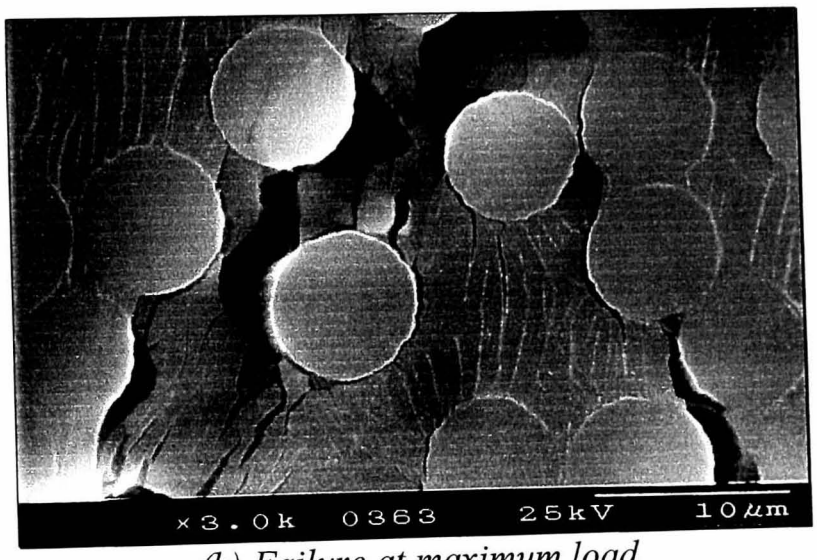

(b) Failure at maximum load

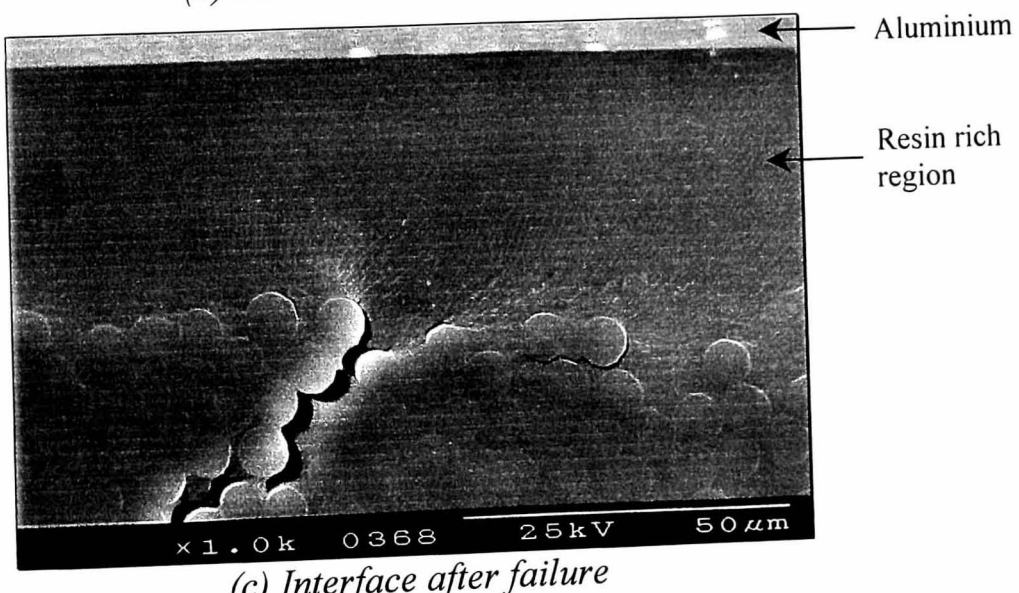

(c) Interface after failure

Figure 4.39 *Scanning electron micrographs showing flexural failure in a (3/2) CFRE-based fibre-metal laminate.*

4.7.2 Glass fibre/polypropylene-based FML

As with the CFRE-based fibre metal laminates, the flexural properties of the GFPP-based fibre-metal laminates shown in Table 3.2 were evaluated. The specimens were loaded at crosshead displacement rates between 3.2 and 8.4 mm/min depending on the thickness (h) and span (L) of the sample. During each test, the load-displacement data were recorded and plotted.

4.7.2.1 Flexural modulus and strength

Typical load-displacement curves for (2/1), (3/2) and (4/3) GFPP-based fibre-metal laminates are shown in Figure 4.40. Here, it is apparent that all systems show a small region of linearity over the initial portion of the trace. Continued loading caused all the samples to undergo non-linear plastic deformation without failing in a catastrophic manner at maximum load. From this figure, it is clear that the (2/1) system undergoes significant flexural deformation before plateauing at its maximum load. As with the (2/1) system, the (3/2) and (4/3) laminates do not exhibit a pronounced loss in properties after the maximum load was reached. It is worth noting that the (2/1) exhibits a typical ductile load-displacement trace. This is believed to be a result of the position of the composite layer within the fibre-metal laminate. Here, the composite ply does not contribute greatly and failure is dominated by the flexural behaviour of the aluminium alloy. Clearly, in passing from the (2/1) to the (3/2) and to the (4/3) laminate, the composite layers play a greater role in determining the flexural properties of the hybrid system because they are further from the neutral axis. In addition, some instabilities are apparent in these traces. This phenomenon is believed to occur as result of failure in the uppermost composite layers. Here, the composite material failed in a compressive manner associated with buckling at the top of the specimen. It is interesting to note that failure in the CFRE-based FML occurred in a tensile mode. This may be attributed to the very low modulus of the polypropylene matrix. Continued loading of the samples resulted in the load being carried by the aluminium plies. This helped to

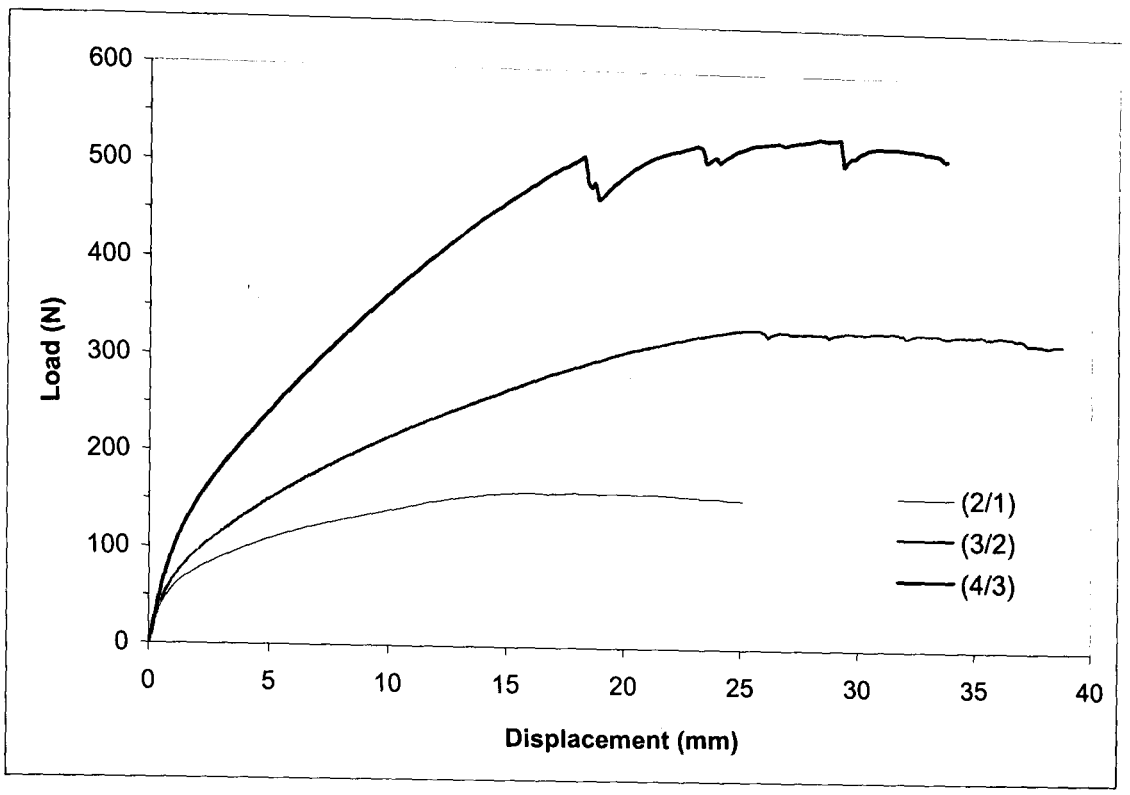

Figure 4.40 *Typical load-displacement curves following flexural tests on the GFPP-based fibre-metal laminates.*

avoid catastrophic failure within this hybrid laminate. The (2/8) laminates exhibited similar trends.

Figure 4.41 shows the variation of the flexural modulus data of the GFPP-based fibre-metal laminates. Once again, the flexural modulus of these systems decreases with increasing composite content again reflecting the lower modulus of the composites. Here, the experimental data exhibits good agreement with Classical Laminate Theory predictions. Once again, Classical Laminate Theory over-estimates the experimental data, an effect that is attributed machine compliance. In addition, it is worth noting that the (2/1), (3/2) and (4/3) laminates offer a flexural modulus that is between 10 and 25% lower that of the monolithic aluminium alloy. It is worth noting that the values of flexural modulus of these systems are lower than those exhibited by the CFRE-based fibre-metal laminates. This is believed to be as a result of the lower flexural modulus of the thermoplastic composite.

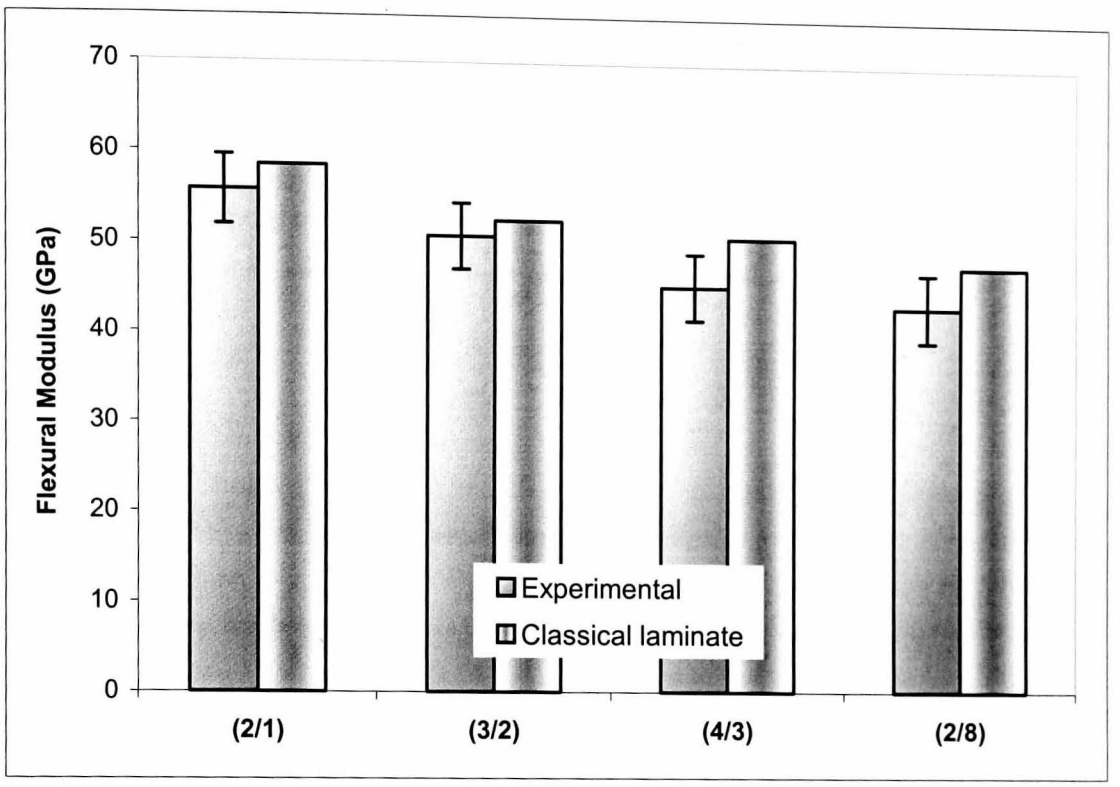

Figure 4.41 *Flexural modulus of GFPP-based fibre-metal laminates following TPB flexural tests and a classical laminate theory prediction.*

Figure 4.42 shows the variation of the flexural strength of the GFPP-based fibre-metal laminates. From this figure, it is clear that increasing the amount of glass fibre/polypropylene in the laminates has a beneficial effect with the flexural strength increasing rapidly with increasing V_f. Here, the (2/1), (3/2) and (4/3) laminates offer flexural strengths that are between 25 and 40 % higher than that of the aluminium alloy. Once again, the data exhibits very little scatter. This evidence suggests that the flexural strength of the GFPP-based fibre metal laminates could be predicted using the constituent properties and the relevant volume fraction of composite. Once again, the CFRE-based fibre-metal laminates exhibited values of flexural strength that are approximately 50 % higher that those offered by the GFPP-based fibre-metal laminates.

4.7.2.2 Flexural failure mechanisms

In order to highlight the flexural failure process occurring during fracture of fibre-metal laminates, the edges of a number of samples were examined during

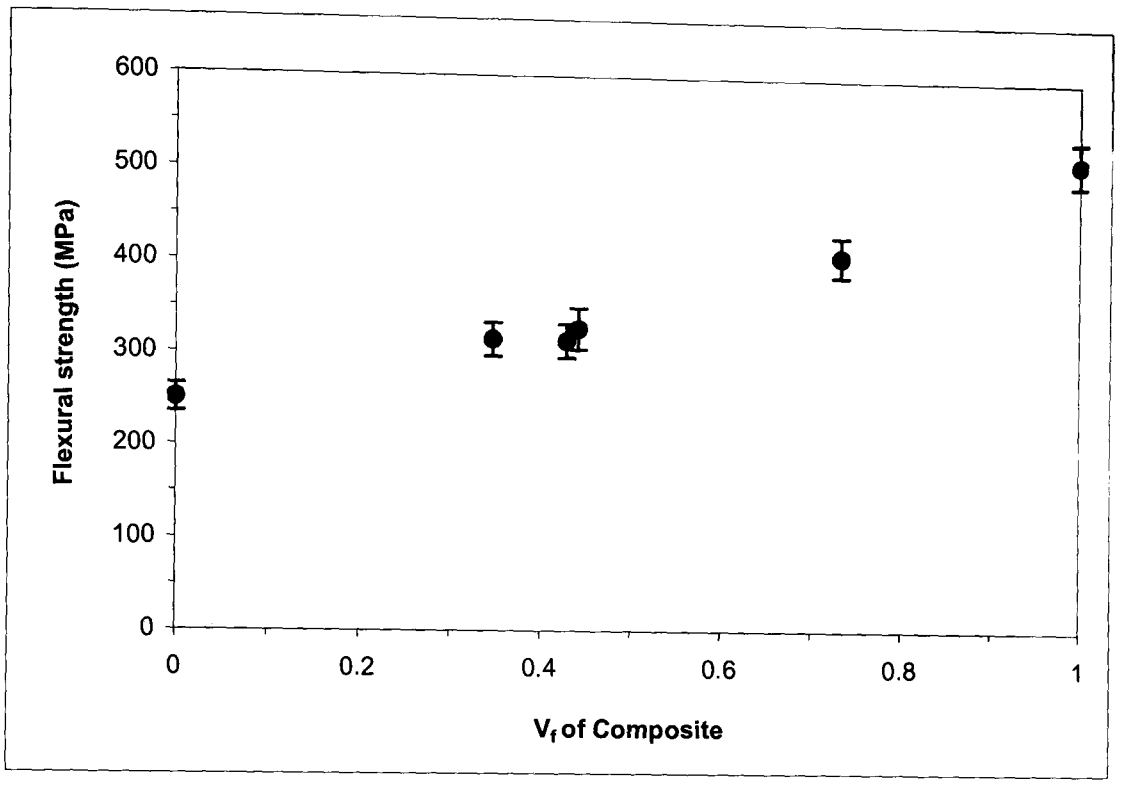

Figure 4.42 *The variation of flexural strength of the GFPP-based fibre-metal laminates with volume fraction of composite material.*

testing. Figure 4.43 shows scanning electron micrographs of the flexural failure of a (3/2) GFPP-based fibre-metal laminate. Here, at 60% of the maximum load, almost no failure is apparent and just a very small amount of fibre/matrix debonding at the top of the composite material can be observed, Figure 4.43a. Continued loading of the samples resulted in the fibre-metal laminates beginning to buckle close to its maximum load before failing in a compressive manner in the uppermost composite layer, Figure 4.43b. Here, it is evident that the material has undergone plastic deformation in the matrix along with extensive fibre/matrix debonding and delamination before failure. An examination of the uppermost bi-material interface

after failure is shown in Figure 4.43c. From this figure, it is evident that the main crack remains within the composite although some delamination at the bi-material interface is also apparent. These results suggest that there is an excellent transfer of load at the bi-material interface. Furthermore, these results suggest that flexural failure in unidirectional GFPP-based fibre-metal laminates occurs within the uppermost composite layer. This was expected, since the compressive properties of the composite material are lower than its tensile properties [35]. Here, the modulus of the composite depends on the stiffness of the supporting matrix, which is very low for the polypropylene (approximately 1 GPa). In addition, these results suggest that the flexural properties of fibre-metal laminates are directly related to the flexural properties of the constituent materials. In addition, the position of each layer within the laminate clearly contributes to the flexural behaviour and failure mode within these systems.

4.8 TENSILE PROPERTIES OF THE FIBRE – METAL LAMINATES

The tensile properties of the plain aluminium, the carbon reinforced plastic and the glass fibre reinforced polypropylene were investigated at quasi-static rates of loading. Following this, the tensile properties of fibre-metal laminates based on both composite systems were evaluated in order to highlight the effect of varying the composite volume fraction (V_f) on the tensile modulus and strength.

4.8.1 Carbon fibre/epoxy-based FML

In order to evaluate the tensile properties of CFRE-based fibre-metal laminates, tensile tests were conducted according to the ASTM D 3039, B557M, and D638 standards. The specimens were cut from the panels parallel to rolling and fibre directions. Dog-bone shape specimens with a 10 x 60 mm working section were used. Testing was conducted at a crosshead displacement rate of 1 mm/min and the load-displacement data were recorded. The tensile stresses were calculated using Equation 3.11.

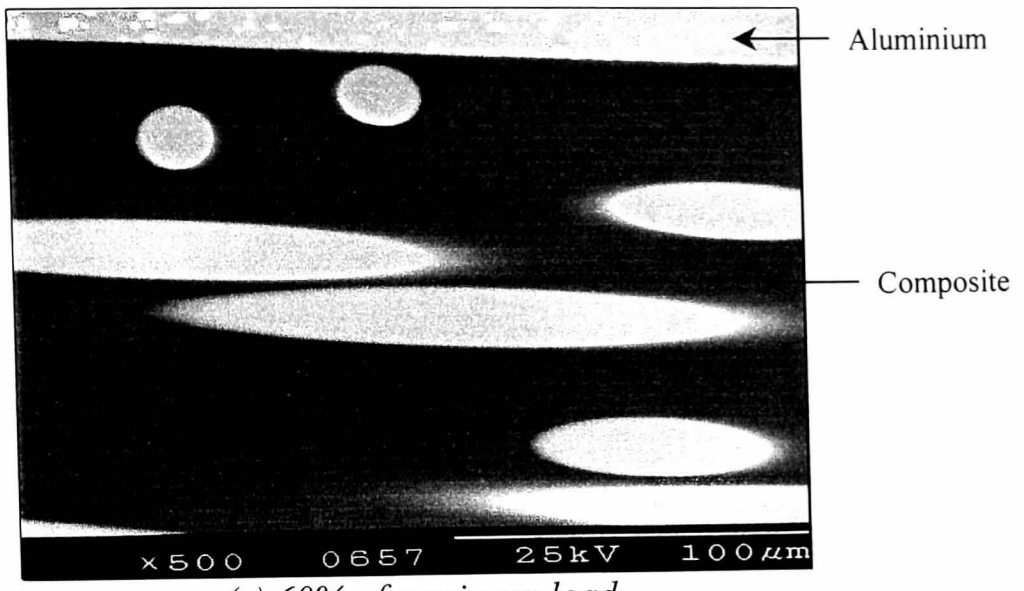

(a) 60% of maximum load

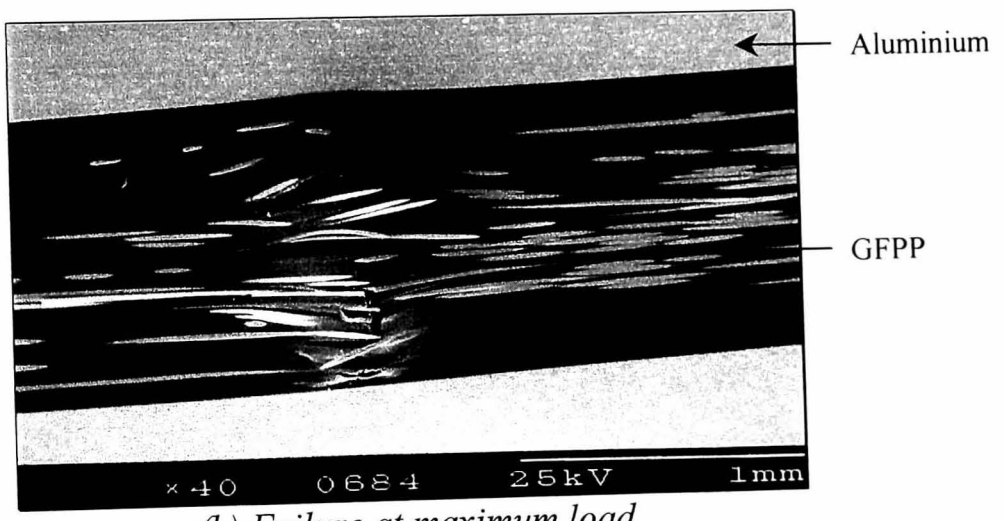

(b) Failure at maximum load

(c) Interface after failure

Figure 4.43 *Scanning electron micrographs showing flexural failure in a (3/2) GFPP-based fibre-metal laminate.*

4.8.1.1 Influence of volume fraction of composite material

Figure 4.44 shows typical stress-strain curves for the (2/1), (3/2) and (4/3) fibre-metal laminates. Also included in the figure are typical stress-strain curves for the plain aluminium and composite. It should be noted that the strain was determined by dividing the crosshead displacement by the working length of the specimen. For this reason, the reported strain is not accurate, however, it is felt that the curves yield a useful comparison of the tensile behaviour of these multi-layered systems. Here, the plain carbon fibre reinforced epoxy exhibited a linear response up to the maximum load point. At the maximum stress, the composite specimen failed in a catastrophic manner across the width of the sample provoking a rapid drop in the stress-strain curve. In contrast, the aluminium alloy exhibited a very ductile failure response with the load plateauing towards the maximum stress. From the figure, it is clear that all three laminates exhibit similar trends with the initial part of the stress-strain curve being roughly linear up to maximum stress. At this point, the composite plies failed and the load was carried by the aluminium layers. Continued loading resulted in extensive plastic flow within the aluminium layers until they failed at high strains.

The modulus of elasticity was measured using a 12.5 mm gauge length clip-on extensometer and calculated using Equation 3.12. Figure 4.45 shows the variation of the tensile modulus of the CFRE-based fibre-metal laminates with the volume fraction of composite material. Also included in the figure are the elastic moduli of the plain aluminium alloy and the carbon fibre reinforced epoxy. The data clearly indicate that there is a roughly linear relationship between the modulus of the laminate and the volume fraction of the composite with the value of the tensile modulus tending to decrease slightly with increasing V_f. The solid line in Figure 4.45 corresponds to a law of mixtures prediction based on the elastic moduli of the aluminium and composite constituents.

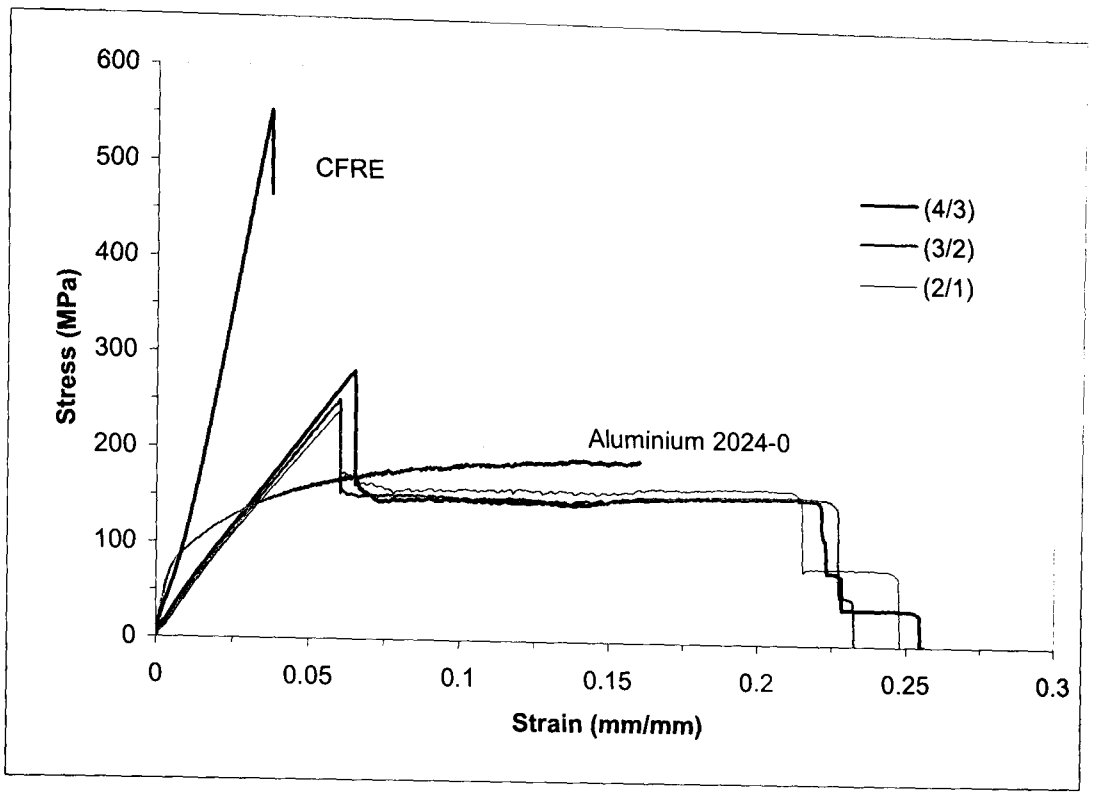

Figure 4.44 *Typical tensile stress-strain curves for the CFRE-based fibre metal laminates.*

Here, the law of mixtures prediction is given by:

$$E_{FML} = E_{Al}V_{Al} + E_{C}V_{C} \tag{4.1}$$

Where E = tensile modulus, V = volume fraction, FML = fibre-metal laminate, Al = aluminium and C = composite.

Clearly, agreement between the experimental results and the law of mixtures prediction is excellent across the range of systems examined.

Figure 4.46 shows the variation of the tensile strength of the CFRE-based fibre-metal laminates with the volume fraction of composite material. This figure clearly shows that the strength of these bi-material laminates increases with increasing composite content.

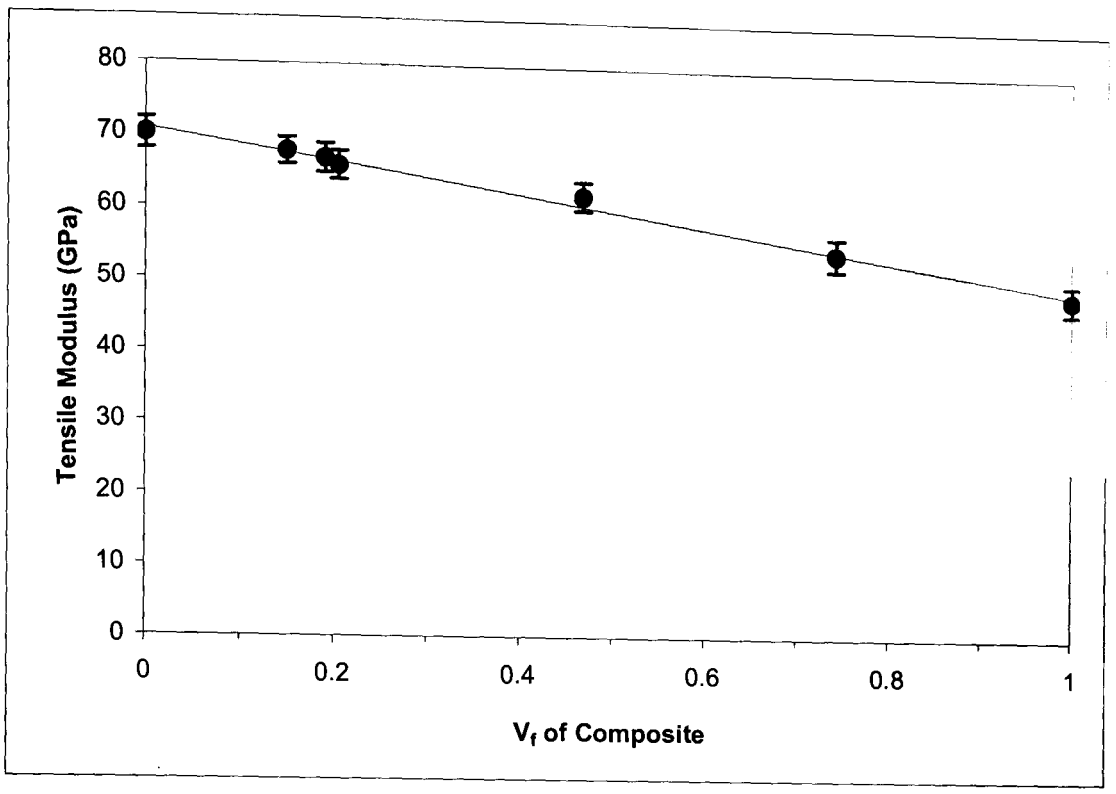

Figure 4.45 *The variation of tensile modulus of the CFRE-based fibre-metal laminates with volume fraction of composite material.*

The three data points on the left of the figure correspond to the fibre-metal laminates shown in Figure 4.44. Increasing the volume fraction of the composite to almost fifty percent resulted in a 120% increase in the tensile strength. In addition, it is encouraging that the data presented in Figures 4.45 and 4.46 exhibited very little scatter suggesting that the laminates were of a high quality. From this figure, it is also apparent that the data appear to agree with the predictions offered by a simple law of mixtures prediction. Wu and Wu reported similar results [36]. Here, a rule of mixtures and metal volume fraction were used for mechanical properties predictions of fibre-reinforced aluminium laminates. These results suggests that a simple rule of mixtures could be successfully used to predict the tensile properties of fibre-metal laminates.

An optical examination of the specimen edges indicated that failure in all laminates initiated in the composite layers. In the (2/1) and (3/2) laminates, the

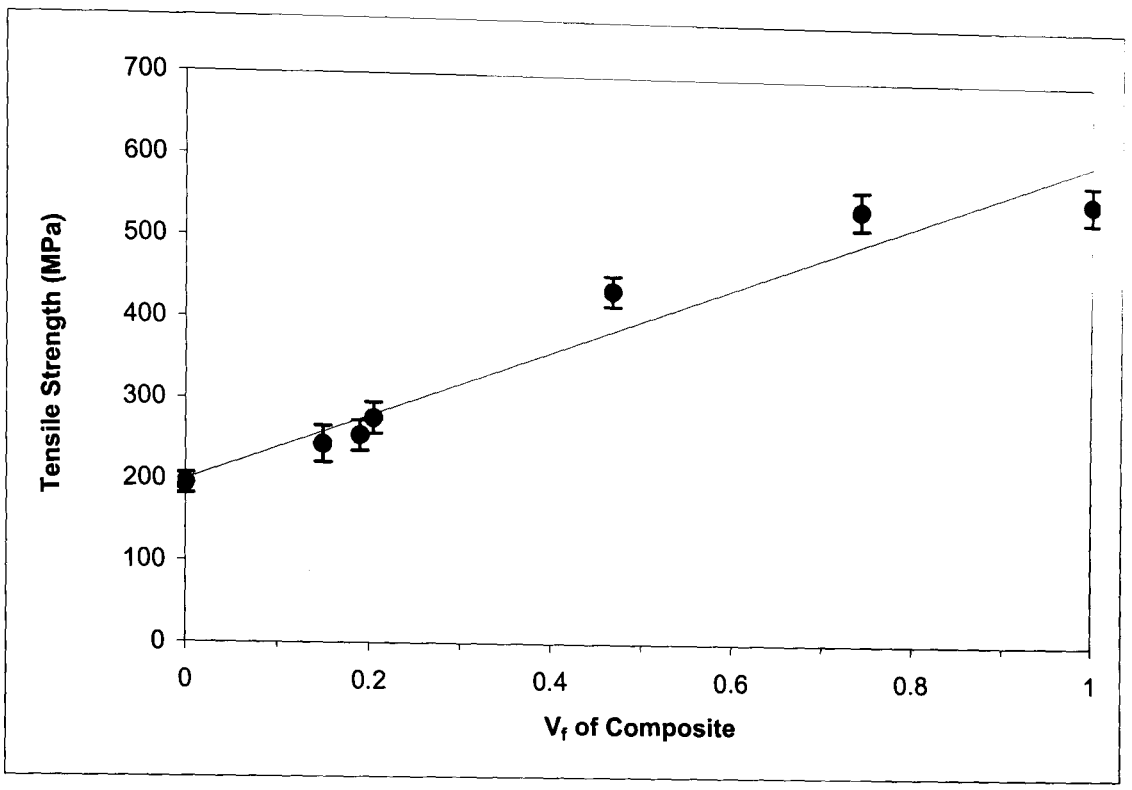

Figure 4.46 *The variation of tensile strength of the CFRE-based fibre-metal laminates with volume fraction of composite material.*

primary crack propagated across the composite to the bi-material interfaces before propagating along the length of the sample in a slow and stable manner. This is surprising since adhesion is very good in this system. In the (2/17) laminate, i.e. that with the highest composite volume fraction, failure occurred in a catastrophic manner involving brittle failure in both the composite and aluminium plies without inducing any delamination at the bi-material interface.

Figure 4.47 shows low magnification optical micrographs of aluminium/CFRE- based fibre-metal laminates following tensile testing at 1 mm/min. An examination of the (2/1) sample indicated that the aluminium plies had not fractured and that the failure had occurred in the composite material. Indeed, a closer examination of the sample indicated that a limited amount of plastic deformation had occurred in the aluminium plies, this is just visible in Figure 4.47a.

In contrast, failure in the (2/17) laminate occurred in a planar manner directly across the aluminium and composite plies, Figure 4.47b. Here, the aluminium exhibited significant plastic flow around the region of fracture. It is interesting to note that the calculated residual stresses in the aluminium plies in the (2/17) laminate were 120 MPa, compare with 16 MPa in the (2/1) laminate. Tension tests on the plain aluminium alloy samples indicated that it offered a tensile strength of 200 MPa.

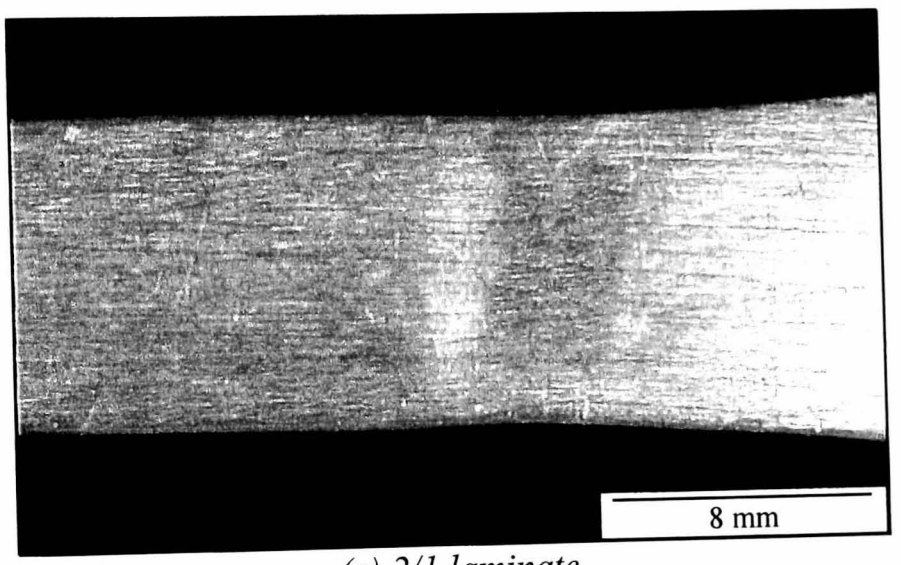

(a) 2/1 laminate

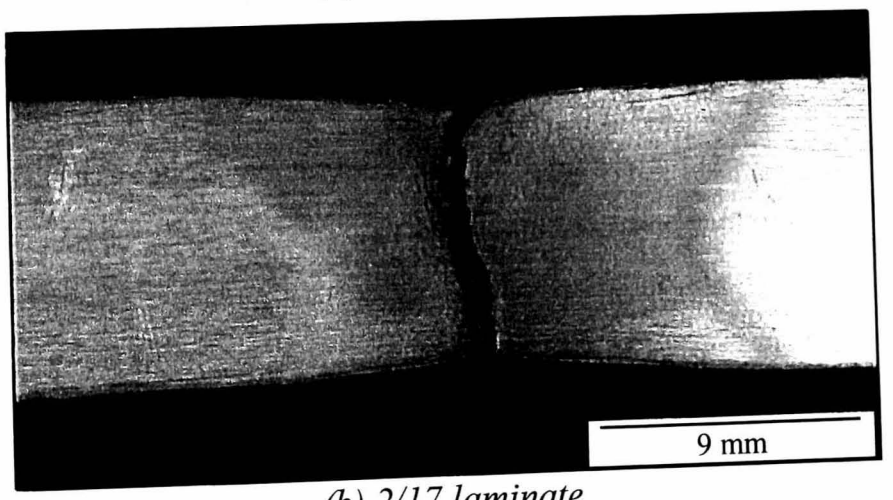

(b) 2/17 laminate

Figure 4.47 *Low magnification optical micrographs of aluminium/CFRE-based fibre-metal laminates following tensile testing at 1 mm/min.*

Clearly, before starting the tests on the (2/17) laminates, the aluminium plies were already effectively loaded to 60 % of their failure strength and were therefore more likely to yield and fail during the tensile test than in the other fibre-metal laminate samples.

4.8.1.2 Tensile failure mechanisms

The tensile failure mechanisms occurring during the fracture process of the CFRE-based fibre-metal laminates were highlighted by polishing a number of specimens to a one micron finish and coating the edges of the specimens with a thin layer of silver. The specimens were then loaded to a pre-determined stress and unloaded. The samples were then examined in a Hitachi S-2460N scanning electron microscope. Once this had been completed, the specimens were loaded to a higher stress and the procedure was repeated. This continued until the specimen had fractured. Figure 4.48 shows scanning electron micrographs of the tensile failure process in a (3/2) CFRE-based fibre-metal laminate. At 75% of the maximum stress, failure is dominated by fibre/matrix debonding in the fibre aligned at 90^{o} within the composite material, Figure 4.48a. A number of microcracks are also apparent in this figure suggesting the presence of plastic deformation in the matrix. In addition, small traces of shear deformation around the 0^{o} fibre are also apparent. As the load was increased, the fibre-metal laminate reached its maximum stress and failed in an unstable manner with the three composite layers failing almost simultaneously, Figure 4.48b. Here, failure occurred initially between the fibres orientated perpendicular to the specimen length with the longitudinal fibres carrying most of the tensile load until failure occurred. A closer examination of the bi-material interface is shown in Figure 7.48c. Here, it is evident that the main crack remains within the composite material and no significant damage to the interface is observed. Furthermore, these results suggest that tensile failure in woven CFRE-based fibre-metal laminates occur in the composite layers rather than at the interface as a result of the strong bond between the aluminium and composite materials.

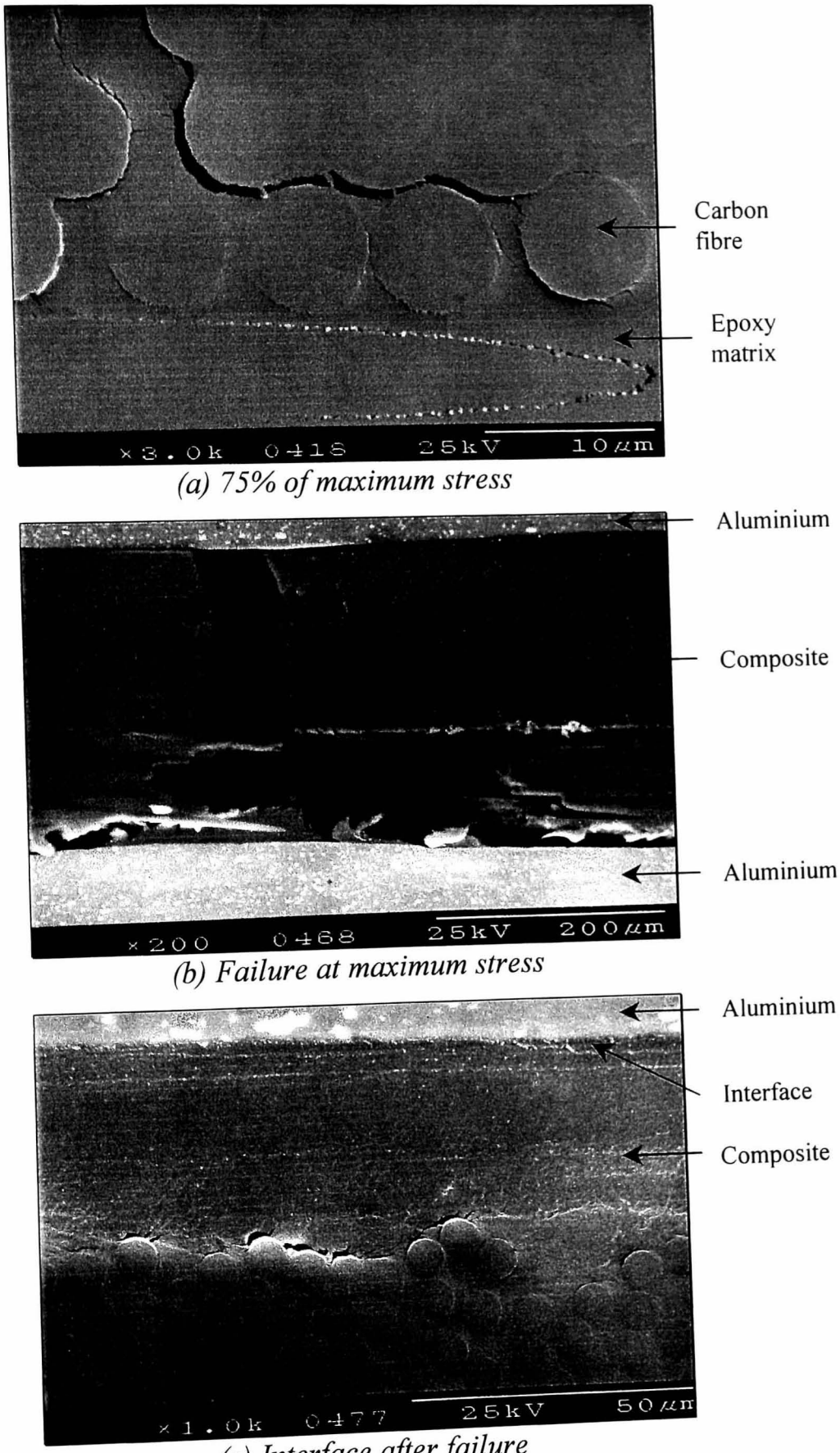

(a) 75% of maximum stress

(b) Failure at maximum stress

(c) Interface after failure

Figure 4.48 *Scanning electron micrographs showing failure in a tensile-loaded (3/2) CFRE-based fibre-metal laminate.*

4.8.2 Glass fibre/polypropylene-based FML

As with the CFRE-based fibre-metal laminates, the tensile properties of the GFPP-based fibre-metal laminates were evaluated using dog-bone shape specimens with a 60 mm long working section. Testing was conducted at a crosshead displacement rate of 1 mm/min and the load-displacement data were recorded. The tensile stresses were calculated using Equation 3.11.

4.8.2.1 Influence of volume fraction of composite material

Typical stress-strain curves for the (2/1), (3/2) and (4/3) GFPP-based fibre-metal laminates are shown in Figure 4.49. Included in the figure are typical stress-strain curves for the plain aluminium and composite. Here, initial failure in the plain glass fibre/polypropylene resulted from longitudinal splitting between the unidirectional glass fibres. This in turn provoked a rapid drop in the stress-strain curve. Continued loading resulted in failure across the fibres at various locations along the length of the sample. The stress-strain curves for all of the laminates exhibited an almost linear response up to a maximum stress at which point the composite layers fractured in a brittle manner. As the load was increased, systematic failure of the aluminium plies was observed until complete fracture of the specimens occurred at relatively high strains.

An examination of the edges of the (2/1) and (3/2) samples indicated that the composite had fractured directly across the fibres without inducing significant amounts of longitudinal splitting. In addition, the sudden release of elastic energy provoked extensive delamination along or close to the bi-material interfaces. In contrast, delamination in the thicker samples was less significant and most of interfaces in the failed (4/3) samples remained intact.

The variation of the tensile modulus of the GFPP-based fibre-metal laminates with the volume fraction of composite is shown in Figure 4.50. Included in the figure is the prediction offered by a simple law of mixtures approach.

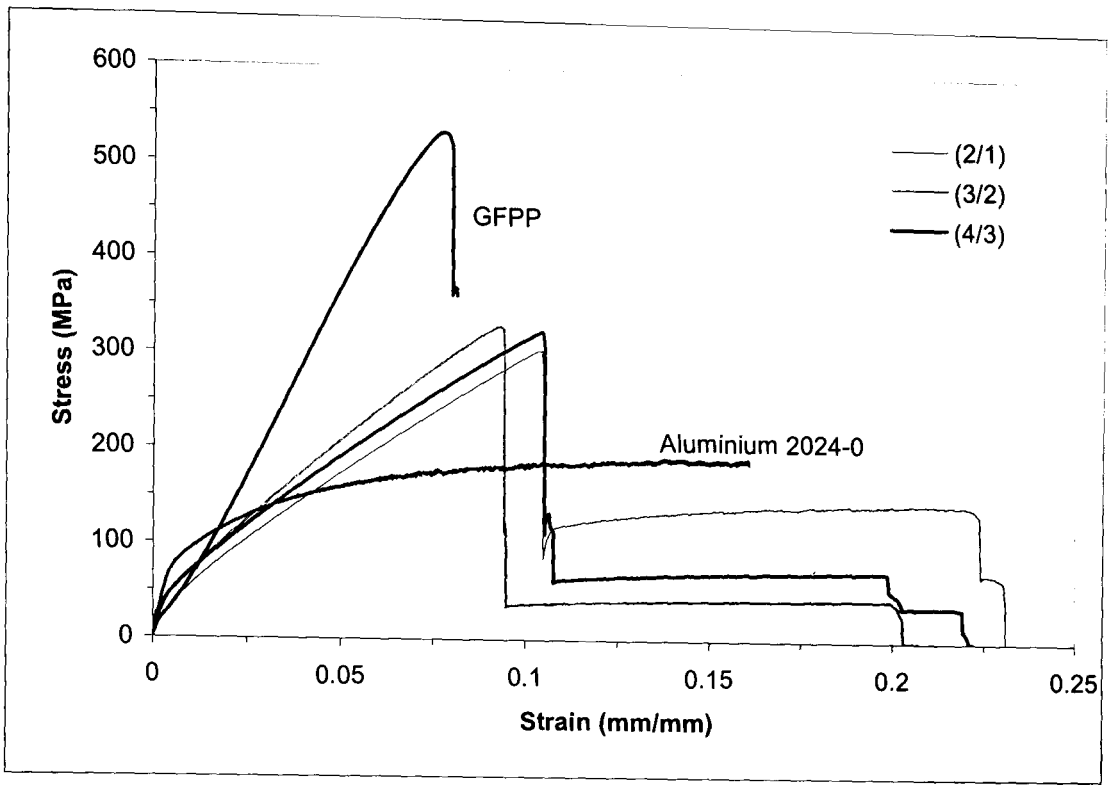

Figure 4.49 *Typical tensile stress-strain curves for the GFPP-based fibre metal laminates.*

From the data, it is clear that the tensile modulus decreases with the addition of glass fibre/polypropylene. It is interesting to note that the data again exhibit very little scatter and follow closely the predictions offered by the rule of mixtures analysis represented by the straight line. It is also worth noting that the (2/1), (3/2) and (4/3) laminates offer a tensile modulus that is between 25 and 30% below to that of the monolithic aluminium alloy. In contrast, the (2/1) (3/2) and (4/3) CFRE-based fibre-metal laminates exhibited a tensile modulus that is between 5 and 10 % below to that of the aluminium. This is believed to be as a result of the higher moduli offered by the carbon fibre-reinforced epoxy in comparison with that of the glass fibre/polypropylene. These results suggest that the modulus of the composite plays an important role on the tensile properties of fibre-metal laminates.

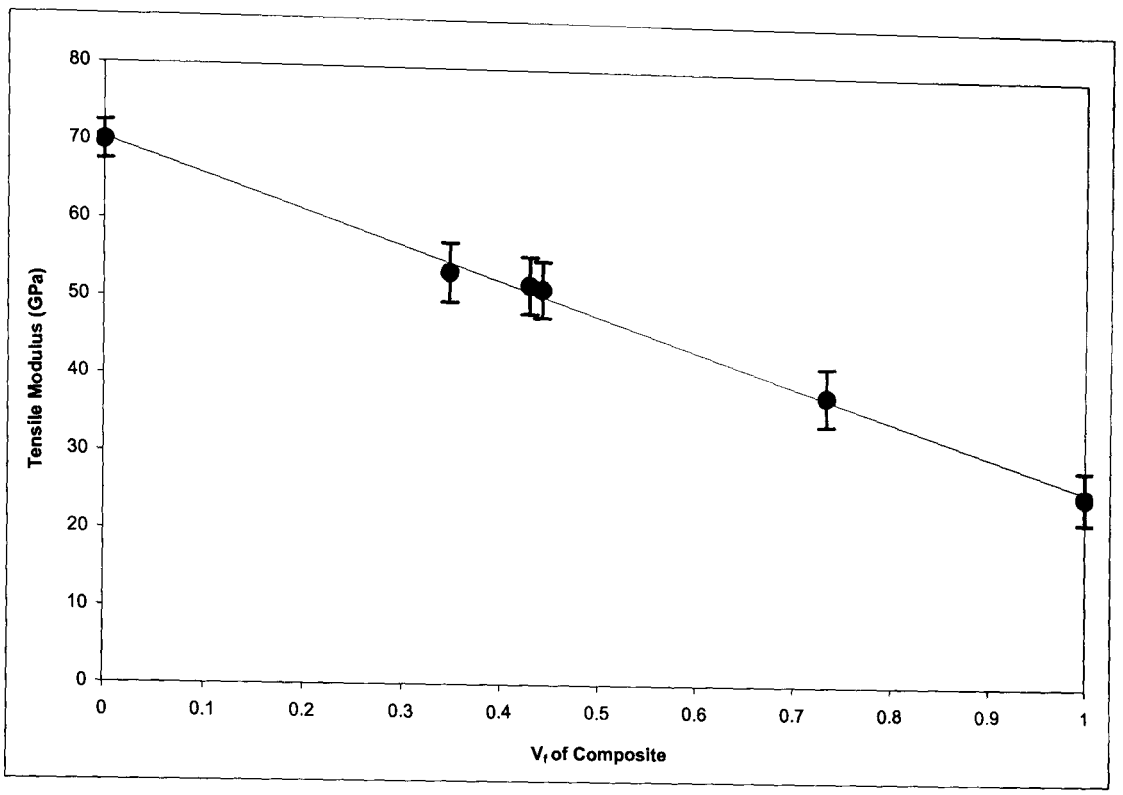

Figure 4.50 *The variation of tensile modulus of the GFPP-based fibre-metal laminates with volume fraction of composite material.*

The variation of the tensile strength of the GFPP-based fibre-metal laminates is shown in Figure 4.51. Here, increasing the amount of glass fibre/polypropylene in the laminates has a beneficial effect with the strength increasing rapidly with increasing composite V_f. In this case, the (2/1), (3/2) and (4/3) laminates offer tensile strengths that are between 50 and 70% higher than that of the aluminium alloy. Here again, the tensile properties of the laminates exhibit low levels of scatter and appear to follow a simple law of mixtures rule.

These results suggest that the tensile properties of the GFPP-based fibre-metal laminates can be easily predicted using the tensile properties of the constituent materials and its corresponding volume fraction.

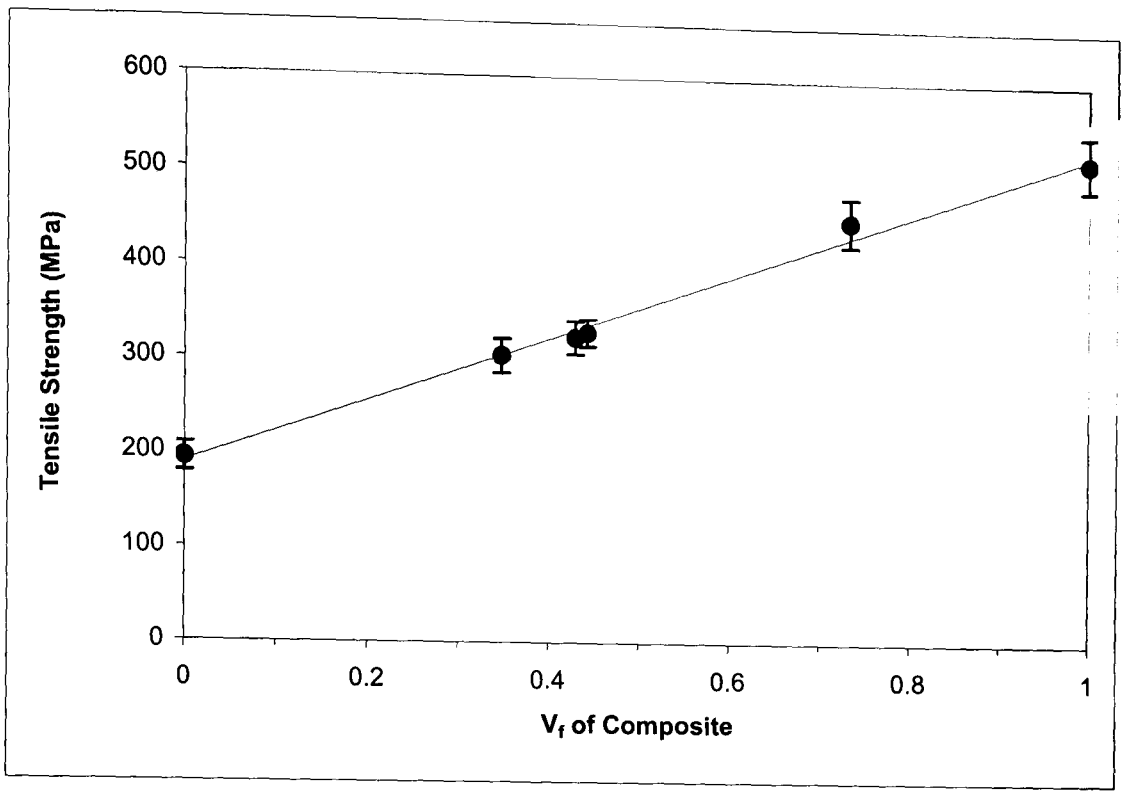

Figure 4.51 *The variation of tensile strength of the GFPP-based fibre-metal laminates with volume fraction of composite material.*

4.8.2.2 Tensile failure mechanisms

As for the CRFE-based fibre-metal laminates, the tensile failure mechanisms in the GFPP-based fibre-metal laminates were highlighted by polishing a number of specimens to a one micron finish and coating the edge of the specimens with a thin layer of silver. The specimens were then loaded to a pre-determined stress and unloaded. The specimens were then examined in a Hitachi S-2460N scanning electron microscope. Once this had been completed, the specimens were loaded to a higher stress and the procedure was repeated. Figure 4.52 shows scanning electron micrographs of the tensile failure of a (3/2) CFRE-based fibre-metal laminate. Here, at 70% maximum stress, failure is dominated by fibre/matrix debonding within the composite material along with small amounts of fibre breakage, Figure 4.52a. In addition, a number of microcracks are also apparent in this figure as a result of

plastic deformation in the matrix. As the fibre-metal laminates reached its maximum stress, failure occurred in an unstable manner with the composite layers failing almost simultaneously, Figure 4.52b. Large amounts of fibre breakage are also apparent, suggesting that the fibres have dominated the failure process. An examination of the bi-material interface after failure is shown in Figure 4.52c. Here, it is evident that failure of this hybrid system is concentrated in the composite plies without inducing significant delamination at the bi-material the interface. In addition, this figure highlights the presence of plastic flow at the resin rich region suggesting that excellent load transfer between aluminium and composite materials has been achieved.

4.9 LOW VELOCITY IMPACT RESPONSE OF THE FIBRE-METAL LAMINATES

The dynamic properties of the fibre-metal laminates were investigated in order to evaluate the effect of varying impact energy on the development of damage within the hybrid materials. Low magnification optical microscopy was used in order to highlight the failure modes of the fibre-metal laminates subjected to low velocity impact energies.

4.9.1 Carbon fibre-based fibre-metal laminates

The low velocity impact response of the carbon fibre-based fibre-metal laminates was investigated by conducting low velocity impact tests on an instrumented falling weight impact tower. Here, a 2 kg carriage was released from heights of up to 0.8 metres onto plates supported on 75 mm internal diameter circular ring. A piezoelectric load cell located just above the 12.7 mm diameter hemispherical impact head was used to measure the impact force and this signal was recorded by a computer. After impact, the carriage was caught in order to avoid secondary impacts.

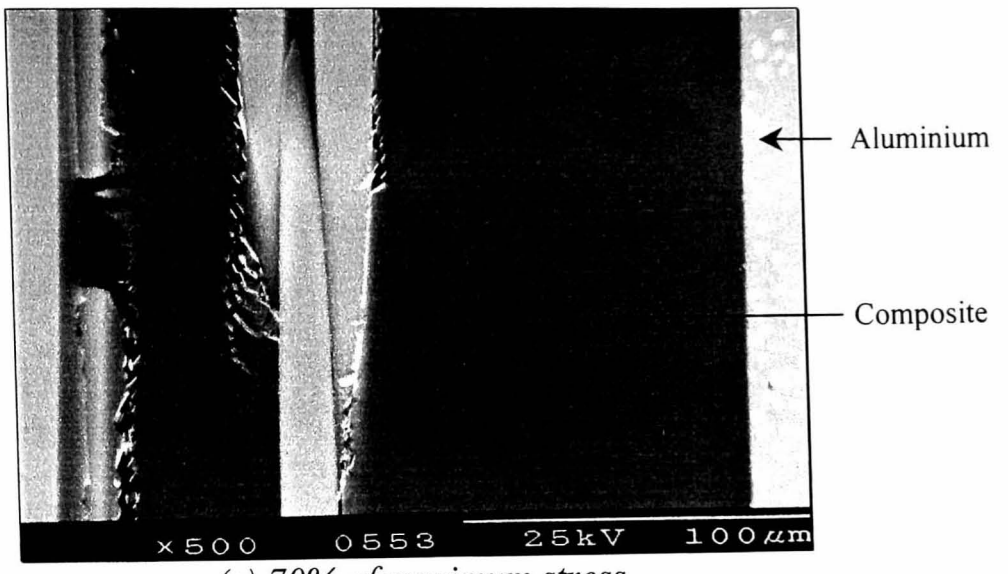

(a) 70% of maximum stress

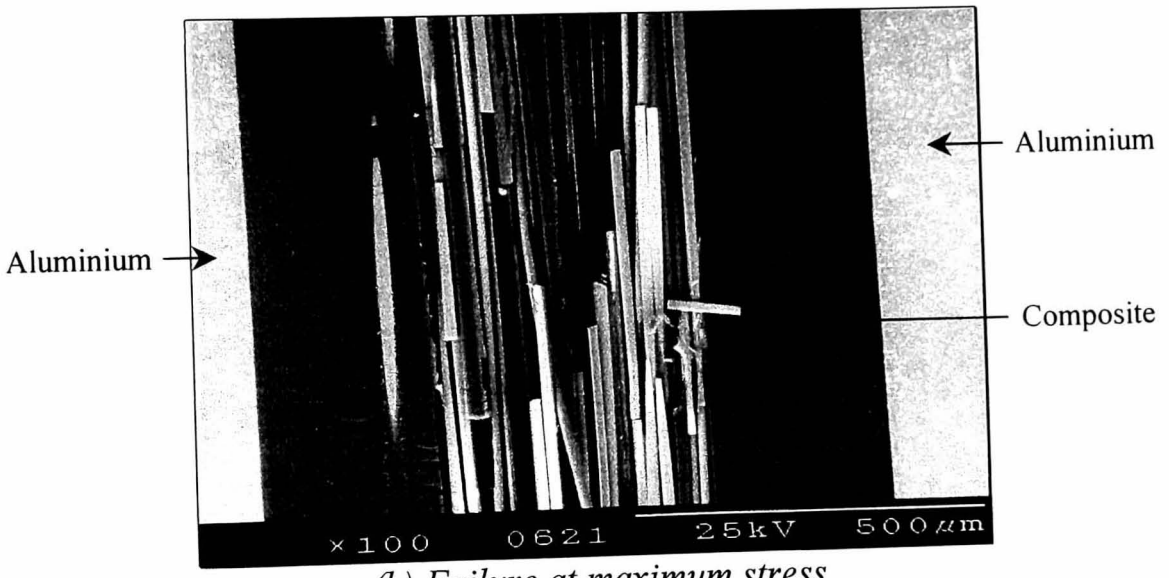

(b) Failure at maximum stress

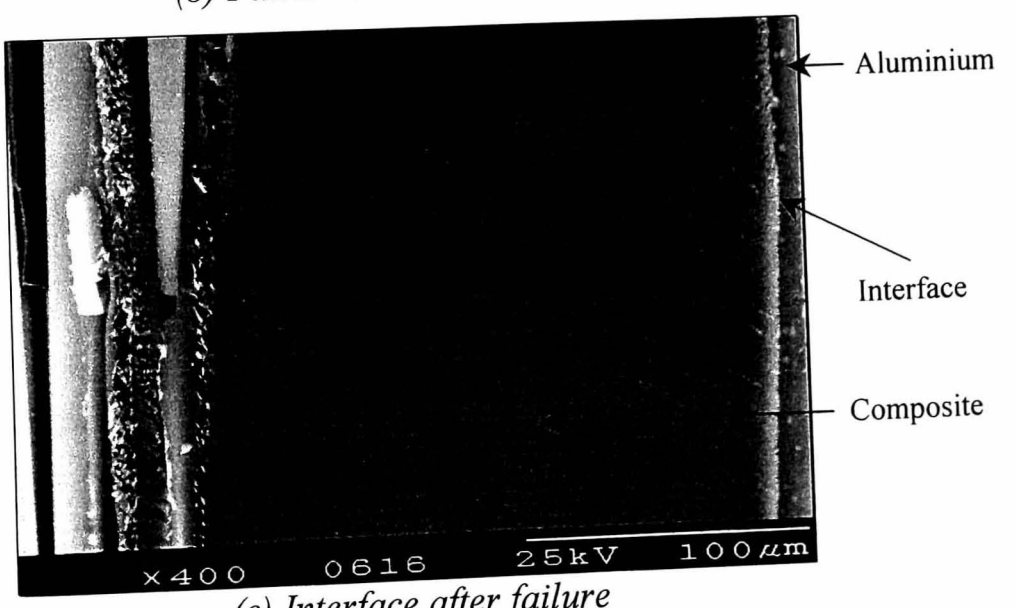

(c) Interface after failure

Figure 4.52 *Scanning electron micrographs showing failure in a tensile-loaded (3/2) GFPP-based fibre-metal laminate.*

The impact tests were performed on 2/1, 3/2 and 4/3 fibre-metal laminates with dimensions of approximately 100 x 100 mm. Impact energies up to 20 Joules were considered.

4.9.1.1 Impact failure mechanisms

Figure 4.53 shows cross-sections of (2/1), (3/2) and (4/3) laminates subjected to impact energies of 7.5, 10.5 and 20 Joules respectively. Damage in the thinner laminate takes the form of cracking and delamination in the composite layer and extensive plastic flow in the outer aluminium plies, Figure 4.53a. From the figure, it is clear that damage is highly localised to the point of impact and no apparent damage to the bi-material interface is visible. Damage in the (3/2) laminate was again quite localised, Figure 4.53b. Here, fracture of the lowermost composite layer is apparent. In addition, a small region of delamination at the uppermost bi-material interface is in evidence. The seven ply (4/3) laminate shows similar types of localised damage to that exhibit by the (2/1) and (3/2) laminates, Figure 4.53c. Here, damage had extended through the thickness of the material.

A closer examination of the micrograph highlights a region of interfacial failure between the uppermost plies and a number of ply fractures in the lowermost composite layers. It is interesting to note that failure in the (3/2) and (4/3) laminates was similar to that observed under flexural loading conditions where fracture of the lowermost composite layer loaded in tension failed as a result of bending. Nevertheless, these results suggest that composite-metal adhesion remains impressive under low velocity impact conditions.

4.9.1.2 Influence of impact energy

The polished sections were used to estimate the size of the damage area in the impact-damaged specimens. Although this method is slightly crude and unlikely to be as accurate as ultrasonic C-scanning, it still offers useful information on the extent of the damage.

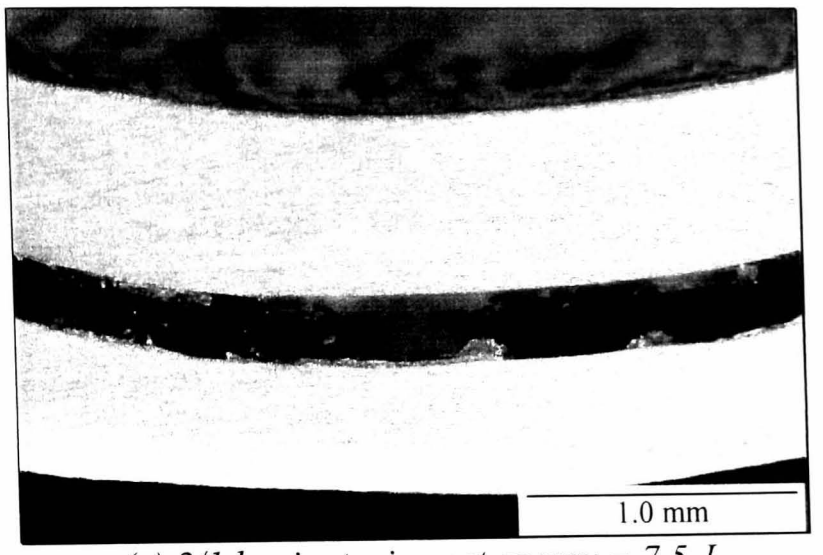

(a) 2/1 laminate, impact energy = 7.5 J

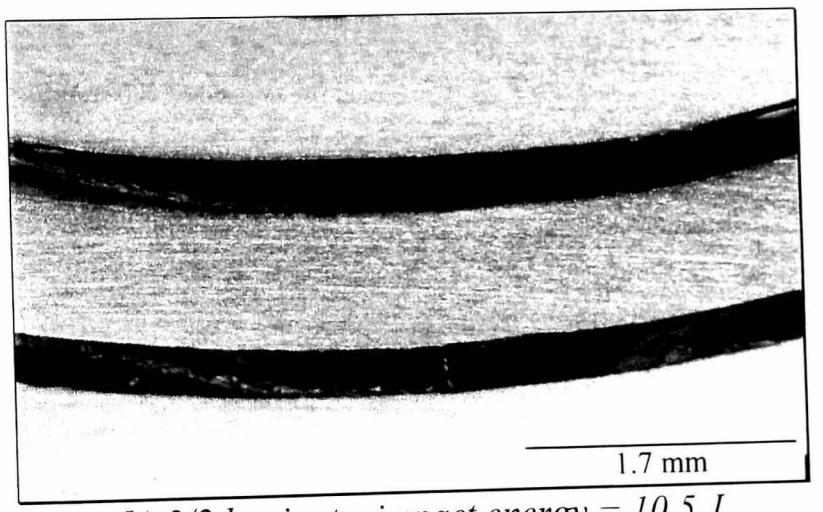

(b) 3/2 laminate, impact energy = 10.5 J

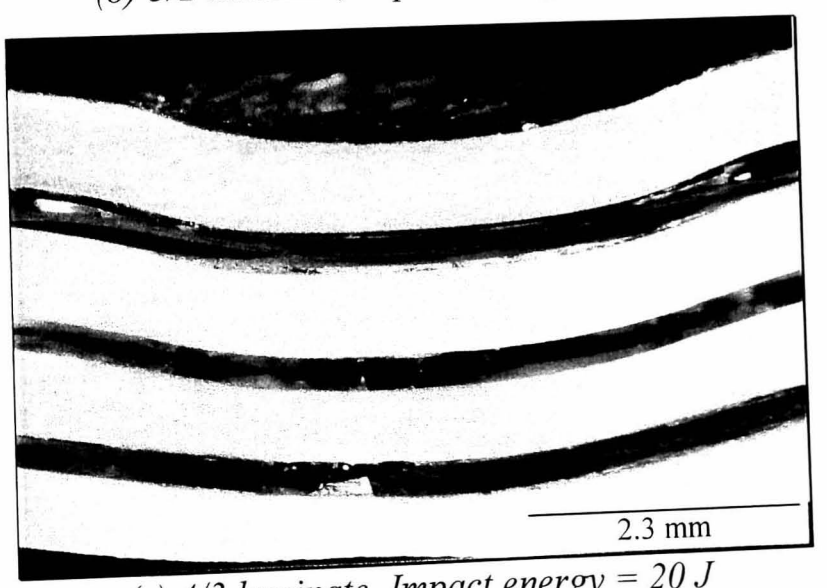

(c) 4/3 laminate, Impact energy = 20 J

Figure 4.53 *Low magnification optical micrographs showing damage in CFRE-based FML subjected to low velocity impact loading conditions.*

Figure 4.54 shows the variation of the damage area (as measured from the polished sections) with impact energy. From this figure, it is clear that the (2/1) and (3/2) laminates exhibit very little damage at impact energies up to 6 Joules. In addition, the data indicate that the damage area increases steadily with increasing impact energy reaching a value of approximately 1200 mm^2 at 20 Joules in the (4/3) laminate. Although direct comparisons of the three laminates are difficult, it is nevertheless interesting to note that all of the carbon fibre-based fibre-metal laminates out perform a sixteen ply (0^o,+/-45^o) carbon fibre reinforced epoxy [37] and offer an impact resistance comparable to that of sixteen ply (0^o,90^o,+/-45^o) carbon fibre reinforced PEEK laminate [38].

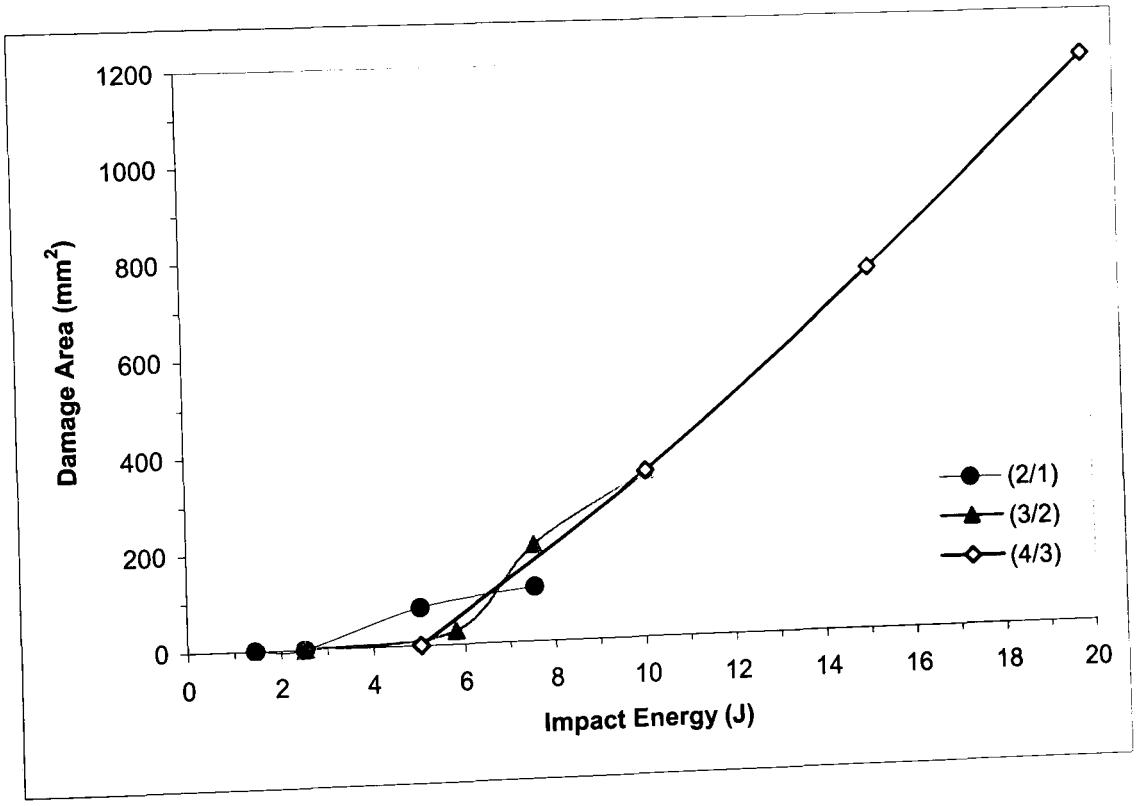

Figure 4.54 *The variation of damage area with impact energy for the CFRE-based fibre-metal laminates.*

4.9.2 Glass fibre-based fibre-metal laminates

As was the case for the CFRE-based fibre-metal laminates, the low velocity impact response of the GFPP-based fibre-metal laminates was investigated by conducting low velocity impact tests on an instrumented falling weight impact tower. Once again, impact tests at energies up to 20 Joules were performed on 2/1, 3/2 and 4/3 fibre-metal laminates with dimensions of approximately 100 x 100 mm approximately. Following impact, a number of specimens were sectioned and polished in order to elucidate the failure mechanisms and processes.

4.9.2.1 Impact failure mechanisms

Figure 4.55 shows low magnification optical micrographs of (2/1), (3/2) and (4/3) laminates subjected to impact energies of 7.5, 10 and 20 Joules respectively. An examination of the cross-section of the (2/1) system, Figure 4.55a, indicated that the sample exhibits significant permanent deformation around the point of impact. A closer examination of the micrograph highlights the presence of a large number of matrix cracks in the highly-deformed region immediately under the point of impact. The extensive damage in these micrographs suggests that the glass fibre reinforced ply has made a significant contribution to the energy-absorbing process in this system. The (3/2) laminate exhibits similar characteristics to those reported above although there is less permanent deformation than in the (2/1) system, Figure 4.55b. A closer examination of this five layer system suggests that the crack had propagated within the composite ply with the bi-material interface remaining intact. The (4/3) laminates exhibits a classical damage zone with the fracture zone exhibiting a conical shape similar to that observed in many plain composites [39], Figure 4.55c. Once again, this micrograph highlights the presence of extensive microcracking within the composite plies. It is interesting to note that after an impact energy of 20 Joules, the bi-material interface remains in excellent condition suggesting the level of adhesion between aluminium and glass fibre/polypropylene remains impressive when subjected to low velocity impact conditions.

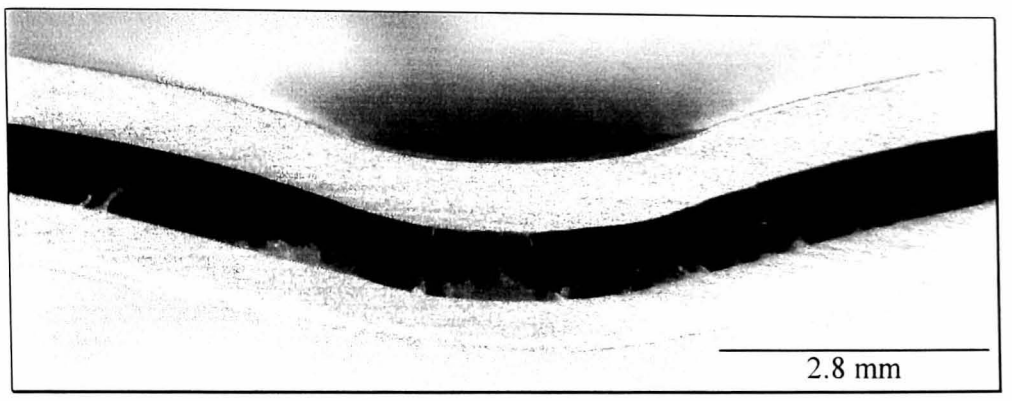

(a) 2/1 laminate, impact energy = 4.5 J

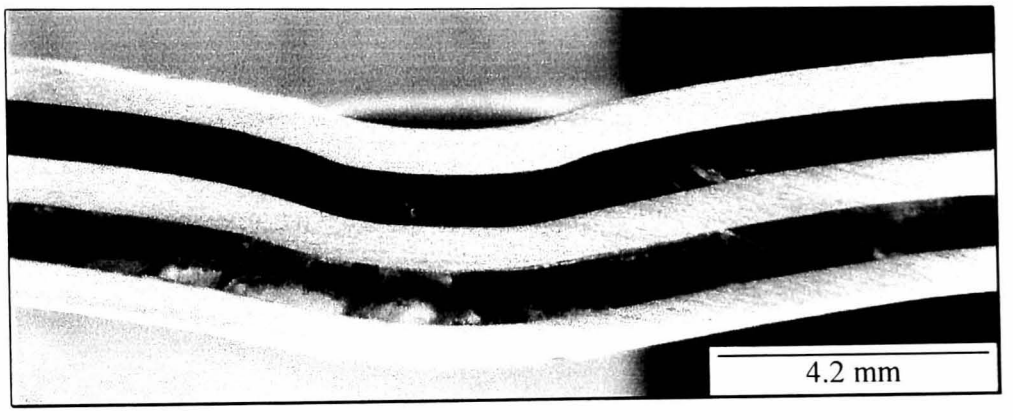

(b) 3/2 laminate, impact energy = 10 J

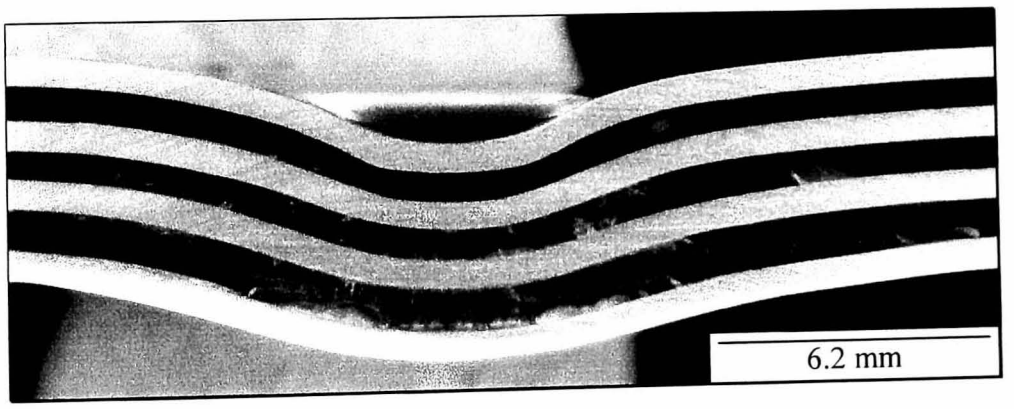

(c) 4/3 laminate, impact energy = 20 J

Figure 4.55 *Low magnification optical micrographs showing damage in GFPP-based FML subjected to low velocity impact loading conditions.*

These results suggests that these hybrid systems were capable of absorbing significant energy through extensive plastic deformation in the aluminium and composite layers and localised microcracking in the GFPP

4.9.2.2 Influence of impact energy

As with to the CFRE-based fibre-metal laminates, the polished sections were used to estimate the size of the damage area with impact energy in the impacted samples. Figure 4.56 shows the variation of the size of the damage zone with impact energy for the (2/1), (3/2) and (4/3) GFPP-based fibre-metal laminates. As expected, the size of the damage zone increases with increasing impact energy in all three systems. It is interesting to note that damage is quite localised and that these results are far superior to those obtained with the CFRE-based fibre-metal laminates. Here, the (4/3) laminate exhibited a damage area of approximately 500 mm^2 after a 20 Joule impact in comparison with the 1200 mm^2 observed in the CFRE-based system. Here, the superiority of the thermoplastic-based system over the CFRE-based is clearly evident. In addition, the GFPP-based fibre-metal laminates exhibited a superior impact resistance to that offered by a sixteen ply (0^o,90^o,+/-45^o) carbon fibre-reinforced PEEK laminate [38]. These results, suggests that the GFPP-based fibre-metal laminates offer excellent energy-absorbing characteristics under low velocity impact loading conditions.

4.10 POST-IMPACT TENSILE PROPERTIES OF THE FIBRE-METAL LAMINATES

The post-impact tensile properties of the fibre-metal laminates were investigated in order to evaluate the effect of varying impact energy on the residual tensile strength of the hybrid materials.

4.10.1 Carbon fibre-epoxy-based FML

The post-impact residual strength of the CFRE-based fibre-metal laminates was investigated by conducting low velocity impact tests using the aforementioned instrumented falling weight impact tower. Here plates with dimensions 200 x

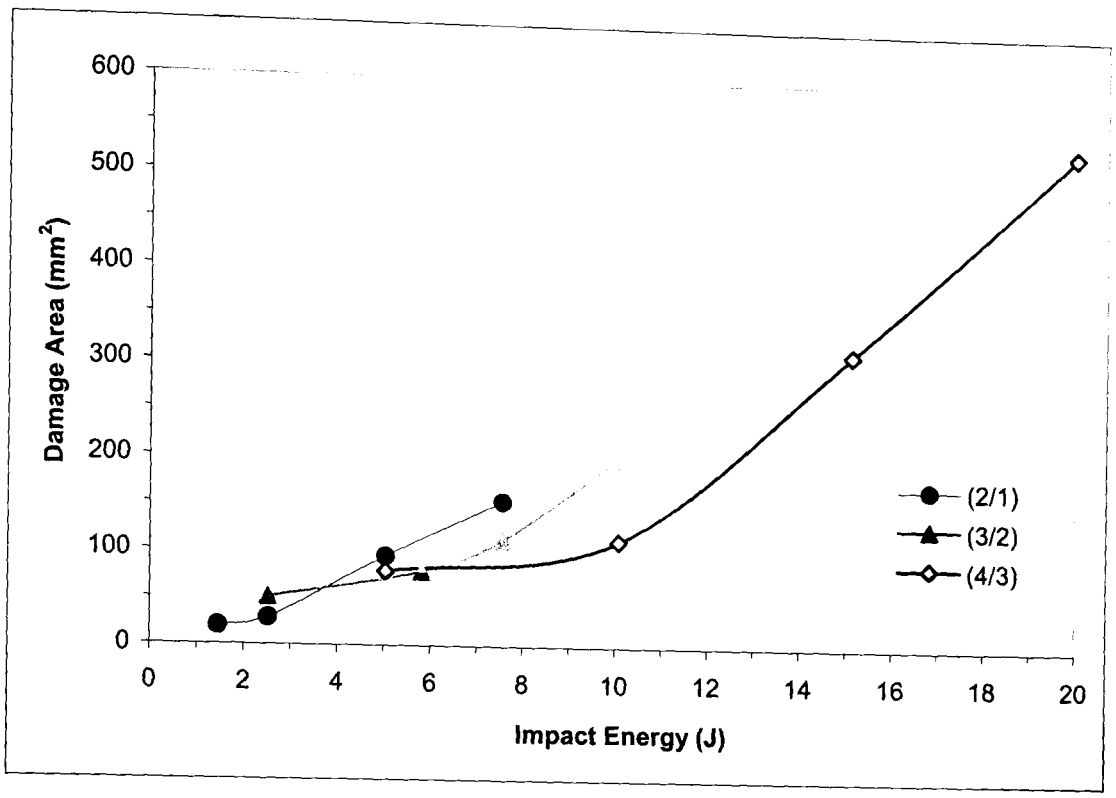

Figure 4.56 *The variation of damage area with impact energy for the GFPP-based fibre-metal laminates.*

240 mm were tested and subjected to impact energies of up to 20 Joules. After impact, specimens with dimensions 200 x 50 mm were removed from the impacted plates and tensile tests were conducted on these samples at 1 mm/min. The tensile strength was then calculated using Equation 3.11.

4.10.1.1 Residual strength

Figure 4.57 shows the variation of the residual tensile strength of the (2/1), (3/2) and (4/3) CFRE-based fibre-metal laminates with impact energy. From the figure, it is clear that increasing impact energy resulted in a moderate reduction in the tensile strength of all three systems. The (2/1) laminates exhibits a more pronounced drop in tensile strength at impact energies between 2 and 6 Joules with no further reduction after a 7.5 Joule impact. The (3/2) and (4/3) systems exhibit a steady reduction in tensile strength with increasing impact energy. It is interesting to note

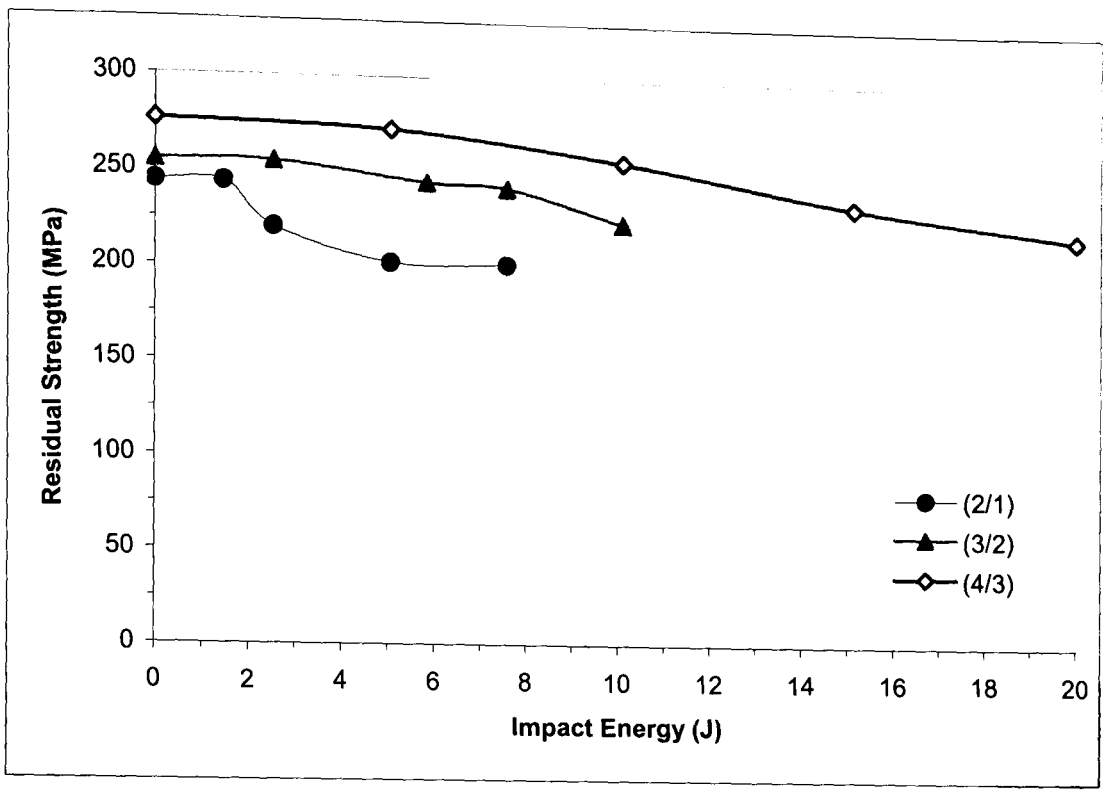

Figure 4.57 *The variation of the residual tensile strength with impact energy for the CFRE-based fibre-metal laminates.*

that the (3/2) and (4/3) laminates suffer a 10 and 20% reduction in tensile strength after 10.5 and 20 Joule impacts respectively. An examination of the laminates subjected to low and intermediate impact energies indicated that tensile failure generally occurred at locations away from the impact zone. In contrast, failure in the specimens subjected to high impact energies occurred close or within the impact zone. Nevertheless, these results suggest that these systems offer a excellent resistance to localised impact loading conditions outperforming a sixteen ply (0^{o},+-45^{o}) carbon fibre/epoxy composite [40]. In addition, these systems offer great potential for use in dynamically-loaded structures.

4.10.2 Glass fibre/polypropylene-based FML

The post-impact residual strength of the GFPP-based fibre-metal laminates was investigated using the same test procedure as that used with the CFRE-based fibre-metal laminates.

4.10.2.1 Residual strength

The tensile properties of the (2/1), (3/2) and (4/3) impact-damaged GFPP-based fibre-metal laminates are summarised in Figure 4.58. The figure shows that the (3/2) and (4/3) laminates suffer a 12 and 19% reduction in tensile strength at the highest energy and the (2/1) laminate incurred a twenty percent reduction in residual tensile strength after a 7.5 joule impact. An inspection of the laminates subjected to low and intermediate impact energies revealed that failure generally occurred at regions away from the impact-damaged zone, often near the zone where the specimens were gripped. These results suggest that thermoplastic-based fibre-metal laminates exhibit an excellent resistance to localised low velocity impact loading. One further advantage of these systems is the likelihood that low and moderate amounts of impact damage can be easily repaired using fusion bonding similar to those used to join thermoplastic components [41]. It is worth noting that the GFPP-based fibre-metal laminates offer superior residual properties over the CFRE-based systems at all impact energies. However, it is interesting to note that the properties of the (4/3) CFRE-based laminate closely mirror those of its thermoplastic counterpart.

4.11 SINGLE EDGE NOTCH BEND PROPERTIES OF THE FIBRE – METAL LAMINATES

The next stage of this programme was to characterise the perforation resistance of the fire-metal laminates. Previous work [42] has shown that it is possible to relate the perforation resistance of a composite to its work of fracture. In this study, the work of fracture W_f of the aluminium, the carbon fibre reinforced epoxy and the glass fibre reinforced polypropylene materials was evaluated using the single edge notch bend (SENB) geometry. Following this, The work of fracture, W_f, of the fibre-metal laminates based on both composite systems was assessed.

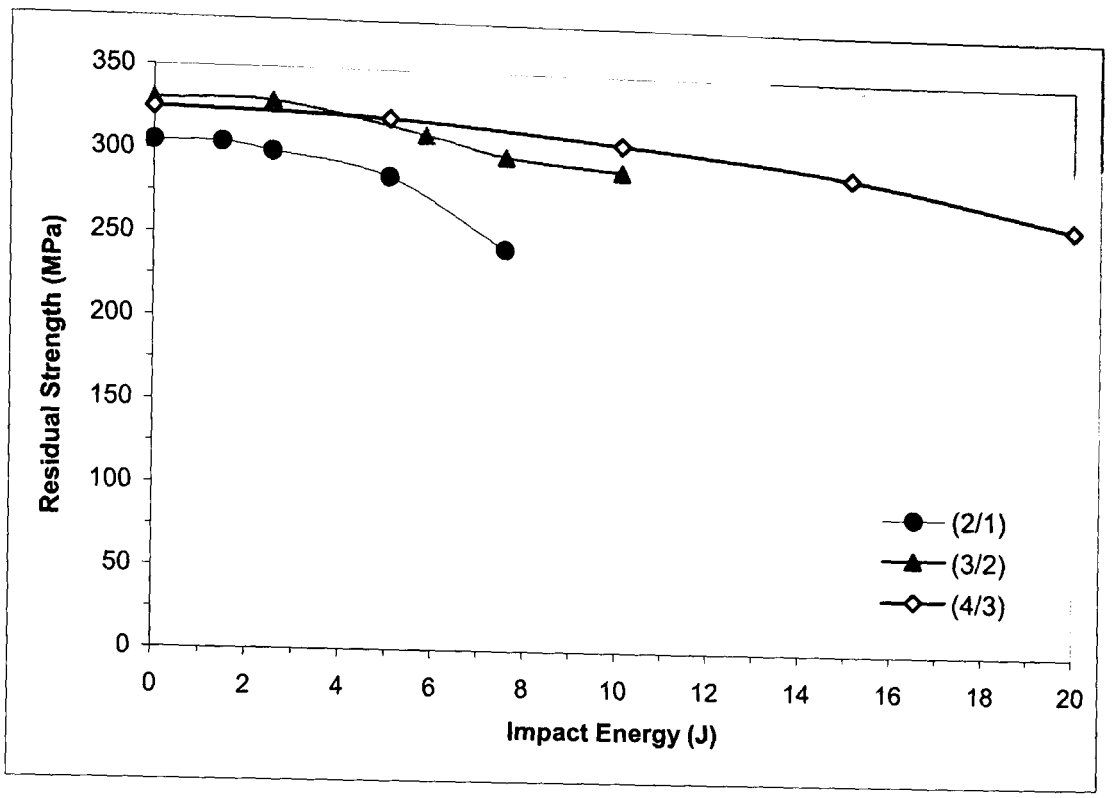

Figure 4.58 *The variation of the residual tensile strength with impact energy for the GFPP-based fibre-metal laminates.*

4.11.1 Carbon fibre/epoxy-based FML

The work of fracture, W_f, of CFRE-based fibre-metal laminates was evaluated using single edge notch bend (SENB) samples having dimensions 75 x 15 mm x thickness. Notches with a length to depth ratio, a/W, of 0.5 were introduced at the mid-span using a saw and sharpened with a fresh razor blade. The specimens were supported on two 6 mm diameter rollers positioned 60 mm apart and loaded at a crosshead displacement rate of 2 mm/min in the Instron 4505 universal test machine. During the test, the crack propagated through the specimen thickness and the load-displacement data were recorded in order to estimate the energy absorbed by the specimen. The work of fracture was calculated using Equation 3.13. After failure, the specimen was removed from the fixture for low magnification optical examination.

4.11.1.1 Influence of the V_f of composite on the work of fracture

Figure 4.59 shows typical load-displacement curves following SENB tests on the CFRE-based fibre-metal laminates. From this figure, it is clear that the initial loading curves for all the laminates exhibited some non-linearity which may be associated with some plasticity in the composite adherends. A closer examination of the curves, highlights the presence of a saw-tooth appearance which is associated with the primary crack propagating in small jumps as a result of the woven nature of the composite. It is interesting to note the laminates exhibited a small amount of crack propagation before maximum load, at this point initial fibre failure occurred within the composite plies and the specimen began failing in a stable manner.

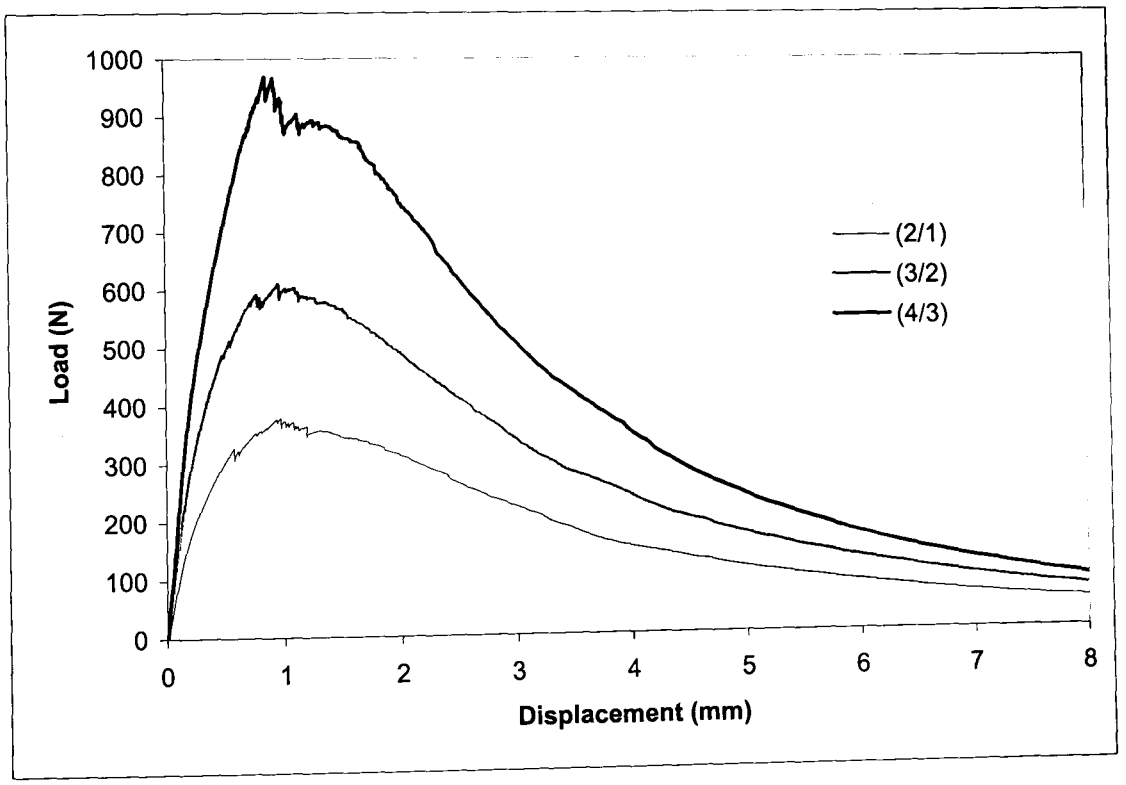

Figure 4.59 *Typical load-displacement curves following SENB tests on the CFRE-based fibre-metal laminates.*

The variation of the work of fracture with volume fraction of composite material is shown in Figure 4.60. Also included in the figure are the work of fracture of the aluminium and carbon fibre reinforced epoxy. The data clearly indicate that there is a roughly linear relationship between the work of fracture of the fibre-metal laminates and the volume fraction of the composite with the value of W_f tending to decrease with increasing V_f. This reduction in work of fracture is as a result of the fact that 50% of the fibres in the carbon fibre reinforced epoxy composite are aligned parallel to crack direction. In consequence, these fibres do not contribute to resisting crack growth. In addition, this reduction is also due to the brittle nature of the carbon fibres. Nevertheless, these results suggest a simple law of mixtures prediction could be applied in order to estimate the work of fracture of CFRE-based fibre-metal laminates. It is encouraging that the data presented in Figure 4.60 exhibited very little scatter suggesting that the laminates were of a high quality.

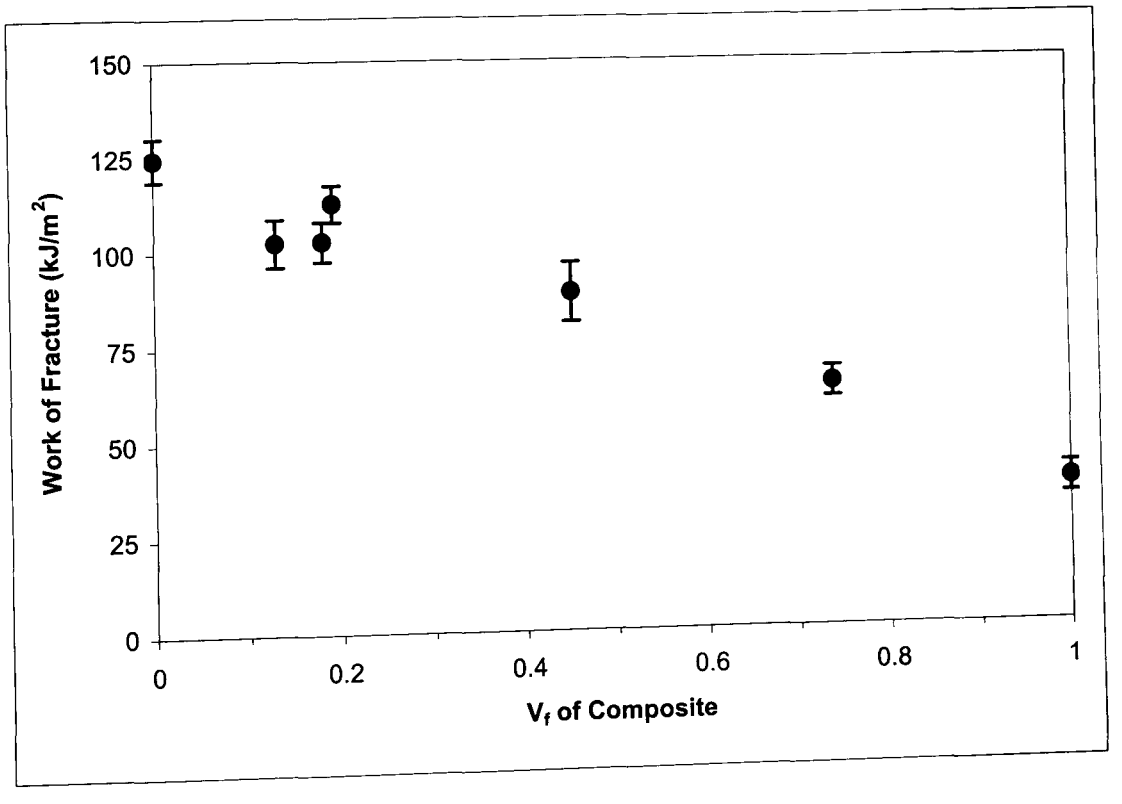

Figure 4.60 *The variation of work of fracture of the CFRE-based fibre-metal laminates with volume fraction of composite material.*

Figure 4.61 shows a typical low magnification optical micrograph of a (3/2) CFRE-based fibre-metal laminate after SENB testing at 2 mm/min. Crack propagation in this figure is from top to bottom. From this figure, it is clear that a small amount of fibre pull-out is apparent. The evidence in Figures 4.60 and 4.61 suggests that the aluminium was the main contributor to resisting crack propagation. As mentioned above, the contribution of the fibres aligned parallel to crack did not enhance the work of fracture.

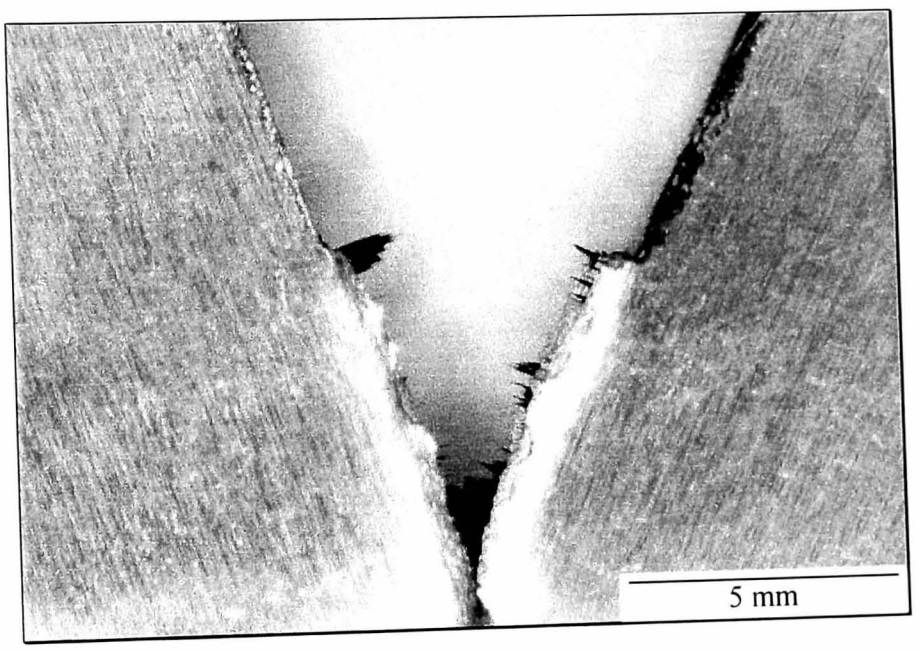

Figure 4.61 *Low magnification optical micrograph of a (3/2) CFRE-based fibre-metal laminate after SENB tests at 2 mm/min.*

4.11.2 Glass fibre/polypropylene-based FML

As for the CFRE-based fibre-metal laminates, The work of fracture, W_f, of GFPP-based fibre-metal laminates was evaluated using the single edge notch bend (SENB) geometry.

Figure 4.62 shows typical load-displacement curves following SENB tests on the GFPP-based fibre-metal laminates. From this figure, it is clear that the initial loading curves for all the laminates exhibited some non-linearity which may be associated with some plasticity in the composite adherends. A closer examination of

the curves highlights the presence stable crack propagation. It is interesting to note the laminates exhibited a noticeable load drop during crack propagation at approximately 4 mm of displacement. This drop in load is believed to be as a result localised aluminium/composite debonding just below the load point. Continued loading of the samples resulted in the material failing in a slow and stable manner.

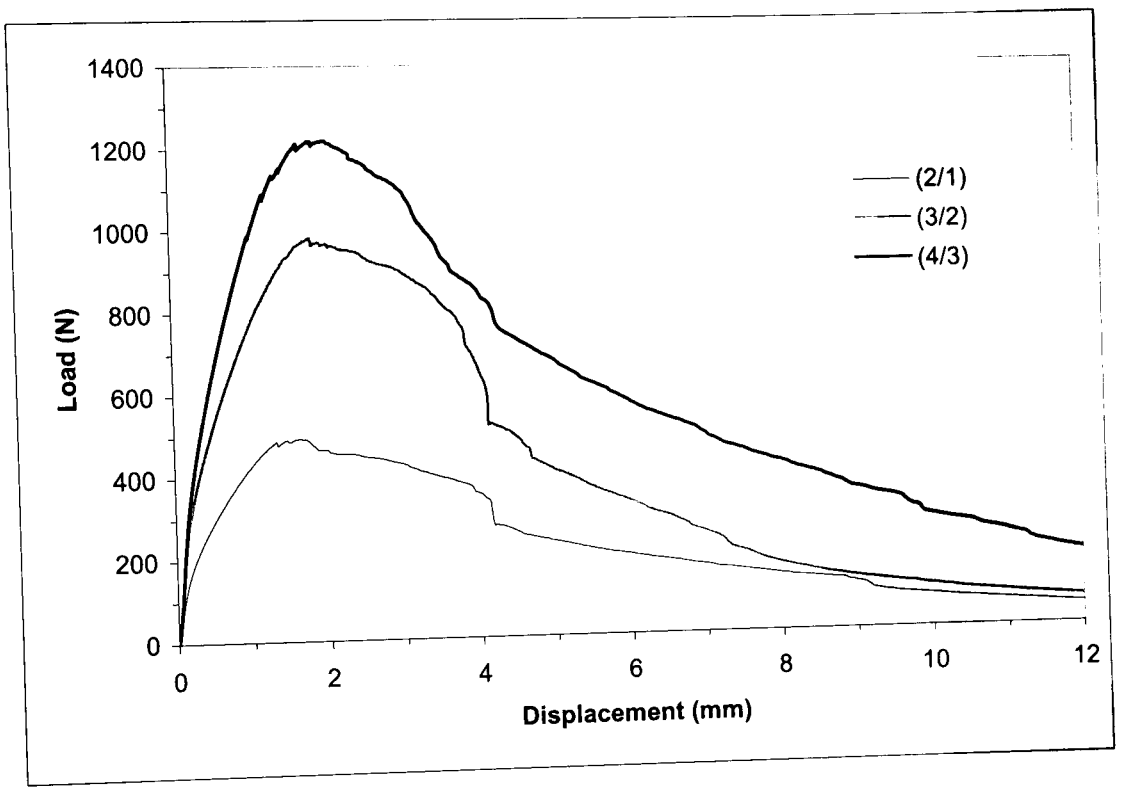

Figure 4.62 *Typical load-displacement curves following SENB tests on the GFPP-based fibre-metal laminates.*

Previous work has shown that glass fibres are rate sensitive [42]. Therefore, tests were undertaken at impact rates of strain using the instrumented falling-weight impact tower. Here, the impact velocity was 3 m/s and the carriage weight was 9.98 kg. During the test, the force-time data were recorded. The impact energy under the load-time trace was calculated using Equation 3.14. The work of fracture was then calculated by dividing the absorbed energy by the ligament of the SENB specimen.

4.11.2.1 Influence of the V_f of composite on the work of fracture

The variation of the work of fracture of the GFPP-based fibre-metal laminates with volume fraction of composite material at quasi-static and dynamic rates of loading is shown in Figure 4.63. Included in the figure are the work of fracture of the aluminium and glass fibre/polypropylene. From this figure, it is clear that increasing the V_f of the composite material had a beneficial effect on the SENB properties of this hybrid systems. At 2 mm/min, the work of fracture steadily increases with increasing V_f of glass fibre/polypropylene.

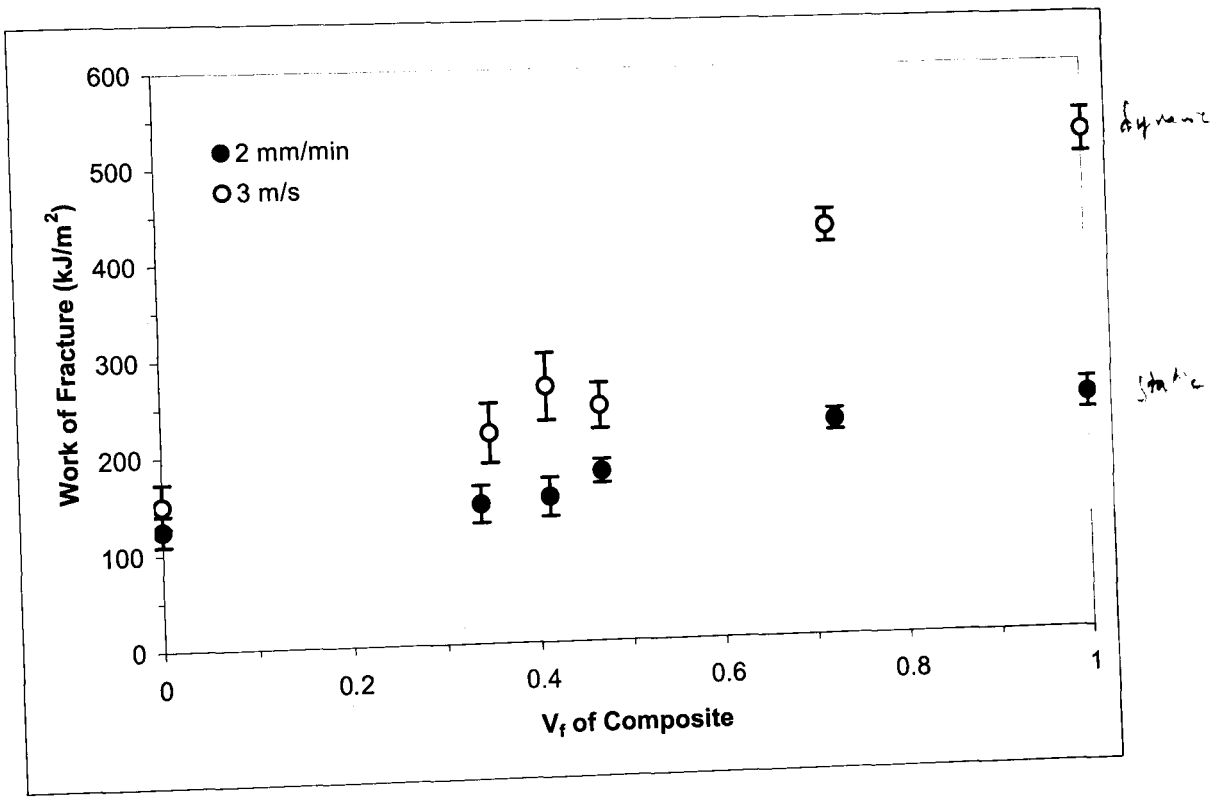

Figure 4.63 *The variation of work of fracture of the GFPP-based fibre-metal laminates with volume fraction of composite material at quasi-static and dynamic rates of loading.*

Here, it is encouraging to note that the data exhibit very little scatter and a roughly linear relationship is also apparent. At 3 m/s the work of fracture exhibits

higher values with increasing V_f of glass fibre/polypropylene, with the plain composite reaching approximately 500 kJ/m^2. This increase in W_f at higher loading rates suggests that the composite material is rate sensitive. Indeed, it has been reported elsewhere [42] that the observed increase in W_f with loading rate is related to the rate-dependent fracture properties of the glass fibres. In addition, these results suggest that the GFPP-based fibre-metal laminates exhibit outstanding fracture properties at high loading conditions being ideal candidates for use in dynamically-loaded structures.

Figure 4.64 shows a typical low magnification optical micrographs of (3/2) GFPP-based fibre-metal laminates after testing at 2 mm/min and 3 m/s. Crack propagation in this figure is from top to bottom. A large amount of fibre breakage and fibre pull-out is apparent in these figures as a result of 100% of the fibres being aligned perpendicular to crack direction. Here the average fibre pullout length was between 2 and 3 mm. This suggests that the glass fibres contributed in a significant manner to the toughness of this material as exhibited in Figure 4.63. In addition, these results suggest that the GFPP-based fibre metal laminates offer excellent through thickness fracture properties at quasi-static rates of loading. It is worth noting that the amount of fibre breakage and pull-out at 3 m/s was very similar to that exhibited at 2 mm/min, Figure 4.64b. Nevertheless, it is believed that increasing the loading rate resulted in an increase in the fibre failure stress and, as a result, the stored elastic energy. This in turn could create a larger damage zone during crack growth which can absorb more energy [42]. It is interesting to note that the GFPP-based fibre metal laminates offer superior work of fracture properties in comparison to the CFRE-based fibre-metal laminates at quasi-static and dynamic rates of loading. This suggests that the thermoplastic-based fibre-metal laminates might exhibit superior perforation resistance properties to those offered the thermosetting-based fibre-metal laminates under high velocity impact loading conditions.

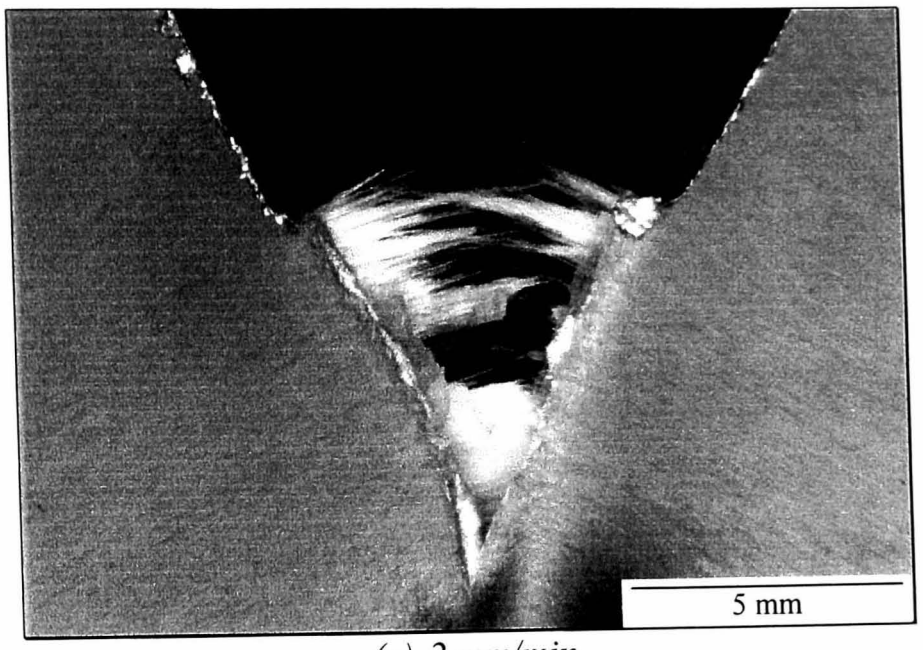

(a) 2 mm/min

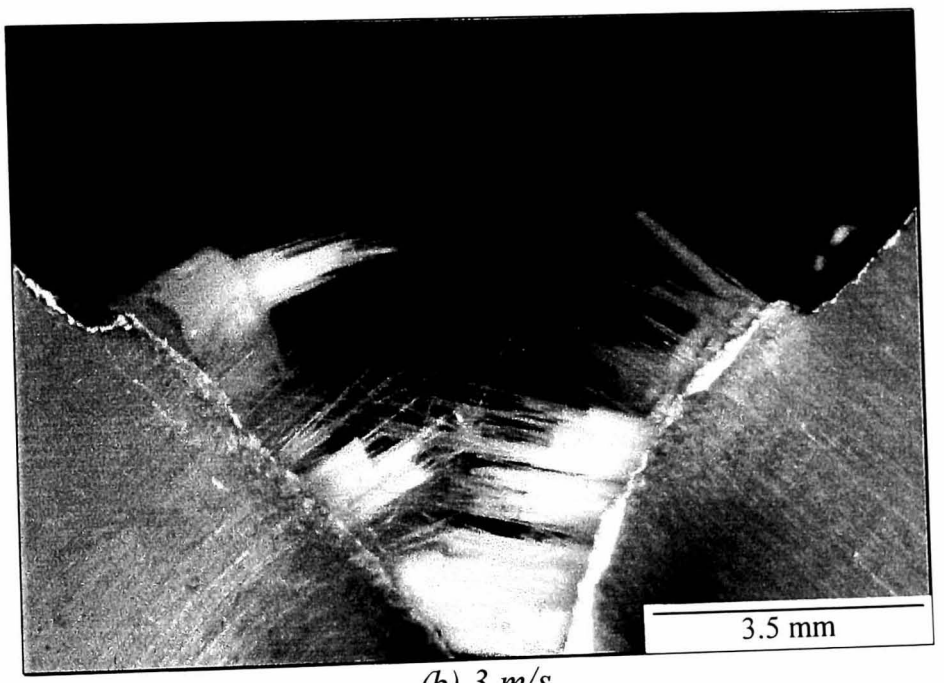

(b) 3 m/s

Figure 4.64 *Low magnification optical micrographs of (3/2) GFPP-based fibre-metal laminates after SENB tests at (a) 2 mm/min and (b) 3 m/s.*

4.12 HIGH VELOCITY IMPACT RESPONSE OF THE FIBRE-METAL LAMINATES

The high velocity impact response of a series of (2/1), (3/2) and (4/3) thermoset and thermoplastic-based fibre-metal laminates was investigated using a

nitrogen gas gun. In order to evaluate the influence of impact energy on the performance of these hybrid systems a range of incident energies were used. After impact, the samples were removed from the supports and sectioned in order to elucidate the failure mechanisms within the impact zone.

4.12.1 Carbon fibre/epoxy-based FML

In order to evaluate the high velocity impact properties of CFRE-based fibre-metal laminates, a nitrogen gas gun was used. Here, plates with dimensions 100 x 100 mm were clamped in a steel support with a 75 x 75 mm square aperture and impacted centrally. Impact testing was performed using a 46.8 g steel projectile with a 12.7 mm diameter hemi-spherical head at velocities between 25 and 84 m/s. The incident impact energy was determined using two photoelectric sensors with a 99.6% guaranteed minimum accuracy. After impact, the samples were removed from the supports and sectioned in order to elucidate the failure mechanisms within the impact zone.

4.12.1.1 Influence of impact energy

In order to evaluate the influence of the incident impact energy on the dynamic response of these layered systems, specimens were impacted at different impact energies until complete perforation of the target was achieved. Figure 4.65 shows low magnification optical micrographs of polished sections from the (3/2) CFRE-based fibre-metal laminates subjected to impact energies between 18 and 81 Joules. At the lowest incident energy, the composite and aluminium plies have clearly undergone permanent plastic deformation, Figure 4.65a. In addition, yielding of the aluminium ply is also apparent in the lowermost aluminium layer as a result of the bending of the sample during impact. After an impact of 42 Joules, greater indentation of the laminate is evident, Figure 4.65b. Here, fracture of the two composite plies and the middle and lowermost aluminium layers is also apparent. It is interesting to note that damage is very localised and the bi-material interface remains in an excellent condition after a 42 Joule impact. As the impact energy is

increased to 61 Joule, failure of the uppermost composite layer occurs, Figure 4.65c. Here, small planes of delamination between the aluminium and composite plies are also apparent. Significant membrane stretching and plastic bending is also evident. After an impact energy of 81 Joule perforation of the laminate had occurred, Figure 4.65d. Here, it is apparent that the upper and middle aluminium plies have been partially severed and removed and the lower aluminium layer has been damaged under the point of impact. Small areas of delamination at the bi-material interface close to the point of impact are also visible. It is interesting to note that damage in the laminates is very localised and that the interface between the aluminium and composite remains in excellent condition after extreme impact loading.

Figure 4.66 shows the perforation energies of the (2/1). (3/2) and (4/3) CFRE-based fibre-metal laminates. From this figure, it is clear that as the thickness of the laminate increases, the energy required to perforate the target also increases reaching values of approximately 48, 81 and 125 Joules for the (2/1), (3/2) and (4/3) laminates respectively. This information was used to evaluate the impact resistance of the CFRE-based fibre-metal laminates. Here, the specific perforation energy was calculated by normalising the perforation energy by the areal density of the target. Figure 4.66 also shows the specific perforation energies for the (2/1), (3/2) and (4/3) CFRE-based fibre-metal laminates after high velocity impact testing. Here it is clear that the (2/1) laminate offers the lowest specific perforation energy with a value of approximately 9.7 Jm^2/kg. In contrast, the (4/3) laminate offers the highest specific perforation energy reaching a value of approximately 13 Jm^2/kg.

4.12.2 Glass fibre/polypropylene-based FML

The high velocity impact properties of the GFPP-based fibre-metal laminates were investigated using the same test procedure as that used with the CFRE-based fibre-metal laminates.

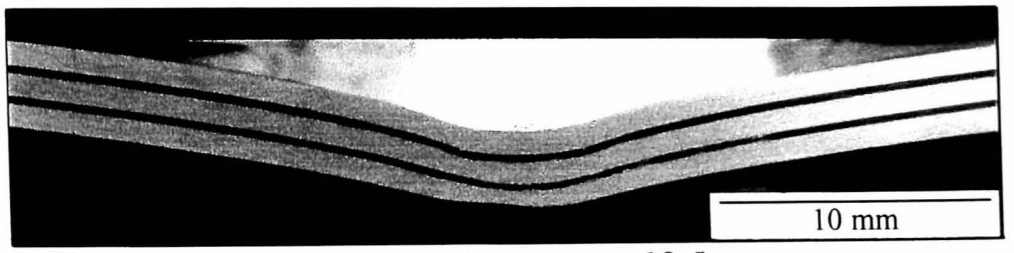

(a) Impact energy = 18 J

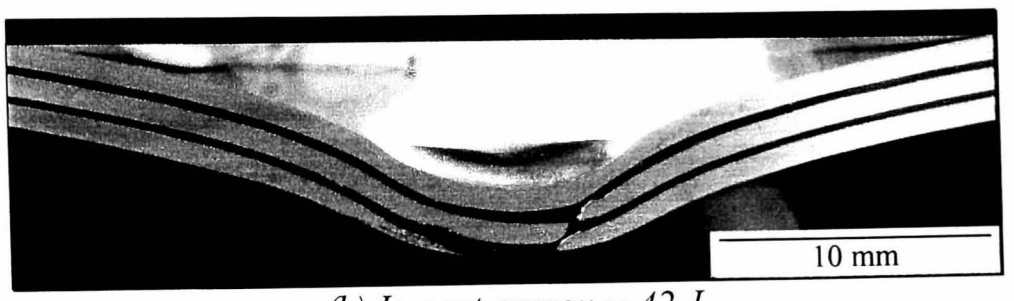

(b) Impact energy = 42 J

(c) Impact energy = 61 J

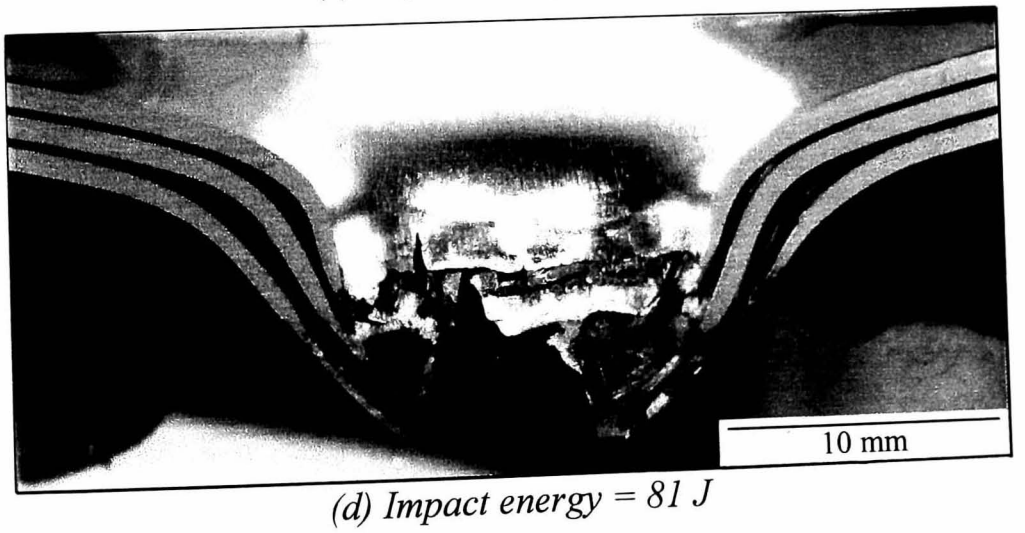

(d) Impact energy = 81 J

Figure 4.65 *Low magnification optical micrographs showing damage in a (3/2) CFRE-based fibre-metal laminate after high velocity impact testing.*

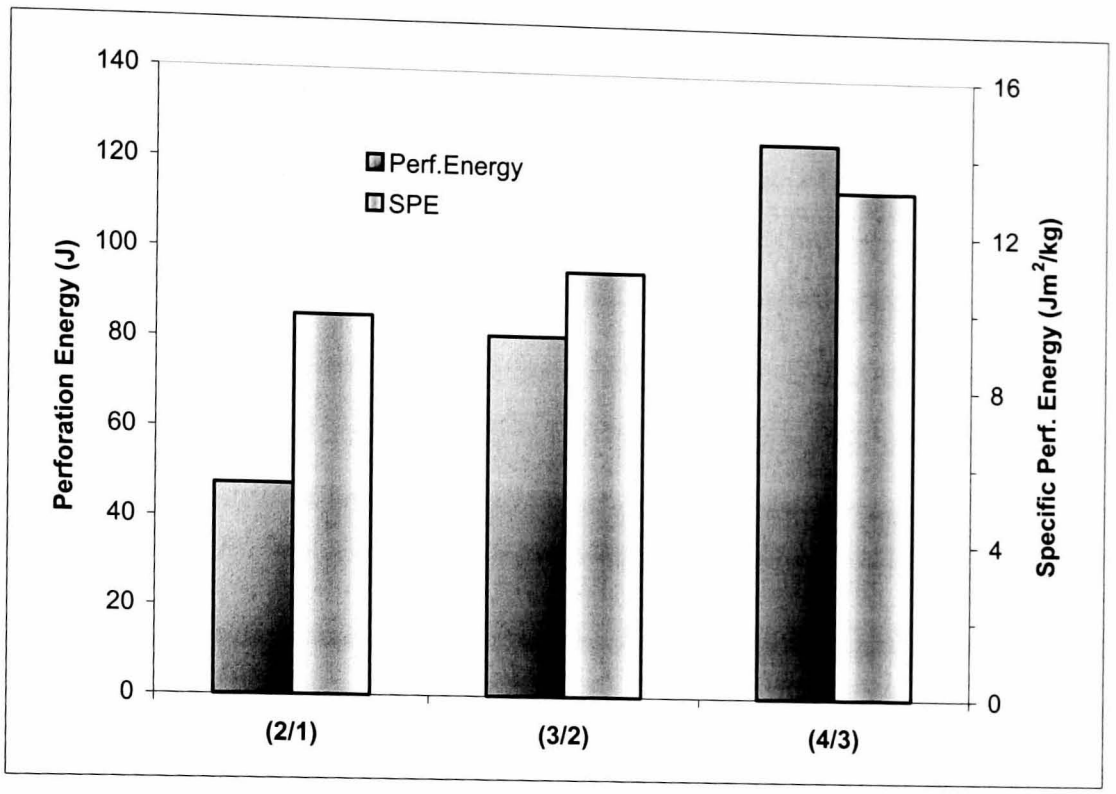

Figure 4.66 *Perforation and specific perforation energies of the CFRE-based fibre-metal laminates after high velocity impact testing.*

4.12.2.1 Influence of impact energy

The influence of impact energy on the dynamic properties of the GFPP-based fibre-metal laminates was also examined. Figure 4.67 shows low magnification optical micrographs of polished sections of a (3/2) laminate subjected to impact energies between 36 and 165 Joules. At the lowest incident energy, it is clear that the laminate has undergone permanent deformation involving plastic deformation of the composite and aluminium plies, Figure 4.67a. A closer examination of the sample highlighted the presence of localised matrix cracking around the point of impact in the two composite plies. Significant membrane stretching and plastic bending is apparent in the sample subjected to an impact energy of 90 Joules, Figure 4.67b.

Here, small planes of delamination between the composite and aluminium plies are also apparent. In addition, a large area of matrix cracking is evident in both composite plies. After an impact of 141 Joules, the upper aluminium ply has been partially severed and removed and the middle and lower aluminium plies have been damaged under the point of loading, Figure 4.67c. A further examination of the micrograph highlights the presence of planes of delamination extending some distance from the point of impact. Damage in the perforated sample is extensive and involves folding of the aluminium plies, extensive fibre fracture in the composite layers as well as delamination and matrix cracking, Figure 4.67d.

The perforation energies of the (2/1). (3/2) and (4/3) GFPP-based fibre-metal laminates is shown in Figure 4.68. Here, it is clear that perforation energy increases with increasing laminate thickness reaching values of approximately 97, 165 and 235 Joules for the (2/1), (3/2) and (4/3) laminates respectively. The high velocity impact response of the thermoplastic-based fibre-metal laminates was investigated on a series of square laminates. Here, the impact resistance of the laminates was characterised by determining the specific perforation energy, defined as the perforation energy normalised by the areal density of the target. Figure 4.68 also exhibits the specific perforation energies for the (2/1), (3/2) and (4/3) GFPP-based fibre-metal laminates after high velocity impact testing. Here it is clear that the (2/1) laminate offers the lowest specific perforation energy with a value of approximately 17 Jm^2/kg. In contrast, the (3/2) laminate offers the highest specific perforation energy with a value of approximately 19.3 Jm^2/kg, a value that is similar to that reported for other thermosetting-based fibre-metal laminates [43].

It is interesting to note that in this case the (4/3) laminate exhibited a specific perforation energy below than that offered by the (3/2) laminate despite its higher perforation energy. This is clearly a result of the higher areal density exhibited by the (4/3) laminate. These results suggests that GFPP-based fibre-metal laminates offer an outstanding perforation resistance when subjected to high velocity impact conditions.

(a) Impact energy = 36 J

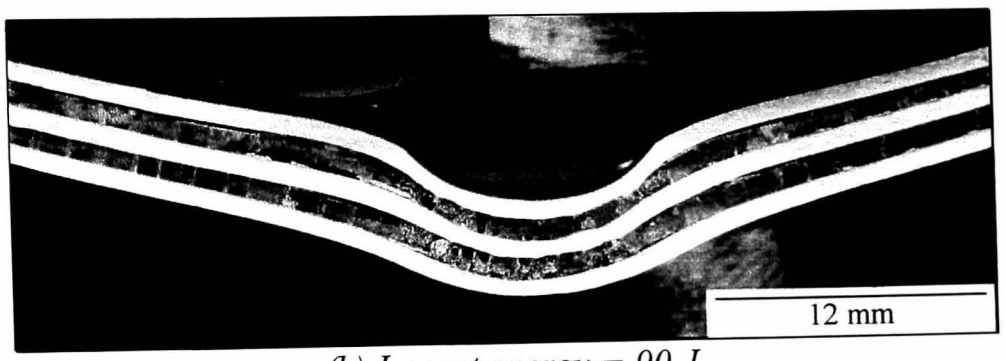

(b) Impact energy = 90 J

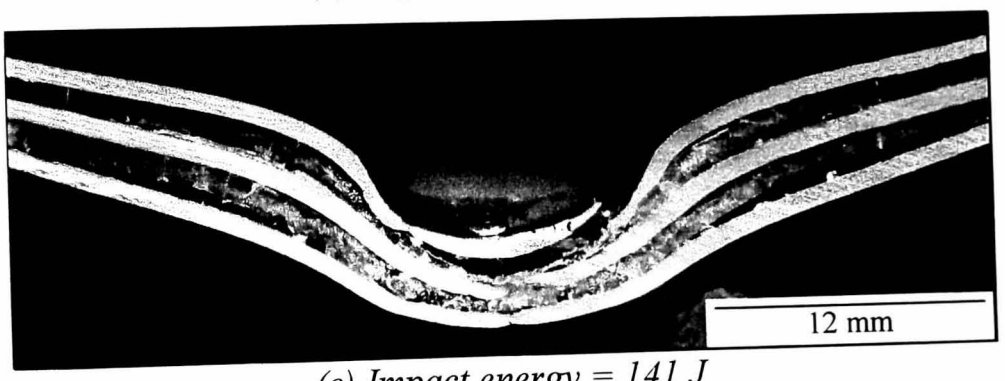

(c) Impact energy = 141 J

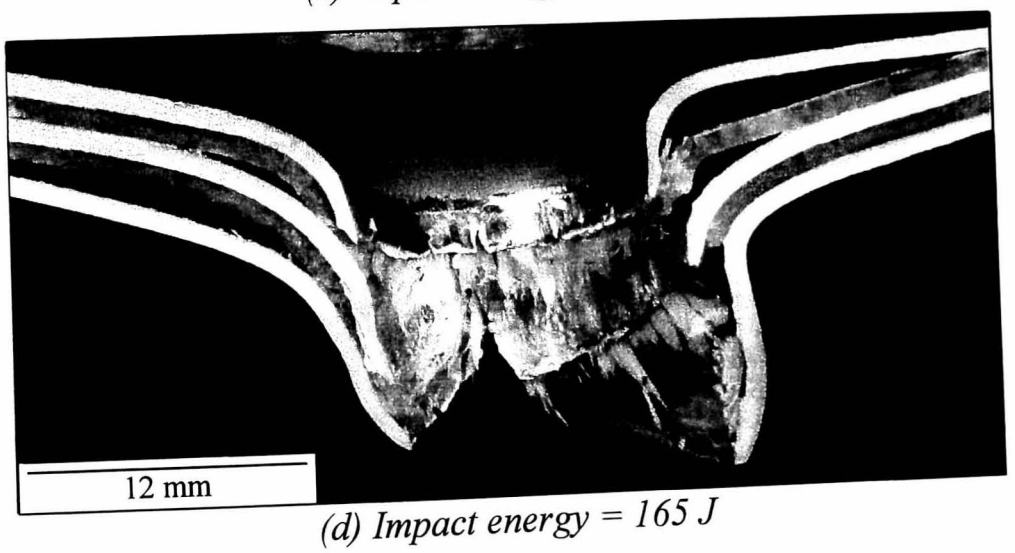

(d) Impact energy = 165 J

Figure 4.67 *Low magnification optical micrographs showing damage in a (3/2) GFPP-based fibre-metal laminate after high velocity impact testing.*

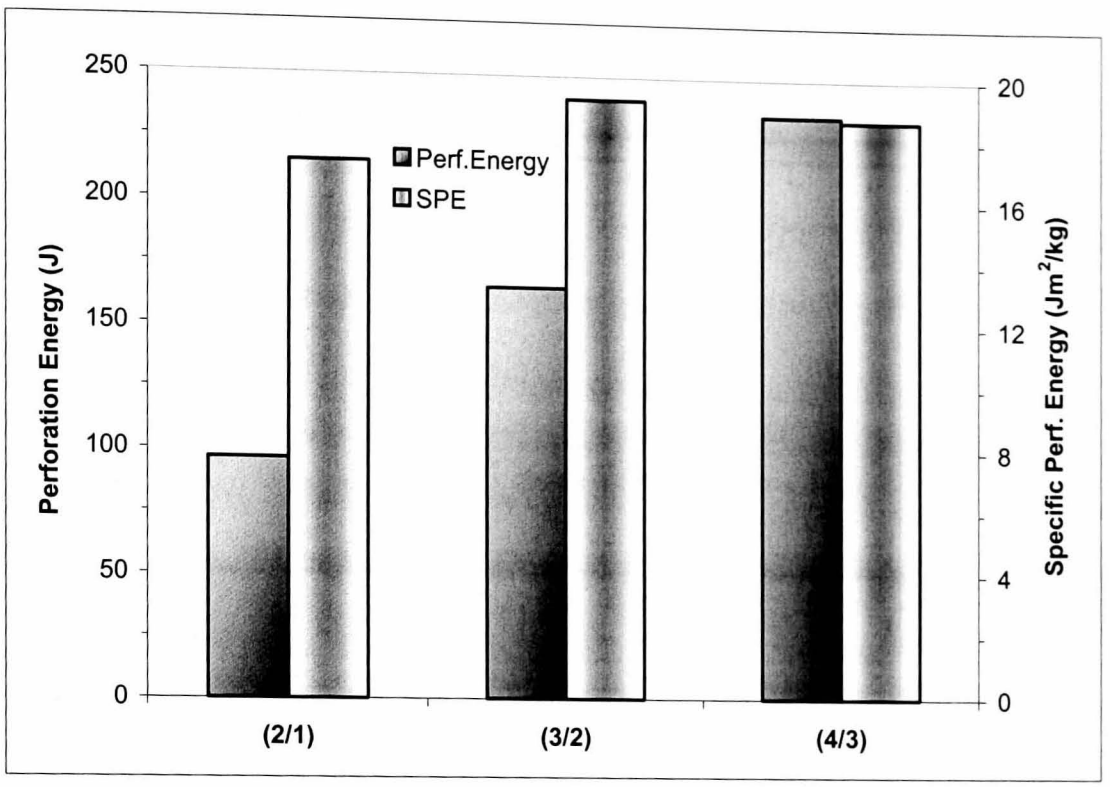

Figure 4.68 *Perforation and specific perforation energies of the GFPP-based fibre-metal laminates after high velocity impact testing.*

Here failure mechanisms such as fibre fracture and matrix cracking in the composite plies and plastic folding within the aluminium layers have been shown to contribute to the impressive perforation resistance of these systems. It is interesting to note that the GFPP-based fibre-metal systems offer superior perforation resistant properties to the CFRE-based fibre-metal laminates under high velocity impact conditions. Indeed, the specific perforation energy of this system was over seventy percent higher than that offered by the thermosetting-based fibre metal laminates. In addition, recent wok have shown that using glass fibre/polypropylene in a cross-ply ($0^o/90^o$) increases by up to 30 % the specific perforation energy of the fibre-metal laminates reaching values of 25 Jm^2/kg [44]. This suggests that the thermoplastic-based fibre-metal laminates offer an excellent candidate for high performance load-bearing applications

4.12 REFERENCES

[1] **Kim, J.K., Sham, M.L.**, Composites Science and Technology, **60** (2000), pp 745-761.

[2] **Cantwell, W.J., Kausch, H.H.**, Mechanics of Composite Materials, **4** (1992), pp 476-483.

[3] **Bradley, W.L., Cohen, R.N.**, Delamination and Debonding of Materials, ASTM STP 876, (1985), pp 389-410.

[4] **Adeyemi, N.B., Shivakumar, K.N., Avva, V.S.**, AIAA Journal, **37** (1998), pp 517-520.

[5] **Charalambides, M. Kinloch, A.J., Wang, Y., Williams, J.G.**, International Journal of Fracture, **54** (1992), pp 269-291.

[6] **Smith, B. and Grove, R.**, Failure Analysis of Composite Structure Materials, AFWAL-TR-87-4001, US Air Force, 1987.

[7] **Smith, B. and Grove, R.**, Post Failure Analysis Techniques for Composite Materials, AFWAL-TR-86-4137, US Air Force, 1987

[8] **Purslow, D.**, Composites, **17** (1983), pp 289-303.

[9] **Shin, S., Jang, J.**, Journal of Materials Science, **34** (1999), pp 5299-5306.

[10] **Samajdar, S., Kishore**, Journal of Materials Science, **26** (1991), pp 977-984.

[11] **Davies, P., Cantwell, W. J.**, Composites, **25** (1994), pp 869-877.

[12] **Alif, N., Carlsson, L.A., Boogh, L.**, Composites part B, **29B** (1998), pp 603-611.

[13] **Mall, S., Law, G.E., Katouzian, M.**, Proceeding of the SEM Spring Conference on Experimental Mechanics, (1986), pp412-417.

[14] **Maikuma, H., Gillespie, J.W., Wilkins, D.J.**, Journal of Composite Materials, **24** (1990), pp 124-149.

[15] **Blyton, M.**, PhD Thesis, The University of Liverpool (1998).

[16] **Cantwell, W.J., Blyton, M., Sixsmith, P., Hiley, M.**, Journal of Materials Science Letters, **17** (1998), pp 1103-1106.

[17] **Gensler,R., Plummer, C.J.G., Grein, C., Kausch, H.H.**, Polymer, **41** (2000), pp 3809-3819.

[18] **Cantwell, W.J., Blyton, M.**, Applied Mechanics Reviews, **52** (1999), pp 199-212.

[19] **Mall, S, Law, G.E., Katouzian, M.**, Journal of Composite Materials, **21** (1987), pp 569-579.

[20] **Cantwell, W.J.**, Journal of Composite Materials, **31** (1997) pp 1363-1380.

[21] **Cantwell, W. J., Morton, J.**, Composites, **22** (1991), pp 347-362.

[22] **Hou, J.P., Ruiz, C.**, Composites Science and Technology, **60** (2000), pp 2829-2834.

[23] **Albers, R.G., White, S.R.**, Proceedings of the American Society for Composites, (2000), pp 587-596.

[24] **Van Horn, K.R.**, Aluminium, III, American Society for Metals, 1967.

[25] **Kinloch, A.J.**, Adhesion and Adhesives, Chapman and Hall Ltd., 1987.

[26] **Chi-Wen, L., Wei-Lun L.**, Journal of Applied Polymer Science, **70** (1998), pp 383-387.

[27] **Chai, H.**, International Journal of Fracture, **60** (1993), pp 311-326.

[28] **Bascom, W.D., Cottington, R.L., Jones, R.L., Peyser, P.**, Journal of Applied Polymer Science, **19** (1975), pp 2545-2562.

[29] **Jones, C.**, Private Communication (1998).

[30] **Chinsirikul, W., Chung, T.C., Harrison, I.R.**, Proceeding of the American Society for Composites, (1992), pp 42-56.

[31] **Denault, J., Joussef, Y.**, ANTEC, (1998), pp 2286-2290.

[32] **Rijsdijk, H.M., Contant, M., Peijs, A.A.J.M.**, Composites Science and Technology, **48** (1993), pp161-172.

[33] **Sharon, G., Dodiuk, H., Kenig, S.**, Journal of Adhesion, **31** (1989), pp 21-31.

[34] Stesalit Ltd., Product Data Sheet, July 1996.

[35] BI Composites Ltd., Product Data Sheet, September 1991.

[36] **Wu, H.F., Wu, L.L.**, Journal of Materials Science, **29** (1994), pp 4583-4591.

[37] **Cantwell, W.J., Curtis, P.T., Morton, J.**, Composites, **14** (1984), pp 301-305.

[38] **Davies, P., Cantwell, W.J., Jar, P.Y., Richard, H., Neville, D.J., Kausch, H.H.**, ASTM STP 1110 Composite Materials: Fatigue and Fracture, Ed. T.K. O'Brien, (1991), pp 70-88.

[39] **Boll, D.J., Bascom, W.D., Weidner, J.C., Murry, W.J.**, Journal of Materials Science, **21** (1986), pp 2667-2677.

[40] **Cantwell, W.J., Curtis, P.T., Morton, J.**, Composites Science and Technology, 25 (1986), pp 133-148.

[41] **Cantwell, W.J., Davies, P., Jar P.Y., Bourban, P.E., Kausch, H.H.**, 11th European SAMPE Conference, (1990), pp 411-426.

[42] **Cantwell, W.J., Youd, S.J.**, Composites Part B, **28B** (1997), pp 635-640.

[43] **Vlot, A., Krull, M.**, Journal de Physique, IV 7(1997), pp.1045-1050.

[44] **Cantwell, W.J., Jones, N., Wade, G.A., Reyes, G., Guillen, J.F.**, Proceedings of the First International Conference on High Performance Structures and Composites, (2002).

5. CONCLUSIONS

The mechanical and fracture properties of novel fibre-metal laminates based on thermosetting and thermoplastic matrices have been characterised and elucidated. The results of this research programme were presented and analysed in the previous chapter and from these results a number of conclusions can be drawn.

5.1 GENERAL SUMMARY

The work presented in this thesis demonstrated that the thermosetting and thermoplastic composite materials studied here exhibit excellent interlaminar fracture properties. Here, the interlaminar fracture toughness of the plain composites was directly related to the ability of the material to dissipate energy in form of plastic deformation within the matrix material. In addition, the GFPP system exhibited a fibre bridging fracture mechanism, which in turn, resulted in higher values of $G_{I/IIc}$ in comparison to its thermosetting counterpart. Mixed-mode tests on the composites studied in this programme have shown that matrix deformation and yielding increased the $G_{I/IIc}$ at low and intermediate loading rates, however, a ductile to brittle transition in the matrix was responsible for a slight drop in $G_{I/IIc}$ at impact rates of loading. Single cantilever beam tests on model aluminium/carbon fibre reinforced epoxy samples have shown that a simple abrasion-wipe procedure is sufficient for achieving an excellent level of adhesion, which in turn resulted in high values of interfacial fracture energy. Tests over a wide range of loading rates have shown that the interfacial fracture energy exhibited a response similar to that of the plain composite, remaining high even under dynamic loading conditions. In addition, SCB tests on the aluminium/glass fibre polypropylene system have shown that excellent adhesion between the metallic and composite plies can be achieved through the combination of an amorphous chromate coating surface treatment applied to the aluminium substrate and the incorporation of an interlayer of maleic anhydride modified PP at the bi-material interface. Tests over a wide rage of loading rates have

shown that the interfacial fracture energy first increased with loading rate and then decreased. These trends have been partly explained by examining the fracture surfaces of the failed specimens. At low and high rates of loading, the crack exhibited a tendency to propagate a long the bi-material interface. At intermediate rates, the crack remained within the composite substrate. Furthermore, DENB tests showed that the level of plastic deformation exhibited by these bi-material specimens was very similar to that in the plain composite. Therefore, the variation of the interfacial fracture toughness with crosshead displacement rate resulted from the presence of a matrix yielding toughening mechanism, coupled with the change in failure locus.

Flexural tests on thermosetting and thermoplastic-based fibre-metal laminates using a number of stacking sequences have shown that increasing the amount of composite material has a beneficial effect on the flexural strength. In contrast, the flexural modulus exhibited a decrease as a result of increasing volume fraction of composite material. Flexural failure in these systems was directly linked to the position of each layer within the layered laminates. In addition, the bi-material interfaces remained in excellent condition after flexural loading. Similarly, tensile tests on both fibre-metal laminate systems have shown that their ultimate strength and elastic modulus follow a simple law of mixtures relationship with the former increasing with the addition of the composite material and the later decreasing. An examination of the edges of the samples highlighted that tensile failure in the thermosetting and thermoplastic-based fibre-metal laminates occurred in the composite layers rather than at the interface as a result of the excellent load transfer between aluminium and composite materials.

The low velocity impact response of the fibre-metal laminates has been investigated by conducting a series of low velocity impact tests on a simple plate configuration. Here, it was shown that the laminates were capable of absorbing significant energy through extensive plastic deformation in the aluminium and composite layers and localised fibre fracture and matrix cracking in the thermosetting and thermoplastic composite layers respectively. In addition, it has been shown that

the thermoplastic-based fibre-metal laminates offer superior resistance to low velocity impact loading than its thermosetting counterpart. Subsequent tensile tests on impact-damaged coupons from both systems have shown that fibre-metal laminates offer excellent residual properties with the (4/3) laminates suffering a maximum 20% reduction in strength following a 20 Joule impact. SENB tests have shown that the GFPP-based fibre metal laminates offer superior work of fracture properties compared to the CFRE-based fibre-metal laminates at quasi-static and dynamic rates of loading. High velocity impact test on a series of thermosetting and thermoplastic-based fibre-metal laminates have shown that the GFPP-based fibre-metal systems offered superior perforation resistant properties over the CFRE-based fibre-metal laminates under high velocity impact conditions. Indeed, the specific perforation energy of this system was over seventy percent higher than that offered by the thermosetting-based fibre metal laminates. Here failure mechanisms such as extensive plastic drawing in the aluminium layers and fibre fracture and matrix cracking in the composite plies have been shown to contribute to the superior perforation resistance of these systems.

5.2 FUTURE WORK

It has been shown that thermoplastic-based fibre-metal laminates offered superior fracture and mechanical properties to those offered by its thermosetting-based FML counterparts. In addition, it is believed that the thermoplastic nature of the GFPP-based fibre-metal laminates will reduce manufacturing times and its corresponding costs. These systems can be moulded, bonded to the aluminium layers and shaped in a simple one-shot manufacturing cycle. Furthermore, it is assumed that a rapid and efficient repair of impact-damaged structures could be achieved in these systems. Therefore, the processing and characterisation of the mechanical and fracture properties of fibre-metal laminates based on a range of tough thermoplastic matrices such as polyetherimide and polyamide can be envisaged as excellent opportunity to continue the development of novel low cost-high strength systems for future aerospace and automotive applications.

APPENDICES

A.1 Analysis of the double cantilever beam (DCB) specimen for mode I testing

The maximum deflection for a DCB specimen can be obtained from beam theory and is given by:

$$\delta = \frac{2PL^3}{3EI} \tag{A.1.1}$$

The compliance is given by:

$$C = \frac{\delta}{P} \tag{A.1.2}$$

Re-writing from equation 1:

$$\frac{\delta}{P} = \frac{2L^3}{3EI} \tag{A.1.3}$$

Therefore the expression for the compliance derived from beam theory is given by:

$$C = \frac{2}{3EI}L^3 \tag{A.1.4}$$

In analysing the results, it is assumed that the relation between the length of the crack in the sample, a, the force applied to its extremities, P, and the total deflection which results, δ, can be represented by the generalised form of the Equation A.1.4 derived from beam theory, yielding [1]:

$$C = Ka^n \tag{A.1.5}$$

Using the general expression for the strain energy release rate

$$G_c = \frac{P^2}{2B}\frac{dC}{da} \tag{A.1.6}$$

and substituting equation A.1.5 into equation A.1.6 yields the strain energy release rate:

$$G_{Ic} = \frac{nP\delta}{2Ba} \tag{A.1.7}$$

A.2 Analysis of the end notched flexure (ENF) specimen for mode II testing

The ENF fracture specimen [2] is a three point bending flexure specimen with an embedded through-width delamination placed at the laminate mid-surface as shown schematically in Figure A.1

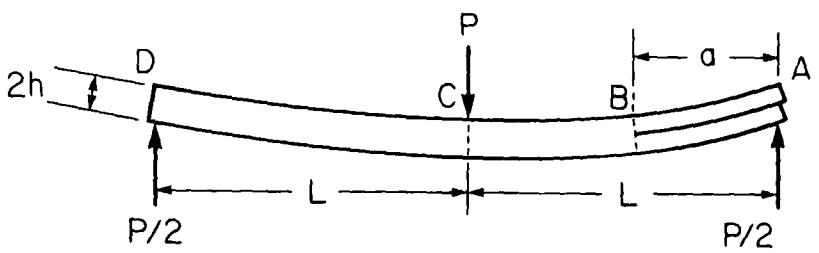

Figure A.1 *End notched flexure (ENF) specimen.*

The derivation of the strain energy release rate for this specimen is based on the change in compliance with crack extension. The compliance of the ENF specimen is defined as the displacement, δ, at the central loading pin divided by the applied load, P. With the notation in Figure A.2, δ may be calculated from:

$$\delta = \frac{\Delta_{AB} + \Delta_{BC} + \Delta_{CD}}{2} \tag{A.2.1}$$

The beams BC and CD are modelled as cantilever beams. For the delaminated region, AB, the displacement Δ_{AB} has two components, one due to the bending and shearing deformations of the beams and the other due to the rotation of the cross-section at point B, see Figures A.1 and A.2. Therefore, the compliance, C, of the ENF specimen is given by:

$$C = \frac{2L^3 + 3a^3}{8EBh^3} \tag{A.2.2}$$

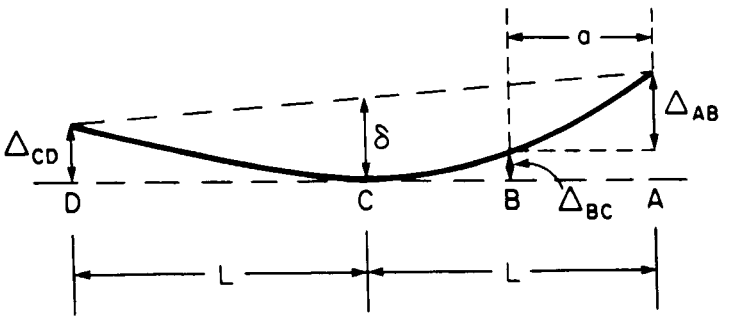

Figure A.2 *Definition of vertical displacements for the ENF specimen [3].*

Using the general expression

$$G_c = \frac{P^2}{2B}\frac{dC}{da} \tag{A.2.3}$$

to obtain the strain energy release rate yields:

$$G_{IIc} = \frac{9a^2P^2}{16EB^2h^3} \tag{A.2.4}$$

where E, is determined from Equation A.2.2, and C = δ/P yielding:

$$E = \frac{P}{\delta}\frac{2L^3 + 3a^3}{8Bh^3} \tag{A.2.5}$$

Therefore, rewriting Equation.4, the strain energy release rate is given by:

$$G_{IIc} = \frac{9a^2P\delta}{2B\left(2L^3 + 3a^3\right)} \tag{A.2.6}$$

A.3 Analysis of the mixed-mode flexure (MMF) specimen for mixed-mode testing

The MMF specimen is similar to the pure mode II specimen except that at the delaminated end the load is applied to the upper arm only, thus providing crack opening as well as shear [2]. An expression for the compliance was derived in a similar manner to that of the ENF specimen [2] and is given by:

$$C = \frac{(7a^3 + 2L^3)}{96EI} \tag{A.3.1}$$

Here, the moment of inertia, I, is given by the expression:

$$I = \frac{Bh^3}{12} \tag{A.3.2}$$

Using the general expression

$$G_c = \frac{P^2}{2B}\frac{dC}{da} \tag{A.3.3}$$

where:

$$\frac{dC}{da} = \frac{21a^2}{8EBh^3} \tag{A.3.4}$$

and

$$E = \frac{(7a^3 + 2L^3)}{8CBh^3} \tag{A.3.5}$$

the strain energy release rate yields:

$$G_{I/IIc} = \frac{21P^2a^2C}{2B(7a^3 + 2L^3)} \tag{A.3.6}$$

A.4 Analysis of the single cantilever beam (SCB) specimen for mixed-mode testing

The maximum deflection for a SCB specimen may be obtained from beam theory and is given by:

$$\delta = \frac{PL^3}{3EI} \tag{A.4.1}$$

The compliance is given by:

$$C = \frac{\delta}{P} \tag{A.4.2}$$

Rewriting from Equation A.4.1:

$$\frac{\delta}{P} = \frac{L^3}{3EI} \tag{A.4.3}$$

Therefore the expression for the compliance derived from beam theory is given by:

$$C = \frac{1}{3EI} L^3 \tag{A.4.4}$$

From measurements of the crack length during the test, an experimental compliance calibration may be determined, allowing dC/da to be obtained. The simplest requires a curve fit such as [4]:

$$C = C_o + ma^3 \tag{A.4.5}$$

This is a generalised form of the Equation A.4.4 derived from beam theory. Here, the intercept, C_o and the slope, m are constants that may be determined from the plot of C vs a^3.

Using the general expression for the strain energy release rate

$$G_c = \frac{P^2}{2B}\frac{dC}{da} \tag{A.4.6}$$

where

$$\frac{dC}{da} = 3ma^2 \tag{A.4.7}$$

and substituting Equation A.4.7 into Equation A.4.6 the strain energy release rate yields:

$$G_{I/IIc} = \frac{3P^2ma^2}{2B} \qquad \text{(A.4.8)}$$

A.5 Elastic and thermal properties used in the Utah Laminates 3.0 software programme

The elastic and thermal properties used for the determination of the residual stresses and flexural moduli are given in table A.1.

	Aluminium	CFRE	GFPP
Tensile modulus, E_{11} (GPa)	70	49	25
E_{22}	70	49	4
Flexural modulus, E_f (GPa)	60	43	21
Poisson's ratio	0.3	0.04	0.33
Shear modulus, G_{12} (GPa)	28	4.1	1.4
Coefficient of thermal expansion, ($x10^{-6}/°C$)	24	4	10

Table A.1 *Thermo-elastic properties of base materials used in this research programme.*

A.6 References

[1] **Berry, J.P.**, Journal of Applied Physics, **34** (1963), pp 62-68.

[2] **Russell, A.J., Street, K.N.**, Delamination and Debonding of Materials, ASTM STP 876, W.S. Johnson, Ed. (1985), pp 349-370.

[3] **Carlsson, L.A., Gillespie, J.W. Jr.,Pipes, R.B.**, Journal of Composites Materials, **20** (1986), pp 594-604.

[4] **European Structural Integrity Society (ESIS)**, Protocols for Interlaminar Fracture Testing, Davies, P.,IFREMER (1993).